Colored Glasses and Glazes from the European Bronze Age to the Early Modern

Technological Developments of Glass Processing in four Examples

Dissertation

(kumulativ)

zur Erlangung des akademischen Grades doctor rerum naturalium
(Dr. rer. nat.)

vorgelegt dem Rat der Chemisch-Geowissenschaftlichen Fakultät der
Friedrich-Schiller-Universität Jena

von Dipl. Chem. Ferdinand Drünert
geboren am 25. Juni 1985 in Bad Oldesloe

Gutachter:

1. Prof. Dr.-ing. Lothar Wondraczek, FSU Jena, Jena, DE
2. Assoc.-Prof. Dr. Doris Möncke, Alfred University, Alfred (NY), USA
3. .....

Tag der Verteidigung: 21. Oktober 2019

"To the king, my lord, my god, my Sun, the Sun from the sky: Message of Yida, your servant, the dirt at your feet, the groom of your horses.

6–13 **I indeed prostrate myself, on the back and on the stomach, at the feet of the king, my lord, 7 times and 7 times. I am indeed guarding the [pl]ace of the king, my lord, and the city of the king, in accordance with the command of the king, my lord, the Sun from the sky.**

13–16 **As to the king, my lord's, having ordered some glass, I [her]ewith send to the k[ing], my [l]ord, 30 (*pieces*) of glass.**

17–23 **Moreover, who is the dog that would not obey the orders of the king, my lord, the Sun fr[o]m the sky, the son of the Sun, [wh]om the Sun loves?" (Moran 1992, p. 353–354)**

Figure 1: Amarna letter E323, 14th century BCE, was found among ca. 300 other letters at the royal city of Akheaten in Egypt, located at the Bureau of Correspondence of the Pharao Akhenaton. The letters were translated into English by Moran (1992) and are now displayed at the British Museum in London.

Acknowledgements

A long research project, such as a PhD, is never accomplished without lots of support. Many people helped me on my way and I want to use the opportunity to express my gratitude.

First of all, I want to thank my supervisors Lothar Wondraczek and Doris Möncke for the long support, input of ideas, advice and help in general. The possibility to delve into the world of archaeometric research is not easy to get, and I am happy that I could conduct my research here in Jena.

Secondly, I thank the late Peter Steppuhn for supplying me with samples. Peter, we will miss you! Many thanks for Ingrid and Uwe Berg for their support and rich collection of samples and to Nikos Zacharias, Eleni Palamara and the Greek Ministry of Culture and Sports for enabling me to study the ancient glass samples.

Also, I thank Courtney, Kristin, Garth and Paul for reviewing my thesis- and paper draft(s), again and again. The many discussions about various aspects of even more things helped me to sort out my ideas and let me stay in- and sometimes also out of focus. The many barbecues (and other occasions to celebrate) with you and all the other colleagues made my time at the institute a lot more cheerful and enjoyable, thanks to all of you.

Finally, I thank my partner Nele and my family for their support. I don't want to know how much I would have messed up without you.

Contents

List of Figures

List of Tables

List of abbreviations

CN	coordination number
CT	charge transfer
FT-IR	Fourier transformed infrared spectroscopy
HLLA	high lime low alkali
HLLM	high lime low magnesia
IR	infrared
IVCT	Intervalence charge transfer
LA-ICP-MS	laser ablation inductively coupled plasma mass spectrometry
LBA	Late Bronze Age
LLHM	low lime high magnesia
MO	molecular orbital
NBO	non-bridging oxygen
PIGE	particle-induced gamma ray emission
Q^n	structural units with n bridging oxygen bonds
SEM-EDX	electron scanning microscopy coupled with energy dispersive X-ray spectroscopy
SIMS	secondary ion mass spectrometry
T_g	glass transition temperature
T_m	melting temperature
UV-Vis-NIR	ultraviolet-, visual and near infrared spectroscopy
XRF	X-ray fluorescence spectroscopy

1 Introduction

Glass is one of the few materials that have been used continuously by human kind since the Stone Age. The use of glass ranges from tools, containers, decorations and technical applications to materials for isolation or energy production. Reworked into scrapers, burins, drills and blades, natural glasses have been employed already at the very beginning of civilization (Emberling et al. 1999). Most likely during advancements in ceramics or metallurgy, first artificial glazes were produced in the 5^{th} to 4^{th} millennium BCE (Peltenburg 1971; Lankton 2003). The development of glass furnaces, approximately in the 16^{th} century BCE, enabled the synthesis of glassy bulk materials. These glasses did not, in contrast to glazes, require ceramic or stone substrates. Such glasses were traded over large distances through the whole Mediterranean and Near East region (Shortland, Rogers, et al. 2007): Early written sources as the Amarna letters (14^{th} century BCE; see Figure 1) document the trade between the earliest known production centers in Mesopotamia and Egypt (Moran 1992). The prominent finding of the Uluburun shipwreck (15^{th} century BCE) reveals that not only finalized glass products were traded during the Aegean Late Bronze Age period, but also raw glass ingots.

The existence of raw glass ingots proves that the very early process of glass production passed two steps. The raw glass was produced in a small number of primary manufacturing sites and formed in ingots, whereas these ingots were used as source for the actual glass products. As of yet, not many of the primary production sites have been discovered. Most prominent are the sites of Amarna (Smirniou and Rehren 2010), Lisht and Qantir (Rehren 2005) in Egypt. Other sites, e. g., in Mesopotamia or Greece, are likely to exist, but have not been excavated until now (Shortland, Rogers, et al. 2007; Smirniou and Rehren 2010).

Appropriate glass furnaces with the capability to keep temperatures of up to 1000 °C stable for a long time are necessary for the manufacture of raw glass. Sites for such primary glass production can be identified rather easily by the presence of glass ingots, glass slags, frit, crucible material and vitrified bricks (Schoer and Rehren 2007). However,

the distinction of secondary sites from primary glass production sites is often challenging due to the the low amounts of remains, the smaller size of the structures and the bad state of preservation. Such sites are often identified by glassy remains, half-prepared products, crucible materials and possibly glass working tools (Panagiotaki et al. 2003; Kemp 2015). Wiesenberg (2018) could demonstrate in some experimental archaeology studies for bead manufacture and similar products, that simple furnace types easily corrode with almost no traces of the furnace material left within a short period of exposure to weathering. Consequently, not only is the identification of production sites more complicated, but also the understanding of applied technologies and techniques becomes more challenging. A detailed chemical analysis of the different features and an experimental archaeological approach therefore extends the existing archaeological knowledge about glass technology in history.

1.1 The scope of archaeometry

As an auxiliary discipline of archaeology, archaeometry can enhance the knowledge about ancient artifacts and their context by detailed scientific analysis based on physical and chemical methods. The results of archaeometric analysis range from dating, determination of the provenience and investigation of corrosion mechanisms to further insight into the processes of manufacture, especially when combined with experimental archaeology. Here I present the most important approaches for the analysis of glasses from a physicochemical perspective.

1.1.1 Quantitative chemical analysis

The quantitative chemical analysis of glass samples is necessary to determine the type of glass, in other words, the recipe used in its manufacture (Tite, Shortland, et al. 2006; Schalm et al. 2007; Wedepohl and Kronz 2009). The amount of coloring ions, such as cobalt or copper, give additional information on the origin of the glasses visual appearance. The most applied techniques for quantitative analysis of archaeological glass samples are the semi-quantitative methods X-ray fluorescence spectroscopy (XRF) and electron scanning microscopy coupled with energy dispersive X-ray spectroscopy (SEM-EDX), while laser ablation inductively coupled plasma mass spectrometry (LA-ICP-MS)

is an relevant method for trace element analysis.

1.1.2 Structural analysis

Archaeological glass samples, especially those from times before the development of the blowpipe, were usually colored and richly decorated. The general information of quantitative analysis regarding coloring ions and, in case of SEM-EDX, sometimes larger crystallites, usually excludes information about oxidation numbers or the exact crystal structure. Redox states of polyvalent ions in a glass are, however, a good indicator for the investigation of historical technologies. They allow conclusions on melting conditions like exclusion of air, as they have already been described in the 11^{th} century by the monk Theophilus Presbyter (Ilg 1874). The standard melting condition and the range of redox states can be estimated by applying ultraviolet-, visual and near infrared spectroscopy (UV-Vis-NIR) (Drünert, Lozier, et al. in press; Drünert, Zacharias, et al. in press). Additionally, optical analysis is suitable to determine the coordination number of coloring agents (Duffy 1990; Tilley 2011; Bingham et al. 2014; Weyl 2016).

In contrast, vibrational spectroscopy enables conclusions about the glass network. Archaeological glass samples are usually affected by corrosion, that is, the depletion of alkaline ions from the glass surface. As a result, the silicate tetrahedrons will repolymerise and reform the glass network. This transformation can be well observed by Fourier transformed infrared spectroscopy (FT-IR; Lynch et al. 2007). The method enables also the investigation of other surface modifications (e. g., alteration through processing) due to the high surface sensitivity of FT-IR spectroscopy (Möncke, Palles, et al. 2013; Drünert, Lind, Vontobel, et al. submitted). The complementary Raman spectroscopy, which probes similarly to infrared (IR) spectroscopy molecule vibrations, has been applied on corrosion studies (Colomban 2008). Furthermore, the high spatial resolution of Raman spectroscopy compared to IR can be used for the identification of crystal phases in a glass matrix (Gedzevičiūtė et al. 2009; Lahlil, Cotte, et al. 2011; Drünert, Palamara, et al. 2018).

1.1.3 Experimental archaeologic approach

The replication of archaeological materials is a modern approach to gain a better understanding of past technologies. Although the method offers opportunities to expand

the understanding of such technologies and can sometimes falsify existing models, it also invites to misinterpretation (Outram 2008). Since verification of a technique by reproduction is not possible, the results of experimental archaeology have to be understood as a model, and as such the limitations of the model have to be considered. Only detailed investigation of the reaction parameters, and therefore the reproducibility of a given approach, separates experimental archaeology from the more educational approach of living history (Outram 2008). A detailed chemical analysis of the archaeological artifact is necessary for the determination of reaction parameters. Still, the reproduction is also very helpful: Unexpected events during the experiment reveal flaws of the former model and show new approaches for the manufacture of such artifacts, while the comparison between artifact and replica bring new insights (Drünert, Blanz, et al. 2018; Drünert, Palamara, et al. 2018). Furthermore, the application of destructive methods on replica aids in finding better analytical methods for archaeological objects (Drünert, Lind, Kästner, et al. in press; Drünert, Lind, Vontobel, et al. submitted).

1.2 Scope of this work

In the following, I will explain technological developments in the history of glass on four very different examples. The focus of this work lies on colored glasses, their origin and manufacture. Therefore, I selected two studies which focus on the Aegean Late Bronze Age (LBA) and the Roman Antiquity in Greece and two studies about Medieval and Early Modern glass in Germany to show, how analysis together with replication can contribute to our understanding of the history of glass technology (Figure 2): We investigated possible routes for the alteration of glass surfaces on blue relief inlay fragments from Epidavros, Greece (late 2^{nd} millennium BCE) and the possible relationship to gold manufacturing of related samples (Drünert, Lind, Kästner, et al. in press; Drünert, Lind, Vontobel, et al. submitted). Opaque white glass mosaic *tesserae* from Messene, Greece, (1^{st} to 4^{th} century CE) were analyzed for their opacifying agents, $CaSb_2O_6$ and $Ca_2Sb_2O_7$; the influence of nucleating agents on the formation of calcium antimonates was also examined (Drünert, Palamara, et al. 2018). We studied Medieval glass samples excavated at the *Philosophicum* in Münster, Germany, 12^{th} to 15^{th} century CE, regarding the employed glass recipe and the range of redox conditions (Drünert, Lozier, et al. in press). And lastly, we analyzed opaque red glasses from Taunus Mountains, Germany (14^{th} cen-

tury CE) and from Wieda, Germany (16^{th} century CE) regarding the oxidation state and size of the copper nanoparticles that give them their deep red color. The calculated backscattering cross-sections that relate to the size of the copper spheres were compared with actual UV/Vis reflection measurements to draw a relationship between optical appearance and particle size (Drünert, Blanz, et al. 2018). In all examples, I focused on chemical analysis and/or replication of the archaeological materials to draw conclusions about the technology which had been used in their manufacture.

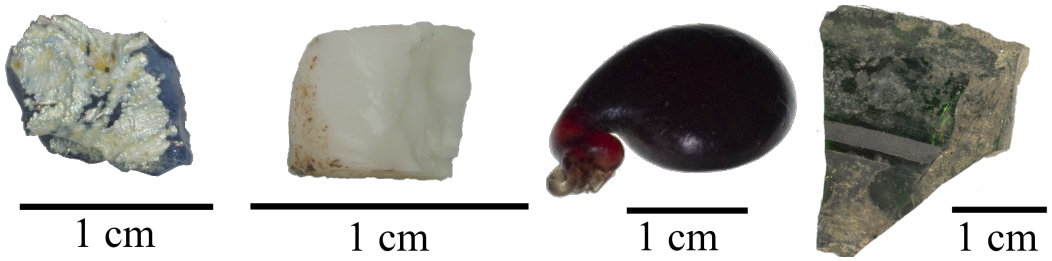

Figure 2: Sample images of the four studies from left to right: LBA glass; Roman mosaic *tessera*; Medieval copper based glass; lead glass shard from Münster.

2 Theoretical Background

2.1 The history of glass compositions

For thousands of years only seven oxides were used as main components for glass synthesis. Modern glass chemistry, utilizing most of the periodic table and expanding to phosphate, borate and even non-oxide glasses, had not been used commercially before the developments of Otto Schott, starting in the late 19th century CE (Vogel 2011). The various silicate glass compositions that have been commonly used during the history of glass manufacture in Europe can be divided into three main groups: (1) soda lime silicate glasses, (2) potassium lime silicate glasses and (3) potassium lead glasses. Silicate sands and powders, usually gathered from beaches or rivers, were used as network former in all three types (e. g., Silvestri, Molin, Salviulo, and Schievenin 2006). In contrast, the glasses vary in the choice of alkali- and alkaline earth sources. Coloring agents were also added to this base glass to modify the appearance (Green and Hart 1987; Möncke, Papageorgiou, et al. 2014). The most important groups and their relevance throughout the history of Europe and the Mediterranean are shown in Table 1. A timeline of their manufacture is shown in Figure 3.

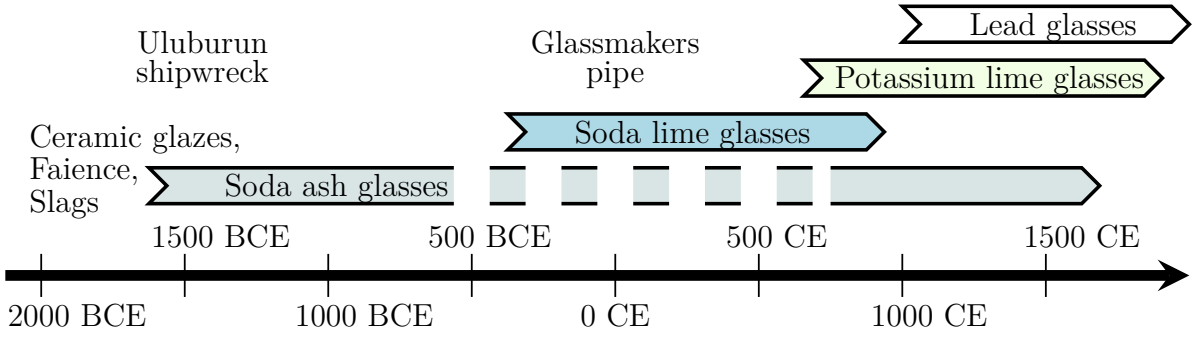

Figure 3: Timeline of glass compositions used in the history of glass manufacture.

Table 1: Approximate chemical compositions (wt%) of archaeological glass samples dependent on the glass type.

Glass type	Soda ash	Soda lime	Potassium lime	Lead
SiO_2	60 to 80	65 to 75	45 to 60	20 to 60
PbO	0 to 5	0 to 5	0 to 10	10 to 80
Na_2O	15 to 20	15 to 20	0.5 to 4	0 to 10
K_2O	2 to 4	< 1	10 to 25	0 to 15
MgO	2 to 4	< 1	2 to 5	< 1
CaO	4 to 10	4 to 10	5 to 30	0 to 15

2.1.1 Soda lime silicate glasses

Soda lime silicate glasses are the first artificial glass types of humankind. They are divided into two main subgroups: *soda ash* glasses and *soda lime* glasses.

Soda ash glasses

The earliest approaches of glass manufacture were based on a *soda ash* glass composition (Lilyquist and Brill 1993; Shortland and Tite 2000). The first written description of glassy materials, utilizing plant ash for glazes, was discovered on a Babylonian stone tablet, dated (although not stratigraphically determined) to the 14th to 12th century BCE (Gadd and Thompson 1936). A later stone tablet from the library of Ashurbanipal at Nineveh (ca. 7th century BCE) mentions the manufacture of glass in further detail (Oppenheim et al. 1970; Brill 1972).

Ashes of halophyte plants, that is from marshland and desert areas, were used as alkali source for *soda ash glasses* (Henderson 1985). Tite, Shortland, et al. (2006) suggest the use of *Salsola kali* ashes for the manufacture of such glasses; yet, the research on compositions of other halophyte ashes, influenced by their soil, and possible purification processes still need further investigation. *Soda ash* glasses were mostly used before the 1st millennium BCE, but similar recipes were used in the 9th century CE and later in today's Northern Italy and in the east Mediterranean region (Hughes et al. 2000; Freestone 2006; Cagno et al. 2012). In the 17th century CE, kelp ashes became a common ingredient for glasses in Northern Europe (Dungworth 2011). Main characteristics of *soda ash* based glasses

are, next to high quantities of sodium and calcium oxide, comparably high amounts of K_2O (roughly 2 wt% to 4 wt%) as well as MgO (ca. 2 % to 7 %) (Lilyquist and Brill 1993; Henderson, McLoughlin, et al. 2004). The glasses usually contain high amounts of impurities due to the rather heterogeneous plant ashes, which vary in composition dependent on the soil, the season and the general influence of the weather in the year of collection (Freestone 2006; Jackson 2008).

Soda lime glasses

Throughout the first millennium BCE new recipes for glass manufacture were employed. The evaporates of salt lakes in Egypt, especially from Wadi Natrun, were collected and used instead of plant ashes. These minerals were mostly trona ($Na_3(HCO_3)(CO_3) \cdot 2\,H_2O$), together with thenardite (Na_2SO_4), burkeite ($Na_6(CO_3)(SO_4)_2$) and halite (NaCl) (Freestone 2006). Such *soda lime* glasses, remarkably similar to modern soda lime silicate glasses, dominated the glass manufacture until the end of the 9th century CE, when political unrest in the delta region of Egypt caused a trade collapse (Shortland, Schachner, et al. 2006).

Soda lime glasses can be identified by the small amount of K_2O and MgO in the glass composition – usually less than 1 wt% (Silvestri, Molin, and Salviulo 2005). *Soda lime* glasses are further separated into a maximum of 14 subgroups according to their impurities. Most of these subgroups originate from the Levant area (Gratuze and Barrandon 1990; Picon and Vichy 2003; Freestone 2004).

2.1.2 Potassium lime silicate glasses

The vast majority of the continental European glass samples from the 9th to 18th century were potassium silicate glasses made from wood ashes. The main difference between these and the *soda ash* type is the ratio of alkalines detected in the glass: While halophyte ashes contain high amounts of sodium ions, wood ash usually contains mostly potassium ions. Potassium lime silicate glasses lost their relevance after the development of the Leblanc process for soda synthesis (Kurkjian and Prindle 1998; Schalm et al. 2007) and were replaced by todays soda lime silicate glasses.

Several Latin recipes for the manufacture of potassium lime silicate glasses are known

today. The earliest instruction found thus far is the third book of Heraclions[1] *De coloribus et artibus Romanorum*, where the use of bracken ashes, young trees and sand is described (Ilg 1873). An unknown monk with the pseudonym Theophilus Presbyter describes a similar recipe in the early 11th century CE: *Schedula diversarum artium*; similarly, he proposes to use three parts of the ashes of beech trunks with one part sand to form clear glass (Ilg 1874). Other recipes of that time, like the *Mappae Clavicula*, provide incomplete instructions or suggest the use of otherwise prepared glass as an ingredient (Smith and Hawthorne 1974). A later recipe is given by G. Agricola in his book "De re metallica" from 1556, translated to English by Hoover and Hoover (1950). In this recipe the ashes of dry, old oak trunks are the preferred raw material. Experiments with different wood ashes showed that all ashes can be used as batch ingredients. Bracken ashes appear to require the highest effort for preparation, they contain around 16 wt% to 33 wt% K_2O and amounts of less than 17 wt% CaO (Jackson 2008). In contrast, beech ashes contain ca. 20 wt% K_2O and 30 wt% CaO, while oak ashes contain more CaO (ca. 65 wt%) and less K_2O (ca. 15 wt%). Therefore, the later recipe would result in a glass type with less alkalines (Jackson et al. 2005). However, employing the ashes of branches and leaves instead of trunks will also decrease the alkali content and increase the amount of CaO (Wedepohl and Kronz 2009).

The actual glass composition of Medieval glass samples changed depending on the place and time of manufacture. The most important subgroups of potassium lime silicate glasses are introduced below, based on the systematic naming of Schalm et al. (2007). Other classifications found in the literature are HLLM (high lime low magnesia) and LLHM (low lime high magnesia) glasses (Kunicki-Goldfinger et al. 2014).

Potash glass

The earliest type of potassium lime silicate based glasses, as found in samples that have been manufactured before the 14th century CE, is known as *potash* glass. According to Schalm et al. (2007), such glasses have a Na_2O content below 6 wt% and a K_2O to CaO ratio higher than unity. This type of glass has also been classified as *early wood ash* glass (8th to 10th century CE) with potassium contents around 12 % and *wood ash* glass

[1]The name Heraclion is not connected to any known historical person. Although the first two books are written by the same person, dated to the 8th to 10th century CE, book III is of younger origin, assumably from the 10th to 11th century (Ilg 1873).

(11^{th} to 14^{th} century CE) with potassium contents around 20 % (e. g., Wedepohl 1997; Wedepohl and Simon 2010). For the earlier glasses presumably more branches and bark were used to generate the ash, which resulted in a comparably higher CaO to K_2O ratio. In contrast, trunks were the preferred ash source for glasses in the 12^{th} century and later (Krueger and Wedepohl 2003). Such glass samples have been found in many regions of central Europe; they most closely resemble the glass type described by Theophilus (Schalm et al. 2007).

High lime low alkali glass

High lime low alkali (HLLA) glasses first occur in the European 14^{th} century (Schalm et al. 2007). They are further separated by Wedepohl and Simon into *early wood ash lime* glasses (14^{th} century CE) with K_2O contents around 12 wt% and *wood ash lime* glasses (15^{th} to 16^{th} century CE) with K_2O contents around 8 % (2010). Another classification used in the literature is based on the difference between *high lime low magnesia* (HLLM) glasses, overlapping with the HLLA type, and *low lime high magnesia* (LLHM) glasses, usually resembling the earlier type (Freestone et al. 2010; Kunicki-Goldfinger et al. 2014). These glasses often have significantly higher CaO to K_2O ratios of up to 5 : 1 (Schalm et al. 2007). In some cases NaCl was added as a flux, which results in a comparably high Na_2O and Cl^- content of 2 wt% to 5 wt% (Schalm et al. 2007; Wedepohl and Kronz 2009; Drünert, Blanz, et al. 2018).

2.1.3 Lead glasses

Lead was known as a colorizing and opacifying agent in the early history of glass manufacture (Shortland 2002) and occurred in a small number of glass beads already in early antiquity (Brill 1999). Clear soda lead silicate glasses have been found in Islamic Spain of the 12^{th} century CE (Carmona et al. 2009), but the soda lead silicate system appears to have been rarely produced and possibly connected to glass of emerald color. In Central Europe, lead glasses based on wood ash appeared first in the 8^{th} century CE (Wedepohl 2003), and became a very characteristic glass type in the Middle Ages (Mecking 2012). The production of emerald green glass from a mixture of sand, lead and wood ashes has been described in *De coloribus et artibus Romanorum* (Ilg 1873) and slightly differently as well by Theophilus Presbyter (Ilg 1874). Such glasses contain 70 wt% to 75 wt% PbO and

can therefore be manufactured at lower temperatures, due to the eutectic region below 800 °C. They have been labeled as *Central European lead ash* glass (Smart and Glasser 1974; Mecking 2012). Two other subgroups, that have been categorized by Mecking as *wood ash lead* glass and *Slavic wood ash lead* glass, usually contain less PbO from ca. 15 wt% to 50 wt% (2012).

2.2 The structure of silicate glasses

2.2.1 The general structure of glasses

In contrast to crystals, the glassy state is characterized as an amorphous network: Although glasses exhibit near order structure, the basic structural units are connected by slightly varying angles and bond lengths and therefore lack any long-range order (Vogel 2011). In the case of silicate glasses, this network consists of interconnected $[SiO_4]^{4-}$-tetrahedra with shared corners. The bonding of these Si−O−Si bonds can be broken up by adding modifier components like alkaline and alkaline earth oxides to the glass matrix and non-bridging oxygen (NBO) bonds are formed. As a result, the melting temperature (T_m) and the glass transition temperature (T_g) decrease.

The general differentiation between network formers and modifiers is defined by the field strength $\frac{Z}{r_c^2}$ of a cation with the charge Z over the distance of an oxygen-cation bond r_c (Dietzel 1942). The radius of the cation depends on the number of surrounding oxygen ions[2] and on the valence of the cation. According to this classification, all cations with a field strength $\frac{Z}{r_c^2} < 0.4$ are considered as modifiers, whereas all cations with $\frac{Z}{r_c^2} > 1.5$ are classified as network formers. All cations that do not fit in one of the two categories are defined as intermediates, that means they can assume both roles (Vogel 2011). Consequently, in silicate glasses, Al^{3+} is known as modifier in six-fold coordination and as network former in four-fold coordination. Cations with multiple redox states are able to switch their function in the network. As an example, six-fold coordinated Fe^{2+} has a field strength of 0.43 and is at the very border between modifiers and intermediates, whereas Fe^{3+}, also six-fold coordinated, is reported with a field strength of 0.76 and is therefore a clear intermediate (Vogel 2011).

[2] In a narrow sense the oxygen bonds are partially of ionic and partially of covalent character. To emphasize the negative polarization of the oxygen I will describe them here as ions.

The only known network formers that occur in archaeological glass samples in relevant quantities are silica, lead and, limited to ash glasses, phosphorus[3]. Typical modifiers are Na^+, K^+, Fe^{2+} and Mn^{2+}, while Al^{3+}, Ca^{2+}, Mg^{2+}, Fe^{3+} and Mn^{3+} are classified as intermediate ions.

2.2.2 The silicate glass network

The amount of non-bridging oxygen (NBO) bonds depends on the presence of modifiers and can theoretically increase to four NBO per silicate ion. The different structures are usually described as structural units with n bridging oxygen bonds $(Q^n)^4$ and $4-n$ non-bridging oxygen ions. The five possible silicate structures are displayed in Figure 4.

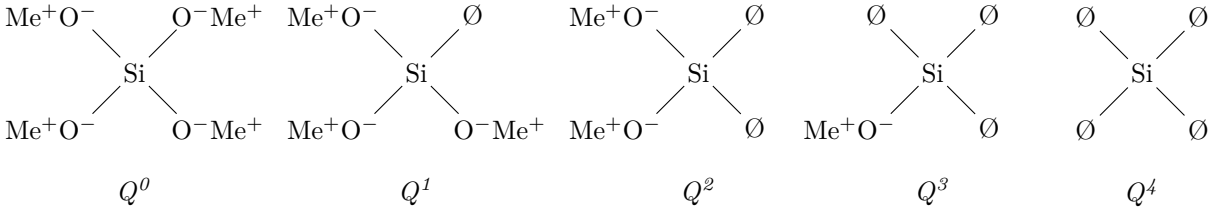

Figure 4: n in Q^n denotes the number of bridging oxygen bonds in a silicate tetrahedron. When more modifier oxides are present in the glass, fewer connections to other silicate tetrahedra are possible. Here, we assume Me^+ to be a monovalent ion, but polyvalent ions connected to multiple non-bridging oxygens are possible as well. The conceivable stereoisomers for Q^0 and Q^1 species are neglected here.

Although all network formers are usually fixed in their average position at room temperature, they still occur in different energy states, which indicates that they vibrate differently. The number of possible vibrations in a structural unit with x atoms is dependent on the degrees of freedom, F. Since rotation of structural units in a fixed network is not possible and movement of all atoms in the same direction can be excluded, $F = 3x-6$ degrees of freedom exist for non-linear units and $F = 3x-5$ degrees of freedom for linear units. All excited states of vibration require a gain of energy, usually in the infrared range. Dependent on the polarizability (Raman) or a changing dipole moment (IR), excitation of the vibrational states is possible by absorption of infrared light (IR) or inelastic scattering of ultraviolet to NIR light (Raman). For further description see section 2.4.3.

[3]Phosphates in ash based glasses can exceed 5 wt%, but generally they have not been added mutually (Stern and Gerber 2004).

[4]The bridging oxygen ions are here denoted as Ø.

2.2.3 The role of intermediate ions

The contribution of intermediate ions, compared to network formers, in the formation of a rigid network is reduced due to the increased ionic (or decreased covalent) nature of the oxygen-intermediate ion bond. Therefore, ions like Ca^{2+} and Mg^{2+} form NBO bonds, but the bonding energy of the $-$Me$-$O bonds is higher than for the predominantly ionic $Me^{+}O^{-}$ bond of modifiers. The elements of the third main group of the periodic table are a special case: Due to their function as a Lewis acid they easily form tetrahedral structures like $Al\emptyset_4^-$ when they are stabilized with another cation, as in $\emptyset_3$Al$-$O$-$CaOX [5] (Jong et al. 1983; Vogel 2011). These tetrahedral units behave similarly to network formers and lead to an increase of the glass transition temperature (e. g., Klyuev and Pevzner 2003; Avramov et al. 2005).

2.2.4 Network modifiers

Modifier-oxygen bonds are predominantly ionic. However, modifiers, as well as intermediate ions, are usually coordinated by more oxygen ions than required for charge balancing reasoning, including bridging oxygen atoms or shared non-bridging oxygen ions (Hoppe et al. 1995). The number of oxygen ions coordinated to a metal ion in the first shell CN usually varies in silicate glasses between four and six (e. g., iron ions; Bingham et al. 2014; Möncke, Papageorgiou, et al. 2014), but they can be as large as CN = 8, e. g., for uranium (Farges et al. 1992).

2.3 Interaction of glassy materials with light

Three coloring mechanisms are known for glasses: The absorption of light due to *d-d* transitions in metal ions (and the similar *d-f* and *f-f* transitions), absorption of light by *charge transfer* (CT) transitions and scattering of light by particles in the glass. The latter will be discussed in detail in section 2.3.2. To understand the nature of *d-d* transitions, I will focus first on the orbital splitting of metal ions coordinated by oxygen ions.

[5] X denotes here any structural unit in the glass network

2.3.1 Attenuation by absorption of light

The attenuation of light can be described empirically by the *Lambert-Beer* law. According to this law, the absorbance A depends on three parameters:

$$A = \log\left(\frac{I_0}{I_t}\right)_\lambda = \epsilon_\lambda \cdot c \cdot d\,, \tag{2.1}$$

where I represents the intensity of light before (I_0) and after the transmission (I_t), λ the wavelength of light, c the concentration of absorption centers, d the thickness of a sample and ϵ the molar attenuation coefficient dependent of the wavelength of light. However, this correlation requires independently reacting, homogeneously spread attenuators, the exclusion of luminescent reactions, the application of monochromatic light and the absence of scattering centers in the glass matrix (Mäntele and Deniz 2017). In a modified version, this equation has also been applied to scattering processes (see equation 2.6).

According to Fermis golden rule, a transition momentum $\vec{R}_{mn}$ different to zero for the transition between two electron wave functions ψ_m and ψ_n,

$$\vec{R}_{mn} = \int \psi^a st_m(x)\vec{\mu}\psi_n(x)\mathrm{d}x \tag{2.2}$$

with a dipole momentum operator $\vec{\mu}$ is required for an absorption process (Huff and Houston 1930; Wedler and Freund 2018). Therefore, only transitions between orbitals with different parity are possible (*Laporte*-rule). Similarly, transitions, where the electron spin changes, are forbidden (spin selection rule, Halstead 2012). In glasses, absorption processes usually occur either within coordination spheres (*d-d* transitions) or by *charge transfer* transitions between polyvalent ions in the matrix (Möncke, Palles, et al. 2013; Weyl 2016).

Orbital splitting of coordinated metal ions in silicate glasses

A coordinative bond is formed when a free electron pair of an anion or molecule (the ligand) is interacting with empty orbitals of a cation. p electrons of an oxygen ligand in a silicate network can form a σ donor bond between a coordinated metal cation. Additionally, one other p orbital of the oxygen can interact with the same cation forming a π donor bond (Janiak et al. 2008).

The interaction of the atomic orbitals can be estimated from molecular orbital theory

by linear combination of orbitals.[6] Since the orbital overlap S_{AB} between two electron wave functions ψ_A and ψ_B,

$$S_{AB} = \int \psi_A \psi_B \mathrm{d}\tau \,, \tag{2.3}$$

has to be different to zero, only orbitals with identical symmetry can interact (Wedler and Freund 2018). Dependent on the polarity of the electron wave function they can interact destructively or constructively, so that the total number of orbitals remains constant. Such linear combined molecular orbitals (MOs) split into different energy levels. An example of orbital splitting, explained for an octahedral complex with σ- and π-donor interactions with oxygen, is shown in Figure 5.

The linear combination of the ligand's σ bonds with the d orbitals of an octahedrally coordinated metal ion will form three degenerate orbitals with t_{2g} symmetry, while the linear combination of the ligand's π bonds with the d orbitals of the metal ion will produce two antibonding orbitals with e_g symmetry (Duffy 1990). The stronger the π donor influence of the ligand is, the more the $2t_{2g}$ orbital will shift to higher energy – the antibonding character will increase (Janiak et al. 2008). Because the 24 electrons of the six oxygen ligands (2 electrons per σ bond and 2 electrons per π bond) will fill the bonding orbitals with an energy $E \leq E(2t_{1u})$, the $2t_{2g}$ orbital and subsequently the e_g^* orbital will be filled with potential electrons of the metal ion d orbitals.[7]

Although the π donor interaction of isolated oxygen ligands can be considered rather weak, this donor function is influenced by the other oxygen bonds (Kläui 1990). This effect has been quantified by Duffy and Ingram (1976) for various glasses in their *optical basicity* concept.

Absorption of light by *d-d* transitions: The energy difference between the $2t_{2g}$ orbitals and the $2e_g^*$, Δ_{O} (see Figure 5), is often in the range of visible light, especially for transition metal ions (Duffy 1990). However, as postulated by the *Laporte* rule, a transition between orbitals of the same parity are forbidden (Huff and Houston 1930; Wedler and Freund 2018). A distortion of the octahedral complex, either permanently

[6] This approach follows the idea of the molecular orbital theory. Other common approaches are the *crystal field theory*, based on the electrostatic interaction of the negative, point-like charge of the ligands, and the complementary *ligand field theory*, describing the interaction of the ligand electrons with the metal ion orbitals.

[7] Similar splitting of orbitals occurs in complexes of other geometries. However, energy levels of the orbitals differ and parity cannot be applied on complexes without point symmetry (e. g., Gray and Ballhausen 1963; Basch et al. 1966).

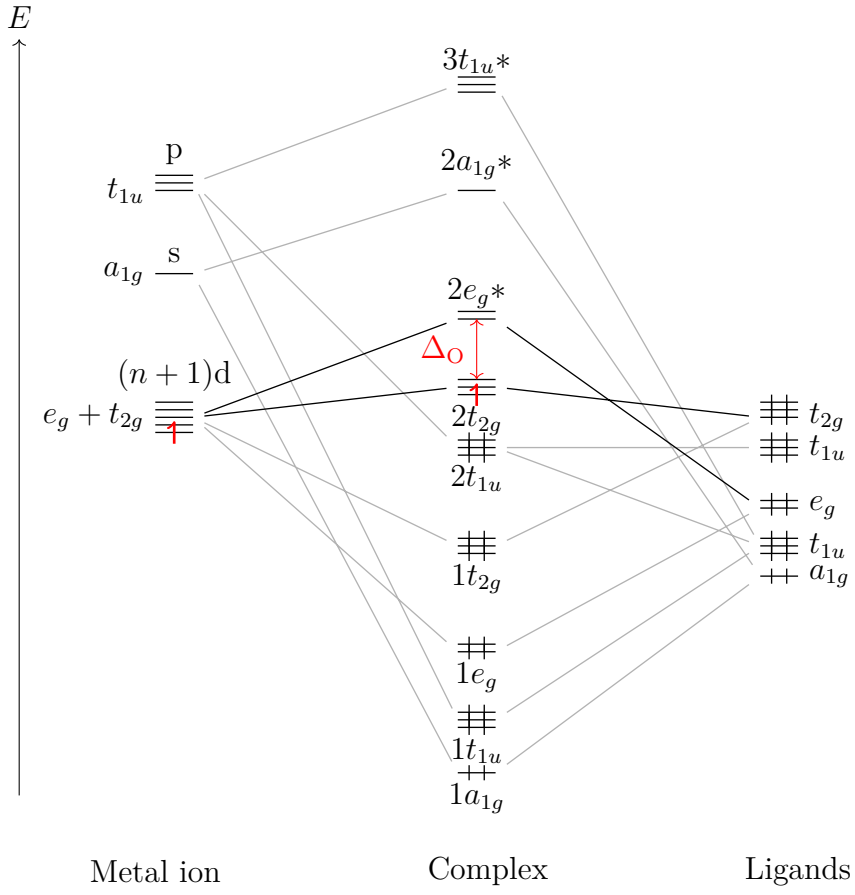

Figure 5: Orbital splitting in an octahedral complex with σ- and π-donor ligands based on Janiak et al. (2008). The crossed orbitals represent filled orbitals. Orbital interactions that are relevant for *d-d* transitions are displayed black. Here, light of the energy Δ_O excites a *d*-electron of the coordinated metal ion (red).

or by vibration, is therefore obligatory for an absorption process. Such a distortion leads to splitting of formerly degenerate orbitals and is known as the *Jahn-Teller* effect[8] (Opik and Pryce 1957; Longuet-Higgins et al. 1958). Since tetrahedral complexes (and many other geometries as well) have no center of inversion, no odd or even symmetry operations are possible. This increase in probability of such electronic transitions results in a significantly higher molar attenuation coefficient ϵ_λ (Duffy 1990; Möncke, Papageorgiou, et al. 2014).

[8]In most cases the *Jahn-Teller* effect is used to describe distortion of octahedral complexes in *z*-axis. However, the effect covers other distortions as well (Sturge 1968)

Absorption of light by *charge transfer* transitions: *Charge transfer* (CT) transitions are observable in complexes when larger amounts of electron density transfer from one ion to another (Tilley 2011). In most cases this transition occurs as *ligand-cation transition* from a negatively charged oxygen ligand ion to a transition metal ion (Me):

$$\mathrm{Me}^{x+} - \mathrm{O}^{2-} \rightleftharpoons \mathrm{Me}^{(x-1)+} - \mathrm{O}^{-}. \tag{2.4}$$

In terms of MOs, this transition arises from orbitals that are mostly composed of the ligand π orbitals, i. e. the $1t_{2g}$ orbitals of octahedral complexes (see Figure 5) to any empty orbital at the cation (Duffy 1990). As a result, CT transitions are of higher energy compared to *d-d* transitions in the same molecule. Since the parity also changes, such transitions have very high attenuation coefficients. Other ligands like S^{2-} ions are known to form CT transitions in glasses as well; the best known example is the $Fe^{3+} - S^{2-}$ complex, where the CT leads to the typical dark brown color as found in beer bottles.

A specific case is given with *Intervalence charge transfer* (IVCT) transitions: Here, a negative charge is transferred from one cation to another. The probability of this transition depends highly on the distance between the two cations, and the charge is always transferred from the lowest oxidation state to the highest (Allen and Hush 1967).

2.3.2 Scattering of light by particles in a glass matrix

Archaeological glass samples often include various types of particles in the glass matrix. The vast majority of archaeological glass samples are rich in bubbles, which cause a loss in transparency, depending on their size and their quantity (Maltoni and Silvestri 2016). Occasionally, residual, undissolved batch ingredients can also be found in the glass matrix (Stapleton and Swanson 2002). In other cases, crystalline opacifiers and colorants were deliberately added to the glass matrix to form a glass ceramic. Depending on the type of opacifier, these crystallites can be introduced into the glass matrix in different ways: They can either crystallize from the glass matrix or they can be synthesized separately and mixed into the glass batch during manufacture (Lahlil, Cotte, et al. 2011; Drünert, Palamara, et al. 2018). Few crystallite types were common for the colorization of archaeological glass samples. However, a rich variety of colors and hues could be achieved by mixing opacifiers with glass colored by dissolved ions (Shortland 2002; Möncke, Palles, et al. 2013). Selected crystallites and their color are given in Table 2.

Table 2: Common crystallites that have been added as opacifiers in archaeological glass samples.

Crystallite	Color	Epoche of application	Example reference
$CaSb_2O_6$ $Ca_2Sb_2O_7$	white	Antiquity, Modern	Drünert, Palamara, et al. 2018 Gedzevičiūtė et al. 2009
SnO_2	white	Bronze Age, Medieval	Tite, Pradell, et al. 2007
$Pb_2Sb_2O_7$	yellow	Antiquity, Early Modern	Lahlil, Cotte, et al. 2011
$PbSnO_3$	yellow	Bronze Age, Medieval	Tite, Pradell, et al. 2007
Cu^0	dark red	Bronze Age to Modern	Drünert, Blanz, et al. 2018
Cu_2O	light red	Bronze Age to Modern	Brill and Cahill 1988; Brun et al. 1991

Effect of particles on the visual appearance of glass

Glasses with significant amounts of crystalline particles are known as glass ceramics. The visual appearance of such glass ceramics is highly influenced by the presence of inclusions. If the refractive index of the glass matrix differs significantly from the refractive index of a particle, light passing through the sample will be scattered. The probability, and therefore the strength of the scattering process depends on the particle size, the difference of the refractive indices and the wavelength of the incoming light. Although light can be scattered inelastically (as in the Raman effect, see section 2.4.3), the probability of elastic scattering is orders of magnitude higher and is therefore considered here as the primary influence on the visual appearance.

The distance between two crystalline particles in such an opacified or colored glass ceramic with more or less randomized particle distribution can usually be considered as large compared to the size of the crystalline particles. Thus, scattered light from each particle is treated as being independent (Hulst 1981; Hendy 2002). Additionally, the size parameter $x = \frac{2\pi r}{\lambda}$ with r as the particle radius and λ as the wavelength will influence the scattering behavior: The electric field E of small particles with $x \ll 1$ can be considered

as homogeneous during the interaction with a photon, whereas attenuation of the E-field cannot be neglected in larger particles (Hulst 1981). The scattering behavior has therefore been described as Rayleigh scattering (particles with $x \ll 1$), as Mie scattering ($x \approx 1$) and as geometric scattering ($x \gg 1$). Optically relevant particles in archaeological glasses are usually in the range of 10^{-8} m to 10^{-5} m and therefore behave like Mie scatterers. We can distinguish two cases of colored archaeological materials: Very thin samples or cameo glasses are partially transparent for visible light; as a result, we see the light that does not interact with the particles in the sample, whereas the scattered light appears attenuated (e. g., in Kunicki-Goldfinger et al. 2014). Other samples are not transparent; in those opaque glasses mostly backwards scattered light is observed (e. g., in Drünert, Blanz, et al. 2018). Few samples, like the famous Lycurgus cup, show both phenomena at the same time (Barber and Freestone 1990; Tilley 2011).

The interaction of the E field with the material is determined by the Maxwell equations (Mishchenko et al. 2006). Today, only scattering processes of a few geometries can be calculated analytically. However, numeric approaches enable the calculation for other geometries that are not covered by analytical techniques (Hulst 1981). A detailed description of scattering mechanisms is found in the literature (e. g., Bohren and Huffman 1998; Mishchenko et al. 2006; Gouesbet and Gréhan 2011). The interaction of light with given refractive indices of matrix and particle can be calculated using the open source software *MiePlot* by Philip Laven (`http://philiplaven.com/mieplot.htm`), as employed in Drünert, Blanz, et al. (2018).

2.4 Analytical techniques in archaeometry

A non-destructive analytical method is always desirable for the investigation of archaeological samples. Particularly richly decorated or rare findings and exceptionally old materials may be prohibited from incurring any damage during the measurement. Spectroscopic techniques are therefore suitable for such analysis due to their usually non-destructive approach (Vandenabeele and Donais 2016). Only when polishing samples for better quality measurements or when trying to look beneath corrosion layers, then alteration of the sample becomes necessary. Large pieces can be analyzed *in-situ* by portable instrumentation (e. g., for UV-Vis, FTIR, Raman, and XRF spectroscopy; Cuevas and Gravie 2011; Miliani et al. 2011; Lauwers et al. 2014; Hunault et al. 2016). However, the

high energy beam of Raman spectroscopy and scanning electron microscopy may cause damage to samples, such as laser-induced crystallization (Kamitsos et al. 1990) or photo-ionization (Stroud 1961). These spectroscopic techniques can be roughly classified by the range of light that induces transitions within the sample. In the following, the principles of selected spectroscopic techniques are introduced.

2.4.1 X-ray spectroscopy

The most important X-ray methods for analysis of archaeological glass samples are SEM-EDX and XRF. In both techniques, core electrons of an ion or atom are excited past the ionization energy threshold I_π. Whereas in SEM-EDX the energy for the excitation comes from the electron beam of the scanning electron microscope, XRF utilizes an X-ray source for excitation. The reaction of the ion, however, is similar in both cases: The electron vacancy caused by the ionization of the atom will be filled with shell electrons, releasing a photon during the transition with a specific energy $E = h\omega$, with ω as the frequency of the light and h as the Planck constant. However, the principal quantum number n, the angular momentum quantum number l and the total momentum quantum number j cannot change randomly: $\Delta n \neq 0$, $\Delta l = \pm 1$ and $\Delta j = \pm\{1, 0\}$ (Janssens 2005). As a result, only specific transition energies are allowed, as Figure 6 demonstrates.

The specific transitions in such processes are usually labeled with the energy level of the initial orbital minus the energy level of the orbital after the transition, e. g., $L_2 - K$. Although this nomenclature has been proposed by Jenkins et al. (1991) for IUPAC, the Siegbahn notation (e. g., $K_{\alpha 1}$ for the $K - L_2$ and $K_{\beta 1}$ for $K - M_2$ transitions) is still widely used in the literature.

The energy of the emitted X-rays depends on the energy difference of the participating orbitals: $E_{photon} = E_{shell} - E_{vacancy}$ (Bertin 1975). Since electron energy levels of heavy elements have a higher difference from core level to outer level, higher energies can be detected from heavier elements. Additionally, the observed atom needs to have at least one electron in the L_1 level, which excludes elements lighter than lithium (Groot and Vogel 2005). Most analytical instruments based on X-ray spectroscopy which are used in archaeometry are not capable of analyzing elements lighter than magnesium with sufficient accuracy (Beckhoff et al. 2006). Since the energy difference between the different levels will increase for heavy atoms, the limit of detection is increasing with the atomic weight. However, the general limit of detection is close to 0.2 wt%, so that these techniques are

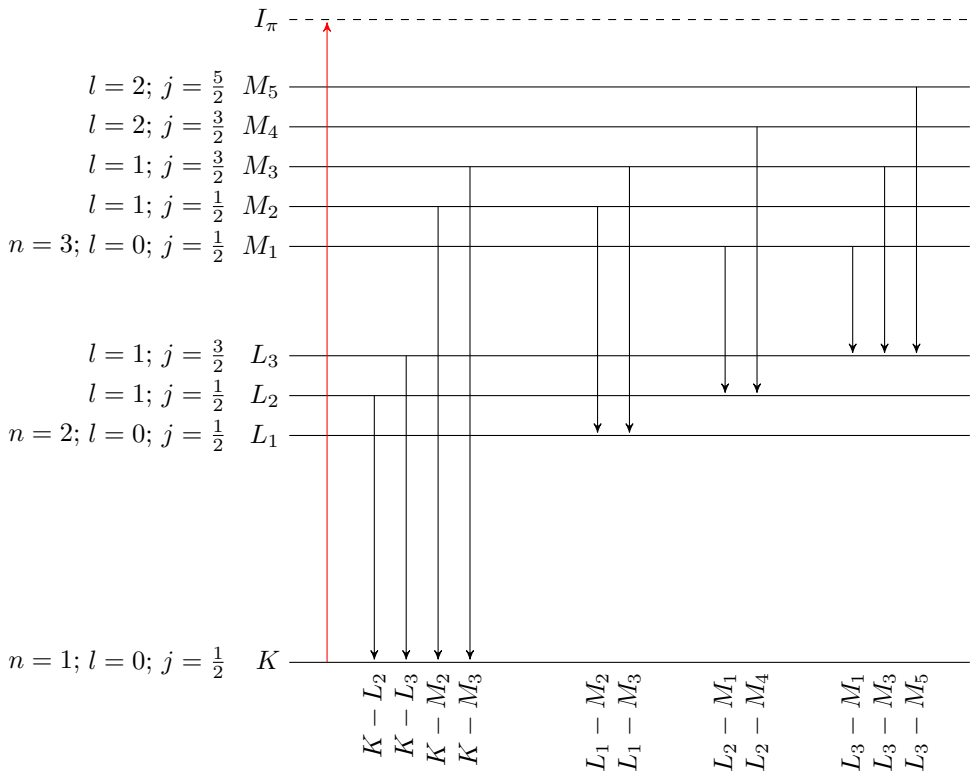

Figure 6: Jablonsky diagram of an atom after excitation by X-ray light or an electron beam. Only transitions with $\Delta n \neq 0$, $\Delta l = \pm 1$ and $\Delta j \pm 1; 0$ are possible. Each atom has a specific energy of transition and therefore enables quantitative analysis of a bulk material. Heavy atoms from the 4^{th} period can lead to higher energy transitions.

more suitable for major and, with limitations, minor element analysis (Beckhoff et al. 2006).

2.4.2 Optical spectroscopy

Despite it being a fast, non-destructive and inexpensive way to determine structural information about transition elements, optical spectroscopy has not been widely used in archaeometry until recently (Duffy and Ingram 1976; Henderson and Imbusch 1989; Möncke, Papageorgiou, et al. 2014; Drünert, Blanz, et al. 2018; Drünert, Zacharias, et al. in press). Although optical spectroscopy specifically denotes any interaction of a material with visible light, I will use this term for UV-Vis-NIR spectroscopy. Other

techniques like fluorescence spectroscopy or atomic absorption spectroscopy (AAS) can also be considered as optical techniques, but are currently rarely used in archaeometry: AAS studies have been conducted previously (Stratis et al. 1988), but today are mostly replaced by less destructive methods. Fluorescence spectroscopy has very specific sample requirements and complicated interactions, thus, only few archaeometric applications are reported (Lazic et al. 2003).

The principle of UV-Vis-NIR spectroscopy is based on the attenuation of light in a material. Reflectance spectroscopy, which measures either diffusely or specularly reflected light, and transmission spectroscopy, utilizing the transmitted light, are the most common methods of UV-Vis-NIR spectroscopy. The incoming light I_0 can be attenuated during transmission by reflection at the sample surface (I_{refl}), scattering processes (I_{sca}) and/or absorption (I_{abs}) to yield the transmitted light I_{trans}:

$$I_{trans} = I_0 - I_{refl} - I_{sca} - I_{abs}\,. \tag{2.5}$$

As long as the concentration of attenuating particles is low, absorption processes are determined by the law of Lambert-Beer (see equation 2.1). A similar approach has been used for scattering S, where a correction factor G based on the geometry of the scattering particles has to be applied to the equation, leading to the *modified Lambert Beer* law (Delpy et al. 1988):

$$S = \log\left(\frac{I_0}{I_t}\right)_\lambda = \epsilon_\lambda \cdot c \cdot d + G\,. \tag{2.6}$$

Although this equation was shown to be an approximation only (Kocsis et al. 2006), it has been used in medical contexts for the analysis of human tissue (Maikala 2010).

Unfortunately, even when scattering particles are present in the sample, scattering and absorption processes cannot be distinguished. Most archaeological glass samples include at least some light-absorbing ions, like Fe^{2+}, causing an overlap of scattered and absorbed light. A better way to estimate scattering of light makes use of an integration sphere for UV-Vis-NIR diffuse reflectance spectroscopy. In both cases, transmission and reflection, the specularly reflected light must be corrected for. In transmission spectroscopy, the reflectivity R can be simply calculated for every interface of two media by applying the Fresnel equations for a reflection angle $\theta = 180°$ on a sample orthogonal to the incident

light beam:

$$R = |\frac{n_1 - n_2}{n_1 + n_2}|^2 , \tag{2.7}$$

with n_1 as the refractive index of the surrounding medium and n_2 as the refractive index of the sample. Although specular reflectance is more difficult to estimate, the light can be excluded in the experimental setup by shifting the reflection angle of the sample slightly on the integration sphere. The diffuse reflection spectra can be obtained by comparison of measurement data including and excluding the specular reflectance.

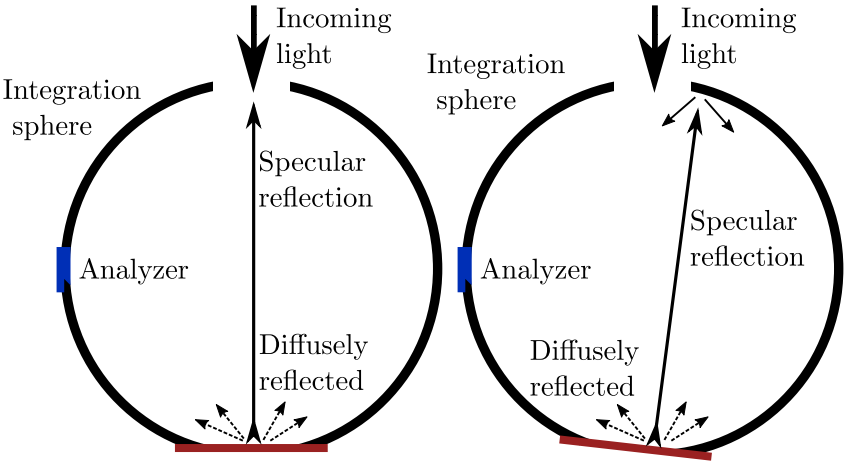

Figure 7: Specular reflection measurements of glass samples can be obtained by comparison of analysis using an integration sphere with different angles. Inside the integration sphere, the light will be diffusely reflected until it reaches the analyzer.

2.4.3 Vibrational spectroscopy

Despite their different methodologies, Raman and IR spectroscopy are complementary techniques. Both techniques detect transitions in the energy range of molecular vibrations, but differ in the physical principle: Only vibrations which include a change in polarizability can be excited by Raman spectroscopy. In contrast, a changing dipole moment during the vibration is necessary for excitation by infrared absorption.

Infrared absorption process

Energy transfer from a photon to a vibrating molecule requires a resonance condition, where the energy of the photon $E = h\omega$ matches the difference between two molecular vibration energies

$$\Delta E = \hbar \left(\frac{k}{\mu} \right)^{\frac{1}{2}} . \tag{2.8}$$

In this equation I assume a molecular vibration to behave like a harmonic oscillator with k as the force constant and μ as the reduced mass $\mu = \frac{m_1 m_2}{m_1 + m_2}$ of two vibrating atoms (Chang and Thoman 2014; Kamitsos 2015). Although molecules do not behave exactly like harmonic oscillators, the anharmonic contribution can be neglected for most transitions, except for the usually much weaker overtones (Chang and Thoman 2014). The condition for a transition between vibrational states is that the dipole moment changes,

$$\langle \mu \rangle_{e0} = \int \psi_e \mu \psi_0 d\tau \neq 0 \, , \tag{2.9}$$

with ψ_e as the wave function of the excited state, ψ_0 as the wave function of the ground state and μ as the dipole moment operator (Diem 2015).

In glass chemistry, infrared absorption of most network structures (except water related bands) is too strong to enable analysis by transmission spectroscopy. To avoid this strong attenuation, glass powder is often mixed with a salt without bands in the region of interest, like KBr or CsBr (Kamitsos 2015).

An alternative to the transmission mode is FT-IR reflectance spectroscopy. The reflected light is influenced by the evanescent field $E_{ev} = E_0 \exp -\gamma z$ (see Fig. 8), that reaches into the sample surface, with E_0 as the incident electric field of a photon, γ as a constant and z as the depth into the sample (Griffiths and Haseth 2007).

The decay of the evanescent field, and therefore the penetration depth of the light beam, is dependent on the wavelength λ of the light, the refractive indices of the surrounding medium n_1 and of the sample n_2, and on the angle of the incidence θ (Griffiths and Haseth 2007):

$$d_p = \frac{\lambda}{2\pi n_1 \sqrt{\sin^2 \theta - (n_2 - N_1)^2}} \, . \tag{2.10}$$

The specular reflectance of the investigated sample, which is influenced by both, real (n) and imaginary (k) part of the complex refractive index, differs from the absorption

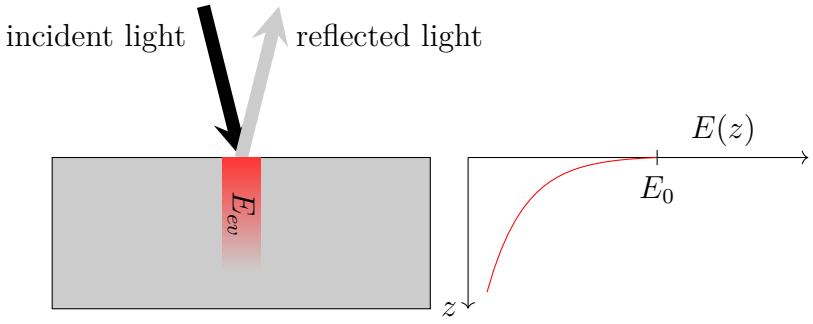

Figure 8: The specularly reflected light interacts with the sample surface. In this process, the evanescent field is attenuated by absorption processes, e. g., due to the excitation of vibrations.

gathered by transmission spectroscopy, which is only dependent on k. Both parts can be separated by the *Kramers-Kronig* relationship (Griffiths and Haseth 2007; Kasap and Capper 2017):

$$n_2(\omega) = n_\infty + \frac{2}{\pi} P \int_0^\infty \frac{\omega' k_2(\omega')}{\omega'^2 - \omega^2} \mathrm{d}\omega' \,, \tag{2.11}$$

$$k_2(\omega) = \frac{2\omega}{\pi} P \int_0^\infty \frac{n_2(\omega')^2}{\omega'^2 - \omega} \mathrm{d}\omega' \,, \tag{2.12}$$

with P as the Cauchy principal value of the integral, ω as the wavenumber and ω' as a wavenumber integration variable. With the relationship $k(\omega) = \frac{\alpha(\omega)}{4\pi\omega}$, the absorption coefficient α can be determined (Griffiths and Haseth 2007). However, samples investigated in such manner may exhibit both, longitudinal and transverse optical vibrational modes and give therefore different results depending on the reflection angle θ (Kamitsos 2015).

Raman scattering process

As opposed to infrared absorption, Raman spectroscopy induces an inelastic scattering process by irradiation with a high intensity laser beam in the UV/Vis/NIR region. The important factor for Raman scattering is a change in polarizability during a vibration. Incoming light induces a dipole moment μ_{ind} that is proportional to the electric field $E = E_0 \cos(\omega_l t)$ of the light with a frequency ω_l (Diem 2015). The proportionality factor,

the polarizability α, can be described with a Taylor series, leading to

$$\alpha = \alpha_0 + \left(\frac{\partial \alpha}{\partial Q_k}\right) Q_k \cos(\omega_k t) + \dots , \tag{2.13}$$

with ω_k as vibrational frequency of a normal mode Q_k. Combining both elements results in the general scattering equation

$$\cos(\omega_l t)\cos(\omega_k t) = \frac{1}{2}\left[\cos(\omega_l + \omega_k)t + \cos(\omega_l - \omega_k t)\right] . \tag{2.14}$$

The first term of this equation describes the elastic Rayleigh scattering, where the wavelength of the incident light equals the wavelength of the observed light. On the other side of the equation the frequency of a vibration energy is either added to (Stokes shift) or subtracted from the observed light (Anti-Stokes shift). In most experimental setups, as the ones used for this study, only the Stokes shift is evaluated. I show an example of energy transitions during a scattering process in Figure 9.

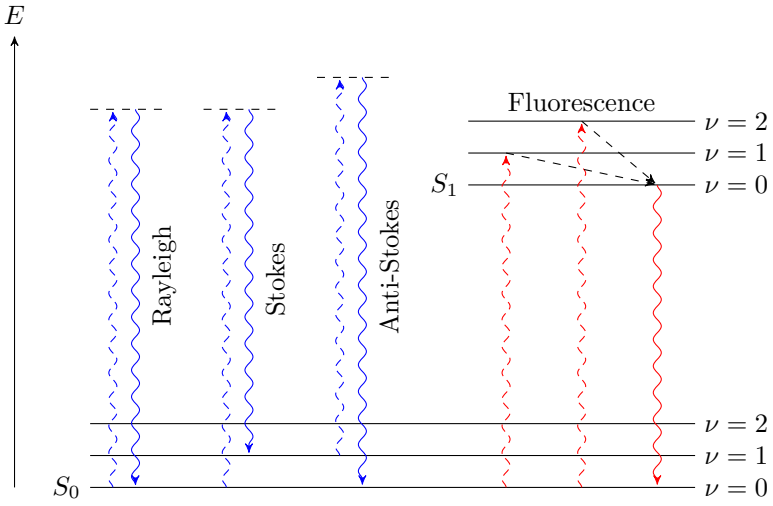

Figure 9: Jablonsky diagram of energy transitions after irradiation (dashed blue). During the interaction of the electrical fields of electrons and photon, a temporary, unstable energy level is created with a subsequent radiative transition (blue). If absorbing energy levels are present, however, fluorescent transitions (red) are possible, usually with much higher intensities than the Raman signal.

The intensity of Raman scattering is given as

$$I_R = \omega^4 I_0 N \left(\frac{\partial \alpha}{\partial Q}\right)^2 , \tag{2.15}$$

with ω as the irradiation wavelength, I_0 as the intensity of the incident light and N as the number of scattering objects (Larkin 2011). The equation shows that the intensity of the Raman signal can be increased by the power of four by increasing the energy of the incident light - however, if fluorescent transitions are possible in a sample, these transitions (see Figure 9) are often up to 10^4 times more intensive. Cu^+, Mn^{2+} and Sb^{3+} ions, among others, are known for their fluorescent behavior and may hinder successful Raman investigations of archaeological samples (Elisa et al. 2009). Theoretically, the fluorescence can be avoided by changing the laser wavelength either to longer wavelengths, which would lack the energy to reach a metastable fluorescent level. In contrast, using an even shorter wavelength source is an option; despite still causing strong fluorescence, the fluorescence might be shifted out of the region of interest. Both approaches are dependent on the availability of the respective lasers (Smith and Clark 2004). A third option is time dependent Raman spectroscopy, using a pulsed laser: Since scattering processes are much faster (ca. 10^{-15} s) than fluorescence processes (ca. 10^{-9} s), the fluorescence signal can be cut off by the instrumentation (Duyne et al. 1974). However, the necessary instruments for this setup are usually too expensive for routine investigations.

General statement about vibrational spectroscopy: Only either Raman or infrared transitions can be observed in point symmetric molecules (Herzberg 1945). In molecules without point symmetry this limitation is not valid; however, due to the required change in dipole moment infrared spectroscopy is generally more sensitive to asymmetric transitions, while symmetric vibrations show higher intensities in Raman spectra (Colomban 2008).

Glasses usually have broad vibrational transitions with comparably low intensity maxima, caused by the broad variety of bond lengths and bond angles. In contrast, crystalline particles show sharp transitions with high intensity maxima. Raman spectroscopy is therefore especially well-suited for fingerprint analysis of crystalline particles in a glass matrix, provided that the samples are not fluorescent (e. g., Welter et al. 2006; Ricciardi et al. 2009; Vandenabeele, Edwards, et al. 2014). Also, the spatial resolution of the

probe site depends on the wavelength of the excitation beam. A Raman spectrometer with a high energy UV-Vis excitation laser can reach resolutions of ca. 0.5 µm, while infrared spectroscopy, even when using a microscope, will probe an area of several µm. Thus, Raman spectroscopy allows the investigation of more detailed structures like larger crystallites in the glass.

2.5 Investigation of archaeomaterials by replication

The comparison of replicated materials with archaeological samples cannot confirm a method of sample preparation. However, it does improve the understanding of manufacturing procedures. A detailed comprehension compasses appropriate materials that are needed for the process and helps to identify other relics in features related to glass manufacture. In contrast, if an attempted replication shows significant differences to an archaeological sample, the method can be excluded from possible routes of manufacture. Most important for an elucidation is, of course, the detailed recording of procedures and the choice of the right measurement tools. I chose the term archaeomaterial here to describe the approach rather than to focus on the archaeological object; instead, the material itself, with inclusions, particles, bubbles, corrosion marks etc. are the focus of this investigation.

Two articles included in this study focus especially on reproduction of archaeomaterial: Firstly, the investigation of calcium antimonates in Roman mosaic *tesserae* (Drünert, Palamara, et al. 2018), and secondly, the formation of borosilicate glass layers on glass samples in respective of vibrational phenomena at the surface of Mycenaean relief fragments (Drünert, Lind, Kästner, et al. in press; Drünert, Lind, Vontobel, et al. submitted). The first study examines induced nucleation after thermal treatment (see section 2.5.1), whereas glass surface alteration methodology was the focus of the second study (section 2.5.2). To a lesser extent, the replication of opaque red glasses is the subject of a third study (Drünert, Blanz, et al. 2018)

2.5.1 Sample opacification by crystallization

Crystallization of glass leads to the formation of glass ceramics. Two basic mechanisms of crystallization can be distinguished: surface crystallization and bulk crystallization

(Höland and Beall 2013). In both cases, crystallites are usually formed due to a heat treatment above the glass transition temperature T_G.

Surface crystallization

The crystallization of a glass starting at its surface is considered as surface crystallization. As described by Tammann in his monography "Der Glaszustand" from 1933, crystallization of glass is preferred at either internal or external surfaces (in Vogel 2011). Different mechanisms for surface catalyzed processes have been put forward.

Multiple parameters are relevant in surface crystallization processes. Müller et al. (2000) summarizes in a review the effects of the surface quality, cracks, foreign particles and of the atmosphere. One approach to explain the crystallization kintetics, according to Gutzow and Schmelzer (2013), is based on strains that are induced into the glass. Such strains, e. g., introduced by foreign particles with a different molar volume than the surrounding matrix, reduce the energy to form crystallites in near surface areas. This effect can be increased by rough and irregular surfaces, as well as high surface area samples, like powders.

Volume crystallization

Volume crystallization, which is any case where the crystallization starts from the bulk of the glass, can occur either directly from the bulk or from any interface found in the glass. The first, also known as *homogeneous crystallization*, is currently rather poorly understood, and large discrepancies between the actual theory and the experimental data exist (Cabral et al. 2004; Schmelzer et al. 2016). In contrast, more research has been conducted on *heterogeneous crystallization*. The theory of crystallization is based on Tammanns concept of nucleation and crystal growth as two separate steps (in Vogel 2011).

The nucleation describes a stage of supersaturation when a glass melt is cooled from the melting temperature T_m below the Ostwald-Miers region (Vogel 2011). Nuclei are understood as small seeding crystallites with a radius r. The formation of such nuclei is dependent on two factors, that is, the energy necessary to form the crystallite and the activation energy that is necessary for the movement of ions (Kleber 1962). The free

energy ΔG of such a nucleus is again dependent on two factors: The energy necessary to form the new surface (ΔG_s) is dependent on r^2,

$$\Delta G_s = 4\pi r^2 \sigma(\Delta g_o)\,, \tag{2.16}$$

with σ as the surface tension and Δg_o as the free enthalpy of the interface. On the other hand, the change in energy from crystallization (ΔG_v) is dependent on the volume of the particle, that is on r^3,

$$\Delta G_v = -\frac{4}{3}\pi r^3 \Delta g_v\,, \tag{2.17}$$

with Δg_v as the free enthalpy of the crystallite. The free energy of the nucleus (ΔG_c) is therefore determined as $\Delta G_c = \Delta G_s + \Delta G_v$. ΔG_c can thus be divided into a region below a critical radius r_c, where the contribution from the surface tension exceeds the energy from crystal formation, and a region above a critical radius r_c, where further crystal growth will lead to a stabilization of the crystalline phase (Figure 10; see also Fokin et al. 2006; Vogel 2011).

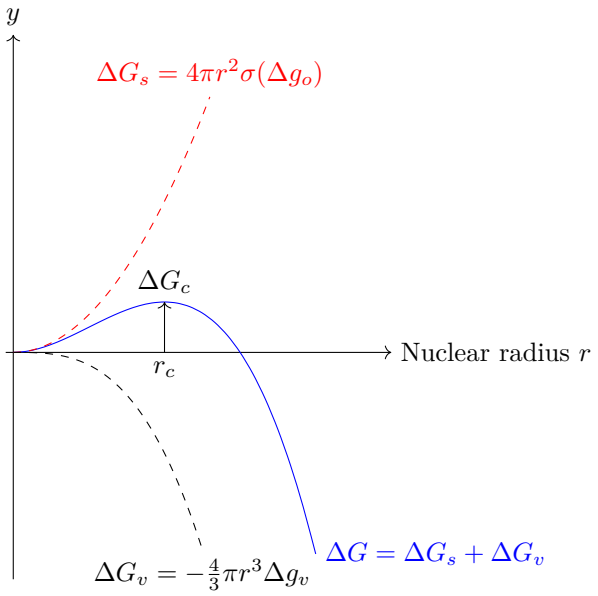

Figure 10: Free enthalpy G_c of a nucleus as a function of the particle radius, as shown in Vogel (2011).

Crystal growth rates attempt to quantify the formation of crystallite layers on top of the nuclei described above. In the case of homogeneous crystallization, the nuclei and the growing crystals are identical, whereas heterogeneous crystallization exploits the possibiity of seeding an insoluble crystal, thereafter another crystal phase grows on top of such crystallites. Generally, crystal growth can be separated in three mechanisms: *normal* growth, *screw dislocation* growth and *two-dimensional surface nucleated* growth (Nascimento and Zanotto 2006). In all cases, the crystal growth is dependent on the effective diffusion coefficients D_u: The model for *normal* and *screw dislocated* growth considers the growth rate u to be

$$u = f\frac{D_u}{\lambda}\left[1 - \exp\left(-\frac{\Delta G}{RT}\right)\right], \tag{2.18}$$

with λ as the diameter of the diffusing ions, R as the ideal gas constant and T as the temperature. The factor f is assumed to be close to one for *normal* growth, while for *screw dislocated* growth f is dependent on the melting temperature T_m and the change of temperature ΔT,

$$f \cong \frac{\Delta T}{2\pi T_m}. \tag{2.19}$$

In contrast u in the *two-dimensional surface nucleated* growth model is considered to be

$$u = C\frac{D_u}{\lambda^2}\exp\left(-\frac{B}{T\Delta G}\right), \tag{2.20}$$

with B dependent on the surface tension σ, and C is a function of λ and ΔG (Nascimento and Zanotto 2006).

Crystallites in archaeological glass samples

Opaque archaeological glass samples usually contain crystalline particles. Common crystalline particles are shown in Table 2; however, a couple of strategies to introduce the crystallites into the glass have been discovered. Heterogeneous nucleation appears to have been used in Roman mosaic *tesserae* containing calcium antimonate (Drünert, Palamara, et al. 2018). In contrast, *ex-situ* formation of crystal phases with subsequent addition to a glass melt have been reported before (Lahlil, Cotte, et al. 2011). As a different example, opaque red glasses based on copper nanoparticles (Drünert, Blanz, et al. 2018) appear

to crystallize homogeneously from the glass melt. Furthermore, the striking method to form copper ruby glasses as an example of sometimes homogeneous, and sometimes heterogeneous crystallization has been the topic of many publications (e. g., Stookey 1949; Câpâţînâ 2005; Weyl 2016).

2.5.2 Surface alteration

Glass corrosion

The most common surface alteration of archaeological glass samples is corrosion. The exposure to humidity causes a change of the glass structure at the surface: Firstly, alkaline and alkaline earth ions are leached out of the glass matrix, being either washed away or reacting with CO_2 in the air and remaining as carbonates, e. g., as $CaCO_3$, on the corroded surface (Vilarigues and Silva 2006). The remaining glass matrix usually consists of an alternating layered structure of Si−O−H containing gel regions and repolymerized, silica rich glass structure (Bunker 1994):

$$2\,\mathrm{Si{-}O{-}H} \rightleftharpoons \mathrm{Si{-}O{-}Si} + \mathrm{H_2O}\,. \tag{2.21}$$

Such characteristic layers are, e. g., shown in Drünert, Blanz, et al. (2018). Corrosion structures can exceed 100 µm in depth and lead to odd results when they are not considered before any analysis.

Mutual sample alteration

Although most of the glass samples found by archaeologists appear, apart from decorative elements, unmodified, in a few cases modification of glass samples has been observed. Especially Mycenaean beads and vessel fragments have frequently been found to be gilded (Panagiotaki 2008; Schallin 2016). In a study that is part of this cumulative thesis, Drünert, Lind, Vontobel, et al. (submitted) could show how an alteration of the surface affects the topmost layer of a glass sample. In this case, boron contamination of gold led to the formation of a borosilicate glass layer, that was observable by infrared spectroscopy. However, the reasons to hide the precious glass behind even more precious gold remain unknown.

3 Publications

The following pages contain the publications presented in this cumulative thesis. Together with my coauthors, I published the following articles in peer-reviewed journals:

- Borosilicate glass layers on Mycenaean glass: surface alterations by glass – borax – gold interactions (submitted to *Journal of Non-Crystalline Solids* on January 28, 2019);
- Ancient Roman nano-technology: Insight into the manufacture of mosaic *tesserae* opacified by calcium antimonate (*Journal of the European Ceramic Society* 38 (2018), pp. 4799–4805; `https://doi.org/10.1016/j.jeurceramsoc.2018.06.031`)
- Copper-based opaque red glasses – Understanding the colouring mechanism of copper nanoparticles in archaeological glass samples (*Optical Materials* 76 (2018), pp. 375–381; `https://doi.org/10.1016/j.optmat.2017.12.054`)

In addition, we contributed to the conference proceedings of the 6th International Symposium on Research to Medieval and Early Modern Glass Works in Europe (May 6 – 8 2016, Buhlbach, Germany) and published a series of contributions in German language (in press):

- Einblick in die Chemie und Physik der Farbigkeit und Opazität von Gläsern
- Untersuchung farbgebender Zusätze im Münsteraner Glasbefund mit Hilfe Optischer Spektroskopie
- Oberflächenanalyse Mykenischer Glasfragmente der späten Bronzezeit: Hinweise auf Vergoldung unter Zuhilfenahme von Borax

Borosilicate glass layers on Mycenaean glass: surface alterations by glass – borax – gold interactions

F. Drünert[a], F. Lind[a], P. Vontobel[b], E. I. Kamitsos[c], L. Wondraczek[a], D. Möncke[c,d,*]

[a] *Otto Schott Institute of Materials Research, University of Jena, Fraunhoferstraße 6, D-07743 Jena, Germany*
[b] *Paul Scherrer Institut, 5232 Villigen PSI, Switzerland*
[c] *Theoretical and Physical Chemistry Institute, National Hellenic Research Foundation, 48 Vassileos Constantinou Avenue, 11635 Athens, Greece*
[d] *Alfred University, 1 Saxon Drive, Alfred, NY 14802, USA*

Abstract

A previous report (Möncke et al., PCG 2013) reports discussed the possible formation of a borosilicate layer on the surface of late Bronze Age glass samples (Mycenaean period) which and had been excavated in Paleia Epidavros, Greece. Here, we investigate potential mechanisms for borate incorporation into the surface of archaeological alkali-lime silicate glasses. Since the former reports on Mycenaean glass relief fragments concerned material that was found together with gold foils featuring identical reliefs, we test here the hypothesis that borates could have been introduced through gold working via the reaction of borax-treated gold foil with the silicate glass surface at elevated temperature. Different ways of fusing a gold sheet to replica glass samples were considered. These experiments indicate that at temperatures above 800 °C, borax could have been used either as a solder for the process of fusing gold sheets to the glass surface, or that borate was transferred from the gold sheet previously in contact with a borax melt, presumably for cleaning or ore extraction. The dimensions of the borosilicate layer in depth and the extent to which it spread across the glass surface were probed by vibrational spectroscopy (IR/Raman) and neutron radiography.

Keywords:
Mycenaean glass, gold processing, borosilicate layer, FT-IR spectroscopy, Raman spectroscopy, neutron radiography, borax

Introduction

The Mycenaean palace epoch (14th to 12th ct. BCE) is not only known for its impressive architecture, bronze weaponry or ceramics, but also for a rich variety of turquoise and blue glass products [1]. Most of the glass objects found in burial sites and residential areas from the Mycenaean era come in the form of beads. Seals and relief inlays are also known [2, 3]. In some cases, relief inlays and relief beads have

*Corresponding author
Email address: moncke@alfred.edu (D. Möncke)

been excavated together with gold sheet of similar shape to the vitreous relief inlays and beads, either alongside or even attached to the glassy material [2, 3, 4, 5, 6].

Previous studies using infrared reflectance spectroscopy on such Mycenaean relief fragments (with provenience Paleia Epidavros, Greece, 13th to 11th century BCE) revealed the characteristics of a typical soda lime silicate glass with mostly Q^3 units[1]. However, the pristine outer surface of the glass was found to exhibit a fully repolymerised, corroded surface; similar formation of a modifier-free SiO_2 layer is an often-observed corrosion product on silicate glass surfaces. In addition, an unexpected absorption band was found at $\sim 930\,\mathrm{cm}^{-1}$, superimposed on the reflectance profile typical of vitreous SiO_2 [7]. Due to the absence of O−H vibrations at $\sim 3600\,\mathrm{cm}^{-1}$, at that time, the authors suggested that this band might originate from the presence of a thin borosilicate glass layer.

Because of its low atomic weight, boron is a challenging element for quantification by common analytical techniques, such as X-ray fluorescence or SEM-EDX, especially when only present in very low levels. Furthermore, the most common analytical techniques are not sensitive to the top layers of a sample. Other techniques are often destructive, like mass spectrometry, or require uncontaminated or coated surfaces (e. g. XPS). Thus, it is not surprising that many earlier studies missed that aspect - especially when boron was present only in a thin layer. In this first observation, the source for boron, or the process by which boron could have been introduced into the glass surface, was addressed only briefly in the earlier publication [7]. In continuation of the earlier study, we now searched for possible sources for boron and/or applications that might have caused the transfer of boron into the archaeological glasses. It is known, for example, that the mineral borax, $Na_2B_4O_7 \cdot 10\,H_2O$, can be used either as a solder [8] or as a simple way to extract gold from ores [9]. The property of borax to bind undesired oxides at the metal surface and, therefore, its application to purify gold is mentioned in modern handbooks of gold smithing [8], although we are not aware if this knowledge would have existed for the Late Bronze Age. It is also known that borates will adhere to the oxidised surface of gold samples [10],and it was speculated already by Schliemann in 1878 [11, p. 266] that this feature was known in Mycenaean times. When gold, extracted from ore by using borax, was later brought into contact with hot glass, a transfer of borate could have occurred. In both cases, we assume that hot glass might have been cast into a mould, in which a gold sheet was already laid out. In all experiments, we focus on the reactivity of boron oxide with a silicate glass surface at elevated temperatures. Thereby, we assume that a better understanding of the reaction mechanism of boron with a silicate glass network will help us to explain the origin of the unexpected infrared signature of Mycenaean glass surfaces. In the absence of suitable experimental (non-destructive) tools for direct chemical analysis, we continue here on this route of speculation where the observed IR spectroscopic features are caused by the presence of a significant amount of boron in

[1] Q^n denotes here a silicate tetrahedral unit with n bridging oxygen atoms [7]

the surface of the glass. We use mostly vibrational spectroscopy to follow structural variations on the surface of the glass samples subjected to different treatments. Depth profiling by infrared reflectance spectroscopy was also conducted on broken edges and obliquely polished samples to probe the extent of the borate-silicate interaction layer. In an attempt to visualise the dimensions of the borosilicate layer and to explore the general applicability of neutron radiography to archaeological glass samples that need to be studied non-destructively, respective experiments were conducted. We note, that while this study can give experimental proof for potential borate transfer reactions to the glass, final proof on the actual mechanisms that caused the layer formation in Mycenaean samples cannot be given.

Materials and Methods

Model glass

Previously published quantitative analysis of Mycenaean glass samples revealed an average composition of approximately $65\,SiO_2 \cdot 7\,CaO \cdot 17\,Na_2O \cdot 2\,Al_2O_3 \cdot 3\,MgO$ (in wt.%); the remaining 5 % including among others K_2O, Fe_2O_3, MnO, Sb_2O_3, Cl and S [12]. Based on this composition, a model soda lime glass (SLS) with similar expected properties and the molar composition $65\,SiO_2 \cdot 15\,CaO \cdot 17\,Na_2O \cdot 3\,Al_2O_3$ (in wt.%: $64\,SiO_2 \cdot 14\,CaO \cdot 17\,Na_2O \cdot 5\,Al_2O_3$) was prepared[2]. Quartz powder, calcium carbonate, sodium carbonate and aluminium hydroxide (all 99.5%) were used as raw materials. The batch was melted at 1400 °C in an electrically heated muffle furnace using a Pt crucible, cast on a brass block, annealed at 550 °C and cooled to room temperature at $2\,K\,min^{-1}$. In order to compare the borate layer with the silicate glass, a sodium diborate glass (SDB, $Na_2B_4O_7$) was prepared from borax, $Na_2B_4O_7 \cdot 10\,H_2O$. The substance was heated to 1200 °C, the melt was cast on a brass block, annealed at ca. 800 °C and cooled to room temperature at $2\,K\,min^{-1}$.

Glass-to-gold fusion experiments between 600 °C *to* 1000 °C *(process A)*

The model soda lime glass (SLS) was cut into slices of 1 mm thickness and polished to replicate an as-cast surface. Samples were covered with fine borax powder and fused to a thin gold plate through exposure for 30 min to different temperatures, selected between 600 °C to 1100 °C. For comparison, blind samples without borax layer and/or gold covering were similarly prepared.

Fusion experiments by direct casting (process B)

A model soda lime glass (SLS) batch was melted at 1400 °C as described above. For direct fusion, a gold plate was coated with borax powder and heated to 800 °C. The glass melt was directly cast on

[2]To simplify the model glass, monovalent components were added to the CaO content and trivalent components to the Al_2O_3 content.

the borax-covered gold plate. A blind sample was prepared by casting the glass melt on a non-borax treated gold sheet. The same procedure was also conducted without preheating the borax-coated gold plate. The general process is schematically visualised in Fig. 1.

Boron transfer from impure gold sheets (process C)

Gold sheets were coated with borax and annealed at 800 °C to simulate a cleaning process during gold purification [8]. The remaining (visual) layer was subsequently removed either by dissolution in hot water or by removing the residual drops of borax mechanically. The so-prepared gold sheets as well as a non-treated blind sample were fused to a model glass at 800 °C.

Vibrational spectroscopy

After treatment, all glass samples were analysed by infrared reflectance micro-spectroscopy (Perkin Elmer Spotlight 200i) at 50x magnitude with a reflectance angle of 0° within a range of 4000 cm^{-1} to 500 cm^{-1}, using a gold mirror as reference. The average of 200 spectral accumulations, at 2 cm^{-1} resolution, from an area covering 200 µm × 200 µm were used for IR analysis. A selection of samples was polished obliquely and analysed in order to get an idea of the depth profile for the boron distribution from the glass surface into the sample. Here, an area of 5 µm × 400 µm was analysed. The such obtained reflectance data was used without any further treatment. Kramers-Kronig transformation was not applied to the reflectance spectra due to the limited accessible wavenumber range, which lacked the far infrared region and, as a consequence, did not allow extrapolation to zero frequency. Reflectance spectra show shifts of band maxima compared to absorption spectra, and emphasise the intensity of low energy bands compared to the intensity of high energy bands. Nevertheless, the direct comparison of reflectance spectra that have been measured under the same conditions gives important information on structural variations. Also, the spectral similarity is close enough to absorption spectra to allow assigning the measured bands to vibrations of various structural entitles.

Some samples were additionally investigated by Raman micro-spectroscopy (Renishaw InVia Raman microspectrometer) at 50x magnification, using a laser wavelength of 514 nm for excitation. Spectra were taken within the range of 100 cm^{-1} to 1650 cm^{-1} and 2 cm^{-1} resolution.

Neutron radiography

One sample of process B (Fig. 1) was selected for neutron radiography in order to visualise boron contaminated glassy material. The measurement was conducted at the Paul Scherrer Institute of Villigen, Switzerland, using the thermal neutron imaging instrument NEUTRA. A scintillator size of 50 µm combined with an *Andor Neo* camera (resolution: 1950 x 1950 pixel) and a 50 s exposure time was used for neutron detection. The sample was rotated at 360° with a step size of ca. 0.5°. For further information, see ref. [13].

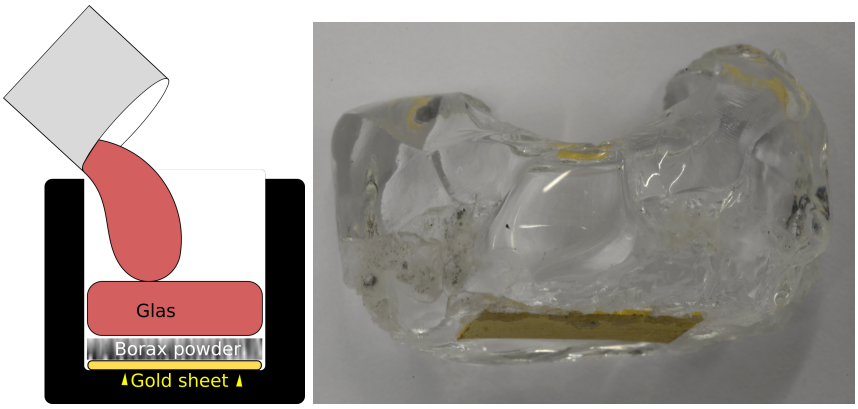

Figure 1: Scheme of the casting process B (left), and the corresponding sample that was investigated by neutron radiography (right).

Results and Discussion

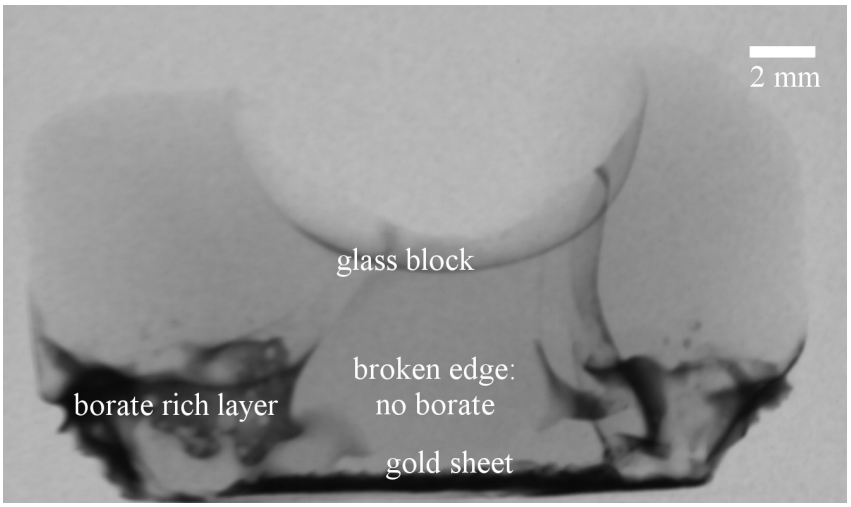

Figure 2: Normalized neutron radiography of a glass cast on a borax-coated gold sheet (process B). The dark area shows high neutron-atom interactions, which is assumed to be due to neutron capture by boron atoms. See supplementary information for a 180° rotation video.

Fusion experiments with borax as flux

We found that heat treatment of polished glass plates with gold (process A) leads to adhesion between glass and gold surfaces, which increases with increasing treatment temperature. Below 700 °C, gold is only weakly attached to the glass surface. We observed no difference between the adhesion of blank samples and those covered with borax. However, surface crystallisation appears in heat-treated samples without a borate layer, whereas crystallisation was inhibited for borax-coated samples. With increasing temperature, the glass becomes softer. Therefore, only samples treated at temperatures below 800 °C

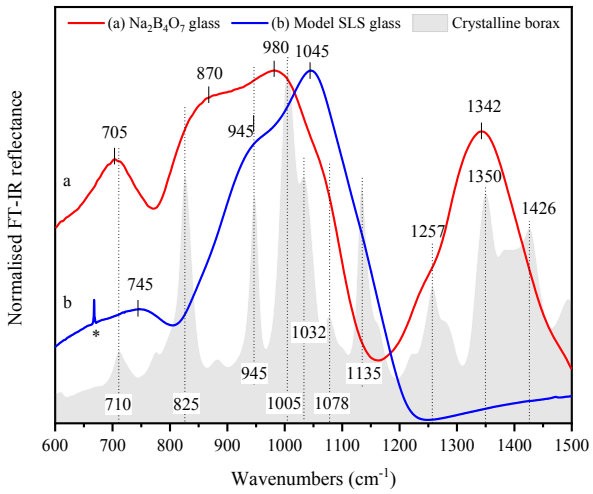

(3.1) FT-IR reflectance spectra of the two model glasses (SDB, a, and SLS, b), together with the fingerprint spectrum of crystalline borax powder. * marks artefacts from CO_2 in the air.

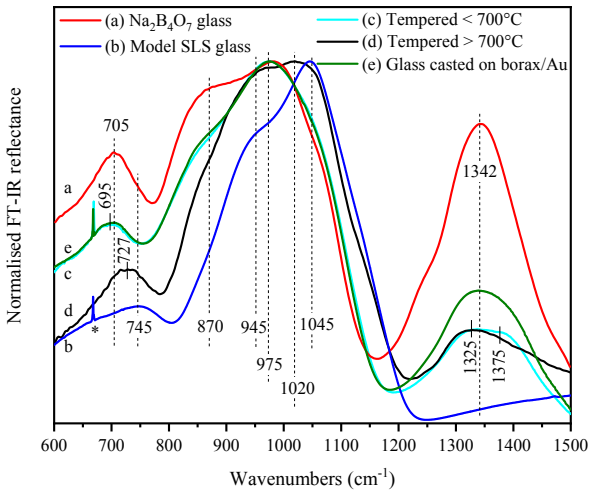

(3.2) Surface FT-IR reflectance spectra of model glass samples after treatment with borax. * marks artefacts from CO_2 in the air.

remained in their original shape. Samples treated at higher temperatures would afford a mould during the heat-treatment to prohibit unwanted deformation.

Casting a model glass on a gold sheet (process B) leads to strong adhesion between glass and gold. As in process A, coating the gold with borax powder did not create a significant difference in adhesion. However, borax appeared to spread further on the surface than expected; Fig. 2 shows the radiography of a model glass cast on a coated gold sheet. As seen from the image, the boron-containing layer spreads rather far on the side of the sample, forming a thin film at the sides.

The modification of gold sheets before fusion (process C) did not affect the adhesion behaviour significantly, similarly to process A. When treating the gold with borax at temperatures $T > 800\,°C$, green coloured drops of borate glass formed at the surface of the gold sheet. The glass could be removed either mechanically by bending the gold sheet or within two hours by dissolution in hot water.

Vibrational studies

Processes A and B

Fig. 3.1 displays the FT-IR reflectance spectra of the two model glasses (SDB, a, and SLS, b) that have been used in this study. Additionally, the spectrum of borax powder was added to the figure for comparison (light grey filled spectrum). The $Na_2B_4O_7$ glass (Fig. 3.1 a) exhibits a B–O–B bending vibration at $705\,cm^{-1}$ (very close to the $710\,cm^{-1}$ band of crystalline borax), and a broad reflectance band from ca. $775\,cm^{-1}$ to $1150\,cm^{-1}$, which forms the envelope of several sharp bands that are also evident in the spectrum of borax. The $775\,cm^{-1}$ to $1150\,cm^{-1}$ envelope of SDB, with apparent reflectance maxima at $870\,cm^{-1}$ and $980\,cm^{-1}$ is due to the asymmetric B–O stretching vibration in tetrahedral borate units

$[B\text{Ø}_4]^-$, where Ø indicates a bridging oxygen atom [14, 15]. In addition, different overlapping bands in the range of 1150 cm^{-1} to 1500 cm^{-1} for both the SDB glass and borax indicate the presence of stretching vibrations of B−O bonds in trigonal borate groups [16, 15]. The SLS model glass spectrum (Fig. 3.1 b) is typical for a soda lime silicate glass. The Si−O−Si bending mode is visible at ca. 745 cm^{-1}, the Si−O stretching profile from ca. 800 cm^{-1} to 1250 cm^{-1} shows its maximum reflectance at 1045 cm^{-1} and designates a dominating presence of Q^3 units, while smaller contributions from Q^2 and Q^4 units add intensity to the lower- and higher-frequency sides of the Q^3 envelope, respectively [7, 17][3].

In comparison to the above two endpoint glasses, SLS and SDB, the spectra of borax coated and heat-treated SLS model glasses (process A) appear to consist of features present in the spectra of both glasses. After treatment at temperatures below 700 °C the coated model glass (Fig. 3.2 c) shows reduced intensity of the high-frequency envelope with apparent maxima at ca. 1325 cm^{-1} and 1375 cm^{-1}, indicating the formation of an amorphous borate phase with trigonal borate groups, in contrast to the starting crystalline phase (grey spectrum in Fig. 3.1). A similar spectrum was obtained for glass casted on borax-coated gold sheet (Fig. 3.2 e), which shows increased content of borate triangles (band at 1342 cm^{-1}) relative to the spectrum in Fig. 3.2 c. Treatment at temperatures above 700 °C (Fig. 3.2 d) reduces further the relative intensity of the infrared profile corresponding to trigonal borate units (1200 cm^{-1} to 1500 cm^{-1}), suggesting a structural reconstruction process. This is supported by additional changes in the 800 cm^{-1} to 1200 cm^{-1} envelope including the reduction in intensity of the borate shoulder at ca. 870 cm^{-1} relative to that of the < 700 °C treatment, and the appearance of a new band maximum at 1020 cm^{-1} which is in between those of the B−O stretching in SDB (980 cm^{-1}). In addition, the band for bending vibrations is measured at 727 cm^{-1} between those of SDB (705 cm^{-1}) and SLS (745 cm^{-1}).

To explore possible interactions between the borate and silicate components, Fig. 4.1 compares weighted averages xSDB+$(1-x)$SLS of the spectra of sodium-diborate glass (SDB, $x = 1$) and the model soda lime glass (SLS, $x = 0$) with the measured spectrum of the borax-coated model glass heat-treated at 800 °C (black, solid). In comparison to the progressive evolution of the weighted average spectra from $x = 1$ to $x = 0$, the experimental coated model glass spectrum shows a shift of its low-frequency band to ca. 695 cm^{-1}, indicating the formation of Si−O−B bonds [7, 15]. Additionally, the high-frequency band of the trigonal borate groups shows two shoulders, one on the lower- (1325 cm^{-1}) and the other at the higher-frequency (1375 cm^{-1}) side of the initial 1342 cm^{-1} band of the SDB glass. This effect suggests a reduction in symmetry of the trigonal borate units [19], which may be the result of trigonal B bonding to Si centres through Si−O−B bridges. Finally, the main reflection maximum of the experimental spectrum in Fig. 4.1 appears at 975 cm^{-1}, whereas no weighted average spectrum x

[3]Strictly speaking, each asymmetric Q^n vibration consists of three vibrational modes with slightly different energies. Here, we will only consider the average band position of the three modes without the application of a band deconvolution. Further information can be found in the literature [e. g. 18]

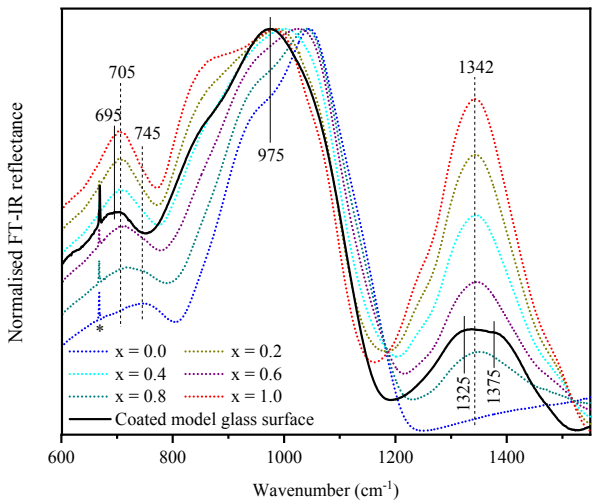

(4.1) Weighted average spectra xSDB+$(1-x)$SLS of sodium diborate glass (SDB) and model soda lime silicate glass (SLS) in comparison to the measured spectrum of the borax-coated model glass heat-treated at 800 °C. * marks artefacts from CO_2 in the air.

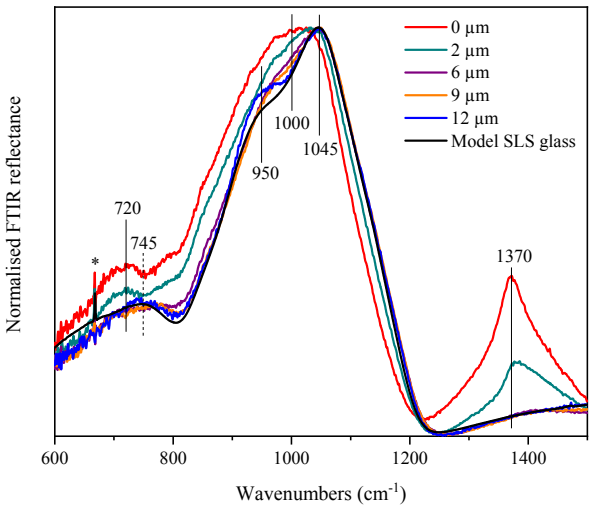

(4.2) Normalised FT-IR line scan spectra of a polished model glass treated with borax at 800 °C. * marks artefacts from CO_2 in the air.

SDB $+(1-x)$ SLS shows maximum at 975 cm^{-1}. These findings show clearly that heat-treatment of the model soda lime silicate glass coated with borax leads to interactions between the silicate and borate structural units.

We have performed a depth profiling of the infrared reflectance spectra to probe the extent of the interactions between the borate/borosilicate layer and the interior of the silicate glass. Samples treated at 800 °C according to process A were polished obliquely and subsequently investigated by infrared reflectance spectroscopy. The evolution of the infrared spectra is presented in Fig. 4.2 in comparison to the spectrum of pristine SLS model glass. According to the previous discussion, the first spectrum in Fig. 4.2 (0 µm spectrum) suggests interactions between the borate and silicate components as manifested by spectral changes at both low- and high-frequency regions compared to the SLS spectrum. The influence of the borate layer is visible very clearly up to ca. 2 µm into the glass bulk. This is especially shown by the gradual disappearance of the high-frequency band of trigonal borate units at about 1370 cm^{-1}, and the shift of the main band from ca. 1000 cm^{-1} (overlapping of the $[B\emptyset_4]^-$ and Q^3 bands) to 1045 cm^{-1} (main Q^3 band in SLS). The influence of borate on the silicate network decreases when measuring deeper into the bulk; in terms of the 1370 cm^{-1} band, Fig. 4.1 indicates that no borate triangles are formed at 6 µm or deeper. However, consideration of reflection at ca. 1000 cm^{-1} shows that there should be some borate-silicate interactions even at 9 µm. The spectrum measured at 12 µm shows that the activity at 1000 cm^{-1} is identical to that of the SLS glass. However, a new shoulder appears at ca. 950 cm^{-1} in the 12 µm spectrum, with relative intensity exceeding that of the similar shoulder for SLS glass. This enhanced 950 cm^{-1} shoulder could be related to the 930 cm^{-1} band which was found superimposed on

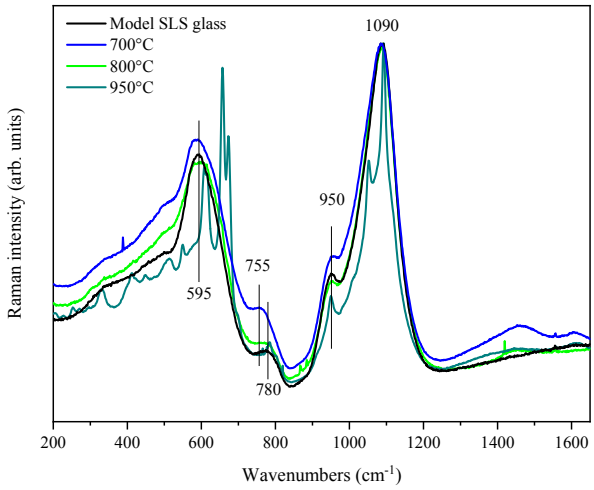

(5.1) Raman spectra of borax-coated model glass samples at different temperatures of heat-treatment (process A).

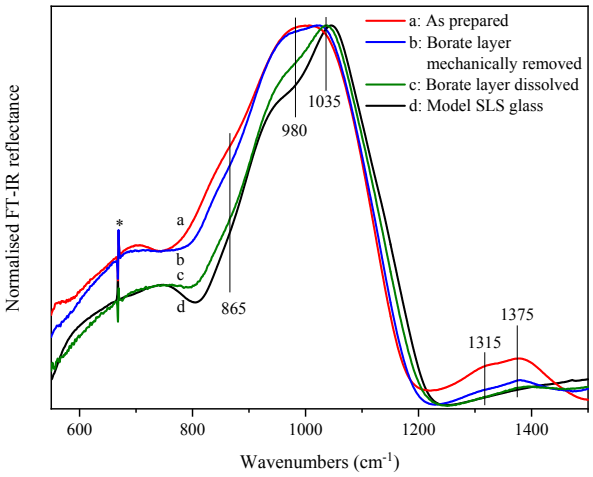

(5.2) Surface FT-IR reflectance spectra of model glass samples after fusing with differently treated gold sheets. * marks artefacts from CO_2 in the air.

the reflectance profile of vitreous SiO_2 measured on Mycenaean glass surfaces [7]. Therefore, this part of this work shows that (i) borate triangles are formed in an amorphous phase with a thickness smaller than 6 µm, (ii) borate tetrahedral units $[B\varnothing_4]^-$ penetrate deeper into the silicate glass, in layers at least 9 µm thick. These results are consistent with earlier findings in ref. [7], where the thickness of the borosilicate layer was estimated to be a few µm.

Raman spectra of heat-treated glass samples (process A) are shown in Fig. 5.1. The spectrum of the model glass SLS is dominated by bands at 1090 cm^{-1} (symmetric stretching of Q^3 units) and 595 cm^{-1} (symmetric stretching-bending of Si–O–Si bridges), while weaker bands are observed at 950 cm^{-1} (symmetric stretching of Q^2Q units) and 780 cm^{-1} (bending of Si–O–Si bridges) [18]. Heat treatments of the SLS glass – cast on borax-coated gold sheet – at temperatures above 700 °C lead to the formation of a broad envelope between 1300 cm^{-1} to 1520 cm^{-1}, which indicates the formation of trigonal borate units [15, 19, 20]. In addition, a shift of the bending mode to 755 cm^{-1} is observed and is consistent with the formation of Si–O–B bridges [7]. In contrast to strong signatures of borate species in the infrared reflectance spectra (Fig. 3.2), no additional Raman evidence is available for the borate species. This is due to the larger depth probed by Raman spectroscopy, leading to spectra dominated by the response of the silicate species. On the other hand, infrared reflectance spectroscopy is a surface-sensitive technique, and, thus, its response comes from the top few µm thick layer where the borate species are found in the studied glass samples. Above 900 °C, crystallisation of sodium silicates and sodium borates dominate the spectra, leading to the formation of multiple sharp peaks [21].

Process C

Fusing the SLS model glass to a gold sheet that had been treated with borax at 800 °C or more, leads to similar vibration bands as seen above. As an example, Figure 5.2 a shows the normalised FT-IR reflectance spectrum of a glass surface that has been fused to a borax-coated and heat-treated gold plate. The presence of the 1315 cm^{-1} and 1375 cm^{-1} bands show the development of a layer containing borate triangles, whereas intensities at ca. 980 cm^{-1} and 865 cm^{-1} which are in addition to those of the SLS glass indicate the presence of borate tetrahedral units as well. Removing mechanically the borate layer results in the decrease of bands due to borate triangles (1315 cm^{-1} and1375 cm^{-1}) and borate tetrahedral units (980 cm^{-1} and 865 cm^{-1}), as seen in Fig. 5.2 b. However, dissolution of the borate layer in water has caused the complete removal of borate triangles as opposed to borate tetrahedral which have retained part of their activity at 980 cm^{-1} and 865 cm^{-1} (Fig. 5.2 c). In addition, the main reflectance maximum shifts to 1350 cm^{-1} in comparison to SLS, manifesting the presence of tetrahedral $[B\emptyset_4]^-$ units and the Si–O–B bonding in the silicate layer (Fig. 5.2 c). The present results demonstrate clearly that the borate triangles are very sensitive to hydrolysis, in very good agreement with ref. [7] which showed that the corroded, over 3000 year period, Mycenaean glass fragments did not have any reflectance activity in the 1300 cm^{-1} to 1500 cm^{-1} range. To the contrary, activity was detected at 930 cm^{-1} and was attributed to $[B\emptyset_4]^-$ units coordinated to Co^{2+} ions [7].

Neutron radiography of cast glass (process B)

Fig. 2 shows the normalized neutron radiograph of a glass block after casting a model glass melt on a gold sheet covered with borax powder. The untreated SLS glass is almost transparent to the neutron beam. Boron with a high neutron absorption and hydrogen with its high scattering cross section are both expected to show in neutron radiography. For the laboratory samples, no significant amount of water is expected, and this assumption was confirmed by optical transmission and reflectance IR spectroscopy in the near IR region.

During the casting process, borax was only present as a thin powder layer on top of the gold sheet. Nevertheless, a thin dark layer (Fig. 2), that – in the absence of water – is indicative for a boron-containing material, is visible even at the sides of the glass sample (except for the missing sides, where edges broke off from the sample at the front and backside of the image's center). The thin layer can be more easily seen in video of the rotating sample (see supplementary information). Thus, we were able to demonstrate that a layer of boron-containing glass can easily be formed and that this layer can spread over a large surface area, without the necessity of a complete and homogeneous covering of the glass sample with borax powder. Borosilicate glass layers could therefore form even though only small parts of the sample were in contact with borate powder.

For the analysis of archaeological glass samples, neutron radiography appears to be a promising method to detect boron even in small quantities. Unfortunately, the sensitivity of neutron imaging

to boron atoms, which absorb neutrons, is similar to that of hydrogen atoms which scatter the neutron beam. Although we could exclude the presence of large hydrogen quantities in our laboratory test sample, this is not the case in the corrosion layers of ancient glass samples. However, we do expect a difference in neutron interaction within the surface of archaeological glass samples due to different process intensities. Moreover, the combination of infrared spectroscopy, confirming water bands in the high frequency IR region, and neutron radiography could support such investigations. In the context of this paper, we focused on the remaking of borosilicate layers. We could confirm that neutron radiography is a useful, non-destructive method for the analysis of small glass fragments, and we plan to follow up with neutron tomography of archaeological glass samples in the future.

Availability of borates in the Aegean region

Recalling the earlier findings regarding the formation of a borosilicate layer on LBA glass samples [7], and without clear evidence that the use of borax was most likely introduced by goldsmiths rather than glassmakers, we want to evaluate the availability of borates in the Aegean region. At the present time, the largest deposits for borates are located in Turkey [22]. Many of these deposits are rather close to the surface and are well conceivable for ancient mining activities. For gold the most important sources for the Late Bronze Age are known today: Next to mining activities on today's Turkish to Greek main land, e.g. in Anatolia, Chalkidiki or Macedonia [23], trade and warfare with the eastern realms supplied the Mycenaean palace culture with gold. Due to the overlap of gold deposits [24] with borate deposits [25] a connection of gold and borate mining is plausible. However, only excavation of such ancient mines will lead to further information.

Conclusions

In our study, we investigated three possible effects that the use of borates may have had in the manufacturing process of glasses covered in gold. Firstly, borax additions inhibit surface crystallisation during heat treatments between 700 °C but below 1000 °C, leading to more appealing surfaces. Secondly, borax could have been used either as a solder between glass and gold, or to avoid undesired darkening by oxidation on the gold surface during the heat treatment. Although, due to the lower melting temperature, borates should have a positive effect on the glass-gold interaction [26], we could not detect an apparent increase of adhesive strength with or without the use of borax. In both cases, glass samples and gold sheets were strongly connected, while the adhesion increased with increasing temperature of heat-treatment. Finally, borax (or other borates) could have been used as a cleansing agent for gold surfaces. In that case we expect borates on the gold surface to react with the glass during fusion.

For all scenarios, we could confirm by infrared reflectance spectroscopy a diffusion of borates into the silicate glass surface at temperatures above 700 °C. While introduction of borates from fusion with

contaminated gold plates will lead to rather small amounts of borates at the glass surface, we could show a diffusion of borates into roughly the first 9 µm of a glass surface when working at temperatures of ca. 800 °C. With our experiments, we demonstrated that the formation of a borosilicate layer can indeed occur. By using purified gold or such that has been extracted by the borax method, the introduction of borates into the glass surface would even be a necessary consequence of fusing gold sheets to glass. The present experiments showed also that borates in trigonal coordination are Lewis base acceptors and as such very sensitive to hydrolysis, as opposed to borates in tetrahedral coordination which can survive hydrolysis due to their 3-dimensional bonding to the glass network.

By neutron radiography we visualised boron contamination of model glasses to occur upon casting on a gold sheet covered with borax. Although a differentiation between boron and hydrogen is not easy in neutron radiography, we assume that surface layers of corroded glass samples will show a difference for a borate layer and a corroded glass layer. In the combination with IR reflectance spectroscopy, neutron radiography could provide further evidence for the formation of such a boron-containing glass layer.

The intentional use of borax as an additional glass-to-gold soldering agent would present a significant step in the understanding of metal-glass interaction. Similarly, the washing of noble metals in borax melts, which is a well-known in contemporary technology, would be a notable feat, reflecting the high level of Mycenaean-age processing of materials.

Acknowledgements

The authors acknowledge the financial support of the Leonardo Program for Lifelong Learning, that made the preliminary experiments of FD at the NHRF in Athens possible, as well as the ProChance program of the University of Jena, which financed parts of this PhD studies at the FSU. This work is partially based on experiments performed at the Swiss spallation neutron source SINQ, Paul Scherrer Institute, Villigen, Switzerland. We are also grateful for the help of A. Kästner when using the ICON and NEUTRA beamlines.

References

References

[1] K. Nikita, Mycenaean glass beads: Technology, forms, and function, Bead Study Trust, London, 2003, pp. 23–37.

[2] G. Nightingale, Mykenisches Glas, in: Althellenistische Technologie und Technik von der prähistorischen bis zur hellenistischen Zeit mit Schwerpunkt auf der prähistorischen Epoche, Verein zur Förderung der Aufarbeitung der Hellenistischen Geschichte, e. V., 2004, pp. 171–189.

[3] M. Panagiotaki, The technological development of Aegean vitreous materials in the Bronze Age, Vitreous Materials in the Late Bronze Age Aegean 9 (2008) 34–63.

[4] T. E. Haevernick, Beiträge zur Geschichte des antiken Glases: Mykenisches Glas, Jahrbuch des Römisch-Germanischen Zentralmuseums Mainz 6 (1960) 36–50.

[5] A.-L. Schallin, Identities and 'precious' commodities at Midea and Dendra in the Mycenaean Argolid, in: Papers and Monographs from the Norwegian Institute at Athens, Vol. 40, The Norwegian Institute at Athens, 2016, p. 1.

[6] M. Panagiotaki, Y. Maniatis, D. Kavoussanaki, G. Hatton, M. S. Tite, The production technology of Aegaean Bronze Age vitreous materials, in: Invention and Innovation. The social context of technological change, Vol. 2, Oxbow Books, 2004, pp. 149–175.

[7] D. Möncke, D. Palles, N. Zacharias, M. Kaparou, E. I. Kamitsos, L. Wondraczek, Formation of an outer borosilicate glass layer on Late Bronze Age Mycenaean blue vitrious relief fragments, Physics and Chemistry of Glasses — European Journal of Glass Science and Technology Part B 54 (1) (2013) 52–59.

[8] E. Brepohl, Theorie und Praxis des Goldschmieds, 5th Edition, VEB Fachbuchverlag, Leipzig, 1978.

[9] P. W. Appel, L. Na-Oy, The borax method of gold extraction for small-scale miners, Journal of Health and Pollution 2 (3) (2012) 5–10. doi:10.5696/2156-9614-2.3.5.

[10] G. A. Holmquist, J. A. Pask, Sodium borate glasses and platinum or gold — wetting and reactions, Lawrence Berkeley National Laboratory LBNL Report #: LBL-3967.
URL https://escholarship.org/uc/item/7dm2n32f

[11] H. Schliemann, Mykenae, Brockhaus, Leipzig, 1878.
URL http://digi.ub.uni-heidelberg.de/diglit/schliemann1878

[12] K. Nikita, J. Henderson, Glass analyses from Mycenaean Thebes and Elateia: Compositional evidence for a Mycenaean glass industry, Journal of Glass Studies 48 (2006) 71–120.

[13] E. H. Lehmann, P. Vontobel, L. Wiezel, Properties of the radiography facility NEUTRA at SINQ and its potential for use as European reference facility, Nondestructive Testing and Evaluation 16 (2-6) (2001) 191–202. doi:10.1080/10589750108953075.

[14] E. I. Kamitsos, A. P. Patsis, G. Kordas, Infrared-reflectance spectra of heat-treated sol-gel-derived silica, Physical Review B 48 (17) (1993) 12499–12505. doi:10.1103/physrevb.48.12499.

[15] D. Möncke, E. I. Kamitsos, D. Palles, R. Limbach, A. Winterstein-Beckmann, T. Honma, Z. Yao, T. Rouxel, L. Wondraczek, Transition and post-transition metal ions in borate glasses: Borate ligand speciation, cluster formation, and their effect on glass transition and mechanical properties, The Journal of Chemical Physics 145 (12) (2016) 124501. doi:10.1063/1.4962323.

[16] E. Kamitsos, A. Patsis, G. Chryssikos, Infrared reflectance investigation of alkali diborate glasses, Journal of Non-Crystalline Solids 152 (2-3) (1993) 246–257. doi:10.1016/0022-3093(93)90258-y.

[17] M. D. Ingram, J. E. Davidson, A. M. Coats, E. I. Kamitsos, J. A. Kapoutsis, Origins of anomalous mixed-cation effects in ion-exchanged glasses, Glastech. Ber. Glass Sci. Technol. 73 (2000) 89–104.

[18] P. Colomban, L. C. Prinsloo, Optical spectroscopy of silicates and glasses, Vol. 40, Royal Society of Chemistry, 2009, pp. 128–149. doi:10.1039/b715005a.

[19] C. P. Varsamis, E. I. Kamitsos, G. D. Chryssikos, Structure of fast-ion-conducting AgI-doped borate glasses in bulk and thin film forms, Physical Review B 60 (6) (1999) 3885–3898. doi:10.1103/physrevb.60.3885.

[20] D. Möncke, G. Tricot, D. Ehrt, E. Kamitsos, Connectivity of borate and silicate groups in a low-alkali borosilicate glass by vibrational and 2D NMR spectroscopy, Journal of Chemical Technology and Metallurgy 50 (2015) 381–386.

[21] T. Furukawa, W. B. White, Raman spectroscopic investigation of sodium borosilicate glass structure, Journal of Materials Science 16 (10) (1981) 2689–2700.

[22] C. Helvaci, R. N. Alonso, Borate deposits of Turkey and Argentina; a summary and geological comparison, Turkish Journal of Earth Sciences 24 (2000) 1–27.

[23] E. Photos, Early extractive iron metallurgy in N Greece: A unified approach to regional archaeometallurgy, Ph.D. thesis, University of London (1987).

[24] O. Yigit, Gold in Turkey — a missing link in Tethyan metallogeny, Ore Geology Reviews 28 (2) (2006) 147–179. doi:10.1016/j.oregeorev.2005.04.003.

[25] R. B. Kistler, C. Helvaci, Boron and borates, Industrial minerals and rocks 6 (1994) 171–186.

[26] R. Frieser, A review of solder glasses, Active and Passive Electronic Components 2 (3) (1975) 163–199.

Journal of the European Ceramic Society 38 (2018) 4799–4805

Contents lists available at ScienceDirect

Journal of the European Ceramic Society

journal homepage: www.elsevier.com/locate/jeurceramsoc

Original Article

Ancient Roman nano-technology: Insight into the manufacture of mosaic *tesserae* opacified by calcium antimonate

Ferdinand Drünert[a,*], Eleni Palamara[b], Nikolaos Zacharias[b], Lothar Wondraczek[a], Doris Möncke[c,d]

[a] Otto Schott Institute of Materials Research, University of Jena, Fraunhoferstraße 6, D-07743 Jena, Germany
[b] Laboratory of Archaeometry, Department of History, Archaeology and Cultural Resources Management, University of the Peloponnese, 24100 Kalamata, Greece
[c] Theoretical and Physical Chemistry Institute, National Hellenic Research Foundation, 48 Vassileos Constantinou Avenue, 11635 Athens, Greece
[d] Department of Built Environment and Energy Technology, Linnæus University, 351 95 Växjö, Sweden

ARTICLE INFO

Keywords:
Roman glass mosaics
Opacification
Calcium antimonate
Mosaic *tesserae*
Nucleation

ABSTRACT

Opaque mosaic glass *tesserae* containing calcium antimonates from Ancient Messene, Greece (1st–4th century CE) were investigated by scanning electron microscopy, Raman spectroscopy and X-ray diffraction. Both trigonal $CaSb_2O_6$ and cubic $Ca_2Sb_2O_7$, with crystallite diameters below 1 µm, were identified as opacifying agents. To better understand ancient technologies, we prepared model glasses that were opacified by crystallisation *via* a secondary heat treatment, by direct crystallisation during the melting process, or by the addition of pre-reacted calcium antimonate to a base glass. We found that direct crystallisation replicated the antique glass artefacts most accurately.

We demonstrated that 0.2 wt% of nucleating agents like TiO_2 and SnO_2 already exert significant influence on the crystallisation behaviour of calcium antimonates. Secondary scattering centres such as silica and carbonates contribute to the optical appearance. Concurrently, we reproduced opaque white glass ceramics in a reconstructed, wood-fired, Roman-type glass furnace built by Wiesenberg (2014).

1. Introduction

One of the earliest applications of manmade glasses was decorative; they were used as brightly coloured materials, in some instances substituting equally precious gemstones [1]. Many inorganic dyes which are found in glasses had already been used earlier in ceramic glazes. However, calcium antimonates appear to have been employed originally as opacifiers in glass decorations [2], *e.g.*, in the white glazes of early Egyptian glass vessels, or later in Hellenic glass decorations [3,4]. During the Roman period these opacifiers also appeared in bulk materials, such as white, green, purple and blue glass mosaic *tesserae* [5–9]. After the fall of the Roman Empire calcium antimonate appears to have been replaced by stannates [10].

The general opacification procedure of opaque white glasses has been the topic of several studies. Most common opacifiers for white materials are the calcium antimonates, $CaSb_2O_6$ and $Ca_2Sb_2O_7$ [11]. Foster and Jackson suggest that opacified glasses were prepared by striking a colourless glass at temperatures below 1200 °C [12]. In contrast, Lahlil et al. [13] describe the formation of calcium antimonates through a secondary heat treatment step at temperatures between 1100 °C and 1300 °C. As raw materials stibnite (Sb_2S_3) and roasted stibnite (Sb_2O_3) have been discussed for the formation of crystalline antimonate particles. However, in a study focussing on the generally pentavalent oxidation state of antimony ions in Egyptian glazes, separately synthesised calcium antimonate added later to a base glass melt is suggested for the manufacture of such glasses [14].

Calcium antimonates can be formed with different stoichiometry and crystal structures. $CaSb_2O_6$ has been described with a trigonal structure (space group $P\bar{3}1m$/No. 162; occasionally also reported as hexagonal [9,15]). On the other side, $Ca_2Sb_2O_7$ occurs in orthorhombic (space group *Imma*/No. 74 [16]) or cubic morphology (space group $Fd\bar{3}m$/No. 227 [9]). The first and the latter are found frequently in glasses and glazes of antique artefacts, where they initiated discussions about the different possible ways of material manufacture [17]. Lahlil et al. analysed the formation of both antimonates during secondary heat treatment and concluded that while $Ca_2Sb_2O_7$ appears to be the phase with higher thermodynamic stability, $CaSb_2O_6$ is formed in the earlier stages of heat treatment [13]. However, the opacification process described by Lahlil is limited to antimonate amounts of 10 wt% and does not take into account the *in-situ* opacification process described by Foster and Jackson [12].

* Corresponding author.
E-mail address: ferdinanddruenert@yahoo.de (F. Drünert).

https://doi.org/10.1016/j.jeurceramsoc.2018.06.031
Received 25 January 2018; Received in revised form 12 June 2018; Accepted 18 June 2018
Available online 20 June 2018
0955-2219/

With the increased availlability of portable Raman instruments, the possibility to study archaeological artefacts becomes more and more important. The selective analysis of inclusions by micro-Raman spectroscopy enables also the identification of many inclusions and inhomogeneities, while X-ray diffraction (XRD) averages over a larger area. In the present study, we applied thermal analysis by differential scanning calorimetry (DSC) and Raman spectroscopy to model glasses for a better understanding of the process of formation of the various antimonate crystals. As confirmation we matched the spectroscopic results to their XRD patterns. The derived mechanistic understanding was subsequently compared to observations on a set of mosaic *tesserae* excavated in 2008 at the archaeological site of Messene, Greece. We focused on different routes of opacification and the effects of minor components like TiO_2 and SnO_2, which are known for their influence on crystallisation processes in glass ceramics manufacture [18]. A common problem for the reproduction of archaeological glass samples is the use of electrically heated furnaces, which typically do not accurately mimic the characteristic atmospheric conditions of wood-fired Roman furnaces. In order to account for the different melting atmospheres, we were fortunate to perform reproduction experiments of opacified glass samples in a reconstructed wood-fired Roman glass furnace in Borg, Germany [19].

2. Materials and methods

2.1. Archaeological glass samples

During the excavation of the archaeological site of Ancient Messene, Peloponnese (Greece), P. Themelis discovered in 2008 large quantities of glass mosaic *tesserae* located at a sanctuary of Isis and Serapis [20].

The *tesserae* were dated to the 1st–4th century CE [8,7]. In this study six glass *tesserae* with elevated antimony levels in white (t1), ivory (t2), greenish (t3, t4) and blue (t5, t6) colour (Fig. 1 and Table 1) were considered. We analysed all samples by scanning electron microscopy (SEM) and energy dispersive X-ray spectroscopy (SEM-EDX). Two samples in white (t1) and (t6) blue colour were investigated in more detail by Raman spectroscopy and X-ray diffraction as described in Section 2.3.

2.2. Laboratory replication of opacified glass

Four experimental setups were used in this study. Their different parameters are summarised in Table 2.

2.2.1. Model glass a: ex-situ synthesis (I)

Ex-situ samples (I) were prepared as follows: Calcium antimonates were synthesised, as described in the literature [21], through a solid state reaction of Sb_2O_3 and $CaCO_3$ for 30 min at 950 °C ($CaSb_2O_6$) and 1150 °C ($Ca_2Sb_2O_7$). Calcium antimonate powder was added to powdered soda lime silicate standard glass (model glass a; see Table 1); the mixture was placed in alumina forms and heated to temperatures between 700 °C–1200 °C for 0.5 h–5 h. A sample photograph is provided in Fig. 2a.

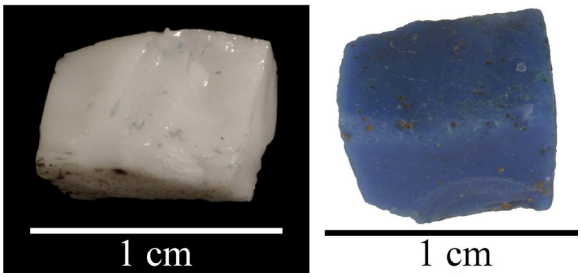

Fig. 1. Photographs of investigated mosaic *tesserae* in white (t1, left) and blue colour (t6, right). The labels refer to Table 1. (For interpretation of the references to colour in this figure legend, the reader is referred to the web version of this article.)

2.2.2. Model glass b: sample sets (II, III and IV)

For the crystallisation of calcium antimonate from the bulk glass (sample set II, III and IV), a model glass with a composition close to that of Roman mosaic *tesserae* was developed (model glass b; see Table 1). Therefore, initial batches were prepared from $Al(OH)_3$, $CaCO_3$, Na_2CO_3, Sb_2O_3 and quartz powder (all 99.5%).

2.2.3. Sample set (II and III): crystallisation by annealing and direct crystallisation

The model glass b was doped with 0.2 wt% TiO_2 and/or SnO_2. Blind samples, without dopant addition, were run parallel through the same heat treatment as the sample sets. The batches were homogenised and calcined in alumina crucibles at 900 °C for 24 h. Subsequently, the mixtures were melted for 3 h at different temperatures between 1100 °C and 1400 °C in an electrical furnace, cast on a brass block and cooled from 550 °C to room temperature with a cooling rate of 2 K min^{-1}.

Set II: Clear glasses were obtained for samples prepared at 1400 °C. These were considered for *annealed* samples (II).

Set III: Glasses molten at 1100 °C–1200 °C were opaque and therefore assigned to sample set (III). Doped and undoped powdered glasses and bulk samples were treated at 700 °C–1200 °C for 0.5 h, 5 h or 50 h. An image of a sample is given in Fig. 2b.

2.2.4. Sample set (IV): experimental archaeology approach

The experiments of sample set (III) were repeated in an experimental clay furnace at the Villa Borg, Perl, Germany, which mimics traditional Roman glass furnaces [19]. Due to limited space, only samples with 0.2 wt% TiO_2 and blind samples were considered for the experiment. The batches were treated at temperatures between 900 °C and 1100 °C in this wood-fired Roman-type furnace for one to three days. Afterwards, the samples were annealed in a wood-fired clay lehr at 400 °C–460 °C for one hour and cooled slowly overnight to room temperature. Glass samples opacified by this process are shown in Fig. 2c and d.

2.3. Methods

Heat capacity data (C_P) of all model glass compositions were collected by differential scanning calorimetry (DSC, Netzsch STA 449F1; reference: sapphire) with a heating rate of 20 K min^{-1} across the temperature range from 100 °C to 1100 °C. The thermal properties of unpolished plane parallel discs of about 2 mm thickness were compared to powdered glass samples to distinguish between bulk and surface crystallisation mechanisms. Possible crystal phases before and after annealing were identified by Raman spectroscopy, conducted over the range of 100 cm^{-1}–1400 cm^{-1} using a 514 nm excitation wavelength at 50x magnification (Renishaw inVia Raman microscope with *Wire 4.1* software). Additionally, all samples were investigated by X-ray diffractometry (XRD, Rigaku Miniflex 600) operated at 40 keV/15 mA using Cu° K_α radiation at a scan rate of 1° over a 2θ range of 5°–75°. Diffraction patterns of archaeological samples were taken from the pristine surface covering an area of 0.1 mm × 5 mm, while powder was used for the model glasses. Scanning electron microscopy investigation of the archaeological glass samples with Electron Dispersive X-ray spectroscopy was employed for the determination of the chemical composition of archaeological glass samples (SEM-EDX; JEOL JSM-6510LV microscope coupled with an energy dispersive spectrometer, Oxford Instruments using INCA software and 1412, NIST610, NIST612 and NIST620 glasses as standards for quantification of the results). Detailed description of the setup used and its accuracy are provided in Moropoulou et al. [22] and Palamara et al. [23].

Table 1
Glass composition (wt%) of used model glasses and selected Roman mosaic *tessera* from Ancient Messene, Greece (1st–4th century CE) containing calcium antimonate, as measured by SEM-EDX.

			Mosaic *tesserae*			Model glass		
	White	Ivory	Green-white	Light green	Turquoise	light blue		
	(t1)	(t2)	(t3)	(t4)	(t5)	(t6)	a	b
SiO_2	69.7 ± 0.9	68.6 ± 0.4	67.8 ± 0.3	67.0 ± 0.4	67.4 ± 0.7	69.0 ± 0.3	74.2	71.3
Al_2O_3	3.0 ± 0.1	2.2 ± 0.1	2.3 ± 0.1	2.8 ± 0.3	2.4 ± 0.4	2.2 ± 0.1		3.2
Na_2O	10.0 ± 0.7	12.2 ± 0.3	12.2 ± 0.1	9.5 ± 0.3	12.9 ± 1.7	15.1 ± 0.1	16.5	14.2
K_2O	1.0 ± 0.2	0.9 ± 0.1	1.3 ± 0.2	1.5 ± 0.1	1.4 ± 0.2	0.8 ± 0.1		
MgO	0.4 ± 0.1	0.6 ± 0.1	0.6 ± 0.1	0.2 ± 0.1	0.5 ± 0.1	0.5 ± 0.1		
CaO	7.4 ± 0.1	6.9 ± 0.1	7.2 ± 0.3	8.3 ± 0.5	6.8 ± 0.6	6.5 ± 0.1	9.3	6.7
CuO_x	< 0.1	< 0.1	0.3 ± 0.1	1.2 ± 0.3	2.4 ± 0.3	< 0.1		
MnO_x	0.3 ± 0.1	0.4 ± 0.1	0.7 ± 0.1	0.4 ± 0.1	< 0.1	0.6 ± 0.1		
FeO_x	0.3 ± 0.1	0.7 ± 0.1	0.7 ± 0.1	0.7 ± 0.3	0.7 ± 0.2	0.5 ± 0.1		
SnO_2	0.4 ± 0.2	0.8 ± 0.4	0.5 ± 0.4	1.4 ± 0.6	0.4 ± 0.4	0.2 ± 0.2		
TiO_2	0.2 ± 0.1	0.3 ± 0.1	< 0.1	< 0.1	< 0.1	0.1 ± 0.1		
PbO	0.6 ± 0.1	0.3 ± 0.1	0.2 ± 0.2	< 0.1	< 0.1	0.2 ± 0.1		
SbO_x	5.4 ± 0.3	4.7 ± 0.3	4.8 ± 0.2	4.9 ± 0.1	3.2 ± 0.4	3.2 ± 0.2		4.6
S^{2-}	0.5 ± 0.1	0.7 ± 0.1	0.6 ± 0.1	0.7 ± 0.1	0.6 ± 0.2	0.4 ± 0.1		

3. Results

3.1. Visual analysis of artefacts and comparison to replicated glass samples

The analysed mosaic *tesserae* of this study are of light colour. Depending on the added chromophor, they vary in appearance from white to ivory, green-white, turquoise and purple. Typical is an increased amount of white diffusely backscattered light. Fig. 1 displays the two glass *tesserae* t1 and t6. Both glass samples are homogeneously opacified and show no granularity. While the white *tessera* appears slightly translucent (Fig. 1a), the blue *tessera* is completely opaque. Magnification of the sample surface shows corrosion marks, but also many bubbles of up to 5 µm in diameter.

Directly crystallised samples (III and IV) show a very similar appearance to the original mosaic *tesserae* (compare Figs. 1 and 2c–d). Of 8 samples, 3 became translucent close to the crucible walls without any apparent correlation to the temperature or other experimental conditions (see Fig. 2c), while the other samples are completely opaque (see Fig. 2d). Unlike the observed Roman glass *tesserae*, the bulk of most glass samples is rich in large bubbles. A correlation between reaction time and the amount of large bubbles could not be found. In contrast, *annealed* glass samples (II) prepared from powdered model glass are homogeneously white, while *ex-situ* samples (I) show a fine granularity and appear more translucent.

3.2. Chemical analysis

Chemical compositions of the investigated glass artefacts as measured by SEM-EDX are shown in Table 1. All archaeological samples considered for this investigation have typical compositions of Roman-type glasses prepared with natron ($Na_3(HCO_3)(CO_3)\cdot 2H_2O$) and silica sand (main component SiO_2) [8]. Broken sea shells ($CaCO_3$), either as a natural component of sea sand or deliberately added, were used as calcium source [24,25]. Relevant minor components considered in this study are tin oxide (SnO_2) and titanium oxide (TiO_2). Whereas tin oxide is found in most *tesserae* in amounts of *ca.* 0.6 wt%, titanium oxide frequently remains below the detection limit of SEM-EDX. As a main constituent of bronze, tin oxide (SnO_2) is usually found with copper oxide ([26]; compare *tesserae* t3 and t4, Table 1), while titanium oxide (TiO_2) is a typical impurity of sands [27]. Detailed investigation by SEM shows the typical structure of a highly corroded glass surface with bubble-like inclusions and many particles, as known from the literature [22]. Due to the small size of the particles we had difficulties to differentiate between bulk glass and particle analysis in most of our experiments. However, we investigated a few particles successfully by SEM-EDX. Most of these approximately 1 µm large particles (see Fig. 3) show elevated levels of calcium and antimony (*e.g.* 60 wt% $Sb^{3+/5+}$ and 20 wt% Ca^{2+}, normalised to oxygen), indicating the presence of calcium antimonate. Some particles also exhibit comparably high levels of sulphur (up to 4% compared to 0.6% average in the glass matrix). Remnants of sulphur may therefore indicate the use of stibnite (Sb_2S_3) as antimonate source, as suggested by Foster et al. [12].

The predominant crystal phase in all mosaic *tesserae*, as investigated by Raman spectroscopy (Fig. 4, Table 3), is cubic $Ca_2Sb_2O_7$ (Fig. 4d: two Raman peaks at 480 cm^{-1} and 620 cm^{-1}). Trigonal $CaSb_2O_6$ (Fig. 4c), recognized by the symmetric stretching peak at 680 cm^{-1}, is found frequently in nearly all samples. Furthermore, calcite (Fig. 4b) was identified in a few cases (1085 cm^{-1}). In contrast, *direct* samples

Table 2
Summary of the three different experimental parameters of the opacification process.

Condition	*Ex-situ* synthesis	Heat treatment	Direct crystallisation	Roman glass furnace
Sample set	*ex-situ* (I)	*annealed* (II)	*direct* (III)	*Borg* (IV)
Batch	model glass (a)	model glass (b)	model glass (b)	model glass (b)
Additives	• 4 wt% prereacted $Ca_2Sb_2O_7$ • 4 wt% prereacted $CaSb_2O_6$	• no dopant • 0.2% TiO_2 • 0.2% SnO_2 • 0.2% TiO_2 • +0.2% SnO_2	• no dopant • 0.2% TiO_2 • 0.2% SnO_2 • 0.2% TiO_2 • +0.2% SnO_2	• no dopant • 0.2% TiO_2
Preparation	annealing at 950 °C ($CaSb_2O_6$) 1100 °C ($Ca_2Sb_2O_7$)	glasses treated at 700 °C–1200 °C for 0.5 h–5 h	Batch preheated at 900 °C	no preheating
Reaction condition	Sintering with powdered glass at 700 °C–1100 °C	1400 °C for 5 h	1100 °C–1300 °C for 5 h	between 950 °C and 1100 °C for 1d–3d

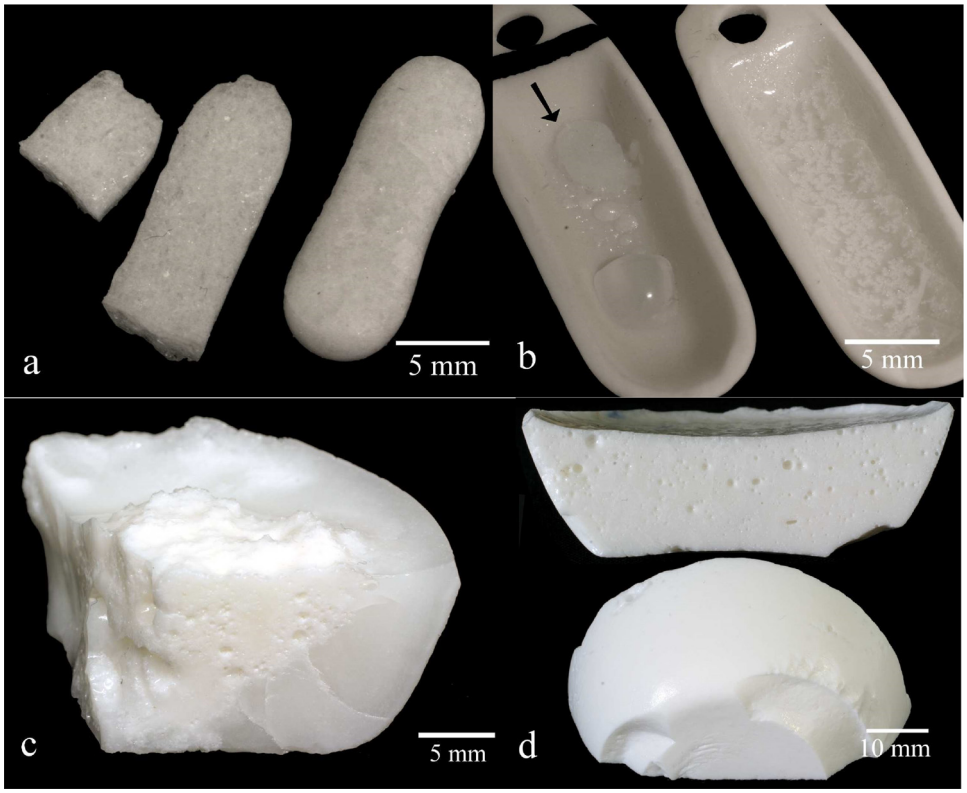

Fig. 2. Images of selected opacified model glasses: (a/I) after sintering of *ex-situ* synthesised calcium antimonate; (b/II) *annealed* glass powder (arrow) or bulk material; (c and d) opacified glass sample as obtained after *direct* crystallisation (III and IV). (c) remained translucent near the crucible walls. Roman numbers refer to the experimental parameters.

(III) contain calcium antimonates, calcite and, occasionally, tridymite and cristobalite; in *annealed* samples (II) either $CaSb_2O_6$ (when heat-treated below 1000 °C) or cristobalite and tridymite (Fig. 4a) (when heat-treated between 1000 °C and 1100 °C) crystallises at the surface. Annealing at temperatures above 1100 °C avoided crystallisation. Bulk crystallisation did generally not occur in any of these samples under the various treatments.

Annealed samples (II) prepared above 850 °C generally show no indication of cubic calcium antimonate. Instead only the trigonal crystal phase was identified by Raman spectroscopy. Heat treatment of bulk samples did not lead to a satisfying opacification, but to surface crystallisation of mostly trigonal calcium antimonate and, for samples treated at temperatures above 1050 °C, also silica. However, the *ex-situ* opacified glass samples (I) contain the expected cubic crystal phase.

X-ray diffraction patterns of the Roman mosaic *tesserae* (Fig. 5) show the presence of calcium antimonates with the typical reflections at (among others) $2\theta = 50^\circ$ (both), 30° (both), 27° ($CaSb_2O_6$) and 15° ($Ca_2Sb_2O_7$). Since all samples were analysed on bulk samples to avoid sample destruction, the obtained signals have to be evaluated carefully. In both observed *tesserae* crystal phases of SiO_2 remained below the limit of detection. Due to the overlap of a calcite and calcium antimonate XRD patterns (especially the strongest peak of calcite at

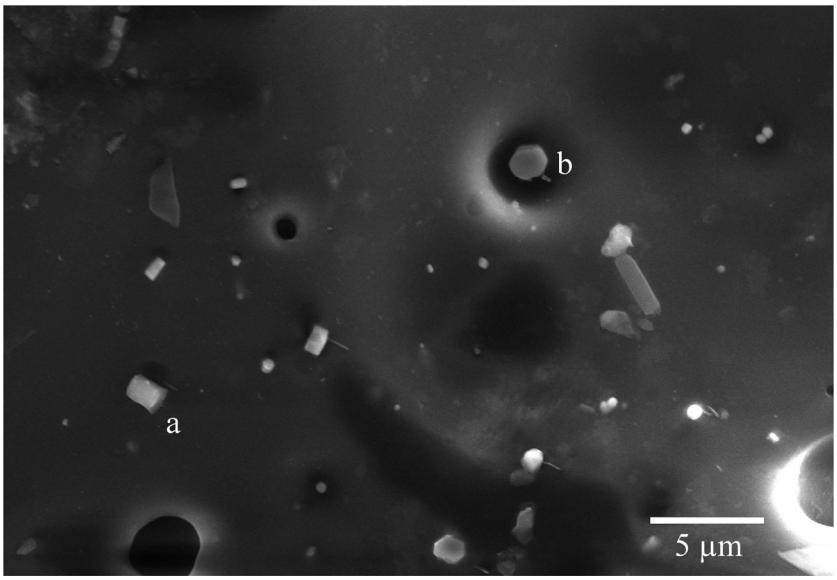

Fig. 3. Differently shaped microcrystals as seen in the electron microscope. Among the crystallites, SiO_2 (a) can be found as well as antimony sulfide (b). Due to their small crystal size, the chemical composition of calcium antimonate crystals was particularly difficult to be determined by SEM-EDX.

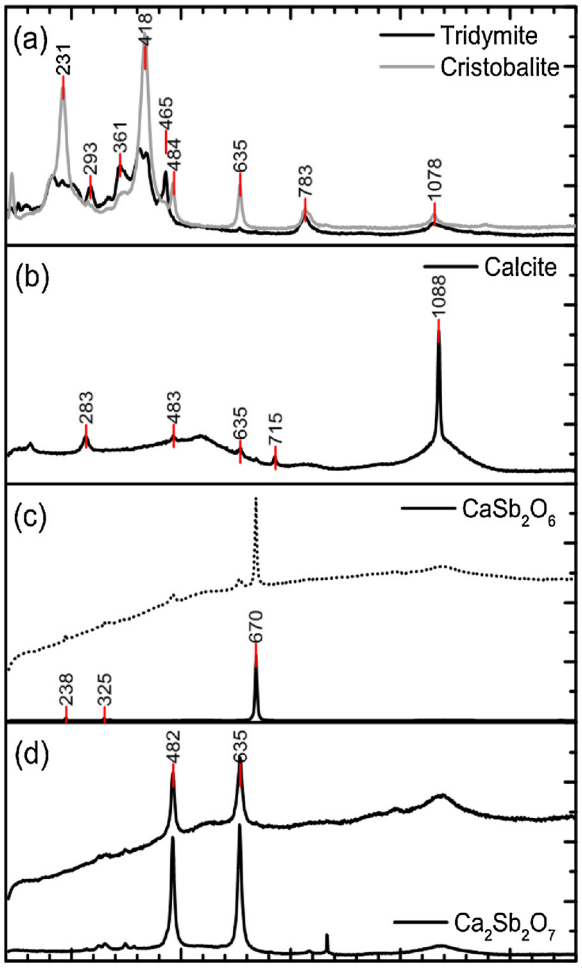

Fig. 4. Main crystal phases as identified by Raman spectroscopy. Solid spectra were taken from exemplary samples of set (III), while dotted spectra were taken from *tessera* t1. For further information see Tab. 3.

$2\theta = 30°$) we could not determine the presence of calcite with sufficient certainty by XRD alone.

XRD patterns of powdered samples of the reproduced glass ceramics (*Direct* III and *Borg* IV; Fig. 5) are dominated by cubic $Ca_2Sb_2O_7$. While more silica occur in glass samples prepared at 1200 °C, trigonal $CaSb_2O_6$ is found only in samples that have not been doped with 0.2 wt % SnO_2.

3.3. Thermal analysis of replicated glass samples

The C_P curves of the model glass samples with or without titanium oxide and/or tin oxide are displayed in Fig. 6. The apparently generally lower measured heat capacity for the undoped glass sample is caused by differences in the experimental setup, in particular, in sample shape. All other four glass compositions appear very similar with a glass transition temperature T_g of 540 °C. While the undoped sample shows a crystallisation peak at *ca.* 900 °C, this peak is shifted to 950 °C for titanium-doped samples. Doping the sample with 0.2% tin oxide leads to a suppressed crystallisation peak at 900 °C; instead a signal at 1000 °C is indicative of another chemical reaction. Doping the model glass with both titanium and tin oxide leads to a shift of the chemical reaction observed for Sn-doped samples to lower temperatures, therefore overlapping with a possible crystallisation peak at 900 °C. It is unclear if the second chemical reaction is a crystallisation or a reduction of Sb^{5+} to Sb^{3+} which would usually be expected at 1180 °C [30].

Table 3
Crystal phases as investigated by Raman spectroscopy. The Raman spectra of the different crystal structures re shown in Fig. 4 a-d.

Crystal type
(a) Tridymite/Cristobalite (SiO_2) – found in:
• directly crystallised samples (III and IV) (frequently, mostly in fully opacified areas) • heat treated samples for $T > 1100$ °C • mosaic *tesserae*: not detected in the current study, but its occurence has been reported in the literature [28,29]
(b) Calcite ($CaCO_3$) – found in:
• all directly crystallised glass samples (occasionally in fully opacified areas) • rarely found in mosaic *tesserae*; reports on archaeological samples can be found in [28]
(c) Trigonal $CaSb_2O_6$ – found in:
• powdered glass samples after heat treatment (as the only phase) • Ti doped, directly crystallised samples (all, frequently) • mosaic *tesserae* (frequently) • surface of bulk glasses after heat treatment • solid state reaction at 950 °C
(d) Cubic $Ca_2Sb_2O_7$ – found in:
• all directly crystallised samples (main phase) • bulk samples after heat treatment (rarely) • mosaic *tesserae* (main phase) • solid state reaction at 1100 °C

4. Discussion

The *ex-situ* synthesis of calcium antimonates leads to a variety of results, depending on the various processing conditions. Lahlil [21] suggests 1100 °C as optimal temperature for the formation of cubic calcium antimonate and 950 °C for the trigonal species. Different reaction temperatures will lead to mixtures of both crystal phases. Exact temperature control without appropriate technological equipment is nearly impossible, so that mixtures of both crystal phases are almost unavoidable in the archaeological materials. The use of thus-prepared calcium antimonate powder therefore explains the broad variety which has been found in the ratio of $Ca_2Sb_2O_7$ to $CaSb_2O_6$. On the other hand, addition of 3 wt% $Ca_2Sb_2O_7$ (*ex-situ*/I) to a powdered glass with additional heat treatment did not lead to a satisfying opacification: In our experiments, as shown in Fig. 2a, sample edges appear uneven and granulated after breaking. Although these factors may be improved by a more sophisticated procedure of material reproduction, such a process might be less representative for the original routes of material manufacture. In contrast, secondary heat treatment (*annealed*/II) seems to be a more promising approach for crystallisation. While bulk glass samples remained transparent, samples from sintered powder appeared completely opacified by trigonal calcium antimonate, as identified by Raman spectroscopy. We could not observe any difference between doped and undoped sintered powder samples. Since $CaSb_2O_6$ is not the dominating crystal phase of the investigated glass *tesserae*, we assume that sintering glass powder was not applied for the production of Messenean mosaic *tesserae*.

Direct crystallisation (III) as well as reproduction in traditional melting environment (*Borg*/IV) led to very heterogeneous products. According to our study, the ratio of trigonal to cubic calcium antimonate is increased for glass melts doped with titanium oxide, while almost no $CaSb_2O_6$ is detected in glasses doped with tin oxide. Adding both, tin and titanium oxide to a glass batch faciliated crystallisation of $Ca_2Sb_2O_7$. Due to the low concentration of nucleating agents in the glass matrix, and also the possibly inhomogeneous distribution in the batch, the formation of calcium antimonate may be only partially influenced by these nucleation agents.

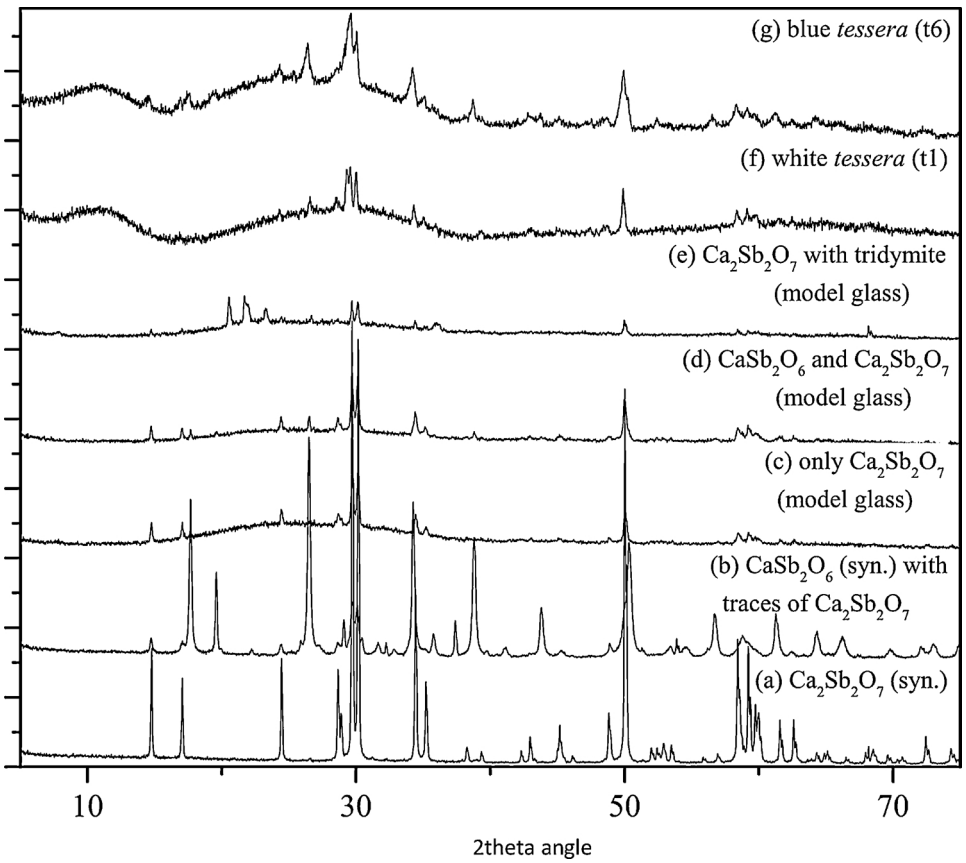

Fig. 5. XRD patterns of *ex-situ* (I) synthesised $Ca_2Sb_2O_7$ (a) and $CaSb_2O_6$ (b); *Direct* (III) glass samples: sample with only $Ca_2Sb_2O_7$ (c) and with additional tridymite (d); two Roman mosaic *tesserae* (e, f).

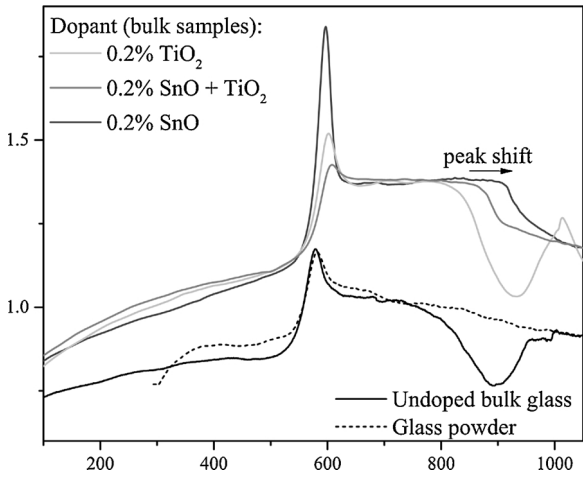

Fig. 6. C_P measurements of doped and undoped model glass (b) samples used for sample set (II).

Tridymite, cristobalite and minor amounts of calcite were additionally observed in our glass samples. Since calcite is known to be a typical corrosion product, we initially connected the presence of carbonates on archaeological glass samples to weathering effects. However, Raman spectroscopy frequently revealed residual calcium carbonate in remade, uncorroded laboratory glasses. Since decomposition of calcite in glass melts is expected to occur at temperatures between 1000 °C–1300 °C [31], we suggest that in this case calcite was not dissolved due to relatively low reaction temperatures of under 1200 °C.

Direct crystallisation (III and IV) leads to opaque, white glass ceramics. However, the variation of crystal phases observed in our experiments complicates the interpretation of temperature ranges and methodology of Roman glass *tessera*manufacture. White glass ceramics are formed in different appearances, varying from completely opaque regions to translucent areas near the surface. Most significant is the frequent presence of silica within the completely opacified parts of the white glass ceramics. Other examples of silica in Roman opaque glasses can be found in the literature [28,29].

Taking into account that temperature control without technical equipment and wood as heating material will lead to widely varying temperatures inside the furnace, we have to consider an increased probability of different crystal structures within the glass matrix. The experimental archaeological approach of Wiesenberg [19] shows that maximum temperatures of at least 1100 °C can be reached using a furnace model based on archaeological findings. For our studies, 1000 °C can be assumed as reasonable temperature estimation, with occasional fluctuations between 900 °C and 1100 °C. Despite all variation of the experimental setup, we could show that opaque glass ceramics can be synthesised with high reproducibility.

5. Conclusion

The technological requirements for producing opaque glasses can only be understood by looking at the whole process of manufacture. Through direct crystallisation of glasses during the melting process at 1000 °C–1200 °C, we could replicate opaque, Roman-type glasses. In comparison to *ex-situ* addition or crystallisation by a secondary heat treatment, directly crystallised samples appear homogeneously opaque, while other samples remained either translucent or inhomogeniously opacified.

The two main opacifiers in Roman, white-opaque glass samples,

$CaSb_2O_6$ and $Ca_2Sb_2O_7$, both formed in our laboratory samples. Additionally, calcite, and the silica types tridymite and cristobalite could be observed as minor components after direct crystallisation, just as the secondary scattering centres known from original Roman opacified materials. By doping glass samples with 0.2 wt% of titanium oxide and tin oxide, we could show that the formation of different antimonates could be enhanced. Thermoanalysis supported the different temperature-dependent crystallisation behaviour of the differently doped samples. Therefore, the appearence of both, trigonal $CaSb_2O_6$ and cubic $Ca_2Sb_2O_7$, can be explained by the presence of nucleating agents in very small amounts.

The synthesis of white opaque glass samples could additionally be reproduced in a wood-fueled Roman-type glass furnace. We could show that operating temperatures of 900 °C–1100 °C were sufficient for the formation of calcium antimonate.

Acknowledgements

This work was financially supported by the ProChance program (A1) of the Friedrich Schiller University Jena.

The authors acknowledge the Ancient Messene excavator Prof. P. Themelis and the Greek Ministry of Culture and Sports for permitting the scientific study of the *tesserae*. The permission to use the experimental archaeological Roman glass furnace at the Villa Borg, Perl (Germany) is also greatly acknowledged.

References

[1] F. Schweizer, Glas des 2. Jahrtausends v. Chr. im Ostmittelmeerraum, Verlag Bernhard Albert Greiner, Remshalden, 2003.
[2] A.J. Shortland, The use and origin of antimonate colorants in early Egyptian glass, Archaeometry 44 (4) (2002) 517–530, http://dx.doi.org/10.1111/1475-4754.t01-1-00083.
[3] M. Tite, A. Shortland, S. Paynter, The beginnings of vitreous materials in the near East and Egypt, Acc. Chem. Res. 35 (8) (2002) 585–593, http://dx.doi.org/10.1021/ar000204k pMID: 12186562. arXiv.
[4] D. Möncke, D. Palles, E. Palamara, M. Papageorgiou, E.I. Kamitsos, N. Zacharias, Coloring vitreous materials: pigments, colloids, and ions in glasses and glazes from the Mycenaean to Medieval periods– probed by spectroscopic techniques, in: N. Zacharias (Ed.), Archaiologiki Erevna Kai Nees Technologies. Proceedings of the 3rd ARCH. RNT, vol. 3, 2014, pp. 153–164.
[5] M. Di Bella, S. Quartieri, G. Sabatino, F. Santalucia, M. Triscari, The glass mosaics *tesserae* of "Villa del Casale" (Piazza Armerina, Italy): a multi-technique archaeometric study, Archaeol. Anthropol. Sci. 6 (4) (2014) 345–362, http://dx.doi.org/10.1007/s12520-013-0172-1.
[6] E. Gliozzo, A.S. Barbone, F. d'Acapito, Waste glass, vessels and window-panes from *Thamusida* (Morrocco): grouping natron-based blue-green and colourless Roman glasses, Archaeometry 55 (4) (2012) 609–639, http://dx.doi.org/10.1111/j.1475-4754.2012.00696.x.
[7] D. Möncke, M. Papageorgiou, A. Winterstein-Beckmann, N. Zacharias, Roman glasses coloured by dissolved transition metal ions: redox-reactions, optical spectroscopy and ligand field theory, J. Archaeol. Sci. 46 (2014) 23–36, http://dx.doi.org/10.1016/j.jas.2014.03.007.
[8] M. Papageorgiou, N. Zacharias, K. Beltsios, Technological and typological investigation of late Roman glass mosaic *tesserae* from Ancient Messene, Greece, in: D. Ignatiadou, A. Antanaras (Eds.), International Association for the History of Glass, Annales du 18e Congrés de l'Association Internationale pour l'Histoire du Verre, Thessalonique, 2009, 2012, pp. 241–248 OCLC: 910107896.
[9] N. Zacharias, F. Karavassili, P. Das, S. Nicolopoulos, A. Oikonomou, A. Galanis, E. Rauch, R. Arenal, J. Portillo, J. Roque, J. Casablanca, I. Margiolaki, A novelty for cultural heritage material analysis: transmission electron microscope (TEM) 3D electron diffraction tomography applied to Roman glass *tesserae*, Microchem. J. 138 (2018) 19–25, http://dx.doi.org/10.1016/j.microc.2017.12.023.
[10] E.V. Sayre, R.W. Smith, Analytical studies of ancient Egyptian glass, Recent Advances in Science and Technology of Materials vol. 3, Plenum Press, New York and London, 1974, pp. 47–70, http://dx.doi.org/10.1007/978-1-4684-7233-2_4.
[11] V. Muros, N. Zacharias, Lines, spots and trails: a microscopic and mineralogical study of antimonate-opacified glass beads from Lofkënd, Albania, J. Archaeol. Anthropol. Sci. 10 (2008) 1–14.
[12] H.E. Foster, C.M. Jackson, 'A whiter shade of pale'? Chemical and experimental investigation of opaque white Roman glass gaming counters, Glass Technol. 46 (5) (2005) 327–333.
[13] S. Lahlil, I. Biron, M. Cotte, J. Susini, New insight on the in situ crystallization of calcium antimonate opacified glass during the Roman period, Appl. Phys. A 100 (3) (2010) 683–692, http://dx.doi.org/10.1007/s00339-010-5650-z.
[14] S. Lahlil, I. Biron, M. Cotte, J. Susini, N. Menguy, Synthesis of calcium antimonate nanocrystals by the 18th dynasty Egyptian glassmakers, Appl. Phys. A 98 (1) (2010) 1–8, http://dx.doi.org/10.1007/s00339-009-5454-1.
[15] B.G. DeBoer, R.A. Young, A. Sakthivel, X-ray Rietveld structure refinement of Ca, Sr and Ba *meta*-antimonates, Acta Crystallogr. Sect. C: Struct. Chem. 50 (1994) 476–482, http://dx.doi.org/10.1107/S0108270193008480.
[16] L. Cai, J.C. Nino, Complex ceramic structures. i. Weberites, Acta Crystallogr. Sect. B: Struct. Sci. 65 (3) (2009) 269–290, http://dx.doi.org/10.1107/s0108768109011355.
[17] V. Gedzevičite˙, N. Welter, U. Schüssler, C. Weiss, Chemical composition and colouring agents of Roman mosaic and millefiori glass, studied by electron microprobe analysis and Raman microspectroscopy, Archaeol. Anthropol. Sci. 1 (1) (2009) 15–29, http://dx.doi.org/10.1007/s12520-009-0005-4.
[18] W. Vogel, Glass Chemistry, URL Springer, 2011, http://www.ebook.de/de/product/19299525/werner_vogel_glass_chemistry.html.
[19] F. Wiesenberg, Experimentelle Archäologie: Römische Glasöfen. Rekonstruktion und Betrieb einer Glashütte nach römischem Vorbild in der Villa Borg, Schriften des Archäologieparks Römische Villa Borg vol. 6, Kulturstiftung Merzig-Wadern, 2014.
[20] P. Themelis, Anaskafe messenes, Praktika tes en Athenais Archaeologekes Etaireias (2008) 31–46.
[21] S. Lahlil, Redécouverte des procédés d'opacification des verres à l'antimoine á travers l'Histoire. Etude des antimoniates de calcium., Ph.D. thesis vol. 12, Université Pierre et Marie Curie, Paris, 2010 URL https://tel.archives-ouvertes.fr/tel-00543276.
[22] A. Moropoulou, N. Zacharias, E. Delegou, B. Maróti, Z. Kasztovszky, Analytical and technological examination of glass *tesserae* from Hagia Sophia, Microchem. J. 125 (2016) 170–184, http://dx.doi.org/10.1016/j.microc.2015.11.020.
[23] E. Palamara, N. Zacharias, L. Papakosta, D. Palles, E. Kamitsos, J. Pérez-Arantegui, Studying a funerary Roman vessel glass collection from Patras, Greece: an interdisciplinary characterisation and use study, STAR: Sci. Technol. Archaeol. Res. 2 (2) (2016) 203–216, http://dx.doi.org/10.1080/20548923.2016.1239868.
[24] J. Henderson, The raw materials of early glass production, Oxf. J. Archaeol. 4 (3) (1985) 267–291, http://dx.doi.org/10.1111/j.1468-0092.1985.tb00248.x.
[25] A. Silvestri, G. Molin, G. Salviulo, R. Schievenin, Sand for Roman glass production: an experimental and philological study on source of supply, Archaeometry 48 (3) (2006) 415–432, http://dx.doi.org/10.1111/j.1475-4754.2006.00264.x.
[26] C.M. Jackson, S. Cottam, 'A green thought in a green shade'; compositional and typological observations concerning the production of emerald green glass vessels in the 1st century AD, J. Archaeol. Sci. 61 (2015) 139–148, http://dx.doi.org/10.1016/j.jas.2015.05.004.
[27] F. Gallo, A. Marcante, A. Silvestri, G. Molin, The glass of the "Casa delle Bestie Ferite": a first systematic archaeometric study on Late Roman vessels from Aquileia, J. Archaeol. Sci. 41 (2014) 7–20, http://dx.doi.org/10.1016/j.jas.2013.07.028.
[28] S. Maltoni, A. Silvestri, Innovation and tradition in the fourth century mosaic of the Casa delle Bestie Ferite in Aquileia, Italy: archaeometric characterisation of the glass *tesserae*, Archaeol. Anthropol. Sci. 10 (2) (2018), http://dx.doi.org/10.1007/s12520-016-0359-3.
[29] G. Molina, G. Odin, T. Pradell, A. Shortland, M. Tite, Production technology and replication of lead antimonate yellow glass from New Kingdom Egypt and the Roman Empire, J. Archaeol. Sci. 41 (2014) 171–184, http://dx.doi.org/10.1016/j.jas.2013.07.030.
[30] W. Johnston, Oxidation-reduction equilibria in molten $Na_2O{\cdot}2SiO_2$ glass, J. Am. Ceram. Soc. 48 (4) (1965) 184–190.
[31] W. Buss, Erhitzungsmikroskopische Untersuchungen von Vorgängen in Glasschmelzen mit und ohne sulfat, Glastechnische Berichte: Glass Sci. Technol. 35 (4) (1962) 167–176.

Optical Materials 76 (2018) 375–381

Contents lists available at ScienceDirect

Optical Materials

journal homepage: www.elsevier.com/locate/optmat

Copper-based opaque red glasses – Understanding the colouring mechanism of copper nanoparticles in archaeological glass samples

F. Drünert [a, *], M. Blanz [a, 1], K. Pollok [b], Z. Pan [a], L. Wondraczek [a], D. Möncke [c, d, *]

[a] Otto Schott Institute of Materials Research, University of Jena, Fraunhoferstraße 6, 07743 Jena, Germany
[b] Institute of Geosciences, University of Jena, Carl-Zeiss-Promenade 10, 07745 Jena, Germany
[c] Theoretical and Physical Chemistry Institute, National Hellenic Research Foundation, 48 Vassileos Constantinou Avenue, 11635 Athens, Greece
[d] Department of Built Environment and Energy Technology, Linnæus University, Hus N 2086, 351 95 Växjö, Sweden

ARTICLE INFO

Article history:
Received 23 October 2017
Received in revised form
15 December 2017
Accepted 29 December 2017
Available online 12 January 2018

Keywords:
Copper ruby
Copper nanoparticles
Mie-scattering
Medieval glasses
Opaque red glasses
Historical glass making practices

ABSTRACT

Red opaque glasses of two different sites in central Germany, a medieval glassworks in Glashütten, Taunus Mountains, and an early modern glassworks in Wieda, Harz Mountains, were analysed with regard to their optical appearance. By scanning electron microscopy and X-ray diffraction, metallic copper nanoparticles were identified as a conspicuous constituent in these glasses. In addition, similar opaque red glasses were reproduced in the laboratory in order to better understand the manufacturing process. Detailed analysis of the optical scattering was conducted in order to evaluate the role of Cu^0 nanoparticles in the colouring mechanism relative to other possible reasons of colouration.

We find clear differences between the possible contributions of Cu_2O (cuprite) particles and metallic copper (Cu^0) nanoparticles. Through simulated backscattering spectra we were able to calculate an average copper particle radius in the archaeological glass samples resulting in a value of up to 95 nm, which matches well the results of SEM investigation (minimum 65 nm). Using the methods we applied in this study, it becomes possible to reconstruct various processing conditions as they were applied in medieval manufacture of these particular materials.

1. Introduction

One of the very first colouring agents which were applied in early glass manufacture is a red dye based on copper, dated to the 15th century BCE [1]. Starting in that time, the number of red-coloured glass artefacts produced until today has increased in countless variants. The underlying mechanism of colouring, however, has become a subject of controversy. In his seminal book on glass colouration, in 1951, Weyl described four different types of copper-based reds, either opaque or transparent, all based on metallic particles [2]. In spite of this, as discussed within the same book, other authors assumed cuprite (Cu_2O) to be the main colouring agent. According to their assumptions, the native red colour of crystalline cuprite gives rise to the appearance of many opaque red glasses (e.g. [3]). Since then, numerous articles have been published, usually following one of the two theories [4–7]. Today we know that either view can be correct in its own right, depending on the glass system and the fabrication process [8,9]: Whereas copper nanoparticles are found in glasses with low amounts of copper and lead oxide, cuprite can precipitate in high-copper-high-lead glasses and leads to a lighter red (often described as 'sealing wax' [9]) to orange colouration. Due to differences in crystal structure, chemistry and morphology the nanoparticles can be distinguished by combining X-ray diffraction and SEM techniques [9,10].

Chemically, the formation of metallic copper nanoparticles in glass matrices was investigated in several studies, usually focusing on particle size and the rules of Ostwald ripening at various temperatures between 500 °C and 800 °C [11–13]. In contrast, the formation of cuprite particles is less investigated; however, it is known from comparable glass systems that cuprite can form at temperatures above 700 °C [14]. In the present context, it should be noted that most of these studies focused on qualitative and quantitative analysis of the particles and did not attempt to correlate the number and type of the observed particles with the visual

* Corresponding authors.
E-mail addresses: ferdinanddruenert@yahoo.de (F. Drünert), dmoencke@eie.gr (D. Möncke).
[1] Present address: Archaeology Institute, University of the Highlands and Islands, Orkney College UHI, Kirkwall KW15 1LX, UK.

https://doi.org/10.1016/j.optmat.2017.12.054
0925-3467/

appearance of their samples.

We now emphasise the difference of interaction between copper nanoparticles and light of specific energies. By solving the Maxwell equations for spherical objects, Mie theory can be used to calculate the backscattering and absorption efficiency factors of particles within the size of visible light wavelengths [15]. The absorption and scattering of nanoparticles of different compositions (e.g. metallic copper or Cu_2O) can be compared to such Mie simulations of the respective optical reflectance spectra. This allows estimating the effect of particle radii in the different samples. Even though Mie theory is fundamentally based on a spherical geometry of the particles, it can be applied in a good approximation to bulk particles.

As a major advantage, optical spectroscopy is a non-destructive technique and therefore is very suitable for the study of archaeological glass samples. When combining this approach with conventional studies on nanoparticle growth in glasses, new insights can be generated using relevant processing parameters of ancient technologies. Vice versa, the same knowledge can also be transferred to modern materials [16].

The archaeological glass fragments of this study originate from two different workshops in central Germany. They were selected because of the unusual abundance of such opaque red samples at these sites. For a more detailed understanding of the manufacturing process and as a reference, we will compare archaeological opaque red glass samples with laboratory-made model glasses.

1.1. Workshop 'Unterhalb Dornsweg', Glashütten/Taunus, Germany (15th century CE)

A large selection of red glass samples originate from a glassworks in the Taunus Mountains, Germany, dated to the mid-15th century CE. The excavation of the experimental workshop 'Unterhalb Dornsweg' in 2001–2005 revealed more than 25 kg of opaque red glass shards, vessel fragments and production residuals [17]. The broad variation of forms and manufacture techniques indicate a focus on high quality glass, presumably for the upper classes. Since the main kiln of the site was destroyed completely, it is assumed that the workshop was closed either for a renewal or as a consequence of a violent dispute. In any case, it was never rebuilt [17,18].

1.2. Weinglashütte Wieda/Harz, Germany (17th century CE)

A second group of glass samples originates from a Weinglashütte (winery glass works) in Wieda, Harz Mountains, Germany, with a documented period of productivity from 1608-1623 CE. It was excavated by the 'Archäologische Arbeitsgemeinschaft Wieda' between 1965 and 1979 as an important regional site of manufacture in its time and a good example of the extreme diversity of glass manufacture in that period. Diverse kinds of glassy vessel fragments of many colours were excavated, among them opaque red shards coloured with copper. Flat glass manufacture is documented in addition to container glass production. The glass manufacture was most likely stopped by hazards imposed by the 30-years war [19].

2. Materials and methods

2.1. Archaeological glass samples

The red glass samples from Glashütten, Taunus Mountains ('Unterhalb Dornsweg') show a broad variety of colour tones ranging from purple-red over red to brown. The hue differs also within the sample between surface and bulk. The latter can be observed at broken edges of the fragments. Some samples appear to be fully opacified (Fig. 1a – c), while other samples are partially transparent (Fig. 1d).

The Wieda glass samples appear more homogeneous. Most of the glasses have a dark-red, wine coloured appearance, sometimes shifted to almost black (Fig. 2a). While some glass fragments display only applications of red decorations on otherwise colourless glass samples (Fig. 2c), others are fully composed of opaque red bulk glass. Of special interest within the feature is a group of dichroic glass fragments, showing a red appearance in reflection, but appearing blue when looked upon in transmission (Fig. 2d).

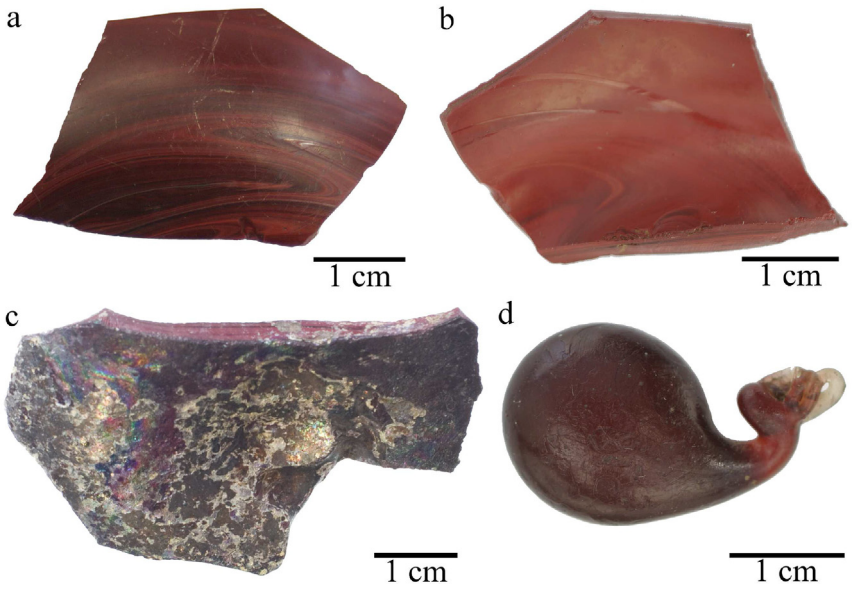

Fig. 1. Selected glass samples from Glashütten/Taunus Mountains: Front- (a) and reverse (b) of a vessel fragment showing a big difference in colour; a strongly corroded glass fragment (c); a partially transparent glass residue in whale shape (d). (For interpretation of the references to colour in this figure legend, the reader is referred to the Web version of this article.)

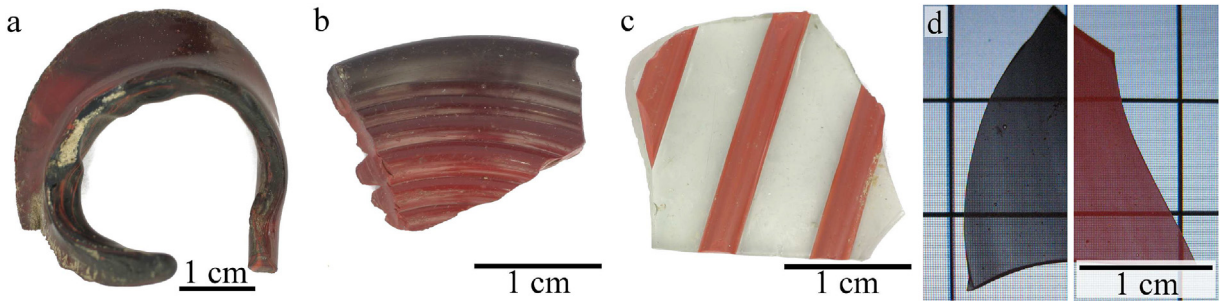

Fig. 2. Selected glass samples from Wieda/Harz Mountains: A piece of scrap that was cut off during production (a); vessel fragment made of opaque red bulk glass (b); colourless transparent base glass with red decoration (c); dichroic glass illuminated from below (d, left side) and the same sample illuminated from above (d, right side). (For interpretation of the references to colour in this figure legend, the reader is referred to the Web version of this article.)

Selected glass samples from the two archaeological excavations were cleaned and optical spectra were taken without further preparation. In addition, a few samples were cut, polished, and the measurements of polished and unpolished samples were compared.

2.2. Modern laboratory glass samples

Based on the glass composition of the Taunus glass samples, a model glass with the molar composition $63SiO_2 \cdot 27CaO \cdot 6Na_2O \cdot 3Al_2O_3 \cdot 1Cu_2O$ (in wt%: 61% SiO_2, 26% CaO, 6% Na_2O, 5% Al_2O_3, 2% Cu_2O) was selected for melting experiments in the laboratory. Quartz powder, calcium carbonate, sodium carbonate, aluminium hydroxide, copper(I) oxide and metallic copper powder (all 99.5%) were used as raw materials. 1% starch was added as a reducing agent; the batch was melted at 1300 °C in an inductive heated furnace under air or under argon atmosphere, to avoid oxidation of copper by oxygen. The glasses were cast on a brass block and subsequently annealed from 550 °C to room temperature at 2 K min^{-1}. No further heat treatment step was used for striking. Example images of the model glasses are shown in Fig. 3.

2.3. Analytical methods

Selected polished glass samples were analysed by scanning electron microscopy (SEM, FEI Quanta 3D FEG). The composition of archaeological samples was determined by energy-dispersive X-ray spectroscopy (SEM-EDX) and X-ray fluorescence (XRF, Eagle III with *Visions 2* software). The reflectivity and, whenever possible, the absorption were analysed from 300 nm to 2000 nm with a UV/Vis/NIR spectrophotometer (Agilent Cary 5000). Reflectivity measurements were performed using an integration sphere with an integration time of 10 s nm^{-1}. Crystalline phases in the glasses were identified by powder X-ray diffraction (XRD, Rigaku Miniflex 600) using the databases of the International Centre for Diffraction Data (ICDD) and the Crystallography Open Database (COD).

2.4. Computation

A Mie scattering model [20] is employed in this work to evaluate the scattering effects arising from interactions between a plane incident light wave and glasses with spherical particles embedded. This model assumes dilute as well as homogeneous particle distributions and calculates wavelength dependent backscattered coefficients at given particle sizes, which serve further as base functions in the fit to the experimental curve. A least square fit is then carried out to find out the coefficients corresponding to base functions for different particle sizes. Finally the particle distribution is obtained by normalizing each of the obtained coefficients to their sum. The fit program is coded in *Matlab* (v. R2017a). The source of wavelength dependent refractive indices in a range of 310 nm–2000 nm of a comparable glass system (standard soda-lime silicate glass NCS 16/10: $74SiO_2 \cdot 16Na_2O \cdot 10CaO$ [21]) and of copper [22] were used for computation.

Table 1
Glass composition of sample sets from Wieda (Harz, Germany) and 'Unterhalb Dornsweg', Glashütten (Taunus, Germany) measured by SEM-EDX quantitative analysis. Differences to 100% occur due to rounding.

	'Unterhalb Dornsweg'				Wieda glassworks			
	R1		R5		H1		H3	
	wt%	mol%	wt%	mol%	wt%	mol%	wt%	mol%
SiO_2	55.0	54.9	54.9	54.8	58.8	56.4	56.4	57.5
Na_2O	2.9	2.8	2.8	2.7	4.7	4.6	4.3	4.3
K_2O	2.9	1.8	2.7	1.7	4.7	3.0	5.1	3.3
Cl^-	1.4	2.3	1.1	1.9	0.9	1.6	0.9	1.5
MgO	3.7	5.5	4.0	5.9	3.4	5.1	3.6	5.4
CaO	25.4	27.2	25.7	27.4	17.5	19.0	18.7	20.5
P_2O_5	3.6	1.5	3.1	1.3	2.4	1.0	2.4	1.1
Al_2O_3	1.8	1.1	2.3	1.3	3.1	1.9	3.7	2.2
TiO_2	0.5	0.4	0.5	0.4	0.5	0.4	0.7	0.5
FeO	0.6	0.5	0.9	0.8	1.5	1.3	1.3	1.1
MnO	1.3	1.1	1.4	1.1	1.7	1.5	1.7	1.5
Cu^0	0.9	0.9	0.6	0.5	1.9	1.8	1.3	1.2

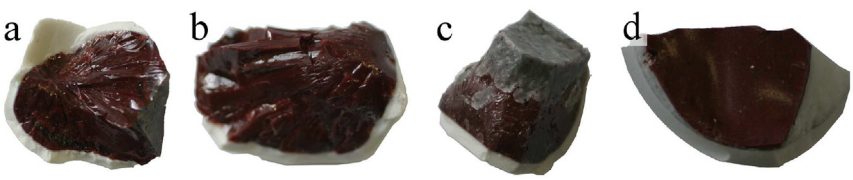

Fig. 3. Modern model glass samples produced by different methods: Glass samples molten under argon atmosphere (a); model glass with addition of iron oxide and manganese oxide (b, c); opacified model glass remolten on top of colourless base glass (d). The white fragments are remains of alumina crucibles used for the melting process.

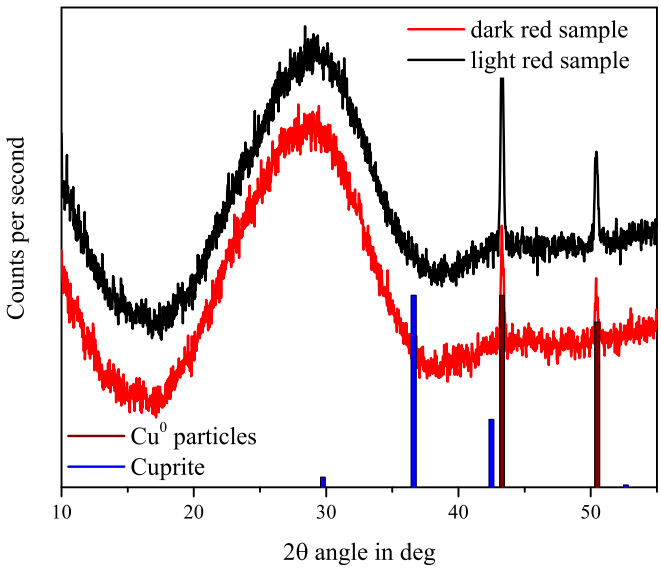

Fig. 4. X-ray diffraction pattern of two powdered, differently coloured archaeological glass samples from Wieda, Harz Mountains. The top spectrum (black) is from a light red sample comparable to Fig. 1b, the bottom spectrum (red) is from a dark red sample comparable to Fig. 2a. (For interpretation of the references to colour in this figure legend, the reader is referred to the Web version of this article.)

3. Results and discussion

3.1. Quantitative chemical analysis

The average chemical composition of selected glass samples from Glashütten (Taunus) and Wieda (Harz) obtained by SEM-EDX is shown in Table 1. The results listed for the Taunus samples are in good agreement with the data given by Wedepohl and Kronz [23]. Comparable to the Taunus samples, the glass samples from Wieda have lower levels of K^+ and higher levels of Ca^{2+} ions and can therefore be classified as a HLLA-type glass (high lime low alkali glass, see Schalm et al. [24]).

A reason for these untypically low K^+ and high Ca^{2+} concentrations could be the use of dead-wood ashes, that is, from ashes of leaves, bark and roots of beech trees, which leads to an increase of the Ca^{2+} to K^+ ratio compared to ashes from tree trunks [25]. Additional use of lime as a raw material is deduced from the Ca^{2+} to Mg^{2+} ratio >4. Such glasses are typically described as wood-ash lime glass [25]. Increased amounts of chloride and sodium ions indicate the use of NaCl as flux to compensate the low amount of potassium ions [23,24,26].

3.2. Phase identification of crystalline particles

The XRD pattern (Fig. 4) shows the usual hump caused by the broad distribution of bond angles in glasses. Furthermore, at $2\theta = 43^\circ$ and 50° the presence of peaks indicate the presence of metallic copper particles. Other peaks, which would be indicative of cuprite (30°, 36° and 42°) or further crystalline compounds, could not be observed.

Inspection of the samples by SEM (Fig. 5) reveals two kinds of particles: Occasional spheres larger than 1μm which are irregularly distributed across the sample, and small crystallites with a diameter up to 130 nm, spread within striae throughout the whole sample. SEM-EDX analysis of the large spheres reveals the presence of only sulphur and copper with a molar ratio of ca. 1:1, possibly indicating residual CuS from the employed raw materials, which hints at the use of slags or copper ores. In contrast, smaller crystallites show elevated amounts of copper in comparison to the bulk

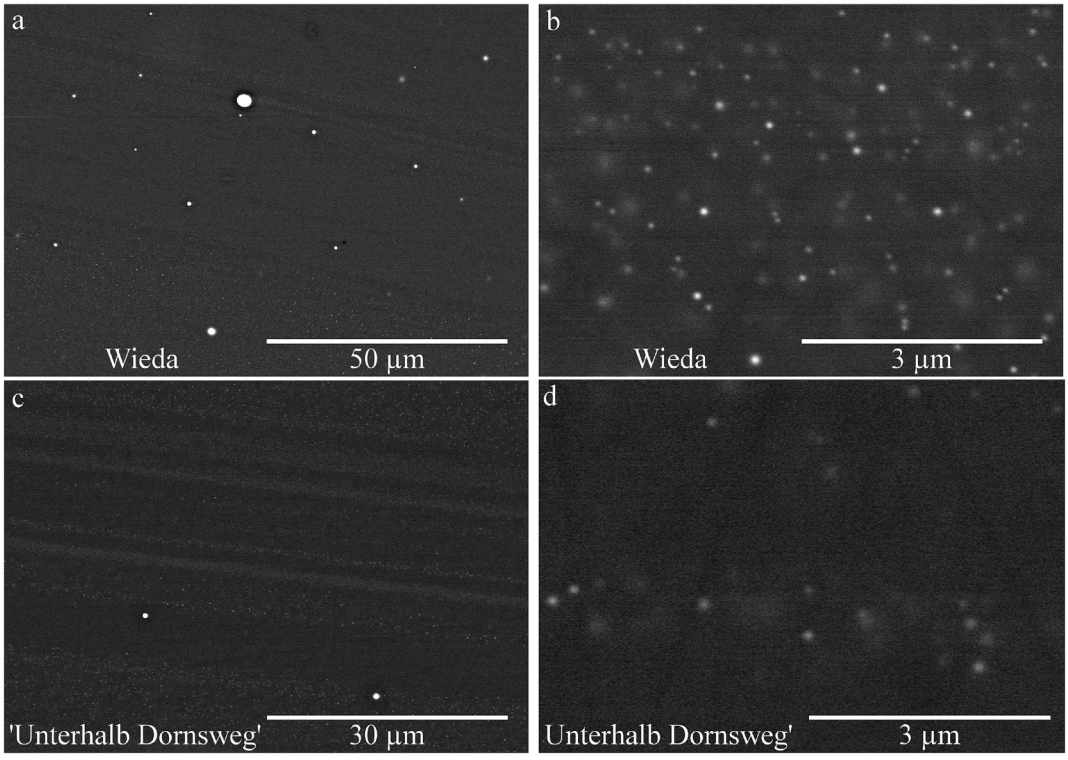

Fig. 5. Representative SEM backscattered electron images (BSE, ETD) of a Taunus sample ('Unterhalb Dornsweg' R1) and a Harz sample (Wieda H3). Both glasses show inclusions of particles (ca. 1μm diameter), while the size distributions of the small particles differ within sample set and striae (see a and c). In both sample sets the small particles are of comparable size (see b and d).

glass, while sulphur is generally below the detection limit of SEM-EDX.

3.3. Optical spectroscopy

Fig. 6 shows representative measurements of spectral absorbance and reflectance from the two sites (reflectance spectra for Wieda only) and from a model glass sample. The absorption band at 560 nm indicates the expected plasmonic resonance band of copper nanoparticles (see [11]), whereas, due to the much lower molar extinction coefficients of electronic *d-d* transitions, no bands from transition metal ions (e.g. Fe^{2+} at 1000 nm or Mn^{3+} at 500 nm) are visible. In contrast to the medieval red samples, the model glass shows a small band of Cu^{2+} with a maximum at 800 nm, due to an incomplete reduction of Cu^{2+} ions during melting.

The reflectivities of both the Taunus glass sample and the model glass sample each show a dominant band, with maxima at 725 nm and 800 nm, respectively. At lower wavelengths a strong decrease at about 575 nm is obvious in both spectra. Values within the noisy range from 800 nm to 900 nm were not considered for analysis because they have too much uncertainty. The noise, as well as the jump observed in other glass samples is caused by a change of monochromators and cannot always be avoided in glasses with inhomogeneities such as striae or scratches.

To understand the interaction of light with the spherical copper nanoparticles in a surrounding glass matrix, we calculated the absorption and backscattering efficiency factors of differently sized particles within a range of 400 nm–1000 nm wavelength (see Fig. 7 top). All spectra show a prominent band at ca. 540 nm, often accompanied by a second, variable band at lower wavelengths. The highest absorption occurs at particle radii between 25 nm and 45 nm, whereas particles with a radius below 10 nm show almost no absorption. In all cases, the observed absorption is limited to wavelengths below 590 nm.

Contrary to the absorption spectra, the first maximum of the backscattering efficiency factor Q_{back} for a particle radius of 45 nm is located at 590 nm, shifting to higher wavelengths with an increasing particle radius (Fig. 7 bottom). In every calculation, a sharp edge towards shorter wavelengths is visible. Furthermore, overtones of this maximum occur at the same wavelength for particle radii $r = 130$ nm, $r = 190$ nm and $r = 270$ nm. Significant backscattering efficiency is limited to particles with a radius smaller than 30 nm.

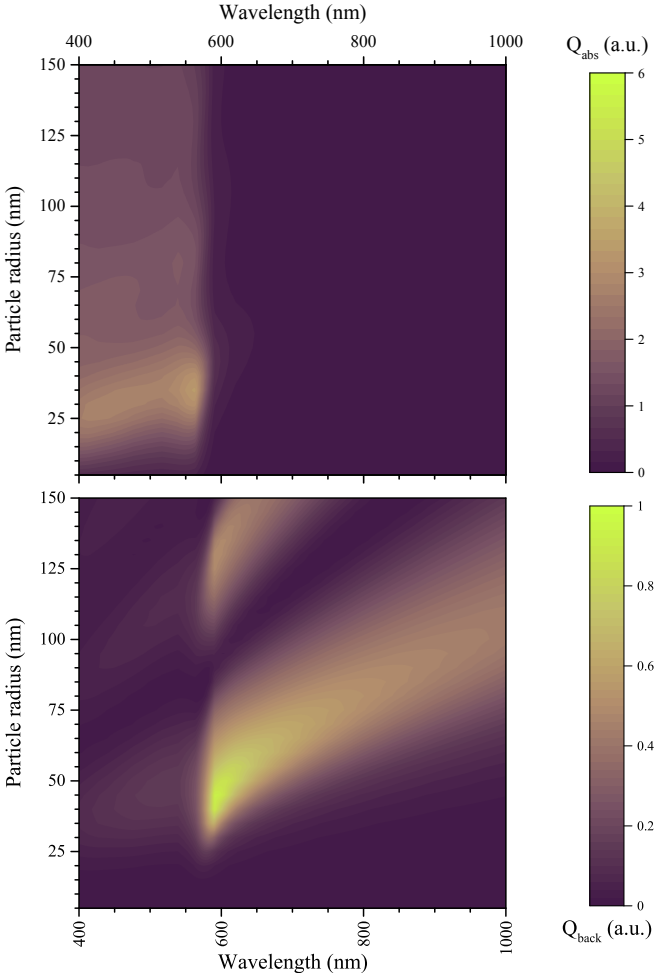

Fig. 7. Computed absorption (top) and backscattering (bottom) efficiency factors of metallic copper nanoparticles dependent on wavelength and particle radius.

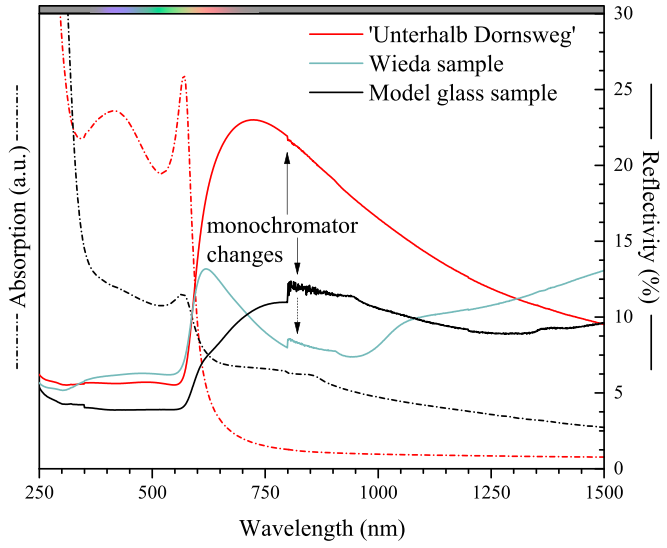

Fig. 6. Comparison of the absorption and reflectance spectra of a polished sample from the Taunus Mountains ('Unterhalb Dornsweg'), a Harz sample (Wieda) and a model glass. Absorption spectra were taken from samples polished to 100 μm thickness. Spectral jumps, as seen in the reflection spectra between 800 nm and 900 nm, often appear in inhomogenous samples with striae or unpolished surfaces.

Unlike metallic copper nanoparticles, cuprite (Fig. 8) shows a broad absorption efficiency not limited to values below 560 nm. The formation is very characteristic of a global maximum, accompanied by several smaller bands (or shoulders) at higher wavelengths. With increasing particle size the band positions shift to higher wavelengths. The maximum of the backscattering efficiency of spherical cuprite particles is strongly wavelength dependent. While the scattering intensity of particle radii below 30 nm is negligible, larger particles lead to a very broad band, where the maximum shifts to higher wavelenghts with increasing particle radii. Additionally, overtones of the first maximum will form for particle radii $r = n \cdot 50$ nm $(n = \{1, 2, 3, \ldots\})$. The overtones' backscattering intensity is usually higher than the first maximum. It should be noted that with increasing particle radius the model of spherical particles may decrease in accuracy due to the usually dendritic shape of Cu_2O crystals.

Comparison of the simulated spectra for cuprite-containing glasses with the actual optical measurements reveal clear differences that support the presence of Cu^0 nanoparticles. All spectra show the very characteristic scattering edge towards shorter

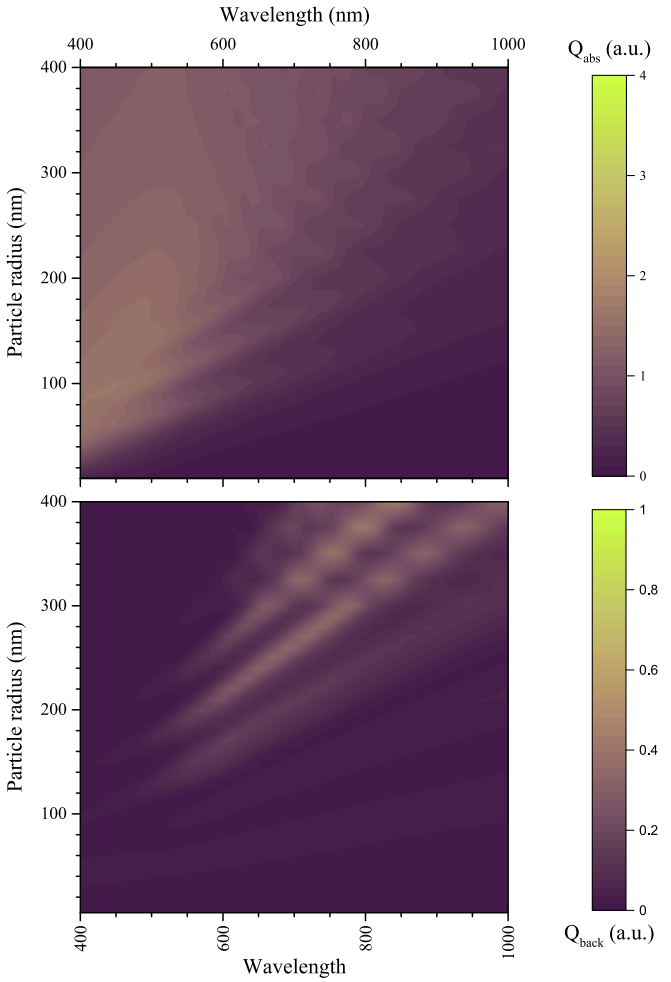

Fig. 8. Computed absorption (top) and backscattering (bottom) efficiency factors of cuprite nanoparticles dependent on wavelength and particle radius.

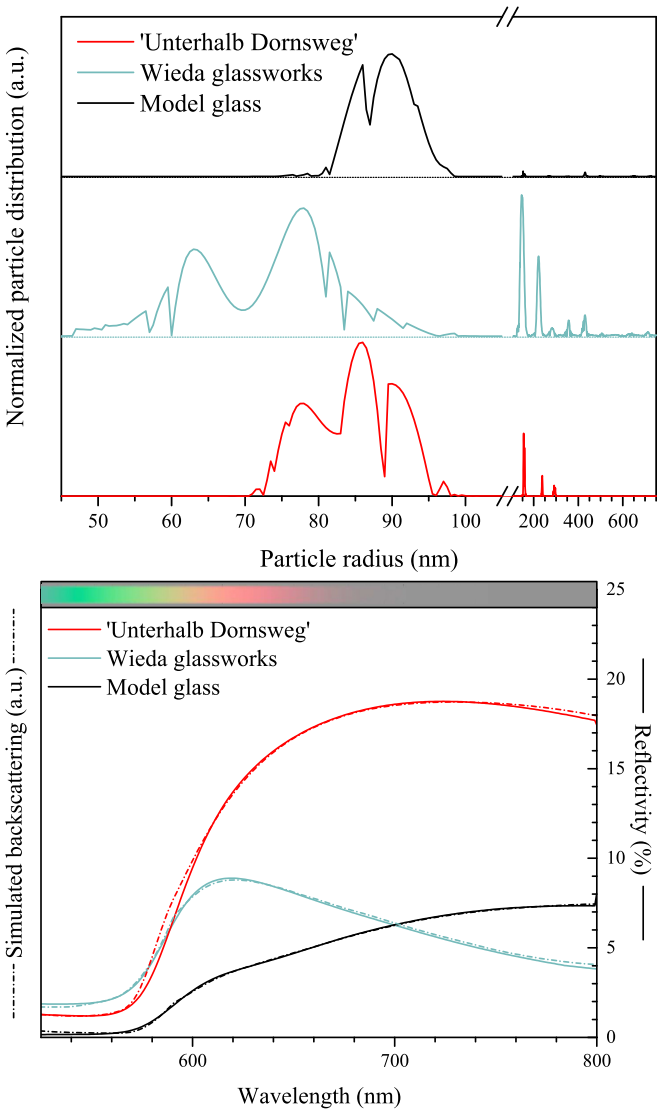

Fig. 9. Particle distribution (top) calculated by fitting the reflection measurements to fitted backscattering spectra (bottom). In the bottom diagram the fit is compared to the actual measurements.

wavelengths, but not the broad scattering band that is expected for cuprite. Furthermore, by fitting a computed curve to the actual reflectivity measurements it is possible to estimate a distribution of particles within our glass samples (Fig. 9). As seen in the figure, the smallest particle radii (between 60 nm and 80 nm) are attributed to the sample from Wieda, Harz Mountains, whereas the particles in the glass samples from 'Unterhalb Dornsweg', Taunus Mountains, are rather large, at 70 nm to 95 nm. The reflectivity of the modern model glass sample is attributed to particles with a radius between 80 nm and 95 nm. Minor deviations, as seen in the bottom figure, may be explained by the poor sample homogeneity (compare Fig. 5c), by differences between the used refractive indices and the ones of the specific glass matrix and by corrosion based phenomena on the surfaces of the archaeological samples.

Different particle radii in the *in-situ* prepared glass samples might occur from varying melting temperatures: The high amount of alkali ions in the Harz glass sample (see Table 1) enable lower melting temperatures compared to the Taunus glass sample ('Unterhalb Dornsweg'). The medieval glasses are assumed to have been prepared at temperatures lower than the model glass melting temperature of 1500 °C. Furthermore, the archaeological samples were formed using a blow pipe or were added as decoration on mouth blown clear glass. Irrespective of the exact production process, repeated reheating at working temperatures of 1100 °C to 1400 °C [27] will also affect nucleation and growth rates [28]. Therefore, particle radii could also be used as a process indicator of the archaeological glass samples.

UV/Vis reflectance spectroscopy can be performed without extensive sample preparation, and is non-destructive. In contrast, multiple corrosion layers on the surface, as known from the literature (e.g. [29]) prohibit SEM investigation of samples without broken edges or polishing, whereas the influence of thin corrosion layers on colour, as for most of our studied samples, is negligible. Since plasmonic resonance is of very strong intensity with high coefficients of attenuation, other effects will be small compared to copper-based light interaction.

4. Conclusion

UV/Vis reflectance spectroscopy is a very useful, non-destructive tool to determine the sizes of plasmonic particles. Optical spectroscopy does not only allow distinguishing different colouring species in transparent glasses or opaque or non-transparent glass ceramics, but fitting the spectra to calculated backscattering efficiency factors even allows us to estimate average particle sizes of

metallic copper nanoparticles. In comparison to the SEM measurements (minimum radius 65 nm), only slightly larger particle radii of up to 95 nm were calculated from the observed spectra. Therefore it could be proven that UV/Vis reflectance spectroscopy is a very good alternative to SEM preparation for the determination of particle radii, despite poor sample homogeneity, corrosion effects and non-planar surfaces.

Furthermore, our experimentation on the reproduction of glasses with nanoparticle colouring showed that an *in-situ* preparation is possible using strongly reducing furnace atmospheres, without the necessity of a second striking process at 500 °C to 800 °C. Due to the guideline 'as simple as possible' and the fact that a separate heat treatment after the formation of the vessels would lead to deformation of the products, we propose that the sampled opaque red glasses of the two sites were produced without a further heat treatment step.

Acknowledgements

This work was financially supported by the ProChance program (A1) of the Friedrich Schiller University Jena, the RISE program of the Deutschen Akademischen Austauschdienst (DAAD) and the Deutsche Forschungsgemeinschaft (DFG LA830/14-1).

The authors also want to thank Ingrid Berg, Ursula Rempel and Peter Steppuhn for providing the archaeological glass samples, Mike Lippold for SEM sample preparation, Vinzenz Mehner for preliminary studies including finding a way to prepare red opaque model glasses and Oliver Mecking for quantitative analysis during these preliminary studies. The authors are also grateful to Kristin Griebenow and Aaron Reupert for fruitful discussions.

References

[1] A.J. Shortland, The use and origin of antimonate colorants in early Egyptian glass, Archaeometry 44 (4) (2002) 517–530, https://doi.org/10.1111/1475-4754.t01-1-00083.
[2] W.A. Weyl, Coloured Glasses, seventh ed., Society of Glass Technology, 2016.
[3] A. Ram, S. Prasad, On the origin of colour in copper ruby glasses, in: Proc. Natl. Inst. Sci. India A vol. 26, 1960, pp. 11–25.
[4] R.H. Brill, N.D. Cahill, A red opaque glass from Sardis and some thoughts on red opaques in general, J. Glass Stud. 30 (1988) 16–27.
[5] A.N. Shugar, Byzantine opaque red glass tesserae from Belt Shean, Israel, Archaeometry 42 (2) (2000) 375–384, https://doi.org/10.1111/j.1475-4754.2000.tb00888.x.
[6] D. Barber, I. Freestone, K. Moulding, From Mine to Microscope, Oxbow Books and the David Brown Book Company, Ch. 11: Ancient Copper Red Glasses: Investigation and Analysis by Microbeam Techniques, 2009, pp. 117–128.
[7] A. Silvestri, S. Tonietto, G. Molin, P. Guerriero, The palaeo-christian glass mosaic of St. Prosdocimus (Padova, Italy): archaeometric characterisation of tesserae with copper- or tin-based opacifiers, J. Archaeolog. Sci. 42 (2014) 51–67, https://doi.org/10.1016/j.jas.2013.10.018.
[8] M.J. Hughes, A technical study of opaque red glass of the Iron Age in Britain, Proc. Prehist. Soc. 38 (1972) 98–107, https://doi.org/10.1017/s0079497x00012068.
[9] N. Brun, L. Mazerolles, M. Pernot, Microstructure of opaque red glass containing copper, J. Mater. Sci. Lett. 10 (23) (1991) 1418–1420, https://doi.org/10.1007/BF00735696.
[10] J. Zhu, Y. Yang, W. Xu, D. Chen, J. Dong, L. Wang, M.D. Glascock, Study of an archeological opaque red glass bead from China by XRD, XRF, and XANES, X Ray Spectrom. 41 (6) (2012) 363–366, https://doi.org/10.1002/xrs.2411.
[11] C. Càpàţînà, The study of copper ruby glass, Ceramics Silikáty 49 (4) (2005) 283–286.
[12] Q. Zhang, G. Chen, G. Dong, G. Zhang, X. Liu, J. Qiu, Q. Zhou, Q. Chen, D. Chen, The reduction of Cu^{2+} to Cu^{+} and optical properties of Cu^{+} ions in Cu-doped and Cu/Al-codoped high silica glasses sintered in an air atmosphere, Chem. Phys. Lett. 482 (4) (2009) 228–233, https://doi.org/10.1016/j.cplett.2009.09.105.
[13] J.J. Kunicki-Goldfinger, I.C. Freestone, I. McDonald, J.A. Hobot, H. Gilderdale-Scott, T. Ayers, Technology, production and chronology of red window glass in the medieval period – rediscovery of a lost technology, J. Archaeolog. Sci. 41 (2014) 89–105, https://doi.org/10.1016/j.jas.2013.07.029.
[14] N.M. Pavlushkin, P.D. Sarkisov, N.Y. Mikhailenko, Phase transformations in Cu-containing glasses of the SiO_2-Al_2O_3-CaO-K_2O system, Glass Ceram. 40 (1) (1983) 20–23, https://doi.org/10.1007/BF00698816.
[15] R.J.D. Tilley, Colour and the Optical Properties of Materials: an Exploration of the Relationship between Light, the Optical Properties of Materials and Colour, 2th ed, Wiley, 2011.
[16] R.A. Ganeev, A.I. Ryasnyanskii, A.L. Stepanov, T. Usmanov, Ganeev, Nonlinear absorption of visible light in silicate glasses doped with copper nanoparticles.pdf, Quant. Electron. 33 (12) (2003) 1081–1084, https://doi.org/10.1070/QE2003v033n12ABEH002557.
[17] P. Steppuhn, Waldglashütten im Taunus, Geschichte, Archäologie, Produkte., Schriftenreihe des Hessischen Freilichtmuseums, Heft 13, Freilichtmuseum Hessenpark, 2006.
[18] P. Steppuhn, Archäologie einer Glashüttenlandschaft – Der Hochtaunus, Ber. d. Komm. f. Arch. Landesforsch. in Hess. 9 (2009) 21–129, 2006/2007.
[19] U. Rempel, Die frühneuzeitliche Weinglashütte bei Wieda/Südharz, in: Glashüttenlandschaft Europa, Verlag Schnell & Steiner GmbH, Regensburg, 2008, pp. 192–196.
[20] C. Bohren, D.R. Huffman, Absorption and Scattering of Light by Small Particles, Wiley Science Paperback Series, 1998, https://doi.org/10.1002/9783527618156.
[21] M. Rubin, Optical properties of soda-lime silica glass, Sol. Energy Mater. 12 (4) (1985) 275–288, https://doi.org/10.1016/0165-1633(85)90052-8.
[22] S. Babar, J.H. Weaver, Optical constants of Cu, Ag, and Au revisited, Appl. Opt. 54 (3) (2015) 477, https://doi.org/10.1364/ao.54.000477.
[23] K.H. Wedepohl, A. Kronz, Die Glaszusammensetzung dreier spätmittelalterlicher Hütten auf dem Taunus-Kamm unweit Glashütten, Ber. d. Komm. f. Arch. Landesforsch. in Hess. 9 (2009) 135–151.
[24] O. Schalm, K. Janssens, H. Wouters, D. Caluwé, Composition of 12–18th century window glass in Belgium: non-figurative windows in secular buildings and stained-glass windows in religious buildings, Spectrochim. Acta Part B 62 (6–7) (2007) 663–668, https://doi.org/10.1016/j.sab.2007.03.006.
[25] K.H. Wedepohl, Chemical composition of medieval glass from excavations in West Germany, Glastechn. Ber. Glass Sci. Technol. 70 (8) (1997) 246–255.
[26] S. Siwadamrongpong, M. Koide, K. Matusita, Prediction of chloride solubility in CaO–Al_2O_3–SiO_{-2} glass systems, J. Non Cryst. Solids 347 (1) (2004) 114–120, https://doi.org/10.1016/j.jnoncrysol.2004.07.063.
[27] G. Eramo, The glass-melting crucibles of Derrière Sairoche (1699–1714 AD, Ct. Bern, Switzerland): a petrological approach, J. Archaeolog. Sci. 33 (3) (2006) 440–452, https://doi.org/10.1016/j.jas.2005.09.002.
[28] W. Vogel, Glass Chemistry, Springer, 2011.
[29] T. Lombardo, L. Gentaz, A. Verney-Carron, A. Chabas, C. Loisel, D. Neff, E. Leroy, Characterisation of complex alteration layers in medieval glasses, Corros. Sci. 72 (2013) 10–19, https://doi.org/10.1016/j.corsci.2013.02.004.

Einblick in die Chemie und Physik der Farbigkeit und Opazität von Gläsern

Ferdinand Drünert[1], Nikolaos Zacharias[2], and Doris Möncke[*1,3]

[1]Friedrich Schiller University Jena, Otto Schott Institute of Materials Research, Germany

[2]University of Peloponnese, Dept. of History, Archaeology and Cultural Resources Management, Laboratory of Archaeometry, Kalamata, Griechenland

[3]Alfred University, Inamori School of Engineering, Alfred (NY), USA

Zusammenfassung

Viele Ionen der Übergangsmetalle bilden in Silicatgläsern Komplexe unterschiedlicher Farbigkeit und Farbintensität aus. In diesem Kapitel werden für die Glasherstellung bedeutende farbgebende Ionen besprochen und wichtige chemische und physikalische Hintergründe der Farbigkeit erklärt. Die unterschiedlichen Blautöne von Cobalt- (Co^{2+}), Kupfer- (Cu^{2+}) und Eisenionen (Fe^{2+}) werden an Hand der optischen Spektren römischer Gasproben (*tesserae* aus dem antiken Messene, Peloponnes, GR) und an Hand nachgeschmolzener Modellgläser diskutiert. Dabei wird auch auf die Sensitivität des menschlichen Auges sowie auf die Abhängigkeit der Farbintensität von der Wahrscheinlichkeit der für den Farbeindruck so wichtigen elektronischen Übergänge eingegangen. Zudem werden am Beispiel der Reaktionen des Kupfers, Eisens und des Mangans Redox-Gleichgewichte erläutert und deren Einfluss auf die Farbigkeit sowie im Fall von Antimon und Mangan auch auf die Läuterung und Entfärbung diskutiert.

*dmoencke@eie.gr

Submitted to: Forschungen und Berichte zur Archäologie in Baden-Württemberg

Summary

The dissolution of transition metal ions in silicate glasses often results in coloured complexes of different hues and intensities. This chapter will discuss important colouring ions and the chemical as well as physical mechanisms that rule colour perception. The different blue hues of cobalt- Co^{2+}, copper- Cu^{2+} und iron ions Fe^{2+} will be discussed on the example of optical spectra of Roman glass *tesserae* (Ancient Messene, Peloponnese, GR) and from remade model glasses. Attention is given to the sensitivity of the human eye, and changes of colouring intensity due to sample thickness, ion concentration and to the probability of electronic transitions, which are fundamental for absorption colours. On the example of cupper, iron and manganese ions, redox equilibria will be discussed in regard to glass colour and in the case of manganese and antimony also on fining and decolourization.

1 Einleitung

Die Vielfalt der Farbtöne, in denen Glas hergestellt werden kann, gibt diesem Material neben seiner Transparenz einen besonderen Reiz. Von einem physikalischen Blickpunkt aus kann aus dem optischen Spektrum eines farbigen Glases auf die Art der Dotierungen und Verunreinigungen geschlossen werden. Weiterhin können aus den vorliegenden Redox-Gleichgewichten auch Informationen zu den Schmelzbedingungen während der Herstellung gewonnen werden.

In der optischen Spektroskopie wird die Änderung der Transmission einer Glasprobe Wellenlänge für Wellenlänge über den gesamten sichtbaren Bereich (380 nm bis 780 nm) gemessen. Kommerzielle Spektrometer schließen dabei den ultravioletten Bereich (von 200 nm bis 380 nm), sowie den nahen infraroten Bereich (780 nm bis 3200 nm) mit ein (Abb. 1).

Die optischen Spektren opaker Glasproben lassen sich im Gegensatz zu transparenten Glasproben nicht in Transmission messen, können aber in Reflexion sehr wohl bestimmt werden. Neben einer Integrationskugel, wie in kommerziellen Laborgeräten, gibt es auch tragbare Alternativen, die über Glasfaserkabel *in-situ* eingesetzt werden können (Fiber Optics Reflectance Spectroscopy, FORS). Auch wenn quantitative Bestimmungen wie das Lambert-Beer'sche Gesetzt für Reflexionsmessungen nicht angewandt werden können, lassen sich doch auch in diesen Proben zerstörungsfrei und relativ einfach Farbkomplexe identifizieren.

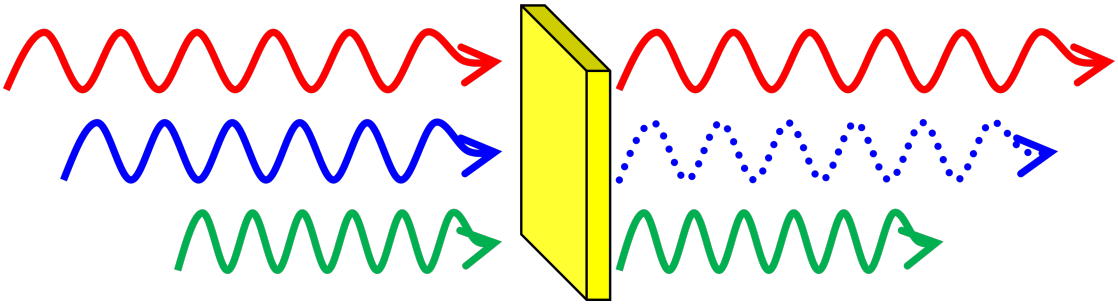

Abbildung 1: Eine Glasprobe absorbiert das Licht verschiedener Wellenlängen und färbt das Licht dadurch in der Komplementärfarbe. Die UV/Vis/NIR-Spektroskopie quantifiziert dieses Licht in Abhängigkeit von der Wellenlänge.

1.1 Färbung durch *d*-*d*-Übergänge

In Übergangsmetallen sind die sogenannten d-Orbitale, d.h. die verschiedenen energetisch fast gleichwertigen möglichen Aufenthaltsbereiche der Außenelektronen, nicht vollständig besetzt. Diese leeren Orbitale können durch andere Außenelektronen des Ions vorübergehend besetzt werden, wenn dem Ion die Energiedifferenz zwischen dem energetisch günstigeren Grundzustand und dem etwas ungünstigeren angeregten Zustand zugeführt werden kann. Bei einer Absorption des Lichts gibt ein Photon einer bestimmten Wellenlänge diese Energie in das System ab, sodass dem vormals weißen Lichtspektrum diese Farbe entnommen wird. In Folge dessen erscheint uns das entsprechende Objekt mit den enthaltenen Übergangsmetallionen farbig in der zugehörigen Komplementärfarbe. Da Gläser amorphe Systeme sind, in denen durch eine Vielzahl von verschiedenen Strukturen und Verzerrungen von Bindungsabständen und Bindungswinkel eine Bandbreite von energetischen Zuständen entstehen, bilden sich für jeden Übergang relativ breite Absorptionsbanden aus, die auch Zustände mit leicht erhöhten und erniedrigten Energien umfassen. In Kristallen mit genau vorgegebenen Kristallgittern werden dagegen viel schmalere Absorptionsbanden als in Gläsern beobachtet.

Übergangsmetallionen haben fünf äußere Orbitale, die, in Abwesenheit eines elektromagnetischen Feldes, insgesamt zehn energetisch gleichwertige Elektronen aufnehmen können. Im Glas werden jedoch die Übergangsmetallionen von den Sauerstoffionen im Silicatnetzwerk umgeben (sie formen einen Komplex), sodass sich die Orbitale je nach Struktur des Komplexes und der Neigung der beteiligten Sauerstoffionen, Elektronen aufzunehmen und abzugeben, in verschiedene energetische Zustände aufspalten. Dies ist, schematisch in Abb. 2 gezeigt, am Beispiel von Cu^{2+} gut zu verstehen: Das d^9-Ion Cu^{2+} hat neun Elektronen in den äußersten Orbitalen (Valenzorbitale, in der Abbil-

dung jeweils als Strich dargestellt). Kupfer-Ionen sind in Gläsern in der Regel von sechs Sauerstoffionen umgeben (man spricht von sechs-facher bzw. oktaedrischer Koordination). Ein Komplex kann zusätzlich, wie im Fall von Kupfer(II)-Ionen, verzerrt auftreten, d.h. die beiden Sauerstoffliganden der Längsachse haben einen etwas anderen Abstand als die vier äquatorialen Liganden. Dieses Phänomen wird auch Jahn-Teller-Verzerrung genannt, wodurch die Orbitale eine weitere Aufspaltung erfahren (Abb. 2c). Cu^+, als d^{10} Ion, hat mit zehn Elektronen eine voll besetzte Außenschale, daher kann kein Elektron in einen energetisch höheren Zustand angehoben werden. Gläser, welche nur Cu^+ Ionen enthalten, sind daher farblos.

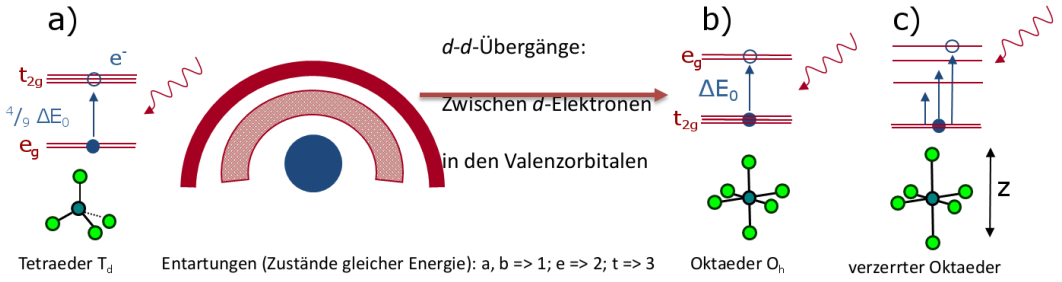

Abbildung 2: Elektronische Übergänge der Valenzelektronen von Übergangsmetallionen. Die Energie des Übergangs zwischen dem Grundzustand und dem angeregten Zustand ($t2g$ und eg) entspricht der Wellenzahl ν (cm^{-1}) oder der Absorptionswellenlänge $\lambda = h/\nu$ in nm (Möncke u. a. 2014).

Die Intensität der *d-d* Übergänge kann durch quantenmechanische Regeln abgeschätzt werden. Ein maßgeblicher Faktor für die Übergangswahrscheinlichkeit ist die Punktsymmetrie, d.h. ob jedes der umgebenden Sauerstoffionen einen Gegenpart auf der gegenüberliegenden Seite hat. Wenn eine Punktsymmetrie vorliegt, wie z.B. bei einer oktaedrischen Koordination, ist ein *d-d* Übergang mit einem Faktor von etwa 0,01 deutlich weniger wahrscheinlich als bei nicht punktsymmetrischer Koordination, wie z.B. bei tetraedrischer Anordnung (Wiberg/Wiberg 2007; Duffy 1990).

1.2 Färbung durch Ladungsaustausch / Charge-Transfer Prozesse

Ähnlich wie die *d-d*-Übergänge können Elektronen auch, angeregt von Licht geeigneter Energie, von einem Ion zum nächsten übertragen werden. In diesen *Charge-Transfer* (CT) Übergängen findet also eine Interaktion zweier benachbarter Ionen statt und ist am Beispiel des Fe^{3+}−O-Übergangs wie folgt zu verstehen: Ein Elektron des zweifach negativ geladenen Sauerstoffions wird kurzfristig zum Eisenion verschoben, sodass folgende

Reaktionsgleichung abläuft:

$$Fe^{3+}{-}O^{2-} \rightleftharpoons Fe^{2+}{-}O^{-} \tag{1}$$

Dieselbe Reaktion kann auch rückwärts ablaufen, verläuft aber üblicherweise durch Energieabgabe ohne Emission von Licht. Da diese Absorption quantenmechanisch nicht verboten ist, sind die Intensitäten der Übergänge üblicherweise extrem hoch. Im Fall der Übergangsmetallionen findet der Übergang im UV-Bereich statt. Ein sehr bekanntes Beispiel für diese CT-Übergänge ist der Übergang zwischen Fe^{3+} und S^{2-}, der für das deutlich leichter polarisierbare Sulfidion in den sichtbaren Bereich verschoben ist (Abb. 3a). Dieser Effekt wird weiter unten ausführlich beschrieben.

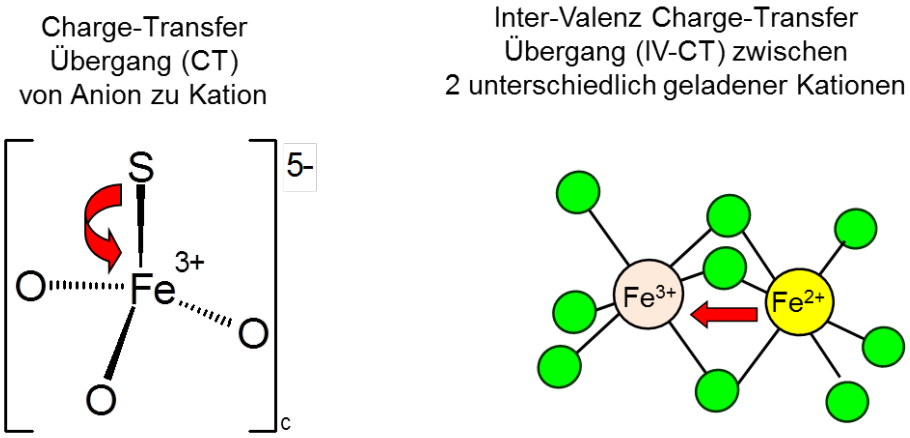

Abbildung 3: (a, links) elektronische *Charge-Transfer* Übergängen von Anionen wie Sauerstoff oder Sulfid-Ionen, zu den Kationen eines Farbkomplexes. (b, rechts) *Intervalence Charge Transfer* Übergänge verschieben Elektronen von einem Metallion zum nächstgelegenen passenden Nachbarion.

Ein Sonderfall der CT-Übergänge sind die *Intervalence Charge Transfer* (IV-CT) Übergänge (Abb. 3b). Der Begriff *Intervalence* beschreibt hier einen Übergang zwischen zwei verschiedenen Metallionen wie z.B. Mn^{2+} und Fe^{3+}, aber auch Fe^{2+} und Fe^{3+}. Auch diese Übergänge sind sehr intensiv, erfordern allerdings höhere Konzentrationen an entsprechenden Metallionen um die entsprechende räumliche Nähe zu gewährleisten (Duffy 1990).

1.3 Färbung durch Lichtstreuung

Elektronische Übergänge der Übergangsmetallionen sind die häufigste, aber nicht die einzige Ursache für Färbungen. Auch kleine, oftmals kristalline Partikel können durch die Streuung des Lichts eine Farbe hervorrufen. Das bekannteste Beispiel für diesen Mechanismus ist das Kupferrubinglas, welches durch die Interaktion der Elektronen dieser etwa 20 nm-80 nm großen metallischen Kupferkügelchen mit dem eingestrahlten Licht bei etwa 520 nm Wellenlänge die typische Farbe erhält. Dabei hängt die Wellenlänge des Absorptionsmaximums von der Größe, Zusammensetzung und Form der Partikel ab (Moores/Goettmann 2006). Weitere Beispiele für in Glas vorkommende Nanopartikel sind Silber- und Goldrubine. Die Herstellung solchermaßen gefärbter Rubingläser ist deutlich komplizierter als die der zuvor beschriebenen Lösungsfarben, da oft eine zusätzliche Temperaturbehandlung der Gläser erforderlich ist, um die Nanopartikel in der gewünschten Größe auszufällen. Für rot gefärbte Glasproben stellten sie lange Zeit jedoch die einzige Färbemöglichkeit dar und wurden erst in neuerer Zeit durch die deutlich günstigeren Cadmiumselenid-Anlaufgläser ersetzt (Weyl 2016; Bamford 1977; Vogel 2011).

Eine auf Lichtstreuung basierende Gruppe von Gläsern sind weiß getrübte Glasproben. Für weiß gefärbtes Glas eignen sich eine ganze Reihe Materialien, von eingebrachten Luftbläschen zu Calcitpartikeln, von untergemengtem Quarzmehl zu entmischten Gläsern (Maltoni/Silvestri 2016). Die älteste bekannte Methode der Herstellung weißer Glasauflagen findet man mit Calciumantimonat bereits in ägyptischen Glasproben (Shortland 2002). In diesen Glasproben wird das Licht weitestgehend wellenlängenunabhängig an der Oberfläche mehrfach gestreut, sodass durch die diffuse Reflexion des Lichts die Probe weiß erscheint. Teilweise wurde dieser Mechanismus auch durch färbende Partikel (z.B. orangerotes Cuprit, Shugar 2000; Neapelgelb / Bleiantimonat, Lahlil u. a. 2011) oder durch Mischung von Lichtstreuung und Absorption durch gelöste Farben (z.B. grünes undurchsichtiges Glas durch Kombination von Neapelgelb mit blauer Glasmatrix, ebd.) kombiniert.

1.4 Das Lambert-Beer'sche Gesetz

Die Farbigkeit einer Glasprobe ist theoretisch genau abschätzbar. Die Absorption A in Abhängigkeit von einer Wellenlänge λ (d.h. der negative dekadische Logarithmus der Differenz aus eingestrahltem Licht I_0 und gemessenem, transmittiertem Licht I_T) ist demnach von der Dicke d der jeweiligen Probe, der Konzentration c der jeweiligen färbenden Ionen und dem zugehörigen molaren Extinktionskoeffizienten ϵ_λ abhängig.

Dieser Zusammenhang wird im Lambert-Beer'schen Gesetz wie folgt zusammengefasst:

$$A_\lambda = \log \frac{I_0}{I_{T\,\lambda}} = \epsilon_\lambda \lambda \cdot c \cdot d \tag{2}$$

Einige molare Extinktionskoeffizienten können der Literatur entnommen werden. Hierbei muss jedoch beachtet werden, dass sich der molare Extinktionskoeffizient nicht nur in Abhängigkeit von der Glaszusammensetzung ändert, sondern auch, dass in der Literatur oftmals der Anteil der jeweiligen Oxidationsstufe verschiedener polyvalenter Ionen nicht bei der Ermittlung berücksichtigt wurde. Der tatsächliche Wert ϵ der absorbierenden Spezies ist dementsprechend oftmals nicht bekannt.

Der molare Extinktionskoeffizient kann als Maß der Übergangswahrscheinlichkeit gesehen werden und zeigt, ob ein Ion oder ein Komplex eine starke oder schwache Farbwirkung hervorrufen wird. In Tabelle 1 sind die molaren Extinktionskoeffizienten verschiedener Ionen in Kalk-Natron-Silicatgläsern aufgeführt.

Tabelle 1

Ion	Übergang	Umgebende Sauerstoffionen	Absorptionsmaximum [nm]	ϵ [$\mathrm{L\,mol^{-1}\,cm^{-1}}$]
Co^{2+}	*dd*	4	595	180 bis 220
Cu^{2+}	*dd*	6	ca. 800	25
Mn^{3+}	*dd*	6	480	135
Mn^{2+}	*dd*	6	420	0.3
Fe^{3+}	*dd*	4 bis 6	435, 555, 770	3 bis 5
Fe^{2+}	*dd*	4 bis 6	1050	30 bis 50
$Fe^{3+} - O$	CT	–	UV	2500
$Fe^{2+} - S$	CT	–	410 nm	9000

Im Folgenden sollen vor allem die bekannteren Lösungsfarben unterschiedlicher Übergangsmetallionen in nachgeschmolzenen Modellgläsern sowie in Glasfragmenten und Mosaik *tesserae* aus dem Antiken Messene in Griechenland, Peloponnes (Papageorgiou/ Zacharias 2010; Papageorgiou u. a. 2012), besprochen werden. Die einzelnen Probenzusammensetzung sind den angegebenen Referenzen (Möncke u. a. 2014) zu entnehmen.

2 Cobalt und Kupfer

Cobaltblau ist ein sehr intensiver Farbkomplex von vierfach koordinierten Co^{2+}-Ionen, der auch in sehr geringen Konzentrationen andere Farben zu überdecken vermag. Cu^{2+}

gibt Gläsern in niedrigen Konzentrationen eine himmelblaue Färbung, die in hohen Konzentrationen tief türkis wirkt. Chemische Analysen blauer Gläser finden häufig ähnliche oder sogar deutlich höhere Gehalte an CuO im Vergleich zu CoO wodurch oft beide oder sogar nur Kupferionen als farbgebendes Ion der Proben angegeben werden. Im Gegensatz zur optischen Spektroskopie können aus quantitativen Analysen jedoch keinerlei Aussage zu dem Cu^{2+}/Cu^{+} Verhältnis getroffen werden. Aus UV/Vis-Spektren können dagegen alle wesentlichen farbgebenden Ionen problemlos bestimmt und teilweise auch quantifiziert werden (z.B. Bamford 1977).

Aus chemischer Perspektive sind die drei charakteristischen Absorptionsbanden mit den entsprechenden Absorptionsmaxima bei 540, 590 und 640 nm auf die tetraedrische Koordination des Co^{2+} zurückzuführen (Möncke u. a. 2014; Bates 1962; Ehrt u. a. 2001; Ferguson 2007; Paul 1990; Mirti u. a. 1993). Der molare Extinktionskoeffzient von Co^{2+} bei 590 nm ist mit etwa $200\,\mathrm{L\,mol^{-1}\,cm^{-1}}$ für einen $d-d$-Übergang vergleichsweise hoch. Diese hohe Intensität wird durch die tetraedrische Koordination des Cobaltions hervorgerufen. Im Vergleich erscheint der Übergang des oktaedrisch koordinierten Kupfer(II)-Ions (d^9) mit einem Bandenmaximum bei 800 nm deutlich weniger intensiv (Duffy 1990; Wong/Austin 1976; Popescu u. a. 2000). Da der für den Menschen sichtbare Wellenlängenbereich nur bis etwa 780 nm reicht, verringert sich die Intensität der Farbwahrnehmung von CuO als Pigment zusätzlich. Weiterhin ist das Redox-Gleichgewicht von $Cu^{2+} + e^{-} \rightleftharpoons Cu^{+}$ zu beachten, was dazu führt, das nicht nur die türkisen Cu^{2+} Ionen, sondern auch ein beträchtlicher Anteil farbloser Cu^{+} Ionen im Glas vorliegen kann. Cobalt tritt dagegen in konventionellen Gläsern immer zweiwertig als Co^{2+} und nicht in anderen Oxidationszahlen auf. Ein Beispiel für die unterschiedliche Farbwahrnehmung von Cobalt- und Kupferhaltigen Gläsern soll in Abb. 4a gezeigt werden: Die optischen Absorptionsspektren verschiedener Natron-Kalk-Silicat-Modellgläser, welche 0.1 ma% CoO bzw. 0.3 ma% CuO enthalten, unterscheiden sich sowohl in ihrem Absorptionsmaximum als auch in der Absorption im sichtbaren Bereich zwischen 400 nm und 750 nm generell erheblich. Zusätzlich ist die Intensität der cobaltblauen Glasproben trotz des geringeren Anteils im Glas erheblich höher im Vergleich zur mit Kupfer gefärbten Glasprobe. Erst bei erheblichen Anteilen an CuO im Glas, hier mit ca. 3 %, tritt eine vergleichbare Farbtiefe ein. Zum Vergleich enthält Abb.4a auch das Spektrum eines Glases, das sowohl 0.1 ma% CoO als auch 0.3 ma% CuO enthält. Wie zu erwarten dominiert auch hier CoO das Erscheinungsbild des Spektrums. Für den Betrachter erscheint die entsprechende Glasprobe als typisches mit Cobalt gefärbtes Glas, während die Farbimpression des Kupfers nur bei cobaltfreien Gläsern auftritt.

Bei intransparenten Glasproben (Abb. 4b) ist die Messung des transmittierten Lichts

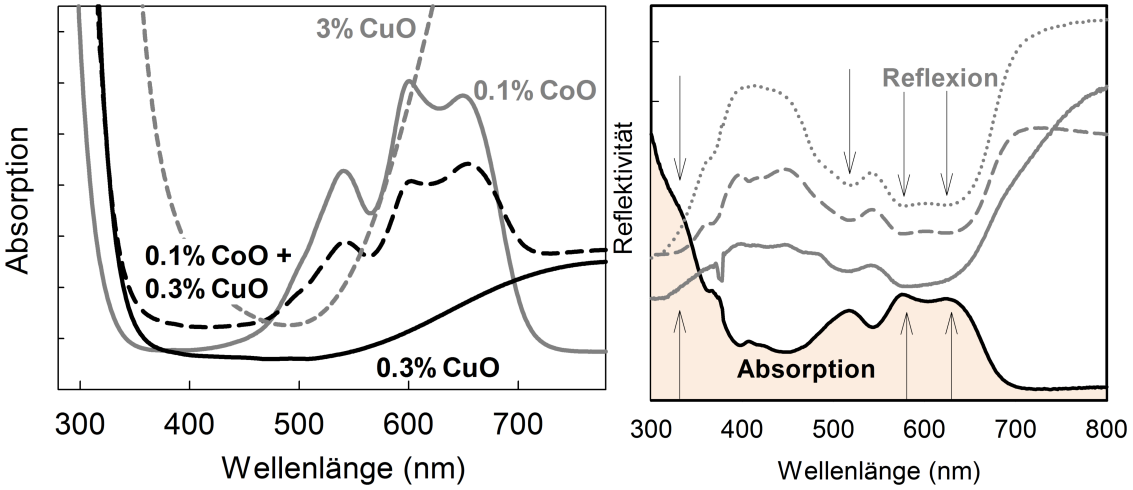

Abbildung 4: (a, links) Optische Absorptionsspektren von Kupfer- und Cobalt-haltigen Glasproben. Selbst bei deutlich höheren Anteilen an CuO tritt das Spektrum von Co^{2+} gut sichtbar hervor. (b, rechts) Optische Reflexionsspektren von Cobalthaltigen Mosaik *tesserae* aus Messene, Griechenland, 1. – 4. Jh. u.Z. im Vergleich mit einem Co^{2+}-Transmissionsspektrum (Möncke u. a. 2014).

nicht möglich. Dennoch können derartige Proben mit Hilfe von Reflexionsmessungen qualitativ analysiert werden: Durch die Streuung des Lichts an etwaigen Partikeln, Blasen o.ä. wird das eingestrahlte Licht diffus reflektiert. Da das Licht sowohl vor- als auch nach dem Streuprozess das Probenmaterial durchfährt, wird ein Teil des reflektierten Lichts absorbiert. Die so erhaltenen Spektren haben Ähnlichkeit mit einem Transmissionsspektrum, wodurch im Vergleich zur Absorption die entsprechenden Banden horizontal gespiegelt erscheinen. Die in Abb. 4b gezeigten Proben sind gleichzeitig ein gutes Beispiel für optische Messungen an historischen Proben: Während das Spektrum der Cobalt-Ionen sehr deutlich hervortritt, sind oftmals Sprünge und unerwartete Signale sichtbar. Diese Sprünge sind auf unregelmäßige Probenoberflächen, streuende Partikel und Bläschen sowie auf Verunreinigungen innerhalb des Glases zurückzuführen.

3 Eisen

Eisen ist in Gläsern entweder in der himmelblauen zweiwertigen, gelben dreiwertigen Form enthalten, oder, was am häufigsten zu sehen ist, in einer grünen Mischform (Bamford 1977; Bingham/Jackson 2008; Kühne 1976; Leistner/Ehrt 1999; Schreurs/Brill 1984; Volotinen u. a. 2008).

3.1 *d-d*-Übergänge

Eisen(III)-Ionen weisen mehrere schwache Banden bei 380, 420 und 435 nm auf. Die drei Banden werden üblicherweise dem tetraedrisch koordinierten Fe^{3+} zugeordnet, wobei sich die etwas breiteren oktaedrischen Banden mit den Tetraederbanden überlagern (Volotinen u. a. 2008).

Eisen(II)-Ionen zeigen in der Regel eine breite Absorptionsbande, deren Maximum wie schon für Cu^{2+}-Ionen besprochen, außerhalb der menschlichen Wahrnehmung liegt. Die Ausläufer dieser breiten Bande absorbieren aber im gelben Wellenlängenbereich, wodurch diese Gläser himmelblau gefärbt sind. Wie für Cu^{2+}, findet sich in silicatischen Gläsern für Fe^{2+} bevorzugt eine vermutlich verzerrte oktaedrische Koordination, während die Banden der tetraedrische Koordination um die 2000 nm teilweise durch die im Glas vorhandenen Banden des gebundenen Wassers (Si−OH) überlagert werden (ebd.). Abb. 5 zeigt die Banden verschiedener geschmolzener Modellgläser mit unterschiedlichen Fe^{2+}:Fe^{3+} Gehalten.

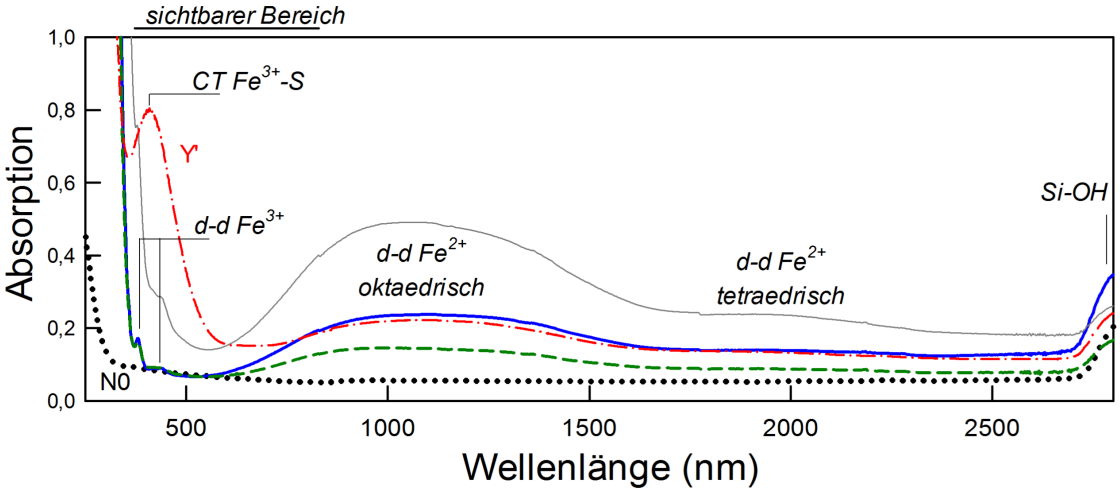

Abbildung 5: Absorptionsspektrum verschiedener eisenhaltiger Glasproben. Sichtbar sind die charakteristischen Banden des Fe^{2+}, Fe^{3+} und des Fe^{3+} − S *CT* Übergangs.

Eisen(II) Ionen haben einen zehnmal höheren molaren Extinktionskoeffizient im Vergleich zu Eisen(III)-Ionen, weshalb eisenhaltige Gläser weniger stark gefärbt erscheinen wenn das Redox-Gleichgewicht der Eisenionen weiter auf die oxidierende Seite geschoben ist. Sorgfältige Betrachtung von Abb. 5 zeigt, dass eine leichte Verschiebung dieses Gleichgewichts nur geringe Auswirkungen auf die Intensität der Banden des Eisen(III) im UV-Bereich hat. Eine Verschiebung des Gleichgewichts wirkt sich aber enorm auf die

Intensität der breiten NIR Bande (1050 nm) des Fe^{2+} aus. Im gezeigten Beispiel wird der Anteil an Fe^{2+} von 10 % auf 15 % des gesamten Eisengehaltes erhöht, was eine Zunahme der breiten Bande bei 1050 nm um 50 % bewirkt. Der Rückgang des Fe^{3+}-Gehaltes von 90 auf 85 % macht sich dagegen kaum in der Intensität der schmaleren 380 nm Bande bemerkbar.

In Abb. 6 soll verdeutlicht werden, welche Schwierigkeit eine akkurate Analyse der Eisenbanden mit sich bringt: Durch die intensive Überlappung diverser Banden ist eine exakte Analyse oftmals schwierig. Da es sowohl für Fe^{2+} als auch für Fe^{3+} mehrere Übergangsmöglichkeiten durch die Verzerrung der jeweiligen Koordinationszentren gibt, muss eine solche Analyse immer sehr genau mit der existierenden Literatur zu den Bandenübergängen (z.B. Volotinen u. a. 2008; Bingham/Jackson 2008 etc) verglichen werden. Für die Betrachtung der Verhältnisse zwischen Fe^{2+} und Fe^{3+} ist allerdings eine genaue Entfaltung aller Banden nicht immer erforderlich. Insbesondere bei Proben ohne störende Banden im Bereich von 380 nm und von 1000 nm nm kann das Verhältnis aus den unterschiedlichen optischen Dichten (d.h. der Intensität der Absorption je cm) berechnet werden (Bamford 1977). Ein Beispiel für eine entsprechende Anwendung ist in Drünert u. a. (in press) in diesem Band beschrieben.

Insgesamt zeigt sich, dass Eisenionen keine so starke Färbewirkung wie Cobalt- oder Kupferionen besitzen. Weiterhin ist wohl in vielen Glasproben Eisen eher als unvermeidliche Verunreinigung, denn bewusst als Färbemittel einzuordnen.

Da die deutlich gelb gefärbten Gläser nur mit Hilfe von oxidierenden Zusätzen zur Glasmasse hergestellt werden können, muss in solchen Proben allerdings von einem bewussten Farbwunsch ausgegangen werden. Ein mögliches Oxidationsmittel für Gläser ist Salpeter ($MeNO_3$).

3.2 Eisensulfid

Einige Glasproben zeigten eine tief gelbe bis braune Färbung, die jedoch nicht auf oxidierende, sondern auf stark reduzierende Schmelzbedingungen zurückzuführen ist. Dies lässt sich an einer starken Bande bei 410 nm erkennen. Im Gegensatz zu der blass gelben Färbung des Fe^{3+}-Ions ($d-d$-Übergang) in oxidierend geschmolzenen Gläsern ist diese tiefgelbe bis tiefbraue Färbung zwar ebenfalls auf Fe^{3+} Ionen zurückzuführen, beruht allerdings auf einem *Charge-Transfer* Übergang zwischen einem Sulfid-Anion (S^{2-}) und Fe^{3+}, d.h. der Ausbildung eines $[Fe^{III}O_3S]$ Komplexes. Um Sulfidionen in der Schmelze zu stabilisieren müssen extrem reduzierende Bedingungen herrschen, z.B. durch die Zugabe von organischen Materialien, da sonst Schwefel zu Sulfationen oxidiert wird. Dies bedeutet, dass die Mehrheit (70 %-90 %) der Eisenionen als reduzierte Fe^{2+} Spezies vorliegen

(Bamford 1977).

Wie bereits in Abb. 3 schematisch gezeigt, unterscheiden sich Charge-Transfer Übergänge, von den in Abb. 2 gezeigten intraatomaren $d-d$-Übergängen nicht nur dadurch, dass der Elektronenübergang zwischen zwei verschiedenen Atomen stattfindet, sondern auch durch ihre viel höhere Farbintensität. Der Charge-Transfer Übergang von Sauerstoffionen zu Fe^{2+} oder Fe^{3+} liegt bei höheren Energien im UV Bereich (etwa 210 nm, Fe^{2+} und 250 nm, Fe^{3+}) (Bamford 1977; Schreurs/Brill 1984; Volotinen u. a. 2008). Der CT-Übergang von S^{2-} zu Fe^{3+} liegt jedoch bei 410 nm und ist damit zu niedrigeren Energien in den sichtbaren Wellenlängenbereich verschoben. Der molare Extinktionskoeffizient für diesen Übergang liegt bei $9000\,\mathrm{L\,mol^{-1}\,cm^{-1}}$ und ist damit fast 50 mal höher als der molare Extinktionskoeffizient der besonders stark färbenden Co^{2+} Ionen ($\epsilon = 200\,\mathrm{L\,mol^{-1}\,cm^{-1}}$) (Bamford 1977; Duffy 1990; Mirti u. a. 1993; Schreurs/Brill 1984).

Beispiele für optische Spektren sind in Drünert u. a. (in press) in diesem Band enthalten.

4 Mangan

Viele der eher reduzierend geschmolzenen leicht grün-gelben eisenhaltigen römischen Glasfragmente zeigen eine schwache, schmale Bande um 420 nm (Abb. 6a). Diese Bande ist auf Mn^{2+} Ionen zurückzuführen, die entweder als Verunreinigungen der Rohmaterialien (Rohstoffe, Scherben) eingetragen wurden oder beim Entfärben der Gläser durch Reduktion höherwertiger Manganionen (z.B. Braunstein, MnO_2) entstanden sind. Die Übergänge der Mn^{2+}-Ionen sind durch die halb besetzten d-Orbitale sowohl nach der Laporte-Regel verboten als auch durch die für den Übergang erforderliche, aber quantenmechanisch unwahrscheinliche Umkehrung des Elektronenspins und haben daher einen sehr niedrigen molaren Extinktionskoeffizienten ($\epsilon = 0.5\,\mathrm{L\,mol^{-1}\,cm^{-1}}$). Unter oxidierenden Bedingungen bildet sich jedoch das sehr intensiv lila gefärbte Mn^{3+}-Ion, welches auf eine breite Absorptionsbande mit Maximum um die 500 nm nm zurückzuführen ist (Bamford 1977; Bates 1962; Duffy 1990; Ferguson 2007; Möncke u. a. 2011). Optische Spektren manganreicher Gläser sind in Abb. 6b dargestellt. Der Übergang der Mn^{3+}-Ionen erfolgt ohne Umkehr des Elektronenspins und hat daher mit $\epsilon = 135\,\mathrm{L\,mol^{-1}\,cm^{-1}}$ einen fast ebenso hohen molaren Extinktionskoeffizienten wie Co^{2+} ($\epsilon = 200\,\mathrm{L\,mol^{-1}\,cm^{-1}}$).

In den meisten antiken Gläsern wurde MnO_2, welches auch untern dem Namen „Glasmacherseife“ bekannt ist, als Entfärbungsmittel zugegeben (Bingham/Jackson 2008).

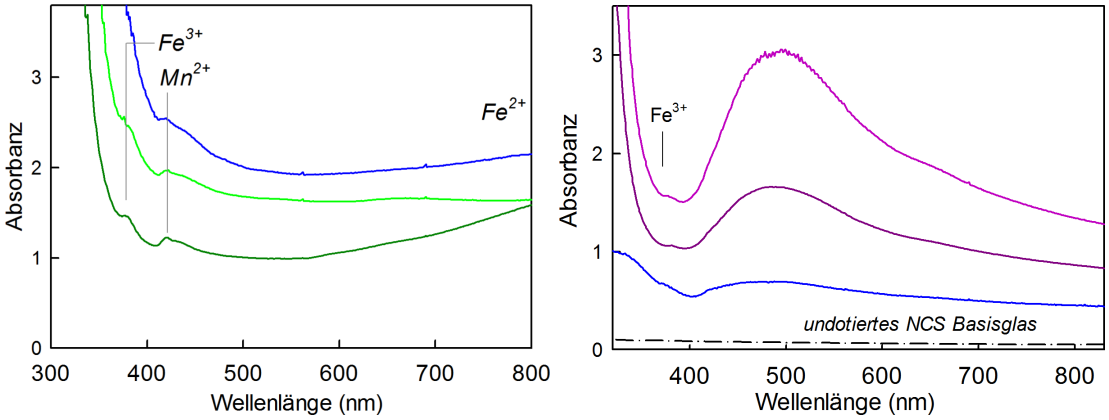

Abbildung 6: (a, links) Mn^{2+} ist als schwache Bande bei ca. 420 nm zu erkennen. (b, rechts) Die Bande des Mn^{3+} ist im Vergleich zum Mn^{2+} deutlich intensiver bei ca. 500 nm und sorgt für eine intensive violette Färbung.

Das Mn^{4+} des Braunsteins ist in Natron-Kalk-Silicatgläsern nicht stabil und wird sofort zu Mn^{3+} oder Mn^{2+} reduziert, wobei andere polyvalenten Ionen oxidiert werden (z.B. $Fe^{2+} \rightleftharpoons Fe^{3+} + e^-$). Dieser Effekt ist in Abb. 7 dargestellt. Die Absorption der Fe^{2+}-Bande nimmt deutlich ab, die der Fe^{3+}-Bande nur wenig zu und zusätzlich ist das resultierende Spektrum im sichtbaren Bereich durch die schwache Absorption der Mn^{3+}-Bande insgesamt relativ ausgeglichen. Durch diese relativ homogene Absorption erscheint das Glas für den Betrachter nahezu farblos. Im Vergleich zu einem aus hochreinen Rohstoffen geschmolzenen Glas wird durch die Erhöhung der grundlegenden Absorptionsbasislinie so chemisch ein entfärbtes Glas in dicken Schichten etwas dunkler erscheinen. Dieses Redoxgleichgewicht und somit auch die Glasfarbe kann auch von anderen polyvalenten Ionen wie Kupfer oder Antimon beeinflusst werden.

5 Schwarzes Glas

Wenn Eisen- und Manganionen in hohen Konzentrationen, also mit mehreren Prozent Massenanteil, in Gläsern vorliegen, sind diese oft so dunkel gefärbt, dass sie nahezu kein Licht mehr durchlassen und intransparent schwarz erscheinen. Dies ist für Obsidian bekannt, aber z.B. auch in verschiedenen römischen Mosaik *tesserae* konnten unterschiedliche Schwarztöne identifiziert werden. In Reflektionsspektren von drei solchen Mosaik *tesserae* oder in sehr dünnen Absplitterungen und Kanten ist zu erkennen, dass die drei schwarzen Proben eigentlich eine grünliche, orangene oder lila-purpurne Grundfarbe besitzen. Durch den Vergleich mit den quantitativen Analysen können diese

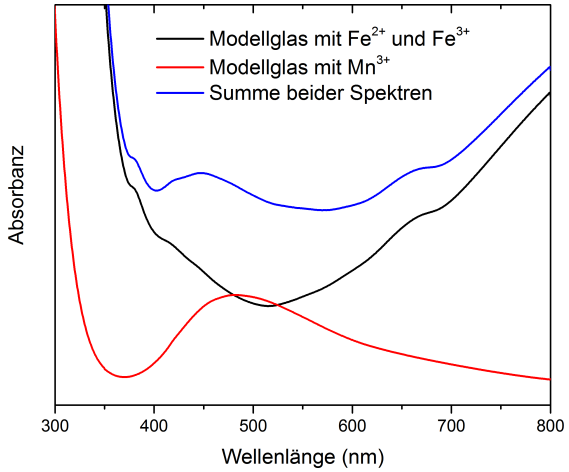

Abbildung 7: Aus der Überlagerung der Spektren von Mn^{3+}, Fe^{2+} und Fe^{3+} resultiert ein für das menschliche Auge homogenes Spektrum, sodass uns die Probe grau erscheint.

Farbzentren unterschiedlichen Komplexen und *CT*-Übergängen zugeordnet werden. In der grünlich-schwarzen Probe (13 Gew % FeO) auf einen $Fe^{2+} - Fe^{3+}$ $IV-CT$-Übergang (vgl. Bamford 1977; Schreurs/Brill 1984). Für die Färbung der schwarz-violetten Probe (1.1 % FeO, 3.8 % MnO) ist der $Mn^{2+} - Fe^{3+}$ $IV - CT$ Übergang (Abb. 8b) verantwortlich, die lila Farbe weist auf $d - d$ Übergänge der Mn^{3+}-Ionen hin. In der orange-schwarzen Probe (3.9 % FeO und 0.8 % SO_3) ist die Farbe auf eine hohe Anzahl des Fe–S *CT* Übergangs zurückzuführen (Abb. 8c).

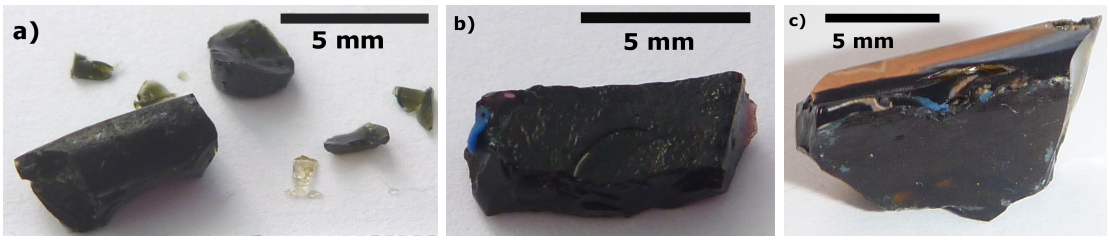

Abbildung 8: Schwarze Mosaik *tesserae*. Aus der intensiven Färbung durch $Fe^{2+} - Fe^{3+}$-*CT*-Übergänge (grün, a), Mn^{3+}-*dd*-Übergänge und $Mn^{2+} - Fe^{3+}$-*IV*-*CT*-Übergänge (violett, b) bzw. Fe^{3+}-S^{2-} CT-Übergänge (braun, c) resultiert ein schwarzes Erscheinungsbild. An Bruchkanten ist die eigentliche Färbung zu erkennen.

6 Undurchsichtige weiße und gelbe Glasproben (Calcium- und Bleiantimonat)

Makroskopische Calciumantimonatkristalle sind farblos. Da die Partikel aber etwas größer als die Wellenlänge des sichtbaren Lichts sind, verlieren Proben, welche die Mikrokristallite enthalten durch Streuung ihre Transparenz und bekommen eine milchig-weiße Farbe. Zusätzlich können diese Glasproben mit den oben beschriebenen Methoden eingefärbt werden und somit z.B. in Kombination mit Cobaltionen zu einem undurchsichtigen blauen Glas führen. Typische weiße Trübungsmittel sind neben Calciumantimonaten ($CaSb_2O_6$ und $Ca_2Sb_2O_7$) noch TiO_2, $CaCO_3$ und Sb_2O_5, aber auch Luftblasen oder feinen SiO_2 Sandkörner können vergleichbare Streueffekte hervorrufen (Basso u. a. 2014; Maltoni/Silvestri 2016; Drünert u. a. 2018). Verschiedene Trübungsmittel können z.B. mit Hilfe von Raman-Spektroskopie, Röntgenbeugung und Elektronenmikroskopie nachgewiesen werden (Papageorgiou/Zacharias 2010). Es gibt allerdings auch mikrokristalline Pigmente, die eine intensive Eigenfärbung besitzen. Eines der ältesten und bekanntesten kristallinen Pigmente, welches eine intensive gelbe Färbung hervorruft, ist sicher Neapelgelb ($Pb_2Sb_2O_7$, ebd.).

Antimon kann in Gläsern auch gelöst vorkommen und wird zum Beispiel als Läutermittel oder als Reduktionsmittel eingesetzt. Beide typischen Oxidationsstufen, Sb^{3+} und Sb^{5+} erscheinen in Gläsern farblos. Das Gleichgewicht zwischen den beiden Oxidationsstufen wird stark von der Schmelztemperatur beeinflusst, daher eignet sich Antimonoxid in modernen Glasschmelzen gut als Läutermittel:

$$Sb_2O_3 + O_2(\text{Schmelze}) \xrightarrow{T<1200\,^\circ C} Sb_2O_5 \tag{3}$$

$$Sb_2O_5 \xrightarrow{T>1200\,^\circ C} Sb_2O_3 + O_2 \tag{4}$$

Bei Temperaturen oberhalb 1200 °C wird Sauerstoff abgegeben, welcher als Gas an die Oberfläche der Schmelze drängt und dabei andere gelöste Gase mit austreibt (Johnston 1965). Durch diese Bewegung wird auch die restliche Schmelze umgewälzt und trägt so weiter zur Homogenisierung des Glases bei. Beim Abkühlen reagiert der in der Schmelze verbliebene, gelöste Sauerstoff bei der Rückreaktion, der Oxidation, zu Sb_2O_5, sodass eine Blasenbildung während des Abkühlens verhindert wird.

Diese Reaktionen beeinflussen jedoch auch das Redox-Gleichgewicht anderer polyvalenter Ionen, wie der farbgebenden Übergangmetalle. So kann zum Beispiel blaues Cu^{2+} leicht zu farblosen Cu^{+} reduziert werden:

$$2\,Cu^{2+} + Sb^{3+} \longrightarrow 2\,Cu^{+} + Sb^{5+} \quad (5)$$

Tatsächlich sind in den Reflexionsspektren der Mosaikglassteine (Abb. 8a-c) trotz gemessener signifikanter Cu-Gehalten von 0.08 Gew % keine Cu^{2+}-Banden zu erkennen.

7 Schlussbemerkung

Die meisten Untersuchungen archäologischer Proben vermögen nicht zwischen Ionenspezies in unterschiedlichen Oxidationsstufen zu unterscheiden. Dabei können besonders technologische Fragen zu den Rohstoffen, einschließlich Recycling, den Schmelzbedingungen oder funktionaler Zusatzstoffe, viel einfacher mit diesen Informationen geklärt werden. Die optische Spektroskopie ist eine zerstörungsfreie, kostengünstige Methode, die auch *in-situ* in Museen oder bei Ausgrabungen eingesetzt werden kann. Mit ihr lässt sich die Funktion polyvalenter Ionen in Gläsern leicht bestimmen. Farbionen lassen sich von nicht oder nur schwach färbenden Spezies unterscheiden, die nun als Verunreinigungen oder in ihrer Funktion als Läutermittel oder Entfärber zu betrachten sind. Auch wenn planparallele polierte Proben die quantitative Analyse erleichtern, können für kleinförmige, korrodierte oder sogar in Reflexion gemessene Proben neben qualitativen Aussagen zumindest auch semiquantitative Aussagen zu den verschiedenen absorbierenden Spezies gemacht werden.

Danksagung

Georgia Papageorgiopoulos und Anja Winterstein waren beide in den grundlegenden Untersuchungen dieser Gläser beteiligt und haben durch quantitative Analysen und Nachschmelzen, respektive, zu den hier gezeigten Beispielen wichtige Informationen beigetragen. Die Autoren möchten dem Direktor der Gesellschaft für Messenische Archäologische Forschungen, Prof. P. Themelis sehr dafür danken, dass er die wissenschaftlichen Untersuchungen des antiken Fundmaterials erlaubt und unterstützt hat. DM und FD danken dem ProChance Programm der Uni Jena für finanzielle Unterstützung.

Literatur

Bamford 1977

C. R. Bamford, Colour generation and colour control in glass 2 (Amsterdam 1977).

Basso u. a. 2014

E. Basso/C. Invernizzi/M. Malagodi/M. F. L. Russa/D. Bersani/P. P. Lottici, Characterization of colorants and opacifiers in Roman glass mosaic *tesserae* through spectroscopic and spectrometric techniques 45 in: 3 2014 238–245.

Bates 1962

T. Bates, Ligand field theory and absorption apectra of transition-metal ions in glasses. In: J. D. Mackenzie (Hrsg.), Modern aspects of the vitreous state 2 (London 1962) 195–254.

Bingham/Jackson 2008

P. A. Bingham/C. M. Jackson, Roman blue-green bottle glass: chemical–optical analysis and high temperature viscosity modelling 35 in: 2 2008 302–309.

Drünert u. a. in press

F. Drünert/E. Lozier/P. Steppuhn/D. Möncke, Untersuchung farbgebender Zusätze im münsteraner Glasbefund mit Hilfe Optischer Spektroskopie. In: Glas und Glashütten: Archäologische Belege zu Rohstoff, Verarbeitung, Handel und Nutzung. Arbeitskreis zur Erforschung des mittelalterlichen Handwerks, 15. Treffen Konstanz 22.-24.05.2014 sowie 6. Internationales Symposium zur Erforschung mittelalterlicher und frühneuzeitlicher Glashütten Europas, Tagung Baiersbronn 6.5.-8.5. 2016 (Esslingen [in press]).

Drünert u. a. 2018

F. Drünert/E. Palamara/N. Zacharias/L. Wondraczek/D. Möncke, Ancient Roman nano-technology: Insight into the manufacture of mosaic *tesserae* opacified by calcium antimonate 38 in: 14 2018 4799–4805.

Duffy 1990

J. A. Duffy, Bonding, energy levels, and bands in inorganic solids (Harlow 1990).

Ehrt u. a. 2001

D. Ehrt/M. Leistner/A. Matthai, Polyvalent elements iron, tin and titanium in silicate, phosphate and fluoride glasses and melts 42 in: 3 2001 231–239.

Ferguson 2007

J. Ferguson, Spectroscopy of $3d$ complexes. In: St. J. Lippard (Hrsg.), Progress in Inorganic Chemistry 12 (New York 2007) 159–293.

Johnston 1965

W. D. Johnston, Oxidation-reduction equilibria in molten $Na_2O \cdot 2\,SiO_2$ glass 48 in: 4 1965 184–190.

Kühne 1976

K. Kühne, Werkstoff Glas (Berlin 1976).

Lahlil u. a. 2011

S. Lahlil/M. Cotte/I. Biron/J. Szlachetko/N. Menguy/J. Susini, Synthesizing lead antimonate in ancient and modern opaque glass. Journal of Analytical Atomic Spectrometry 26, 5, 2011, 1040.

Leistner/Ehrt 1999

M. Leistner/D. Ehrt, Redox behavior of iron and vanadium ions in silicate melts at temperatures up to 2000 °C 72 in: 5 1999 153–160.

Maltoni/Silvestri 2016

S. Maltoni/A. Silvestri, Innovation and tradition in the fourth century mosaic of the Casa delle Bestie Ferite in Aquileia, Italy: archaeometric characterisation of the glass tesserae in: 2016.

Mirti u. a. 1993

P. Mirti/R. P. Ferrari/E. Laurenti/A. Casoli, A study of Roman glass by reflectance and electron paramagnetic resonance spectroscopies 49 in: 9 1993 1361–1371.

Möncke u. a. 2011

D. Möncke/E. I. Kamitsos/A. Herrmann/D. Ehrt/M. Friedrich, Bonding and ion–ion interactions of Mn^{2+} ions in fluoride-phosphate and boro-silicate glasses probed by EPR and fluorescence spectroscopy 357 in: 14 2011 2542–2551.

Möncke u. a. 2014

D. Möncke/M. Papageorgiou/A. Winterstein-Beckmann/N. Zacharias, Ro-

man glasses coloured by dissolved transition metal ions: redox-reactions, optical spectroscopy and ligand field theory. Journal of Archaeological Science 46, 2014, 23–36.

Moores/Goettmann 2006

A. Moores/F. Goettmann, The plasmon band in noble metal nanoparticles: an introduction to theory and applications 30 in: 8 2006 1121–1132.

Papageorgiou/Zacharias 2010

M. Papageorgiou/N. Zacharias, Comparative and analytical study of late antiquity vessel glass: Collections from Peloponnese and Magnesia. In: Proc. 2nd ARCH_RNT Symposium: Archaeological Research and New Technologies, Kalamata, 21.–23. Oktober 2010 ([o. O.] 2010) 163–170.

Papageorgiou u. a. 2012

M. Papageorgiou/N. Zacharias/K. Beltsios, Technological and typological investigation of late Roman glass mosaic tesserae from Anient Messene, Greece. In: Annales du 18e Congrés de l'Association Internationale pour l'Histoire du Verre: Thessalonique, 2009 ([o. O.] 2012).

Paul 1990

A. Paul, Chemistry of glasses[2] (London 1990).

Popescu u. a. 2000

M. A. Popescu/M. R. Leonovici/A. Ioanid/F. Iova, Thermal annealing effects in pure and copper doped $Na_2O \cdot 4\,B_2O_3$ glass 41 in: 5 2000 313–316.

Schreurs/Brill 1984

J. W. H. Schreurs/R. H. Brill, Iron and sulfur related colors in ancient glasses 26 in: 2 1984 199–209.

Shortland 2002

A. J. Shortland, The use and origin of antimonate colorants in early Egyptian glass 44 in: 4 2002 517–530.

Shugar 2000

A. N. Shugar, Byzantine opaque red glass *tesserae* from Beit Shean, Israel 42 in: 2 2000 375–384.

Vogel 2011

W. Vogel, Glass chemistry^{2} (Berlin 2011).

Volotinen u. a. 2008

T. T. Volotinen/J. M. Parker/P. A. Bingham, Concentrations and site partitioning of Fe^{2+} and Fe^{3+} ions in a sodalimesilica glass obtained by optical absorbance spectroscopy 49 in: 5 2008 258–270.

Weyl 2016

W. A. Weyl, Coloured glasses^{7} (Sheffield 2016).

Wiberg/Wiberg 2007

N. Wiberg/E. Wiberg, Lehrbuch der Anorganischen Chemie^{102} (Berlin 2007).

Wong/Austin 1976

J. Wong/A. C. Austin, Glass structure by spectroscopy (New York 1976).

Untersuchung farbgebender Zusätze im Münsteraner Glasbefund mit Hilfe Optischer Spektroskopie

Ferdinand Drünert[1], Emilie Lozier[1], Oliver Mecking[2], Peter Steppuhn[3], and Doris Möncke*[1,4]

[1]Friedrich Schiller University Jena, Otto Schott Institute of Materials Research, Germany

[2]Thüringer Landesamt für Archäometrie und Denkmalpflege, Weimar, Deutschland

[3]Landesamt für Kultur und Denkmalpflege Mecklenburg-Vorpommern, Schwerin, Deutschland

[4]Alfred University, Inamori School of Engineering, Alfred (NY), USA

1 Einleitung

Der sehr umfangreiche Befund des Münsteraner Philosophicum zeigt eine beeindruckende Menge an Glasproben aus dem 12. – 16. Jh. u.Z. (Steppuhn in press). Der überwiegend aus grünen Flachglasscherben in diversen Facetten bestehende Befund erscheint für den Betrachter zwar homogen, aber ob die verschiedensten Glasproben aus einer Werkstatt oder aus verschiedenen Produktionsstandorten stammen ist ohne weiteres nicht unterscheidbar. In der vorliegenden Publikation wird dieses Problem aus einer archäometrischen Perspektive untersucht: Während die quantitative Analyse der Glasproben dabei helfen soll, diese in verschiedene Gruppen mit unterschiedlichen Produktionsweisen zuzuordnen, werden mit Hilfe der optischen Spektroskopie semiquantitativ farbgebende Bestandteile untersucht, um über die verschiedenen Redoxzustände der farbgebenden Ionen Hinweise auf die Schmelzbedingungen im Ofen zu erhalten.

Farbige Gläser sind schon seit dem frühesten Beginn der Geschichte des Glases bekannt (z.B. Oppenheim u. a. 1970; Hen-

*dmoencke@eie.gr

Submitted to: Forschungen und Berichte zur Archäologie in Baden-Württemberg

DERSON 1985). Obwohl Gläser in der Vergangenheit schon in den schillerndsten Facetten hergestellt worden sind, ist nur eine kleine Auswahl an Ionen für den Großteil der farbigen Gläser verantwortlich: Kupfer in Glas kann zu türkisen oder rot gefärbten Gläsern führen, manganhaltige Gläser sind farblos oder violett, Cobalt führt zu einer intensiven Blaufärbung und die Schattierungen eisenhaltiger Gläser reicht von braungelb über grün zu blassblau (vgl. BAMFORD 1977; DUFFY 1990; MÖNCKE u. a. 2014; DRÜNERT u. a. in press). Häufig ist es bei der Betrachtung mittelalterlicher Glasproben unklar, ob ein farbgebendes Ion absichtlich mit in die Glasschmelze gegeben worden ist oder ob eine Zugabe unwissentlich als Verunreinigung der Rohstoffe erfolgte. Insbesondere Eisen ist in fast allen Rohstoffen, zumindest in Spuren, vorhanden, teilweise sogar im Bereich von mehreren Gewichtsprozenten (vgl. STERN/GERBER 2004; JACKSON u. a. 2005; JACKSON 2008). Die charakteristische blassblaue Farbe vieler Glasproben ist auf die färbende Wirkung von Fe^{2+} zurückzuführen, bei einem signifikanten Anteil an Fe^{3+} oberhalb 0.5 ma% Gewichtsanteil tritt eine grünliche Färbung auf, zurückzuführen auf die Mischung von gelber und blauer Absorption (ZOLEO u. a. 2015; DRÜNERT u. a. eingereicht, in diesem Band). Das Gleichgewicht zwischen Fe^{2+} und Fe^{3+} ist sehr stark von der Glasmatrix, der Schmelztemperatur und möglichen Reaktionspartnern abhängig, sodass, um dieser Färbung entgegenzuwirken, gelegentlich Manganoxid zum Entfärben in die Glasschmelze gegeben wurde. Da Mangan allerdings ebenfalls zu signifikanten Anteilen in Pflanzenasche enthalten ist, reicht eine einfache quantitative chemische Analyse der Bestandteile nicht aus, um eine intentionale Zugabe des Mangans vorauszusetzen oder auszuschließen (JACKSON u. a. 2005).

In dieser Arbeit soll die optische Spektroskopie genutzt werden, um das Zusammenspiel zwischen Mangan und Eisen etwas genauer betrachten zu können. Mit Hilfe des von BAMFORD (1977) entwickelten Ansatzes soll das Verhältnis von Fe^{2+} zu Fe^{3+} abgeschätzt werden: In diesem Verfahren wird die Absorptionsbande bei 380 nm mit der Absorptionsbande bei 1000 nm verglichen und daraus das Verhältnis wie folgt berechnet.

$$\frac{P}{1-P} = 0,133 \frac{OD_{1000} - R_{1000}}{OD_{380} - R_{380}}\,, \qquad (1)$$

wobei OD die optische Dichte einer Glasprobe bei 1000 nm bzw. bei 380 nm beschreibt. Der Korrekturfaktor R beschreibt die Reflexion des Lichts bei entsprechender Wellenlänge, während der Faktor von $0,133$ das Intensitätsverhältnis der beiden Eisenbanden wiederspiegelt. Für Glasproben, in denen die Gegenwart von Kupferionen sowie von Charge-Transfer Übergängen im Bereich von 400 nm ausgeschlossen werden kann, ist diese Gleichung gut anwendbar, da die Absorptionsbanden des Cobalt

und des Mangan in dem Bereich sehr geringe Intensitäten aufweisen.

2 Experimentelle Durchführung

Die Glasproben des Befunds wurden zunächst anhand optischer Kriterien vorsortiert, gruppiert und anschließend so weit wie möglich gereinigt. Anschließend wurden die Proben in ihrem ursprünglichen Zustand mit Hilfe eines UV/Vis Photospektrometers (Carey 5000 Photospectrometer) analysiert. Ausgewählte Proben wurden beidseitig auf etwa 1 mm Dicke poliert und zunächst mit Röntgenfluoreszenzspektroskopie (RFA - Eagle III Microröntgenfluorenzspektroskop mit der zugehörigen Software Visons v.2; jeweils drei Messpunkte je Glasprobe; die Auswertung erfolgte mit Hilfe von Standards) quantitativ auf die chemischen Bestandteile hin untersucht. Anschließend erfolgte eine erneute optische Analyse (UV/Vis), um farbgebende Korrosionsprodukte ausschließen zu können. Die Verarbeitung der Spektren erfolgte nach dem folgenden Schema: Aus dem wellenlängenabhängigen Brechungsindex des Glases wurde zunächst die zu erwartende Reflexion an jeder Phasengrenze gemäß der Fresnel'schen Gleichung für senkrechten Strahleneinfall

$$R = \frac{(n+1)^2}{(n-1)} \qquad (2)$$

berechnet und den jeweiligen Absorptionsspektren unter Berücksichtigung von zwei Reflexionsvorgängen abgezogen. Anschließend erfolgte eine Normierung der Spektren auf eine Probendicke von 1 mm gemäß des Lambert-Beer'schen Gesetzes (3),

$$A = \frac{1}{\log(T)} = \sum \epsilon_i c_i d\,, \qquad (3)$$

mit der Absorbanz A, der Konzentration des jeweiligen farbgebenden Ions c_i und dem zugehörigen Extinktionskoeffizienten ϵ_i und der Probendicke d.

3 Auswertung und Diskussion

3.1 Die Auswahl der Glasproben

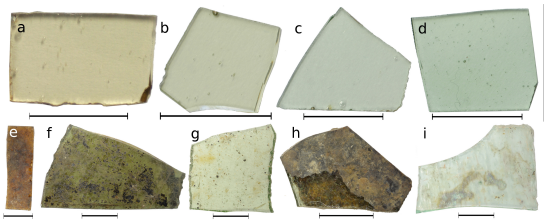

Abbildung 1: Blassgrün bis blassgelb gefärbte Glasproben. Der Übergang der Farbe erfolgt fließend, ist aber in den stark korrodierten Glasproben (unten) nicht gut zu erkennen.

Aus dem rund 270 kg umfassenden Fundkomplex wurden einige Proben nach visuellen Unterscheidungsmerkmalen (Farbe, Bemalung) ausgewählt und gruppiert. Der gesamte Komplex ist in Steppuhn (in press) in diesem Band beschrieben; an dieser Stelle sollen daher nur die für die archäometrische Analyse ausgewählten Proben vor-

gestellt werden. In den Abbildungen 1 bis 3 sind die analysierten Gruppen kurz vorgestellt. Die deutliche Mehrzahl der Glasproben (etwa 95 % Massenanteil, vgl. Abb. 1) ist nur geringfügig gefärbt, wobei der Übergang von blassgelb (Abb. 1 a) bis blaugrün (Abb. 1 e) fließend ist. Teilweise wird der Farbeindruck durch die Korrosion derart verändert, dass die eigentliche Färbung nur nach der Politur der Proben zu erkennen ist.

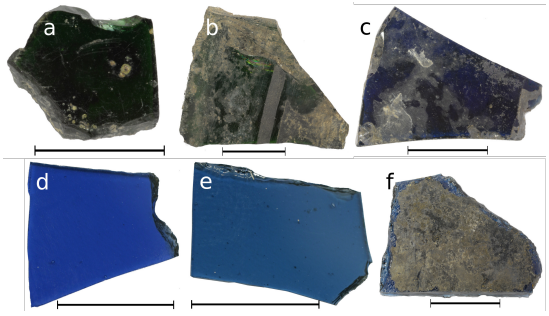

Abbildung 2: Dunkelgrüne (a, b) und dunkelblaue (c-f) Glasproben. Während die dunkelgrünen Glasproben überwiegend gut erhalten sind, variiert die Korrosion der dunkelblauen Proben stark. Die eigentliche Farbe ist nach Politur gut zu erkennen (d, e).

Während in den nahezu farblosen Glasproben die Korrosion der Oberflächen überwiegt, zeigen dunkelgrüne Glasproben (ca. 3 % der Proben) kaum erkennbare Veränderung, zu sehen in Abb. 2 a. Die Korrosion reicht von einer dicken dunkelgrauen Schicht (Abb. 2 f) bis zu einer nahezu ursprünglicher Oberfläche (Abb. 2 c). Letzterer Anteil im Befund beträgt etwa 0.8 %. Deutlich bei den roten Überfanggläsern sichtbar ist das nach der Politur übrig bleibende grüne Grundglas (Abb. 3 a), während die dünne rote Glasschicht (Abb. 3 b – d) vergleichsweise geringfügig angegriffen ist. Nur relativ selten vorhanden sind gelbe bis braune Glasproben, der Anteil beträgt etwa 0.2 % Massenanteil (Abb. 3 e – h). Zur besseren Farbwahrnehmung und für die optische Analyse wurden Beispiele für jede Farbe poliert und für die weitere Analyse verwendet.

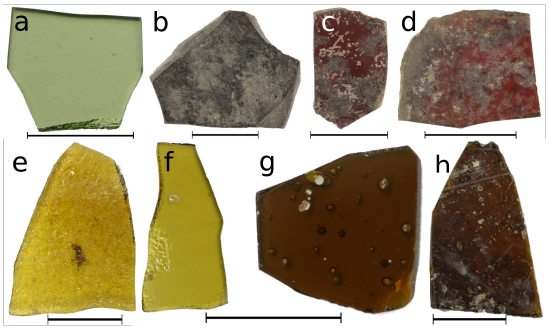

Abbildung 3: Rote Überfanggläser (oben): poliertes Grundglas (a), Glasproben mit unterschiedlichem Erhaltungszustand (b-d). Unten abgebildet sind braune und deutlich gelb gefärbte Glasproben vor und nach Bearbeitung (e-h).

3.2 Quantitative Analyse

Die Zusammensetzung und Probenerscheinung ausgewählter Proben ist in Tabelle 1 gezeigt. Anhand der deutlich unterschiedlichen Anteile an Calcium-, Natrium- und Kaliumoxid (Abb. 4 a - b) kann zwischen drei Gruppen von Gläsern differenziert werden: Beim Großteil der analysierten Gläser handelt es sich um typische Kalk-Kalium-Silicatgläser mit einem kon-

Tabelle 1: Quantitative chemische Analyse ausgewählter Glasproben des Münsteraner Befunds gemäß Röntgenfluoreszenzanalyse (ma%).

Probennr	Farbe	Na_2O	MgO	Al_2O_3	SiO_2	P_2O_5	K_2O	CaO	TiO_2	PbO_2	MnO	Fe_2O_3	CoO	CuO
030-1	grünes Grundglas	0.6	2.8	2.2	50.4	1.2	16.7	22.0	0.4	0.7	1.9	0.8	n.d.	0.10
031-2	roter Überfang	0.8	3.0	2.0	48.8	4.4	12.2	25.7	0.3	n.d.	1.2	0.6	n.d.	0.82
037-2	dunkelblau	0.4	1.9	3.5	52.9	1.1	21.0	16.0	0.3	0.2	0.6	1.4	0.13	0.19
216-5	dunkelblau	1.2	3.6	3.4	50.4	1.7	10.9	26.6	0.4	n.d.	1.0	0.6	0.02	n.d.
220-4	dunkelbraun	1.2	3.9	2.5	49.6	4.4	10.7	25.1	0.3	n.d.	1.2	0.8	0.05	n.d.
213-7	dunkelbraun	0.8	3.3	2.2	52.0	1.9	16.2	21.3	0.2	0.1	1.1	0.6	n.d.	0.02
213-9	hellbraun	0.6	3.1	2.1	52.5	2.3	15.9	20.8	0.3	0.7	1.1	0.5	0.02	n.d.
213-11	gelb	0.7	2.8	1.7	54.5	1.4	18.7	18.4	0.2	n.d.	0.9	0.6	0.03	n.d.
174-1	hellgrün	0.9	2.8	2.4	55.8	1.1	15.4	19.3	0.3	n.d.	1.5	0.3	n.d.	0.01
220-3	hellgrün	1.1	3.9	2.2	51.1	3.3	13.4	22.1	0.3	0.0	0.7	1.5	0.10	0.16
222-1	hellgrün	2.4	3.2	2.6	59.6	1.9	4.8	23.4	0.3	n.d.	1.1	0.6	n.d.	0.01
223-2	hellgrün	2.8	2.8	2.2	62.4	2.0	3.9	21.9	0.3	n.d.	1.0	0.6	0.04	n.d.
223-5	hellgrün	3.6	3.4	1.9	65.2	1.7	2.7	19.6	0.2	0.0	0.8	0.6	n.d.	0.01
223-7	hellgrün	4.2	4.4	4.4	53.5	2.9	5.0	23.0	0.3	n.d.	1.3	0.8	0.01	n.d.
064-1	dunkelgrün	1.0	1.2	1.6	51.9	1.9	4.6	8.5	0.2	26.9	0.5	0.3	n.d.	0.99

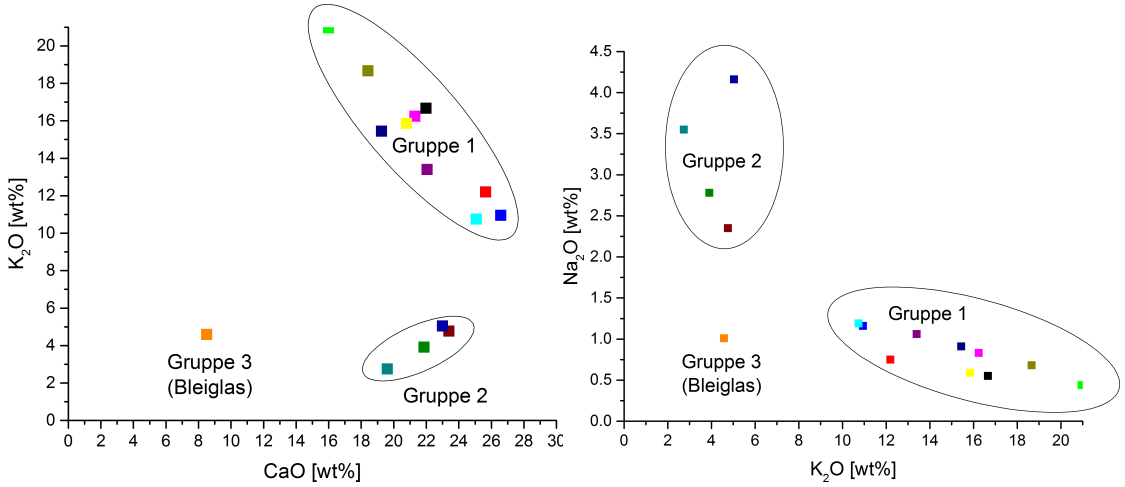

Abbildung 4: Anhand der Anteile an Na_2O, K_2O und CaO können die Glasproben in drei Gruppen eingeteilt werden.

stantem Anteil von CaO + K_2O von etwa 35 ma% mit geringen Anteilen an Na_2O (Abb. 5). Das Farbspektrum dieser Gläser reicht von Cobalt-blauen Glasproben, roten Überfanggläsern und Glasproben mit charakteristischem Grünstich bis hin zu intensiv braun gefärbten Glasproben. Das Verhältnis von CaO zu K_2O schwankt in diesen Glasproben zwischen 1 und 2.4. Die Zusammensetzung dieser Glasproben ist vergleichbar mit der von Theophilus Presbyter im 12. Jh. veröffentlichten Rezeptur für die Glasherstellung (Theophilus Presbyter 1979), Wedepohl/Simon (2010) spricht diese Gläser als Holzasche-Gläser an.

Eine zweite Gruppe besteht ausschließlich aus grünen Glasproben und weist einen deutlichen Anteil an Na_2O im Glas auf. Diese Glasproben haben im Schnitt einen deutlich geringeren Anteil an K_2O von weniger als 10 ma% auf, der Anteil an Calciumoxid ist in diesen Glasproben ebenfalls reduziert. Das Verhältnis zwischen CaO zu K_2O liegt bei diesen Glasproben im Bereich von etwa fünf zu eins. Diese beiden Glastypen werden auch bei anderen Fenstergläsern in Kirchen beobachtet (Brill 1999).

Eine separate Gruppe bilden Bleigläser mit einem signifikanten Anteil an PbO von etwa 20 ma%; diese Gläser werden üblicherweise als Holzasche-Blei-Gläser bezeichnet und sind in zahlreichen Kirchen im deutschsprachigen Raum als Fensterglas nachgewiesen (Mecking 2012). Diese Proben zeichnen sich durch ihre intensive grüne Farbe aus. Von dieser Gruppe wurde nur eine Glasprobe quantitativ untersucht.

3.3 Qualitative Analyse

Die normierten und reflexionskorrigierten Spektren der verschieden gefärbten Gruppen sind in den Abbildungen 6 – 8 gezeigt. Deutlich sichtbar sind die Unterschie-

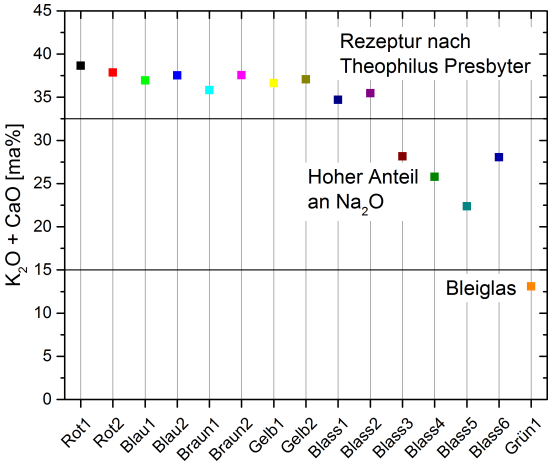

Abbildung 5: Während die Glasproben der Gruppe eins vergleichbar mit Glasproben gemäß der Rezeptur von Theophilus Presbyter (11. Jh.) sind, ist die Zusammensetzung der anderen Glasproben insbesondere durch den hohen Na_2O-Anteil beeinflusst.

de zwischen den blauen (Abb. 6 a) und dunkelgrünen Glasproben (Abb. 6 b), den roten Überfanggläsern (Abb. 7), den braunen Glasproben (Abb. 8) und den blassgelben bis hellblauen Glasproben (ebenfalls Abb. 8).

3.3.1 Cobalt-blaue und mit Kupfer gefärbte Glasproben

Vor allem die Gruppen *FD 037* und *FD 216* zeigen die typische, intensiv dunkelblaue Farbe Cobalt-gefärbter Glasproben (Abb. 6 a). Im Vergleich zwischen polierten und unpolierten Proben ist ersichtlich, dass selbst bei hohen Korrosionsschäden (Probe *FD 216-5*) die Banden des Cobalts deutlich sichtbar sind. Der Anteil an Co^{2+} in diesen Glasproben ist mit etwa 0.1 ma% zwar relativ gering, durch den hohen molaren Extinktionskoeffizienten des Co^{2+} für eine intensive Blaufärbung allerdings deutlich ausreichend. Die Absorption des Kupfer, wo vorhanden, ist bei 12 500 cm^{-1} höchstens zu erahnen, während bei etwa 1000 cm^{-1} zusätzlich zu den zu erwartenden Cobalt-Banden noch Fe^{2+} und bei etwa 26 000 cm^{-1} Fe^{3+} sichtbar ist.

Durch die Überlagerung der Absorption von Co^{2+} und Fe^{2+} ist eine Berechnung des Verhältnisses von Fe^{2+} zu Fe^{3+} nach Bamford (1977) zwar eingeschränkt, aber durch die geringe Überlappung der beiden Peaks möglich. Der berechnete Anteil an Fe^{2+} zum Gesamtanteil an Eisen beträgt dabei zwischen 10 und 15 % (in einem elektrisch beheizten Ofen bei ca. 1300 °C in Luft beträgt der Anteil an Fe^{2+} etwa 40 %, vgl. Tab. 2). Da die bewusste Verwendung von Reduktions- oder Oxidationsmitteln keine nennenswerte sichtbare Veränderung auf cobalthaltige Glasproben mit sich bringt, ist die Verwendung solcher Zusätze in diesen Proben unwahrscheinlich. Aus diesem Grund kann der hier ermittelte Wert gut als Referenzwert für eisenhaltige Glasproben verwendet werden.

Die dunkelgrün gefärbten Glasproben der Gruppe 3, welche den Bleigläsern zugeordnet sind, zeigen alle ein sehr ähnliches Absorptionsspektrum (Abb. 6 b). Für die Grünfärbung ist in diesen Glasproben Cu^{2+} verantwortlich: Während in reinen Silicatgläsern das Maximum der Cu^{2+}-Bande bei etwa 800 nm (12 500 cm^{-1}) und die

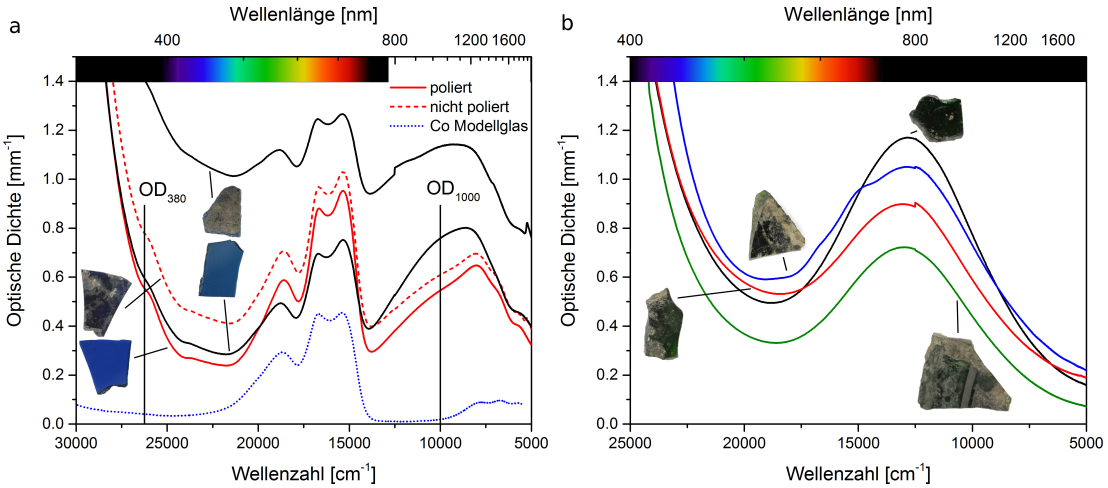

Abbildung 6: Optische Spektren der mit Co^{2+} (a) bzw. mit Cu^{2+} (b) gefärbten Glasproben. Durch den hohen Bleianteil der Gläser in (b) ist die eigentliche türkise Farbe ins Grüne verschoben.

Tabelle 2: Verhältnis von Fe^{2+} zum Gesamtanteil an Fe in dunkelblauen Glasproben. Die Zugabe von MnO_2 als Oxidationsmittel hat in diesen Glasproben keinen Effekt auf die Farbe.

Probe	OD_{380}	OD_{1000}	$\frac{Fe^{2+}}{Fe}$
037-1	0.92	0.66	16 %
037-2	0.56	0.55	12 %
037-3	0.82	0.61	15 %
037-4	0.81	0.64	14 %
216-3	0.63	0.64	12 %
216-5	0.60	0.76	10 %
216-6	0.49	0.50	12 %
Elektr. Heizofen, 1300 °C (Luft)			40 %

UV-Absorptionskante bei etwa 30 000 cm^{-1} liegt, ist die UV-Absorptionskante in stark bleihaltigen Gläsern durch die Absorption der Pb − O-Bindung auf bis zu 22 500 cm^{-1} deutlich in den sichtbaren Bereich verschoben, wodurch statt der ursprünglich türkisen Farbe eine grüne Mischfarbe entsteht. Etwas ungewöhnlich ist die dreigeteilte Schulter der Probe *FD 67-4* (Abb. 6 b, blau) oberhalb von 15 000 cm^{-1}. Die in diesem Bereich auftretenden Signale sind sehr vergleichbar mit den Cobalt-Banden (Abb. 6 a), sodass von einer Verunreinigung mit Co^{2+}-Ionen ausgegangen werden kann.

3.3.2 Kupfer-gefärbte rote Überfanggläser

Der rote Überfang der Glasproben zu *FD 030* und *FD 031* zeigt in der quantitativen Analyse (Tab. 1) mit 0.8 ma% einen deutlich erhöhten Anteil an Kupferionen. Da Kupfer ähnlich wie z.B. Eisen oder Mangan in verschiedenen Valenzen vorkommen kann, nämlich dem türkis färbenden Cu^{2+}, dem farblosen Cu^{+} und dem zur roten Kolloidbildung neigenden Cu^{0}, ist eine rein

quantitative Analyse der Bestandsanteile mitunter irreführend. Bereits geringste Anteile der Kupferkolloide sind in der Lage, eine sehr intensive rote Färbung hervorzurufen, während für die türkis gefärbten Glasproben durch den geringeren molaren Extinktionskoeffizienten ϵ von etwa $30\,\mathrm{L\,cm^{-1}\,mol^{-1}}$ relativ große Mengen an Cu^{2+} im Glas enthalten sein müssen. Da alle Valenzen des Kupfers miteinander über ein Gleichgewicht verknüpft sind, ist eine Rotfärbung des Glases nur bei einem deutlichen Überschuss an reduzierten Kupferspezies (d.h. Cu^{+} oder Cu^{0}) zu erwarten.

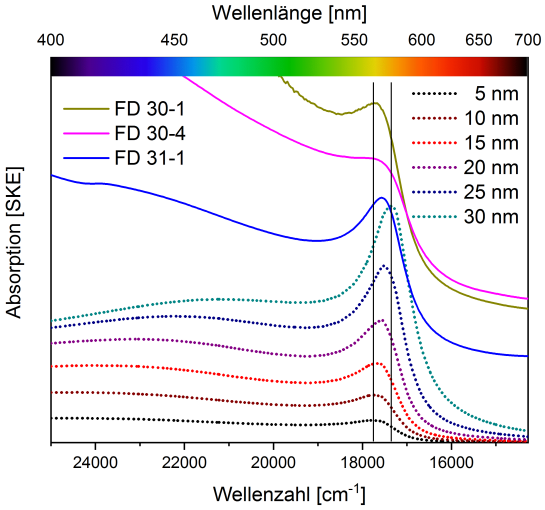

Abbildung 7: Rote Überfanggläser sind an der Plasmonenresonanz bei ca. $17\,500\,\mathrm{cm^{-1}}$ leicht zu erkennen. Das Maximum dieser Glasproben ist vergleichbar mit den von etwa 20 nm großen Kupferpartikeln (unten gezeigt).

In Abbildung 7 sind die optischen Spektren einiger Überfanggläser abgebildet. Da sich die Farbpigmente überwiegend im sehr dünnen Überfang befinden, sind diese Spektren nicht auf die Dicke der Probe normiert. Die Absorption des Lichts durch Kupferpartikel ist von der jeweiligen Partikelgröße abhängig, sodass die Größe der in diesen Glasproben vorhandenen Partikel anhand der Peakposition abgeschätzt werden kann. Simulationsdaten mit Hilfe der Software MiePlot0.46 legen hierbei einen Partikeldurchmesser von etwa 20 nm nahe. Diese Werte stimmen mit den Größenordnungen roter Überfanggläser in der Literatur überein (Brun u. a. 1991).

3.3.3 Blassgrüne bis braune Glasproben

In den blassgrünen bis braunen Glasproben der Gruppen 1 und 2 können sowohl Eisen- als auch Manganionen zur Farbgebung beitragen, deren optische Spektren teilweise überlappen. In Abbildung 8 a sind die Übergänge von grünen zu braunen Glasproben abgebildet. Während in den nur geringfügig gefärbten Proben die Banden des Fe^{3+} bei $24\,000\,\mathrm{cm^{-1}}$ und $26\,500\,\mathrm{cm^{-1}}$ gut sichtbar sind, werden diese Signale in den grünlichen bis braunen Proben durch eine sehr breite Bande bei $25\,300\,\mathrm{cm^{-1}}$ überlagert, welche am ehesten einem Fe^{3+}–S^{2-} Charge-Transfer Übergang zuzuordnen ist. Da geringste Mengen an Schwefel im Glas ausreichend sind, um diese intensive Färbung hervorzurufen (vgl. Drünert u. a. eingereicht, in diesem Band), ist es auch nicht verwunderlich, dass Schwefel in der quantitativen Analyse der Glasproben unterhalb der Nachweisgrenze von etwa 0.1 ma% enthalten ist. Um

die Färbung hervorrufen zu können, ist allerdings die Verwendung von starken Reduktionsmitteln erforderlich, da Sulfidionen (S^{2-}) in der Schmelze nicht stabil sind und schnell zum Sulfit (SO_3^{2-}) oder zum Sulfat (SO_4^{2-}) oxidiert werden.

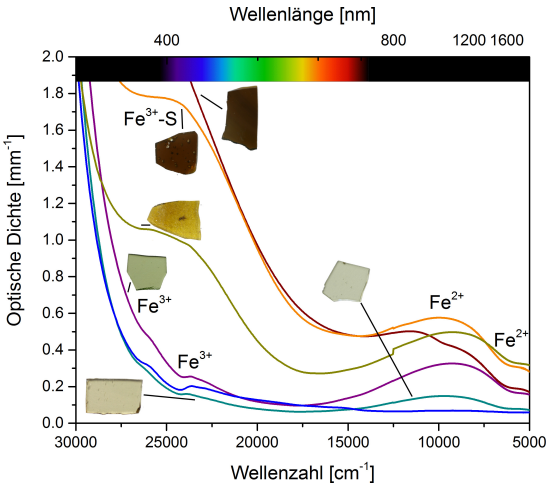

Abbildung 8: Optische Spektren der braunen und blassgrünen / blassgelben Glasproben (links); Das Verhältnis von Fe^{2+} zum Gesamtanteil an Fe korreliert nicht mit dem Anteil an MnO im Glas, sodass eine Verwendung von MnO als Glasmacherseife unwahrscheinlich ist (rechts).

Trotz der Gegenwart von 0.6 ma% bis 1.9 ma% in allen Glasproben ist ohne eine Bandenentfaltung in keiner der gemessenen Glasproben ein eindeutig dem Mn^{3+} zuzuordnendes Signal zu finden, sodass eine Verwendung als violettes Farbpigment auszuschließen ist, sondern mehr für einen Nebenbestandteil aus der Pflanzenasche spricht. Ebenfalls denkbar ist die primäre Verwendung des Manganoxids als Oxidationsmittel zur Entfärbung der Glasproben. Daher sind in Tabelle 3 bzw. in Abbildung 8 b die Redoxverhältnisse von Fe^{2+} zu Fe^{3+} neben dem Anteil an Manganoxid abgebildet. In Anbetracht der Annahme, dass Fe^{2+} in Gegenwart von Mn^{3+} unter Bildung von Mn^{2+} zu Fe^{3+} oxidiert wird, müsste der Anteil an Fe^{2+}mit steigenden Anteilen an Manganoxid in der Glasschmelze absinken. Ein derartiger Trend ist aus den optischen Spektren jedoch nicht zu entnehmen, weshalb die Verwendung als „Glasmacherseife“ auszuschließen ist.

4 Zusammenfassung

Die quantitative Analyse der Glasproben zeigt, dass für die Herstellung der Glasproben im Münsteraner Befund mindestens drei verschiedene Rezepturen für die Glasherstellung verwendet worden sind. Während eine Gruppe große Ähnlichkeit zu der von Theophilus Presbyter veröffentlichten Glasrezeptur hat, sind dunkelgrüne Glasproben (Gruppe drei) aus stark bleihaltigen Gläsern hergestellt worden. Die zweite Gruppe an Glasproben zeigt deutliche Anteile an Natriumoxid zwischen 1 ma% und 5 ma%, sodass entweder von Recycling durch Kalk-Natron-Silicatgläser oder von der Beimengung alternativer Rohstoffe wie z.B. Seetang (vgl. Dungworth 2012) zur Herstellung der Glasproben auszugehen ist. Da Glasproben der ersten und der dritten Gruppe farblich teilweise sehr deutlich überlappen, ist es wahrscheinlich, dass diese Glasproben aus unterschiedlichen, von-

Tabelle 3: Anteil von Fe^{2+} am Fe-Gesamtanteil in den geringfügig gefärbten Glasproben.

Probe	OD_{380}	OD_{1000}	$\frac{Fe^{2+}}{Fe}$	FeO in ma%	MnO in ma%
223-7	0.37	0.26	16 %	0.8	1.3
223-5	0.24	0.23	12 %	0.6	0.8
223-2	0.28	0.37	9 %	0.6	1.0
222-1	0.30	0.44	8 %	0.6	1.1
220-3	0.23	0.25	11 %	1.5	0.7
30-1	0.51	0.32	17 %	0.8	1.9
174-1	0.31	0.15	22 %	0.3	1.5
Elektr. Heizofen, 1300 °C (Luft)			40 %		

einander unabhängigen Produktionsstandorten kommen.

Mit Hilfe der Optischen Spektroskopie ist es zusätzlich möglich, die Bandbreite an Redoxverhältnissen innerhalb mittelalterlicher Glasproben abzuschätzen. Während ein Großteil der blassgrünen Glasproben scheinbar ohne weitere Zusätze an reduzierend oder oxidierend wirkenden Glasproben hergestellt wurde und somit den Standard für Schmelzbedingungen darzustellen scheint, sind braune Glasproben gezielt reduziert worden, um den stark färbenden gelben Fe^{3+}–S^{2-} Charge-Transfer Übergang zu erhalten. Es konnte weiterhin gezeigt werden, dass Manganoxid nicht zur Färbung oder Entfärbung der Glasproben eingesetzt wurde, sondern höchstwahrscheinlich als Nebenbestandteil in der Asche in das Glas eingebracht wurde.

Literatur

Bamford 1977

C. R. Bamford, Colour generation and colour control in glass 2 (Amsterdam 1977).

Brill 1999

R. H. Brill, Chemical analyses of early glass, vols. I/II, The catalogue / The tables 1999.

Brun u. a. 1991

N. Brun/L. Mazerolles/M. Pernot, Microstructure of opaque red glass containing copper 10 in: 23 1991 1418–1420.

Drünert u. a. eingereicht

F. Drünert/F. Lind/P. Vontobel/E. I. Kamitsos/N. Zacharias/L. Wondraczek/D. Möncke, Borosilicate glass layers on Mycenaean glass: surface alterations by glass — borax — gold interactions in: [eingereicht].

Drünert u. a. in press

F. Drünert/N. Zacharias/D. Möncke, Einblick in die Chemie und Physik der Farbigkeit und Opazität von Gläsern. In: Glas und Glashütten: Archäologische Belege zu Rohstoff, Verarbeitung, Handel und Nutzung. Arbeitskreis zur Erforschung des mittelalterlichen Handwerks, 15. Treffen Konstanz 22.-24.05.2014 sowie 6. Internationales Symposium zur Erforschung mittelalterlicher und frühneuzeitlicher Glashütten Europas, Tagung Baiersbronn 6.5.-8.5. 2016 (Esslingen [in press]).

Duffy 1990

J. A. Duffy, Bonding, energy levels, and bands in inorganic solids (Harlow 1990).

Dungworth 2012

D. Dungworth, Historic window glass 18 in: 1 2012 7–25.

Henderson 1985

J. Henderson, The raw materials of early glass production 4 in: 3 1985 267–291.

Jackson 2008

C. Jackson, Theophilus and the use of beech ash as a glassmaking alkali. In: M. Martinon-Torres/Th. Rehren (Hrsg.), Archaeology, history and science. Integrating approaches to ancient materials (New York 2008) 117–130.

Jackson u. a. 2005

C. M. Jackson/C. A. Booth/J. W. Smedley, Glass by design? Raw materials, recipes and compositional data 47 in: 4 2005 781–795.

Mecking 2012

O. Mecking, Medieval lead glass in Central Europe 55 in: 4 2012 640–662.

Möncke u. a. 2014
D. Möncke/M. Papageorgiou/A. Winterstein-Beckmann/N. Zacharias, Roman glasses coloured by dissolved transition metal ions: redox-reactions, optical spectroscopy and ligand field theory. Journal of Archaeological Science 46, 2014, 23–36.

Oppenheim u. a. 1970
A. L. Oppenheim/R. H. Brill/D. Barag/A. Von Saldern, The chemical interpretation of the texts. In: Glass and glassmaking in ancient Mesopotamia 3 (New York 1970) 105–128.

Steppuhn in press
P. Steppuhn, 270 kg Flachglas in der Grube – Ein Fundkomplex des späten 12. bis frühen 16. Jahrhunderts vom Areal der Domimmunität in Münster (Westfalen). In: Glas und Glashütten: Archäologische Belege zu Rohstoff, Verarbeitung, Handel und Nutzung. Arbeitskreis zur Erforschung des mittelalterlichen Handwerks, 15. Treffen Konstanz 22.-24.05.2014 sowie 6. Internationales Symposium zur Erforschung mittelalterlicher und frühneuzeitlicher Glashütten Europas, Tagung Baiersbronn 6.5.-8.5. 2016 (Esslingen [in press]).

Stern/Gerber 2004
W. B. Stern/Y. Gerber, Potassium-calcium glass: New data and experiments 46 in: 1 2004 137–156.

Theophilus Presbyter 1979
Theophilus Presbyter, On divers arts[2] (New York 1979).

Wedepohl/Simon 2010
K. H. Wedepohl/K. Simon, The chemical composition of medieval wood ash glass from Central Europe 70 in: 1 2010 89–97.

Zoleo u. a. 2015
A. Zoleo/M. Brustolon/A. Barbon/A. Silvestri/G. Molin/S. Tonietto, Fe(III) and Mn(II) EPR quantitation in glass fragments from the palaeo-Christian mosaic of St. Prosdocimus (Padova, NE Italy): Archaeometric and colour correlations 16 in: 3 2015 322–328.

Oberflächenanalyse Mykenischer Glasfragmente der späten Bronzezeit – Hinweise auf Vergoldung unter Zuhilfenahme von Borax

Ferdinand Drünert[1], Felix Lind[1], Anders Kästner[2], Peter Vontobel[2], Efstratios I. Kamitsos[3], Nikolaos Zacharias[4], and Doris Möncke*[1,5]

[1]Friedrich Schiller University Jena, Otto Schott Institute of Materials Research, Germany

[2]Laboratory for Neutron Scattering and Imaging, PSI, CH-5232 Villigen PSI, Switzerland

[3]Theoretical and Physical Chemistry Institute, National Hellenic Research Foundation, 48 Vassileos Konstaninou Avenue, 11635 Athen, Griechenland

[4]University of Peloponnese, Dept. of History, Archaeology and Cultural Resources Management, Laboratory of Archaeometry, Kalamata, Griechenland

[5]Alfred University, Inamori School of Engineering, Alfred (NY), USA

Zusammenfassung

In einer früheren Studie wurden die Infrarot-Reflexionsspektren mykenischer Glasfragmente schon ausführlich diskutiert und auf die Möglichkeit hingewiesen, dass sich eine oberflächennahe Borosilicatschicht ausgebildet haben könnte (Möncke u. a. 2013). Die Ergebnisse der Infrarotspektroskopie (IR) allein könnten auch als Korrosionsschicht gedeutet werden, jedoch sprachen einige Details der Untersuchungen gegen reine Korrosionseffekte. In der Fortführung dieser Untersuchungen galt es zum einen experimentell die Ausbildung einer Borosilicatschicht nachzustellen und zum anderen eine unabhängige weitere Analysenmetho-

*dmoencke@eie.gr

Submitted to: Forschungen und Berichte zur Archäologie in Baden-Württemberg

de zu finden, die eine Boranalyse auch in dünnen Schichten ermöglicht. Mit der Neutronentomographie (NT) haben wir wegen des hohen Absorptionsvermögens von ^{10}B eine solche Methode gefunden. Mit den Neutronenradiographieanlagen NEUTRA und ICON am Paul-Scherrer-Institut (PSI) in Villigen in der Schweiz war es möglich, auch sehr dünne Borosilicatschichten auf der Oberfläche eines mit Borax behandelten Kalk-Natron-Silicatglases nachzuweisen. In der Tat kann sich eine Borosilicatschicht durch die Reaktion von Borax mit einem Natron-Kalk-Silicat Glas an dessen Oberfläche bilden. Ähnliche Bedingungen könnten zum Beispiel auch bei einer möglichen Vergoldung bronzezeitlicher Reliefgläser geherrscht haben. Wegen des hohen Streuvermögens von ^{1}H waren die Ergebnisse der Neutronentomographie an korrodierten mykenischen Proben leider nicht eindeutig. In der Kombination der zerstörungsfreien Techniken IR- und Neutronenabsorption sollte jedoch zukünftig eine eindeutige Zuordnung möglich sein.

Summary

In an earlier publication we discussed infrared spectroscopic studies (IR) and the possible presence of a highly polymerized borosilicate glass layer on a Late Bronze age Mycenaean vitreous relief fragment (Möncke et al. 2013). We favored the explanation of surface modifications during gilding of the fragments through the use of borax. However, we were not able to exclude weathering as explanation for some of the observed spectral features. In order to follow up on this discussion we tried in the current study to find additional analytical tools for the analysis of a modified glass surface containing boron. Furthermore, we tried to recreate the formation of such a borosilicate layer in the laboratory, through contact of a soda-lime-silicate glass melt with borax powder. Neutron tomography (NT), using the NEUTRA and ICON beam lines at the Paul Scherrer Institute (PSI) in Villigen in Switzerland, was able to show the presence of a thin absorbing layer not only in archaeological samples, but also on remade model glasses. This emerging borosilicate layer was also confirmed on the laboratory species by infrared spectroscopy.

The combination of NT and IR is able to detect the light element boron nondestructively even in low concentrations and in very thin layers. Some ambiguity exists still in regard to the presence of $Si-OH$ groups, due to the high neutron scattering ability of hydrogen. However, a combined approach by IR (quick screening of promising samples, excluding significant hydroxyl groups) and NT should be able to illustrate the extend of the formed borosilicate surface layer on Mycenaean glasses.

1 Einleitung

Auf den Außenseiten mehrerer cobaltblauer Glasfragmente der späten Bronzezeit (LBAIIIb, 1330 - 1190 BC, Palia Epidavros, Peleponnes, Griechenland; Zacharias u. a. 2013; Zacharias/Palamara 2016) konnte mittels Infrarot-Reflexionsspektroskopie eine hochpolymerisierte Oberfläche identifiziert werden, bei der es sich vermutlich um eine Borosilicatschicht handelt (Möncke u. a. 2013; Drünert u. a. 2013). Die Fragmente, gezeigt in Abb. 1, zeigen spiralförmige Reliefs auf der Oberseite, sind aber auf der Rückseite undekoriert und flach. Die Funde stammen aus einer Grabkammer, die 1989 ausgegraben wurde und waren wohl ursprünglich nicht nur als Ketten beigegeben, sondern auch an den Kleidern der Toten befestigt (Nightingale 2005). Wie für entsprechende Funde aus anderen mykenischen Gräbern wurden auch hier viele den Reliefs entsprechende Goldhüllen gefunden (ebd). Es muss daher davon ausgegangen werden, dass auch bei den hier untersuchten Funden eine signifikante Zahl der Proben ursprünglich vergoldet war und somit als Goldfolienschmuck einzuordnen ist (Nightingale 1998; Nightingale 2005). Auch wenn wir die Goldhüllen selber nicht untersuchen konnten, gab es doch indirekt Hinweise für die Existenz einer Borosilicatschicht an den Glasoberflächen, die auch auf eine mögliche Vergoldung hinweisen (Möncke u. a. 2013).

Quantitative Analyse der Gläser mittels Rasterelektronenmikroskopie und energiedispersiver Röntgenspektroskopie (REM-EDX), wurden später durch Messungen der Protonen-induzierten Gamma-Emission (PIGE) und Protonen-induzierten Röntgen-Emission (PIXE) bestätigt. Die Zusammensetzung der Proben entspricht derer typischer Soda-Asche-Gläser, welche unter Verwendung von Halophytenasche sowie gegebenenfalls einer mineralischen Natriumcarbonatquelle erschmolzen wurden (siehe Tabelle 1; Zacharias u. a. 2013, vgl. auch Tite u. a. 2006; Nikita u. a. 2006; Walton u. a. 2009; Möncke u. a. 2013). Die blaue Färbung geht auf geringen Zugaben von CoO (0.1 Gew%) zurück. Neben cobaltblauen Fragmenten sind auch türkise, Cu^{2+} haltige Fundstücke bekannt.

Tabelle 1: Durchschnittliche Zusammensetzung von drei mykenischen Glasproben im Vergleich zu einem Modellglas (Gew%).

	Mykenisches Glas	Modellglas
SiO_2	64.71	64.0
Na_2O	17.3	17.3
K_2O	0.8	–
CaO	8.1	13.8
MgO	5.3	–
Al_2O_3	1.3	5.0
CuO	0.3	–
CoO	0.1	–
Rest	2.09	0
Q^2-Gruppen	5 %	
Q^3-Gruppen	95 %	

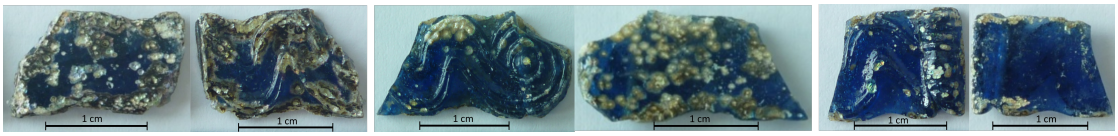

Abbildung 1: Fotografien der mykenischen Reliefgläser.

Die anfänglichen Infrarot-Messungen (Abb. 2) zeigten eine vollpolymerisierte Glasstruktur an den Glasoberflächen. Eine Bande um $940\,\mathrm{cm}^{-1}$ kann sowohl auf B-O Streckschwingungen von $[BO_4]^-$-Tetraedern, als auch auf Si − OH Einheiten hinweisen. Messungen mit dem IR-Mikroskop an gut erhaltenen Glasoberflächen zeigen jedoch keine Anzeichen für O − H Schwingungen, wie sie um $3000\,\mathrm{cm}^{-1}$ in den Spektren, die an sichtbar korrodierten Arealen aufgenommen wurden, zu erkennen sind (Möncke u. a. 2013).

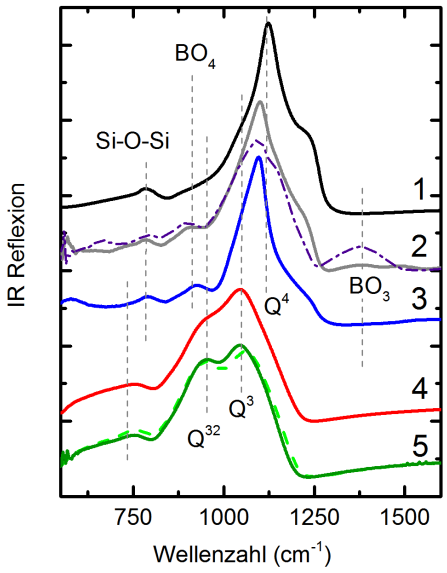

Abbildung 2: IR Reflexionsspektren: (1) reines SiO_2 Glas; (2) völlig polymerisiertes Borosilicatglas (10 Jahre alte Probe, durchgezogen; frische Probe, gestrichelt); (3) korrodierte Glasoberfläche eines mykenischen Glases; (4) Nachschmelze einer mykenischen Probe; (5) korrodierte Bruchfläche der mykenischen Probe (durchgezogen) im Vergleich zu einem depolymerisierten Bio-Glas (gestrichelt).

Die Ähnlichkeit dieser gut erhaltenen glasigen Oberflächen der mykenischen Glasfragmente im Vergleich zu den Spektren technischer alkaliarmer Borosilicatgläser des Duran-Typs ist aus den IR-Reflexionsspektren gut zu erkennen. Messungen an seitlichen Bruchstellen (5) zeigen jedoch, dass die polymerisierte Schicht auf der Glasoberfläche sehr dünn ist und dass die darunterliegenden Glasareale (3) eher Korrosionsspuren aufweisen, welche einer Depolymerisation entsprechen, d.h. einem Aufbrechen des Silicatnetzwerkes (Möncke u. a. 2013).

$$-\mathrm{OSiO_2}-\mathrm{O}-\mathrm{SiO_2O^-}+\mathrm{H_2O} \rightleftharpoons -\mathrm{OSiO_2}-\mathrm{OH}+\mathrm{HO}-\mathrm{SiO_2O}- \quad (1)$$

Die verschiedenen Glasbausteine mit den

jeweils wichtigsten IR-Schwingungen sind in Tabelle 2 zusammengefasst. Die Streckschwingungen zwischen und $900\,\mathrm{cm}^{-1}$ und $1200\,\mathrm{cm}^{-1}$ sind am stärksten ausgeprägt, die dazugehörigen Biegeschwingungen ($500\,\mathrm{cm}^{-1}$ bis $800\,\mathrm{cm}^{-1}$) haben geringere Intensitäten. Die Lage der asymmetrischen Si - O Streckschwingungen verschiebt sich von $Q^4 > Q^3 > Q^2 > Q^1$ zu niedrigeren Energien. Dabei ist zu berücksichtigen, dass auch die Verknüpfung dieser SiO_4-Tetraeder die Lage beeinflusst, und dass eine Q^2 Gruppe, die an eine Q^3 gebunden ist, bzw. eine Q^3 Gruppe, die an eine Q^2 Gruppe gebunden ist, niedrigere Energien aufweisen als eine Q^3/Q^3 Verknüpfung und eine höhere Energie als eine Q^2/Q^2 Verknüpfung (Stavrou u. a. 2014). Wenn Schwingungen verschiedener Gruppen zufällig ähnliche Bandenlagen haben, wie $\mathrm{Si-OH}$ oder BO_4 und Q^2, erfolgt die Zuordnung über die Lage der dazugehörigen Biegeschwingungen oder im Falle einer OH-Gruppe auch der Oberschwingungen bei ca. $3000\,\mathrm{cm}^{-1}$.

In den im Folgenden beschriebenen Experimenten ging es zum einen darum, die Existenz einer Borosilicatschicht mittels eines zweiten unabhängigen Verfahrens zu bestätigen oder zu widerlegen. Weiterhin galt es zu versuchen, die in Möncke u. a. (2013) vorgeschlagene Reaktion zur Ausbildung einer möglichen Borosilicatschicht während der Vergoldung eines Silicatglases im Labor nachzustellen. Letzteres gelang, indem eine Kalk-Natron-Silicatglasschmelze auf ein mit Borax-Pulver bestreutes Goldplättchen gegossen wurde. Diese Situation simuliert z.B. ein Verfahren in dem eine Steatitform (wie aus Funden bekannt, Nightingale 1998), erst mit Goldfolie ausgelegt wird, mit Borax bestreut und dann mit der Glasschmelze befüllt wurde. Da viele Methoden der Boranalytik (SEM, PIGE, Raman etc.) durch energiereiche Messmethoden oft tiefere Schichten beproben, ist ein entsprechender Nachweis in dünnen Schichten schwierig. Hier bietet sich jedoch wegen des hohen Absorptionsvermögens von ^{10}B für Neutronen die Neutronentomographie als zerstörungsfreie Alternative an.

2 Ergebnisse und Diskussion

Ohne die Diskussion in Möncke u. a. (2013) wiederholen zu wollen hat sich natürlich nach der Identifikation der Borosilicatschicht sofort die Frage gestellt, wie sich so eine Schicht überhaupt ausbilden konnte, auf welchem Weg und warum Bor in das Glas eingeführt wurde. Auf diese eben genannten Fragen möchten wir hier eine vorläufige Antwort vorschlagen, die sich auf die Nachstellung im Labor und einigen Literaturstellen stützt.

2.1 Vergoldung von Glas

Wie in der Einleitung erwähnt, sind die mykenischen Glasfragmente in einem Grabkontext zusammen mit Goldfolien gefunden worden, die, wie in vielen Museen in Grie-

Tabelle 2: Übersicht über die gängigsten Netzwerkstrukturen in Borosilicatglas und deren Infrarot-Schwingungsfrequenzen.

Bezeichnung	Q^4	Q^3	Q^2	$[BO_4]^-$	BO_3
Netzwerk-struktur	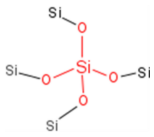	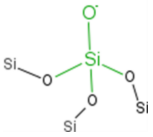	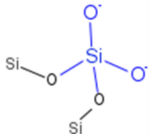	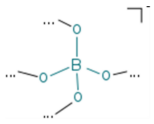	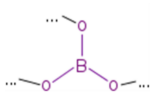
Streck-schwingung	1100 cm^{-1}, 1200 cm^{-1}	1080 cm^{-1}	950 cm^{-1}	940 cm^{-1}	1400 cm^{-1}
Biege-schwingung	800 cm^{-1}	700 cm^{-1}	500 cm^{-1} - 750 cm^{-1}	700 cm^{-1}	700 cm^{-1}

chenland zu sehen, oft die Glasreliefs der späten Bronzezeit umgeben haben.

Schon bei Schliemann (1878) findet sich ein Zitat in dem die Verwendung von Borax von mykenischen Goldschmieden erwähnt wird: 'Da ich hier von Löthen spreche, so erwähne ich, dass nach den Mittheilungen des Professor Landerer die mykenischen Goldschmiede das Gold mittels Sodium-Borax lötheten, welches bis heute zu dem gleichen Zweck gebraucht [...] und aus Persien und Indien unter dem Namen Baurac Pounxa Tinkal [...] importirt wurde'. (*H. Schliemann: Mykene - Bericht über meine Forschungen und Entdeckungen, 1878. Digitale Version der Universität Heidelberg, <http://digi.ub.uni-heidelberg.de/diglit/schliemann1878>, S. 266*)

Auch in anderen Quellen wird auf die frühe Verwendung von Borax von Glasschmieden hingewiesen. So sollen möglicherweise schon die Babylonier Borax beim Schweißen bzw. Löten genutzt haben (Woods 1994). Auch heutzutage wird Borax von Goldschmieden genutzt um die Dunkelfärbung von Gold beim Nachbearbeiten in der Flamme zu verhindern (Brepohl 1978). Borax wird auch als Flux angepriesen, um Rohgold aus Silicaterzen zu lösen (ebd.).

2.2 Reaktion von Borax mit Glas

Mit einem einfachen Experiment wollten wir sehen, ob die Kombination von Borax mit einem Kalk-Natron-Silicat-Glas unter Hitzeeinwirkung tatsächlich zur Ausbildung einer Borosilicatschicht führen kann. Im ersten Versuch wurde eine Kalk-Natron-Silicat-Glasschmelze auf eine mit Borax bestreute Goldfolie gegossen, schematisch dargestellt in Abb. 3 dargestellt. Eine Fotographie des entstehenden Glasblocks ist in Abb. 4 gezeigt. Die Goldfolie hat ihren Glanz erhalten.

Unter dem Infrarotmikroskop ist deutlich zu sehen, dass sich außen auf der Glasprobe eine Borosilicatschicht gebildet hat. In Abb. 5 sind die Infrarotreflexionsspek-

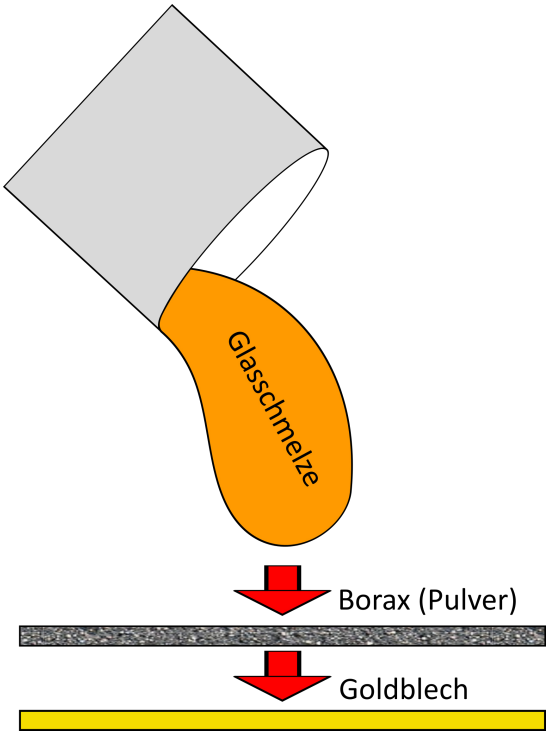

Abbildung 3: Schema der Herstellung einer Borosilicatschicht.

tren dieser Schicht im Vergleich zur nicht mit Borax kontaminierten Probenoberseite gezeigt. Zum Vergleich ist auch ein Spektrum des nicht reagierten Borax gezeigt, von dem sich neben der Goldfolie noch Reste fanden, sowie eines aus Borax hergestelltes Natriumboratglases. Während kristallines Borax ein Infrarotspektrum mit vielen scharfen Banden zeigt, ähneln die Spektren der Borosilicatschicht denen des reinen Silicatnetzwerkes mit seinen wenigen breiten Banden. Allerdings zeigen sich deutlich drei Bandenbereiche in denen sich eindeutig der Einbau von Bor im Glasnetzwerk widerspiegelt. Erstens, im Wellenlängenbereich hoher Energien zwischen 1250 cm^{-1} und

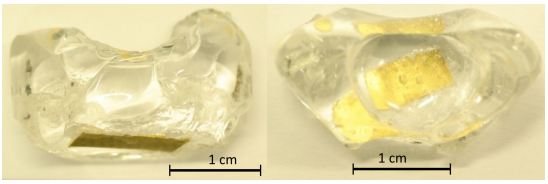

Abbildung 4: Fotografien der nachgestellten Kalk-Natron-Silicat Glasproben mit einer Borosilicatschicht auf der Glasoberfläche.

1600 cm^{-1}. Dieses Bandensystem ist auf Streckschwingungen $B - O$ in trigonalen BO_3 Gruppen zuzuordnen. Kristallines Borax hat dort sehr scharfe Banden, während reines Kalk-Natron-Silicatglas bei so hohen Energien keine Banden hat. Trigonale Borate bilden mit Wasser einen Lewis-Säure-Basen Komplex und lösen sich damit schon bei normaler Luftfeuchtigkeit langsam auf, sodass solche Banden in Glasfragmenten der späten Bronzezeit sehr unwahrscheinlich sind (Möncke u. a. 2013). Ein zweites Borspezifisches Signal ist in den wasserfreien Borosilicatschichten in der Schulter bei 950 cm^{-1} zu erkennen. Weiterhin unterscheidet sich das Bandensystem der chSi - O - Si Biegeschwingungen in den Borosilicatschichten deutlich von denen der borfreien Kalknatronsilicatgläser, sodass zusätzliche Schultern, die auf $B - O - Si$ und $B - O - B$ Biegeschwingungen zurückzuführen sind, sichtbar werden.

2.3 Neutronentomographie

Neutronentomographieaufnahmen (Abb. 6) zeigen das Ausmaß der Borosilicatschicht. Es ist zu erkennen, dass sich die

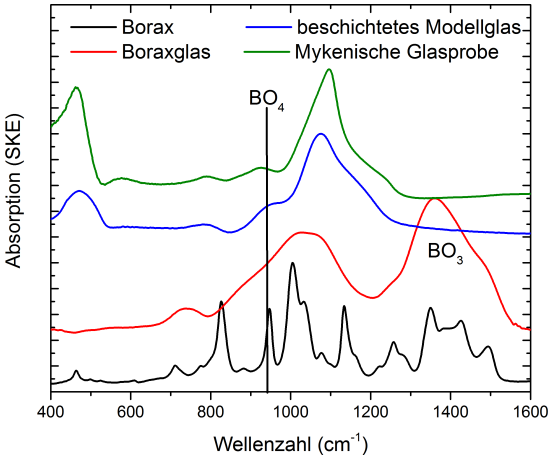

Abbildung 5: IR-Spektren der mykensichen Glasprobe im Vergleich zu einer beschichteten und gewaschenen Modellglasprobe, einem reinen Boraxglas und zu kristallinem Borax.

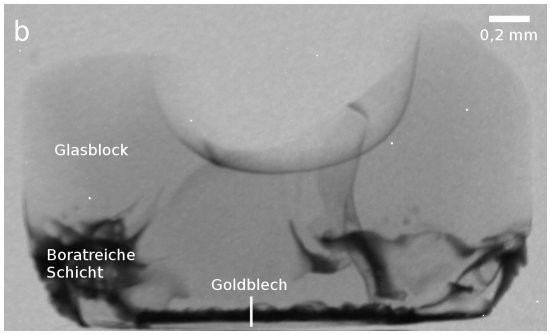

Abbildung 6: Neutronenradiographische Abbildung des Modellglases aufgenommen in NEUTRA. Die hellen Bereiche zeigen für unterschiedliche Orientierungen, welche besonders stark Neutronen absorbieren, d.h. in diesem Fall die Borosilicatschicht.

Borosilicatschicht nur auf der Außenseite der Probe befindet. Die große Ausbreitung der Borosilicatschicht lässt sich durch das Fließverhalten der Glasschmelze erklären. Der erste Tropfen der Glasschmelze reagiert auf der Unterseite mit Borax zum Borosilicatglas; während mehr Glasmasse in die sich formende Glasblase nachfließt, dehnt sich die Außenhaut auf dem langsam erkaltenden Tropfen aus und wandert mit höherer Fülltiefe an den Rändern des Glasblockes nach oben.

Dieser Versuch zeigt, dass grundsätzlich die Reaktion von Borax mit einem Kalknatron-Silicat-Glas unter Hitzeeinwirkung zu der Ausbildung einer äußeren Borosilicatschicht führt. Allerdings ist zum einen der Zeitaufwand jeder einzelnen Messung relativ hoch, zum anderen führen die während der Messung absorbierten Neutronen zu der Bildung radioaktiver Kerne, weshalb die Proben anschließend erst bis zum vollständigen Abklingen der strahlenden Übergänge mehrere Wochen verwahrt werden müssen. Auch die Kosten des Versuchsaufbaus sind sehr hoch, sodass man auf Bestrahlungszeiten an entsprechenden Forschungsinstituten angewiesen ist.

Die Messungen an den spätbronzezeitlichen Proben waren leider nicht so eindeutig wie die der im Labor hergestellten Modellgläser. Da wir die für NEUTRA beantragte Messzeit sehr kurzfristig erhalten hatten blieb uns zu wenig Zeit, gezielt mykenische Proben auszuwählen, mittels der Infrarotspektroskopie zu untersuchen und die Erlaubnisse der griechischen Regierung für die entsprechenden Messungen einzuholen. Die wenigen archäologischen Proben, die wir bei dieser Messkampagne in Villigen untersuchen konnten, waren sehr klein und für Rasterelektronenmikroskopie-

Aufnahmen präpariert; zum Teil war die äußere Schicht wegpoliert oder sie wiesen sehr starke Korrosionsspuren auf. Leider ist die Neutronentomographie nicht nur besonders sensitiv für Atome, die Neutronen besonders stark absorbieren (wie Bor, ^{10}B), sondern auch für Atome mit hoher Streuwirkung (wie Wasserstoff ^{1}H). Durch die Anlagerung von Wasser an die chSi - O - Si-Bindungen bilden sich allerdings an Glasoberflächen häufig Hydroxylgruppen,

$$\equiv\mathrm{Si} - \mathrm{O} - \mathrm{Si}\equiv + \mathrm{H_2O} \rightleftharpoons 2\,\equiv\mathrm{Si} - \mathrm{O} - \mathrm{H}\ , \quad (2)$$

sodass diese Bereiche in den mykenischen Glasfragmenten nicht eindeutig Boratgruppen zugeordnet werden können.

Abb. 7 zeigt den rekonstruierten Querschnitt der Neutronentomographie einer solchen mykenischen Glasprobe. welche am Messplatz ICON aufgenommen wurde. Im Gegensatz zu NEUTRA (21 ţm/px) ermöglicht ICON eine deutlich bessere Auflösung von 13.5 ţm/px, sodass Veränderungen der Glasoberfläche viel deutlicher sichtbar gemacht werden können. Das untersuchte Mykenische Glasfragment zeigte an den Rändern deutliche Korrosionserscheinungen. Im Gegensatz zu den anfangs beschriebenen Proben ist diese durch Cu^{2+} Ionen, nicht Co^{2+}, gefärbt und weist daher eine türkise Farbe auf. Die hellen Bereiche deuten auf eine geringe Transmission hin, was entweder durch hohe Absorption (^{10}B) oder durch Streuung von Wasserstoffatomen hervorgerufen wird.

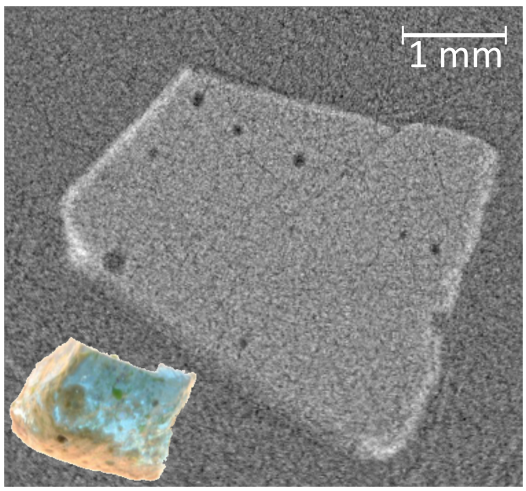

Abbildung 7: Rekonstruierter Querschnitt, Neutronentomographie (ICON), eines mykenischen Glasfragments. Die hellen Bereiche deuten auf eine geringe Transmission hin, was entweder durch hohe Absorption (^{10}B) oder, was in dem Fall dieser an den Rändern stark korrodierten Proben sehr wahrscheinlich ist, durch Streuung (^{1}H) von Hydroxylgruppen und Wassermolekülen bedingt ist.

3 Schlussfolgerung

Nach dem vorläufigen Stand der Untersuchung können wir bestätigen, dass die Vergoldung von Kalk-Natron-Silicat-Glasschmelzen unter Zuhilfenahme von Borax zur Bildung einer Borosilicatschicht führt. Die Glasstruktur dieser Schicht lässt sich sehr gut mittels Infrarot-Reflexions-Spektroskopie nachweisen. Das Ausmaß der Borosilicatschicht über einen weiten Bereich der Glasoberfläche sowie die geringe Schichtdicke war wiederum gut in der Neu-

tronentomographie zu erkennen. Beide Methoden sind zerstörungsfrei und können damit ohne weitere Probenpräparation auch an archäologischen Proben eingesetzt werden.

Die Daten der mykenischen Glasfragmente waren leider nicht eindeutig, da wir zu diesem Zeitpunkt nur stark korrodierte Fragmente zur Verfügung hatten. Allerdings bestätigte sich in diesen ersten Versuchen die grundlegende Eignung der zerstörungsfreien Neutronentomographie für archäologische Proben. Die Unterscheidung einer hohen Neutronenabsorption von Boratomen von der einer hohen Neutronenstreuung durch Wasserstoffatome wird vermutlich nur in Kombination mit IR-Reflexionsspektroskopie erfolgen können. Wegen der Kosten und dem Zeitfaktor, bietet es sich an, erst einmal mit dem IR-Mikroskop geeignete mykenische Glasfragmente zu untersuchen. Dies kann sogar mit einem tragbaren IR-Spektroskop erfolgen. Proben, die deutliche Zeichen einer Borosilicatschicht aufweisen, d.h. eine deutlich ausgeprägte Bande bei $940\,\mathrm{cm}^{-1}$ ohne entsprechende Wasserbanden um die $2700\,\mathrm{cm}^{-1}$ bis $3200\,\mathrm{cm}^{-1}$, sollten anschließend für Messungen und Neutronentomographie ausgewählt werden. Im Anschluss an die Neutronentomographie sollte an diesen Proben zusätzlich ein IR-Mapping durchgeführt werden, um die Intensität der Boratbande ($940\,\mathrm{cm}^{-1}$) und die der Wasserbanden im NIR mit den Bereichen niedriger Neutronentransmission abgleichen zu können. Wenn Bereiche wasserfreier IR-Spektren mit stark absorbierenden Flächen zusammenfallen, kann von der Bildung einer Borosilicatschicht ausgegangen werden.

Wir konnten zeigen, dass es möglich ist eine dünne Borosilicatschicht auf einem Kalk-Natron-Silicatglas zu erzeugen, wenn die heiße Glasmasse mit Borax in Berührung kommt. Weitere Versuche, zum Beispiel ob es genügt die Goldfolie, Borax und das kalte Glas in einem zweiten Schritt zu erhitzen, oder eine Steatitform zu nutzen und dort die Goldfolie, Borax und Glasschmelze einzufüllen, stehen noch aus.

Die Versuche werfen natürlich weitere Fragen auf: Wie üblich war die Technik der Vergoldung mit Borax? Wie weiträumig war die Verwendung von Borax unter Goldschmieden der damaligen Zeit? Wurde Borax auch sonst genutzt (Glasuren, Desinfektionsmittel , ...)? Welche Boraxquellen standen damals zur Verfügung? Die letzte Frage lässt sich am einfachsten beantworten. So haben wir in Abb. 8 einmal die oberflächennahen Boraxvorkommen Westanatoliens aufgezeichnet und mit bekannten Goldvorkommen abgeglichen. Wie weit diese Vorkommen in die Ägäis oder in mykenische Gebiete reichen ist noch abzuklären.

4 Danksagung

Die Autoren sind dem ProChance Programm der Universität Jena, dem Leonardo da Vinci Programm und dem ERAMUS

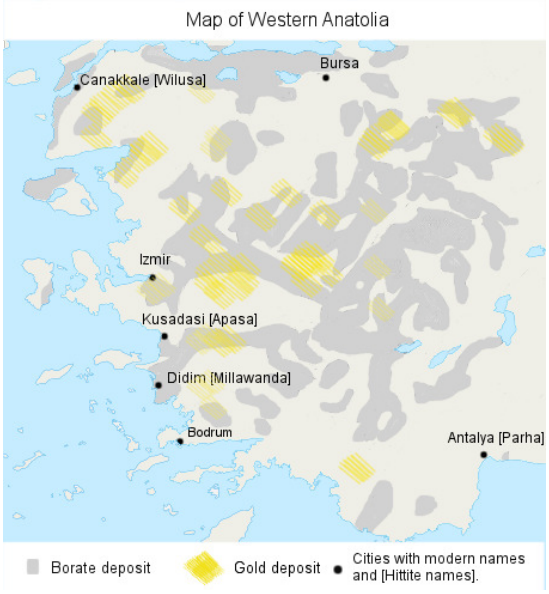

Abbildung 8: Karte der Gold und Borat-Vorkommen im heutigen Anatolien nach Yigit (2006) bzw. Kistler/Helvaci (1994).

Programm der EU sowie dem Programm der Förderung des Deutsch-Griechischen Wissenschaftsaustausches (IKYDA) für finanzielle Förderung zu Dank verpflichtet. Die Autoren danken zudem den griechischen Behörden für die Erlaubnis die beschriebenen Proben zu untersuchen, besonderer Dank gilt hier der 4. Ephorie für Prähistorische und Klassische Altertümer in Argolis des Griechischen Kultusministeriums.

Literatur

Brepohl 1978
E. Brepohl, Theorie und Praxis des Goldschmieds[5] (Leipzig 1978).

Drünert u. a. 2013
F. Drünert/M. Kaparou/E. Palamara/D. Palles/D. Möncke/E. I. Kamitsos/N. Zacharias, Laborversuche zur Bildung von Borosilicatschichten auf Kalk-Natron-Silikat Gläsern. Vergoldung Mykenischer Glasfragmente unter Zuhilfenahme von Borax als Flux. 6 in: 2013 279–283.

Kistler/Helvaci 1994
R. B. Kistler/C. Helvaci, Boron and borates. Industrial Minerals and Rocks 6, 1994, 171–186.

Möncke u. a. 2013
D. Möncke/D. Palles/N. Zacharias/M. Kaparou/E. I. Kamitsos/L. Wondraczek, Formation of an outer borosilicate glass layer on Late Bronze age Mycenaean blue vitrious relief fragments. Physics and Chemistry of Glasses — European Journal of Glass Science and Technology Part B 54, 1, 2013, 52–59.

Nightingale 1998
G. Nightingale, Glass and Mycenaean palaces of the Aegean. In: P. McGray/W. D. Kingery (Hrsg.), The prehistory & history of glassmaking technology 8 (Westerville 1998) 205–226.

Nightingale 2005
ders., Welche Verteilungsmechanismen verbanden Produzenten und Konsumen-

ten in der mykenischen Welt? In: R. Lafer (Hrsg.), Die Geschichte der Antike aktuell: Methoden, Ergebnisse und Rezeption ([o. O.] 2005) 47–62.

Nikita u. a. 2006
K. Nikita/J. Henderson/G. Nightingale, An archaeological and scientific study of Mycenaean glass from Elateia-Alonaki, Greece. In: Annales of the 17th Congress of the International Assiciation for the History of Glass ([o. O.] 2006) 39–46.

Schliemann 1878
H. Schliemann, Mykenae. Bericht über meine Forschungen und Entdeckungen in Mykenae (Leipzig 1878).

Stavrou u. a. 2014
E. Stavrou/D. Palles/E. I. Kamitsos/A. Lipovskii/D. Tagantsev/Y. Svirko/S. Honkanen, Vibrational study of thermally ion-exchanged sodium aluminoborosilicate glasses. Journal of Non-Crystalline Solids 401, 2014, 232–236.

Tite u. a. 2006
M. Tite/A. Shortland/Y. Maniatis/D. Kavoussanaki/S. Harris, The composition of the soda-rich and mixed alkali plant ashes used in the production of glass. Journal of Archaeological Science 33, 9, 2006, 1284–1292.

Walton u. a. 2009
M. S. Walton/A. Shortland/S. Kirk/P. Degryse, Evidence for the trade of Mesopotamian and Egyptian glass to Mycenaean Greece 36 in: 7 2009 1496–1503.

Woods 1994
W. G. Woods, An introduction to boron: History, sources, uses, and chemistry. 102 in: suppl 7 1994 5–11.

Yigit 2006
O. Yigit, Gold in Turkey — a missing link in Tethyan metallogeny. Ore Geology Reviews 28, 2, 2006, 147–179.

Zacharias u. a. 2013
N. Zacharias/M. Kaparou/S. Kastovszky/B. Maroti/K. Beltsios/J. Murphy/V. Kantarelou/A. G. Karydas, An alteration and provenance study of Mycenaean glass objects using neutron beam and X-ray methods 10 in: 2 2013 127–140.

Zacharias/Palamara 2016
N. Zacharias/E. Palamara, Glass corrosion: Issues and approaches for archaeological science. In: F. Gan (Hrsg.), Recent advances in the scientific research on ancient glass and glaze 2 ([o. O.] 2016) 233–247.

4 Discussion

The presented publications give an impression on how spectroscopic techniques can be applied to archaeological materials and emphasize the necessity of a methodological replication. My main focus is the investigation of technological developments in different periods of glass manufacture. Here, I will discuss the benefit of the included studies to the investigation of the specific period and in general about the history of glass technology.

4.1 Investigation of borosilicate glass layers on glass samples treated with gold

Using borax in the Aegean Bronze Age has been intensively discussed in the literature before (Schliemann 1878; Jüngst 1986; Reitzenstein 2016). However, there is no direct proof, e. g., excavated samples, for any borates in early history. The only direct evidence is a forged coin investigated by Landerer (1859), who does not supply the reader with any information on the provenience or exact age. Keeping in mind that the earliest documented coin usage is connected to the mythical Lydian King Midas and his successors (7^{th} century BCE; Davies 2002), this report can hardly be considered as a convincing proof for a Bronze Age sample[9]. The investigations of Möncke, Palles, et al. (2013), however, present indications for mutual surface alterations by borate usage in the Late Bronze Age period. The subsequent survey about the reproducibility of such altered glass layers (Drünert, Lind, Kästner, et al. in press; Drünert, Lind, Vontobel, et al. submitted) is therefore the necessary addendum to understand this alteration process. Here, we present the transfer of borates into a glass matrix by heat treatment of glass samples with borax and boron containing gold sheets.

By such heat treatment, borosilicate glass layers can indeed be realized. In both

[9]Nonetheless, this source must be considered significantly earlier than the first description of *chrysokolla* by Pliny the Elder in his *Naturalis Historia*, 1^{st} century CE (Reitzenstein 2016)

scenarios, contact of hot glass with borax and with boron contaminated gold, boron is introduced into a thin surface layer below 5 µm. Contaminated gold sheets could either indicate the use of a purification agent, or it is possible that borates were used for extracting gold from ores (Brepohl 1978; Appel and Na-Oy 2012). Alternatively, borates could be introduced as a potential solder or to prevent surface crystallization. All these scenarios fit the theory of gold covered glass findings, as implied by Panagiotaki (2008), and emphasize the depth of understanding gold manufacture in a Mycenaean society.

However, the analysis of boron in the Mycenaean glass artifacts requires further confirmation. The most characteristic infrared band at 940 cm^{-1} may be misinterpreted in archaeological samples due to the overlap of silanol bands with the $B\emptyset_4^-$ vibrations in the infrared spectra. Although the absence of O−H vibrations in the near infrared region at 3500 cm^{-1} favor the borate theory, direct analysis of borates in a very thin layer at a glass surface could improve the plausibility of these results. Possible techniques to measure such a layer could include particle-induced gamma ray emission (PIGE) or secondary ion mass spectrometry (SIMS).

4.2 Calcium antimonates as opacifying agents in Roman mosaic *tesserae*

Calcium antimonates have been known as opacifiers in antique opaque glasses for a long time (Shortland 2002). One of the first objects with calcium antimonate opacified glazes are blue Egyptian glass vessels with their characteristic white and yellow zigzag patterns (Mass et al. 2002). Such glazes were usually opacified by the calcium antimonates $CaSb_2O_6$ and $Ca_2Sb_2O_7$ (Mass et al. 2001; Lahlil, Biron, Cotte, Susini, and Menguy 2010). In the early years of the first millennium CE such opacifiers were also applied on Roman mosaic *tesserae*, usually with rather irregular occurrence of both crystal types (e. g., Mirti et al. 2001; Arletti et al. 2008). The recreation of such opacifiers in bulk glasses have been conducted before (Foster and Jackson 2005; Lahlil, Biron, Cotte, and Susini 2010), but the inhomogeneity of the two opacifiers has not been explained completely. By recreation of opaque bulk glasses with slightly modified composition, we examined the influence of TiO_2 and SnO_2 traces on the nucleation of antimonate crystallites (Drünert, Palamara, et al. 2018). Such impurities are regularly found in archaeological glass

samples and have to be considered for crystallization processes. However, since they only occur in traces below 1 wt%, we think they were not deliberately added to the glass batch. Regional differences in composition of such traces may also influence the ratio of $CaSb_2O_6$ to $Ca_2Sb_2O_7$ and could therefore result in the variations of reported opacifiers in the literature.

The successful replication of opaque glasses in a controlled experimental archaeological environment confirms the method of *in-situ* opacification by reducing the melting temperature. In contrast to flashed copper ruby glasses, no two-step melting temperature process was needed. Our experiments illustrate that the suggested process is simple and reproducible (Drünert, Palamara, et al. 2018). Further investigations should now focus on a quantitative investigation of crystallites in opaque white glasses and relate these quantities to the occurrence of nucleation agents. Furthermore, a multi-sample statistical analysis could also improve the understanding of the manufacture process.

4.3 Analysis of a glass feature nearby the Münster Philosophicum

Selected glass fragments of a mass feature excavated by Steppuhn (in press), close to the Philosophicum in Münster, were analyzed in our study (Drünert, Lozier, et al. in press), for their chemical composition. Such mass findings are often difficult to evaluate: the visual appearance of all glass samples is usually too similar to differentiate; moreover, the glass samples of this feature appear to be related to restorations conducted in the late Medieval or Early Modern period and must have been disposed together. Neither the proveniences of these glasses nor their original placement could be determined by stratigraphic relationship. By analysis of exemplary glass samples, we proved that indeed glasses from at least three sources have been employed in the original arrangement.

The studied glass samples prove not only the existence of several production sites, but emphasize the knowledge of glass manufacturers in the Medieval period. At least one group of glasses was prepared similar to the recipes provided by Theophilus Presbyter in the 11^{th} century CE (Ilg 1874). A second group contained relatively high amounts of sodium oxide and could have been produced using NaCl as flux. Such glass compositions have been found in later samples, as seen in Schalm et al. (2007). The third group

consisted of emerald lead glasses, as they have been described by Heraclius (Ilg 1873) and Theophilus Presbyter (Ilg 1874).

The investigation of the $Fe^{2+} - Fe^{3+}$ redox ratios in such glass samples enabled an estimation of a typical atmosphere in Medieval glass furnaces. We demonstrated by comparison with cobalt blue glass samples, that in most cases the atmosphere in the furnace remained steady for the majority of the glass samples. The typical ratio of $\frac{Fe^{2+}}{Fe_{total}}$ was around 10 %. A next step of investigation could be the reproduction of colorless glass in a wood fired glass furnace and comparison of different reducing agents after specific melting periods. Such results could possibly strengthen other reproduction experiments, e. g., those conducted by Wiesenberg (2014).

4.4 Copper nanoparticles: The influence of particle size on the visual appearance of opaque red glasses

The chemistry of copper in red opaque glasses has been the topic of many debates (e. g., Hughes 1972; Brill and Cahill 1988; Shugar 2000). Although both phases, metallic Cu^0 spheres and Cu_2O crystallites, can colorize glass, the visual appearance of Cu_2O particles differs from the appearance of Cu^0 spheres. In our study (Drünert, Blanz, et al. 2018), we explain the different UV-Vis-NIR reflectance spectra of such opaque red glasses by simulating the backscattering of nanoparticles with various sizes. We prove that the identity and size of the scatterer of Medieval and Early Modern opaque red glasses can be determined by comparison of the UV-Vis-NIR reflectance spectra with simulated scattering efficiencies. Furthermore, the application on other glass systems with metallic nanoparticles of undetermined size is possible.

The reproduction of opaque red glasses in this study also demonstrates that copper nanoparticles form in a one step process under strongly reducing conditions. The manufacture of opaque red vessels, as found in some Medieval features (Steppuhn 2006; Rempel 2008), could be explained using such conditions to form copper nanoparticles, as opposed to the typical flashed cameo glass.

4.5 Conclusion

The development in historical techniques occurred often through multiple, separate small steps. Many technologies continued for long periods of time without major changes. Today we can only analyze fragmentary remains, based on which we aim to understand the processes, proveniences and usage of the findings. The analysis of such samples and interpretation of the results is therefore an essential element of the investigation. In all four studies, the analysis of archaeological glass samples and the reproduction of the archaeomaterials improved the understanding of manufacture significantly. The results include sample treatment and surface alteration (Drünert, Lind, Kästner, et al. in press; Drünert, Lind, Vontobel, et al. submitted), opacification processes (Drünert, Palamara, et al. 2018) and production conditions and the understanding of the visual appearance (Drünert, Blanz, et al. 2018; Drünert, Lozier, et al. in press). The investigations therefore contribute to the general knowledge about ancient technologies. This information can be used to explain the processes to an interested audience, in the form of experimental archaeological studies, but also the information can broaden the understanding of the chemistry behind the ancient processes. The knowledge of glass manipulation is therefore not only a key to ancient technologies, but also to investigations of modern glasses and their applications.

5 Summary

The present study focuses on technological developments in the history of glass technology. I selected four aspects of glass manufacture from different periods, beginning in the earliest period of artificial glass and ending in the Early Modern time.

5.1 Borosilicate glass layers on Mycenaean glass samples

Gold covered glass samples originating from the Mycenaean epoch have been found in several contexts (Haevernick 1960; Nightingale 2004; Panagiotaki 2008). In a previous study, Möncke, Palles, et al. (2013) discovered unusual infrared absorption bands around 930 cm^{-1}, typical for $B\emptyset_4^-$-units in a borosilicate glass. However, the relief inlays showed no indication for borate in the quantitative analysis. Based on this study, we investigated possibilities of boron contaminations in the surface of reproduced glass samples (Drünert, Lind, Vontobel, et al. submitted). Focus was the interaction of gold sheets with glass samples during heat treatments, using borax either as a solder to attach the glass to the gold or as a cleaning agent for the gold sheets before treatment. We could demonstrate by infrared reflection spectroscopy that both borate contamination on gold and borax powder interact with the glass surface at temperatures above 800 °C. Borate units in the glass were identified by the presence of a B−OH band at ca. 1370 cm^{-1}. The interaction between the silicate matrix and the borate layer formed a borosilicate structure leading to Si−O−B vibrations at 690 cm^{-1}. An interaction between borate and silicate groups was additionally detected by Raman scattering bands at 450 cm^{-1} to 550 cm^{-1}.

The suggested borate contamination in the glass surface could arise due to at least three mechanisms: Firstly, borax or similar chemicals could have been used as a solder to attach gold to a glass at high temperatures. The glass could either be cast directly on a gold sheet covered with a borate layer or both glass and gold could be annealed at temperatures above 800 °C. Secondly, borax may have been used to extract gold from

ores, as later discovered by Appel and Na-Oy (2012), or to purify gold (Brepohl 1978). The glass could therefore be attached by heat treatment without using a solder. As of yet no source of boron has been discovered during excavations. An unambiguous free identification of boron in the top layer of the glass would therefore prove that borates were known as a solder or a material to process gold in the Late Bronze Age. Neutron tomography may be a promising method for the detection of boron in the glass surface: The combination of neutron absorption with infrared reflection spectroscopy has good prospects – while being non-destructive – to detect borosilicate structures in the glass surface.

5.2 Calcium antimonate opacifiers in Roman mosaic *tesserae*

Calcium antimonates are often found in opaque white glass ceramics and glazes from the Roman period and before (Shortland 2002; Arletti et al. 2008; Lahlil, Biron, Cotte, and Susini 2010). The occurrence of both known crystal structures, trigonal $CaSb_2O_6$ and cubic $Ca_2Sb_2O_7$, seems to be random in most archaeological samples (e. g., Mirti et al. 2001). The presented study compares different procedures of opacification, that is by *in-situ* crystallization, by *ex-situ* addition of separately synthesized calcium antimonates or by secondary heat treatment of clear glass samples, with mosaic *tesserae* from Messene, Greece, 1st to 4th century CE (Drünert, Palamara, et al. 2018). Furthermore, we investigated the influence of traces of TiO_2 and SnO_2 on the crystallization behavior. All samples were examined by Raman spectroscopy and X-ray diffraction. We demonstrated that the *in-situ* crystallization at temperatures below 1200 °C produces the most reliable opacification. Additionally the presence of SnO_2 and TiO_2 influences the crystallization behavior of the glass, even if present in traces of ca. 0.2 wt% in the glass matrix. Together with cubic and trigonal calcium antimonate, the minerals tridymite, cristobalite and calcite were found in the opaque samples. The process of opacification was reproduced in an experimental archaeological glass furnace at an average temperature of ca. 1050 °C.

5.3 Investigation of glass samples from the Münster philosophicum

A selection of glass samples excavated near the *philosophicum* in Münster (Steppuhn in press) was investigated by X-ray fluorescence and optical spectroscopy. The analyzed glasses were differently colored glass shards originating from a 278 kg mass feature and were dated to the 12th to 16th century CE. In this study we could demonstrate that the glass samples of this feature were made by at least three recipes: The X-ray fluorescence analysis revealed that one group of glass samples contained significantly higher amounts of K_2O (8 wt% to 20 wt%) and 0.5 wt% to 1.5 wt% Na_2O. This group was most similar to glasses that can be obtained following the recipe of Theophilus Presbyter (Ilg 1874). A second group contained between 2 wt% and 6 wt% K_2O and 2 wt% to 5 wt% Na_2O. Such glasses are more typical for late medieval glasses and could possibly be prepared using NaCl as an additional alkali source. A third group consisted of emerald green lead glasses.

The optical analysis showed that the content of Fe^{2+} in most of the investigated glass samples was 10 % to 20 % of the total amount of Fe ions in the glass. We could therefore confirm that the furnace atmosphere of the glass furnaces used for the preparation of these samples were much more reducing compared to ambient condition in an electric glass furnace (40 % Fe^{2+}). The relation of $\frac{Fe^{2+}}{Fe_{total}}$ to the manganese content indicated that glass maker soap was not used to influence the color of the glass.

5.4 The influence of particle size and type on the visual appearance of copper reds

Opaque red glasses are known since the beginning of glass manufacture (Shortland 2002). Two main theories have been reported to explain the color of such glasses: one based on metallic copper (Hughes 1972; Weyl 2016) and the other on cuprite particles (Brill and Cahill 1988). This study focuses on the scattering properties of Cu_2O and Cu^0 particles with different sizes (Drünert, Blanz, et al. 2018). We show by simulation of the Mie backscattering and absorption cross sections of such particles in a soda lime silicate matrix, how the optical spectra change depending on the particle size and the wavelength

of light. We compared these results with a sample set from Glashütten, Germany, 12$^{\text{th}}$ to 14$^{\text{th}}$ century CE, and a sample set from Wieda, Germany, 17$^{\text{th}}$ century CE. By fitting the expected backscattering curves into the UV/Vis/NIR reflectance spectra, we estimated an average Cu^0 particle radius of 80 nm to 95 nm for the samples from Glashütten and 60 nm to 80 nm for samples from Wieda. The fitting of simulated cuprite spectra did not give reasonable results.

We compared the estimated values with electron microscopy images of a polished sample surface. The determined particle radius $r > 65$ nm match the results of UV/Vis/NIR reflectance spectroscopy. Lastly, we reproduced opaque red glasses in a strongly reducing atmosphere. We demonstrated that copper nanoparticles of a similar radius form in a one-step melting process at 1400 °C under reducing atmosphere.

5.5 General summary

The technology of glass manufacture was investigated by analysis of archaeological glass samples and the reproduction of the used materials. I demonstrated developments in glass processing by four examples to highlight the technological state of the art in the respective epoch. The experimental approach enabled a detailed understanding of the challenges and specifications during the manufacture.

6 Zusammenfassung

Die dargestellten Studien fokussieren die technologischen Entwicklungen innerhalb der Geschichte der Glastechnologie. Ich habe vier Aspekte der Glasherstellung aus verschiedenen Epochen ausgewählt. Sie umfassen den Zeitraum vom Anfang des menschengemachten Glases bis zur frühen Moderne.

6.1 Borosilicat-Glasschichten auf mykenischen Glasproben

Mit Goldfolie bedeckte Glasproben aus mykenischer Zeit sind aus verschiedenen Kontexten bekannt (Haevernick 1960; Nightingale 2004; Panagiotaki 2008). In einer vorhergehenden Studie entdeckten Möncke, Palles u. a. (2013) ungewöhnliche Infrarot-Absorptionsbanden bei einer Energie von etwa $930\,\mathrm{cm}^{-1}$, die typisch für $\mathrm{B}\emptyset_4^-$-Gruppen in Borosilicatgläsern sind. Der direkte Nachweis von Bor in den oberflächennahen Bereichen verblieb allerdings negativ, vor allem beeinflusst durch die niedrige Konzentration und die dünne Schichtdicke im Zusammenspiel mit der schwierigen Analyse dieses leichten Elements durch Rasterelektronenmikroskopie und Röntgenfluoreszenz. Von dieser Beobachtung ausgehend untersuchten wir mögliche Ursachen der Borkontamination in der Oberfläche von reproduzierten Modellglasproben (Drünert, Lind, Vontobel u. a. eingereicht). Fokus war insbesondere die Interaktion von Blattgold mit Glasproben während einer Temperaturbehandlung unter Verwendung von Bor als Lötmittel und zum Reinigen von Gold. Wir konnten durch infrarotspektroskopische Untersuchungen zeigen, dass sowohl durch Borverbindungen kontaminierte Goldplättchen als auch Borax als Lötmittel zwischen dem Gold und der Glasprobe zu einer Oberflächenreaktion bei Temperaturen oberhalb 800 °C führten. Boratgruppen im Glas wurden durch die B−OH Infrarotbande bei ca. $1370\,\mathrm{cm}^{-1}$ identifiziert. Die Interaktion zwischen der silicatreichen Glasmatrix und der gebildeten Boratschicht führte zu der Ausbildung von Si−O−B Schwingungen

mit Energien um 690 cm^{-1}. Eine solche Interaktion konnte mit Raman-Spektroskopie anhand von Banden im Bereich zwischen 450 cm^{-1} und 550 cm^{-1} bestätigt werden.

Die vorgeschlagene Kontamination durch Borverbindungen in der Glasoberfläche ist durch mindestens drei Mechanismen möglich: Erstens könnte Borax oder eine ähnliche Verbindung als Lötmittel verwendet worden sein, um die Verbindung von Glas und Gold zu stärken. Dabei könnte sowohl das Glas auf eine mit Boraxpulver beschichtete Goldprobe gegossen, als auch eine Glasprobe zusammen mit einer Goldprobe bei Temperaturen oberhalb 800 °C behandelt worden sein. Als zweites könnte Borax zur Extraktion von Gold aus Erzen (Appel und Na-Oy 2012, vgl.) oder zur Reinigund von Gold (Brepohl 1978) verwendet worden sein. In diesem Fall gehen wir nicht von der Verwendung eines Lötmittels aus. Bis heute ist allerdings kein Fall bekannt, in welchem die Verwendung von Boraten in der späten Bronzezeit nachgewiesen worden sind. Der eindeutige Nachweis von Bor in der Glasoberfläche wäre daher ein erstmaliger Beweis für die Kenntnis von Boraten als Lötmittel oder zur Verarbeitung von Gold in der späten Bronzezeit. Eine vielversprechende Methode für die Detektion von Bor ist die Kombination von Neutronentomographie mit Infrarotspektroskopie.

6.2 Calciumantimonat als Trübungsmittel in römischen Mosaik-*tesserae*

Calciumantimonate sind in weißen Glaskeramiken und Glasuren vor- und seit der Römerzeit nachgewiesen worden (Shortland 2002; Arletti u. a. 2008; Lahlil, Biron, Cotte und Susini 2010). Die beiden bekannten Kristallstrukturen, trigonales $CaSb_2O_6$ und kubisches $Ca_2Sb_2O_7$, scheinen in archäologischen Proben zufällig aufzutreten (z. B. Mirti u. a. 2001). In der hier gezeigten Studie vergleichen wir verschiedene Methoden der Trübung von Kalk-Natron-Silicatglas, namentlich *in-situ*-Kristallisation, *ex-situ*-Zugabe von Calciumantimonat zur Glasschmelze und gesteuerte Kristallisation durch Temperaturbehandlung, mit römischen Mosaikgläsern aus Messene, Griechenland, erstes bis viertes Jahrhundert u. Z. (Drünert, Palamara u. a. 2018). Weiterhin untersuchten wir den Einfluss von Titan- und Zinndioxid auf die Kristallisation. Die Analyse der Glasproben erfolgte durch Raman-Spektroskopie und Röntgendiffraktometrie. Wir konnten zeigen, dass *in-situ*-Kristallisation unterhalb von 1200 °C die Glasproben am zuverlässigsten trübte. Die

Gegenwart von TiO_2 und SnO_2 im Gemenge beeinflusste das Kristallisationsverhalten, sogar wenn sie nur in Spuren in der Größenordnung von 0.2 Masse% in der Glasmatrix vorhanden waren. Neben kubischem und trigonalem Calciumantimonat konnten wir Tridymit, Cristobalit und Calcit in den getrübten Proben nachweisen. Die Trübung wurde anschließend in einem experimentell-archäologischen Glasofen nach römischem Vorbild bei einer Durchschnittstemperatur von etwa 1050 °C reproduziert.

6.3 Untersuchung der Glasproben des Münsteraner *philosophicum*

Wir untersuchten eine Auswahl an Glasproben, welche in der Nähe des Münsteraner *Philosophicum* ausgegraben wurden (Steppuhn in press), mit Röntgenfluoreszenzspektroskopie und optischer Spektroskopie. Die Glasproben bestanden aus verschieden farbiger Glasscherben, welche aus einem etwa 278 kg umfassenden Befund stammten und auf das 12. bis 16. Jahrhundert u. Z. datiert wurden. Die Studie zeigt, dass mindestens drei verschiedene Rezepturen zur Herstellung der Glasproben verwendet wurden: Die Röntgenfluoreszenzanalyse ergab dass eine Gruppe signifikant höhere Mengen K_2O (8 Masse% bis 20 Masse%) und geringe Mengen Na_2O (0.5 Masse% bis 1.5 Masse%). Diese Gruppe ähnelt dadurch am ehesten Gläsern, die nach der Rezeptur von Theophilus Presbyter (Ilg 1874) erschmolzen wurden. Eine zweite Gruppe enthielt zwischen 2 Masse% und 6 Masse% K_2O und 2 Masse% bis 5 Masse% Na_2O. Solche Gläser sind typischer für spätmittelalterliche Glasproben und weisen auf die Verwendung von NaCl als Flussmittel hin. Eine dritte Gruppe waren smaragdgrüne Bleigläser.

Die optische Analyse zeigte, dass der Anteil an Fe^{2+} in den meisten Glasproben 10 % bis 20 % des Gesamtanteils an Eisenionen entsprach. Dadurch konnten wir zeigen, dass die Ofenatmosphäre deutlich niedriger als in einem elektrisch geheizten Ofen war (ca. 40 % Fe^{2+}). Die Relation von $\frac{Fe^{2+}}{Fe_{gesamt}}$ zu dem Mangananteil im Glas deutet darauf hin, dass keine Glasmacherseife zur Beeinflussung der Glasfarbe verwendet wurde.

6.4 Der Einfluss von Partikelgröße und -art auf die optische Erscheinung von Kupfer-roten opaken Gläsern

Opake rote Gläser sind seit Beginn der Glasherstellung bekannt (Shortland 2002). Zwei Theorien zur Färbung des Glases wurden entwickelt: zum einen basierend auf metallischen Kupferpartikeln (Hughes 1972; Weyl 2016) und zum anderen auf Cuprit (Brill und Cahill 1988), In dieser Studie behandeln wir die Streueigenschaften sowohl von Cu_2O- als auch von Cu^0-Partikeln verschiedener Größe in einer Glasmatrix (Drünert, Blanz u. a. 2018). Wir konnten durch Simulation der Streuquerschnitte durch Mie-Rückstreuung und Absorption in einem Kalk-Natron-Silicatglas zeigen, wie sich die optischen Spektren in Abhängigkeit von Partikelgröße und verwendeter Wellenlänge des Lichts verändern. Diese Ergebnisse wurden mit Glasproben aus Glashütten, Deutschland, 12. bis 14. Jahrhundert u. Z. und aus Wieda, Deutschland, 17. Jahrhundert u. Z. verglichen. Durch das Simulieren der UV-Vis-NIR Reflexionsmessungen und die Kombination verschiedener berechneter Streukurven konnten wir eine durchschnittliche Partikelgröße von 80 nm bis 95 nm (Glashütten) bzw. 60 nm bis 80 nm (Wieda) bestimmen. Die entsprechende Simulation der experimentellen Reflexionsmessungen mithilfe von Streukurven durch Cuprit führte zu inkonsistenten Ergebnissen.

Die berechneten Werte wurden anschließend mit Messungen durch Elektronenmikroskopie an der polierten Glasoberfläche verglichen. Der gemessene Partikelradius $r > 65\,\text{nm}$ stimmt gut mit den Ergebnissen der UV-Vis-NIR Reflexionsspektroskopie überein. Wir zeigten weiterhin, dass Kupfer-Nanopartikel in vergleichbarer Größenordnung durch einen einstufigen Schmelzprozess bei 1400 °C unter reduzierenden Bedingungen möglich ist.

6.5 Generelle Zusammenfassung

Die Technologie der Glasproduktion wurde durch die Analyse archäologischer Glasproben und durch die Reproduktion der Gläser untersucht. Ich konnte anhand von vier Beispielen Entwicklungen der Glasverarbeitung in der jeweiligen Zeit zeigen. Der experimentelle Ansatz ermöglichte ein vertiefendes Verständnis der Herstellungsprozesse und ihrer Schwierigkeiten.

Bibliography

Allen, G. C. and N. S. Hush (1967). "Intervalence-transfer absorption. Part 1. Qualitative evidence for intervalence-transfer absorption in inorganic systems in solution and in the solid state". In: *Progress in Inorganic Chemistry*. Ed. by F. A. Cotton. Vol. 8. New York: Wiley, pp. 357–389. DOI: 10.1002/9780470166093.ch6.

Appel, P. W. and L. Na-Oy (2012). "The Borax Method of Gold Extraction for Small-Scale Miners". In: *Journal of Health and Pollution* 2.3, pp. 5–10. DOI: 10.5696/2156-9614-2.3.5.

Arletti, R., G. Vezzalini, S. Quartieri, D. Ferrari, M. Merlini, and M. Cotte (2008). "Polychrome glass from Etruscan sites: first non-destructive characterization with synchrotron μ-XRF, μ-XANES and XRPD". In: *Applied Physics A* 92.1, pp. 127–135. DOI: 10.1007/s00339-008-4462-x.

Avramov, I., T. Vassilev, and I. Penkov (2005). "The glass transition temperature of silicate and borate glasses". In: *Journal of Non-Crystalline Solids* 351.6-7, pp. 472–476. DOI: 10.1016/j.jnoncrysol.2005.01.044.

Barber, D. J. and I. C. Freestone (Feb. 1990). "An investigation of the origin of the colour of the Lycurgus cup by analytical TEM". In: *Archaeometry* 32.1, pp. 33–45. DOI: 10.1111/j.1475-4754.1990.tb01079.x. URL: http://dx.doi.org/10.1111/j.1475-4754.1990.tb01079.x (visited on 09/13/2016).

Basch, H., A. Viste, and H. B. Gray (1966). "Molecular orbital theory for octahedral and tetrahedral metal complexes". In: *The Journal of Chemical Physics* 44.1, pp. 10–19. DOI: 10.1063/1.1726431.

Beckhoff, B., B. Kanngießer, N. Langhoff, R. Wedell, and H. Wolff, eds. (2006). *Handbook of practical X-ray fluorescence analysis*. Berlin: Springer-Verlag. ISBN: 3540286039.

Bertin, E. P. (1975). *Principles and Practice of X-Ray Spectrometric Analysis*. New York: Plenum Press. DOI: 10.1007/978-1-4613-4416-2.

Bingham, P. A., O. M. Hannant, N. Reeves-McLaren, M. C. Stennett, and R. J. Hand (2014). "Selective behaviour of dilute Fe^{3+} ions in silicate glasses: an Fe K-edge EXAFS

and XANES study". In: *Journal of Non-Crystalline Solids* 387, pp. 47–56. DOI: 10.1016/j.jnoncrysol.2013.12.034.

Bohren, C. F. and D. R. Huffman, eds. (1998). *Absorption and scattering of light by small particles*. New York: Wiley-VCH. DOI: 10.1002/9783527618156.

Brepohl, E. (1978). *Theorie und Praxis des Goldschmieds*. 5th ed. Leipzig: VEB Fachbuchverlag.

Brill, R. H. (1972). "Some chemical observations on the cuneiform glassmaking texts". In: *Annales du 5e Congrés de l'Association Internationale pour l'Historie du Verre*, pp. 329–351.

– (1999). *Chemical analyses of early glass, vols. I/II, The catalogue / The tables*. Tech. rep. The Corning Museum of Glass, New York.

Brill, R. H. and N. D. Cahill (1988). "A red opaque glass from Sardis and some thoughts on red opaques in general". In: *Journal of Glass Studies* 30, pp. 16–27.

Brun, N., L. Mazerolles, and M. Pernot (1991). "Microstructure of opaque red glass containing copper". In: *Journal of Materials Science Letters* 10.23, pp. 1418–1420. DOI: 10.1007/BF00735696.

Bunker, B. C. (1994). "Molecular mechanisms for corrosion of silica and silicate glasses". In: *Journal of Non-Crystalline Solids* 179, pp. 300–308. DOI: 10.1016/0022-3093(94)90708-0.

Cabral, A. A., V. M. Fokin, and E. D. Zanotto (2004). "Nanocrystallization of fresnoite glass. II. Analysis of homogeneous nucleation kinetics". In: *Journal of Non-Crystalline Solids* 343.1-3, pp. 85–90. DOI: 10.1016/j.jnoncrysol.2004.06.020.

Cagno, S., L. Favaretto, M. Mendera, A. Izmer, F. Vanhaecke, and K. Janssens (2012). "Evidence of early medieval soda ash glass in the archaeological site of San Genesio (Tuscany)". In: *Journal of Archaeological Science* 39.5, pp. 1540–1552. DOI: 10.1016/j.jas.2011.12.031.

Câpâţînâ, C. (2005). "The study of copper ruby glass". In: *Ceramics-Silikáty* 49.4, pp. 283–286. URL: http://pdf.easechem.com/pdf/05/2005_04_283.pdf (visited on 09/13/2016).

Carmona, N., M. A. Villegas, P. Jiménez, J. Navarro, and M. García-Heras (2009). "Islamic glasses from Al-Andalus. Characterisation of materials from a Murcian workshop (12th century AD, Spain)". In: *Journal of Cultural Heritage* 10.3, pp. 439–445. DOI: 10.1016/j.culher.2008.12.005.

Chang, R. and J. W. Thoman Jr. (2014). *Physical chemistry for the chemical sciences*. Sausalito: University Science Books. 951 pp. ISBN: 1891389696. URL: https://www.ebook.de/de/product/22026129/raymond_chang_physical_chemistry_for_the_chemical_sciences.html.

Colomban, P. (2008). "On-site Raman identification and dating of ancient glasses: A review of procedures and tools". In: *Journal of Cultural Heritage* 9, pp. 55–60. DOI: 10.1016/j.culher.2008.06.005.

Cuevas, A. M. and H. P. Gravie (2011). "Portable energy dispersive X-ray fluorescence and X-ray diffraction and radiography system for archaeometry". In: *Nuclear Instruments and Methods in Physics Research Section A: Accelerators, Spectrometers, Detectors and Associated Equipment* 633.1, pp. 72–78. DOI: 10.1016/j.nima.2010.12.178.

Davies, G. (2002). *History of money: From ancient times to the present day*. 3rd ed. Cardiff: University of Wales Press. ISBN: 978-0-7083-1717-4.

Delpy, D. T., M. Cope, P. van der Zee, S. Arridge, S. Wray, and J. Wyatt (1988). "Estimation of optical pathlength through tissue from direct time of flight measurement". In: *Physics in Medicine and Biology* 33.12, pp. 1433–1442. DOI: 10.1088/0031-9155/33/12/008.

Diem, M. (2015). *Modern vibrational spectroscopy and micro-spectroscopy*. New York: John Wiley & Sons. DOI: 10.1002/9781118824924.

Dietzel, A. (1942). "Die Kationenfeldstärken und ihre Beziehungen zu Entglasungsvorgängen, zur Verbindungsbildung und zu den Schmelzpunkten von Silicaten". In: *Zeitschrift für Elektrochemie und angewandter physikalischer Chemie* 48.1, pp. 9–23.

Drünert, F., M. Blanz, K. Pollok, Z. Pan, L. Wondraczek, and D. Möncke (2018). "Copper-based opaque red glasses. Understanding the colouring mechanism of copper nanoparticles in archaeological glass samples". In: *Optical Materials* 76, pp. 375–381. DOI: https://doi.org/10.1016/j.optmat.2017.12.054.

Drünert, F., E. Lozier, P. Steppuhn, and D. Möncke (in press). "Untersuchung farbgebender Zusätze im münsteraner Glasbefund mit Hilfe Optischer Spektroskopie". In: *Glas und Glashütten: Archäologische Belege zu Rohstoff, Verarbeitung, Handel und Nutzung. Arbeitskreis zur Erforschung des mittelalterlichen Handwerks, 15. Treffen Konstanz 22.-24.05.2014 sowie 6. Internationales Symposium zur Erforschung mittelalterlicher und frühneuzeitlicher Glashütten Europas, Tagung Baiersbronn 6.5.-8.5. 2016*. Forschun-

gen und Berichte zur Archäologie in Baden-Württemberg. Esslingen: Landesamt für Denkmalpflege Baden-Württemberg. in press.

Drünert, F., F. Lind, A. Kästner, P. Vontobel, E. I. Kamitsos, N. Zacharias, and D. Möncke (in press). "Oberflächenanalyse Mykenischer Glasfragmente der späten Bronzezeit – Hinweise auf Vergoldung unter Zuhilfenahme von Borax". In: *Glas und Glashütten: Archäologische Belege zu Rohstoff, Verarbeitung, Handel und Nutzung. Arbeitskreis zur Erforschung des mittelalterlichen Handwerks, 15. Treffen Konstanz 22.-24.05.2014 sowie 6. Internationales Symposium zur Erforschung mittelalterlicher und frühneuzeitlicher Glashütten Europas, Tagung Baiersbronn 6.5.-8.5. 2016*. Forschungen und Berichte zur Archäologie in Baden-Württemberg. Esslingen: Landesamt für Denkmalpflege Baden-Württemberg. in press.

Drünert, F., F. Lind, P. Vontobel, E. I. Kamitsos, N. Zacharias, L. Wondraczek, and D. Möncke (submitted). "Borosilicate glass layers on Mycenaean glass: surface alterations by glass — borax — gold interactions". In: *Frontiers in Materials* (). Submitted.

Drünert, F., E. Palamara, N. Zacharias, L. Wondraczek, and D. Möncke (2018). "Ancient Roman nano-technology: Insight into the manufacture of mosaic *tesserae* opacified by calcium antimonate". In: *Journal of the European Ceramic Society* 38.14, pp. 4799–4805. DOI: 10.1016/j.jeurceramsoc.2018.06.031.

Drünert, F., N. Zacharias, and D. Möncke (in press). "Einblick in die Chemie und Physik der Farbigkeit und Opazität von Gläsern". In: *Glas und Glashütten: Archäologische Belege zu Rohstoff, Verarbeitung, Handel und Nutzung. Arbeitskreis zur Erforschung des mittelalterlichen Handwerks, 15. Treffen Konstanz 22.-24.05.2014 sowie 6. Internationales Symposium zur Erforschung mittelalterlicher und frühneuzeitlicher Glashütten Europas, Tagung Baiersbronn 6.5.-8.5. 2016*. Forschungen und Berichte zur Archäologie in Baden-Württemberg. Esslingen: Landesamt für Denkmalpflege Baden-Württemberg. in press.

Duffy, J. A. and M. D. Ingram (1976). "An interpretation of glass chemistry in terms of the optical basicity concept". In: *Journal of Non-Crystalline Solids* 21.3, pp. 373–410. DOI: 10.1016/0022-3093(76)90027-2.

Duffy, J. A. (1990). *Bonding, energy levels, and bands in inorganic solids*. Harlow: Longman.

Dungworth, D. (2011). "The value of historic window glass". In: *The Historic Environment: Policy & Practice* 2.1, pp. 21–48. DOI: 10.1179/175675011x12943261434567.

Duyne van, R. P., D. L. Jeanmaire, and D. F. Shriver (1974). "Mode-locked laser Raman spectroscopy. New technique for the rejection of interfering background luminescence signals". In: *Analytical Chemistry* 46.2, pp. 213–222. DOI: 10.1021/ac60338a012.

Elisa, M., B. Sava, A. Diaconu, D. Ursu, and R. Patrascu (2009). "Fluorescence of copper, manganese and antimony ions in phosphate glass host". In: *Journal of Non-Crystalline Solids* 355.37-42, pp. 1877–1879. DOI: 10.1016/j.jnoncrysol.2009.03.010.

Emberling, G., J. Cheng, T. E. Larsen, H. Pittman, T. B. B. Skuldboel, J. Weber, and H. T. Wright (1999). "Excavations at Tell Brak 1998: Preliminary report". In: *Iraq* 61, pp. 1–41. DOI: 10.2307/4200465.

Farges, F., C. W. Ponader, G. Calas, and G. E. Brown (1992). "Structural environments of incompatible elements in silicate glass/melt systems: II. U^{IV}, U^{V}, and U^{VI}". In: *Geochimica et Cosmochimica Acta* 56.12, pp. 4205–4220. DOI: 10.1016/0016-7037(92)90261-g.

Fokin, V. M., E. D. Zanotto, N. S. Yuritsyn, and J. W. P. Schmelzer (2006). "Homogeneous crystal nucleation in silicate glasses: A 40 dates perspective". In: *Journal of Non-Crystalline Solids* 352.26-27, pp. 2681–2714. DOI: 10.1016/j.jnoncrysol.2006.02.074.

Foster, H. E. and C. M. Jackson (2005). "'A whiter shade of pale'? Chemical and experimental investigation of opaque white Roman glass gaming counters". In: *Glass Technology* 46.5, pp. 327–333. ISSN: 0017-1050.

Freestone, I., J. J. Kunicki-Goldfinger, H. Gilderdale-Scott, and T. Ayres (2010). "Multidisciplinary investigation of the windows of John Thornton, focusing on the Great East Window of York Minster". In: *The Art of Collaboration: Stained-Glass Conservation in the 21st Century*. Ed. by M. B. Shepard, L. Pilosi, and S. Strobl. Turnhout: Brepols/Harvey Miller Publications for the American Corpus Vitrearum, pp. 151–160.

Freestone, I. C. (2004). "The provenance of ancient glass through compositional analysis". In: *MRS Proceedings* 852. DOI: 10.1557/proc-852-oo8.1.

– (2006). "Glass production in Late Antiquity and the Early Islamic period: a geochemical perspective". In: *Geological Society, London, Special Publications* 257.1, pp. 201–216. DOI: 10.1144/gsl.sp.2006.257.01.16.

Gadd, C. J. and R. C. Thompson (1936). "A Middle-Babylonian chemical text". In: *Iraq* 3.1, p. 87. DOI: 10.2307/4241587.

Gedzevičiūtė, V., N. Welter, U. Schüssler, and C. Weiss (2009). "Chemical composition and colouring agents of Roman mosaic and millefiori glass, studied by electron microprobe analysis and Raman microspectroscopy". In: *Archaeological and Anthropological Sciences* 1.1, pp. 15–29.

Gouesbet, G. and G. Gréhan (2011). *Generalized Lorenz-Mie theories*. Berlin: Springer. DOI: 10.1007/978-3-642-17194-9.

Gratuze, B. and J.-N. Barrandon (1990). "Islamic glass weights and stamps: Analysis using nuclear techniques". In: *Archaeometry* 32.2, pp. 155–162. DOI: 10.1111/j.1475-4754.1990.tb00462.x.

Gray, H. B. and C. J. Ballhausen (1963). "A molecular orbital theory for square planar metal complexes". In: *Journal of the American Chemical Society* 85.3, pp. 260–265. DOI: 10.1021/ja00886a002.

Green, L. R. and F. A. Hart (1987). "Colour and chemical composition in ancient glass: An examination of some Roman and Wealden glass by means of ultraviolet-visible-infra-red spectrometry and electron microprobe analysis". In: *Journal of Archaeological Science* 14.3, pp. 271–282. DOI: 10.1016/0305-4403(87)90015-x.

Griffiths, P. R. and J. A. de Haseth (May 11, 2007). *Fourier transform infrared spectrometry*. Ed. by J. D. Winefordner. Hoboken, New Jersey: Wiley John + Sons. 700 pp. ISBN: 0471194042.

Groot de, F. and J. Vogel (2005). "X-ray spectroscopy". In: *Neutron and X-ray spectroscopy*. Ed. by F. Hippert, E. Geissler, J. L. Hodeau, E. Lelièvre-Berna, and J.-R. Regnard. Dordrecht: Springer, pp. 3–66. ISBN: 9781402033377.

Gutzow, I. S. and J. W. P. Schmelzer (2013). *The vitreous state. Thermodynamics, structure, rheology, and crystallization*. 2nd ed. Heidelberg: Springer.

Haevernick, T. E. (1960). "Beiträge zur Geschichte des antiken Glases: Mykenisches Glas". In: *Jahrbuch des Römisch-Germanischen Zentralmuseums Mainz* 6, pp. 36–50.

Halstead, J. A. (2012). "Teaching the spin selection rule: An inductive approach". In: *Journal of Chemical Education* 90.1, pp. 70–75. DOI: 10.1021/ed200795t.

Henderson, B. and G. F. Imbusch (1989). *Optical spectroscopy of inorganic solids*. Vol. 44. Monographs on the physics and chemistry of materials. Oxford: Oxford University Press. ISBN: 0-19-851372-0.

Henderson, J., S. D. McLoughlin, and D. S. McPhail (2004). "Radical changes in Islamic glass technology: evidence for conservatism and experimentation with new glass recipes

from early and middle Islamic Raqqa, Syria". In: *Archaeometry* 46.3, pp. 439–468. DOI: 10.1111/j.1475-4754.2004.00167.x.

Henderson, J. (1985). "The raw materials of early glass production". In: *Oxford Journal of Archaeology* 4.3, pp. 267–291. DOI: 10.1111/j.1468-0092.1985.tb00248.x.

Hendy, S. (2002). "Light scattering in transparent glass ceramics". In: *Applied Physics Letters* 81.7, pp. 1171–1173. DOI: 10.1063/1.1499989.

Herzberg, G. (1945). *Infrared and Raman spectra of polyatomic molecules.* New York: D. van Nostrand Company, pp. 288–288. DOI: 10.1021/j150447a021.

Höland, W. and G. H. Beall (2013). "Glass-ceramics". In: *Handbook of Advanced Ceramics.* Ed. by S. Somiya. 2nd edition. Amsterdam: Elsevier, pp. 371–381. DOI: 10.1016/b978-0-12-385469-8.00021-6.

Hoover, H. C. and L. H. Hoover, eds. and trans. (1950). Georgius Agricola*: De re metallica* (1556). Mineola, New York: Dover Publications.

Hoppe, U., D. Stachel, and D. Beyer (1995). "The oxygen coordination of metal ions in phosphate and silicate glasses studied by a combination of X-ray and neutron diffraction". In: *Physica Scripta* T57, pp. 122–126. DOI: 10.1088/0031-8949/1995/t57/021.

Huff, L. D. and W. V. Houston (1930). "The appearance of 'forbidden lines' in spectra". In: *Physical Review* 36 (5), pp. 842–846. DOI: 10.1103/PhysRev.36.842. URL: https://link.aps.org/doi/10.1103/PhysRev.36.842.

Hughes, M. J. (1972). "A technical study of opaque red glass of the Iron Age in Britain." In: *Proceedings of the Prehistoric Society* 38, pp. 98–107. DOI: 10.1017/s0079497x00012068.

Hughes, M. J., I. C. Freestone, and Y. Gorin-Rosen (2000). "Primary glass from Israel and the production of glass in Late Antiquity and the Early Islamic period. Colloque organisé en 1989 par l'Association française pour l'Archéologie du Verre (AFAV)". In: *La Route du verre. Ateliers primaires et secondaires du second millénaire av. J.-C. au Moyen Âge. Colloque organisé en 1989 par l'Association française pour l'Archéologie du Verre (AFAV).* Lyon: Maison de l'Orient et de la Méditerranée Jean Pouilloux. URL: https://www.persee.fr/doc/mom_1274-6525_2000_act_33_1_1874.

Hulst, H. C. van de (1981). *Light scattering by small particles.* Dover edition. Mineola, New York: Dover Publications.

Hunault, M., G. Lelong, M. Gauthier, F. Gélébart, S. Ismael, L. Galoisy, F. Bauchau, C. Loisel, and G. Calas (2016). "Assessment of transition element speciation in glasses us-

ing a portable transmission ultraviolet–visible–near-infrared (UV-Vis-NIR) spectrometer". In: *Applied Spectroscopy* 70.5, pp. 778–784. DOI: 10.1177/0003702816638236.

Ilg, A., ed. and trans. (1873). Heraclius*: De coloribus et artibus romanorum* (9^{th} – 12^{th} century CE). Wien: Wilhelm Braumüller. URL: https://babel.hathitrust.org/cgi/pt?id=wu.89054764725;view=1up;seq=1.

– ed. and trans. (1874). Theophilus Presbyter*: Schedula diversarum artium* (11^{th} century CE). Wien: Wilhelm Braumüller. URL: http://www.mdz-nbn-resolving.de/urn/resolver.pl?urn=urn:nbn:de:bvb:12-bsb11181503-5.

Jackson, C. M., C. A. Booth, and J. W. Smedley (2005). "Glass by design? Raw materials, recipes and compositional data". In: *Archaeometry* 47.4, pp. 781–795. DOI: 10.1111/j.1475-4754.2005.00232.x.

Jackson, C. (2008). "Theophilus and the use of beech ash as a glassmaking alkali". In: *Archaeology, history and science. Integrating approaches to ancient materials*. Ed. by M. Martinon-Torres and T. Rehren. New York: Routledge, pp. 117–130.

Janiak, C., T. Klapötke, H.-J. Meyer, and R. Alsfasser (2008). *Moderne Anorganische Chemie*. Ed. by E. Riedel. 3rd ed. Berlin: De Gruyter. ISBN: 978-3-11-020685-2.

Janssens, K. (2005). "X-ray fluorescence analysis". In: *Handbook of Spectroscopy*. Weinheim: Wiley-VCH Verlag GmbH & Co. KGaA, pp. 363–420. DOI: 10.1002/3527602305.ch11.

Jenkins, R., R. Manne, R. Robin, and C. Senemaud (1991). "IUPAC—nomenclature system for X-ray spectroscopy". In: *X-Ray Spectrometry* 20.3, pp. 149–155. DOI: 10.1002/xrs.1300200308.

Jong de, B. H. W. S., C. M. Schramm, and V. E. Parziale (1983). "Polymerization of silicate and aluminate tetrahedra in glasses, melts, and aqueous solutions—IV. Aluminum coordination in glasses and aqueous solutions and comments on the aluminum avoidance principle". In: *Geochimica et Cosmochimica Acta* 47.7, pp. 1223–1236. DOI: 10.1016/0016-7037(83)90064-9.

Jüngst, H. (1986). "Supposed References to Reaction Soldering in Alcman, Sophocles and Antiphanes". In: *American Journal of Archaeology*, pp. 95–98.

Kamitsos, E. I. (2015). "Infrared spectroscopy of glasses". In: *Modern Glass Characterization*. Ed. by M. Affatigato. Hoboken, New Jersy: John Wiley & Sons, Inc., pp. 32–73. DOI: 10.1002/9781119051862.ch2.

Kamitsos, E. I., M. A. Karakassides, A. P. Patsis, and G. D. Chryssikos (1990). "Laser-induced crystallization of glassy caesium metaborate studied by Raman spectroscopy". In: *Journal of Non-Crystalline Solids* 116.1, pp. 115–122. DOI: 10.1016/0022-3093(90)91053-t.

Kasap, S. and P. Capper, eds. (2017). *Springer handbook of electronic and photonic materials*. Cham: Springer International Publishing. DOI: 10.1007/978-3-319-48933-9.

Kemp, B. (2015). "Tell El-Amarna, 2014–15". In: *The Journal of Egyptian Archaeology* 101.1, pp. 1–35. DOI: 10.1177/030751331510100101.

Kläui, W. (1990). "The coordination chemistry and organometallic chemistry of tridentate oxygen ligands with π-donor properties". In: *Angewandte Chemie International Edition in English* 29.6, pp. 627–637. DOI: 10.1002/anie.199006271.

Kleber, W. (1962). "Zur thermodynamisch-kinetischen Theorie der heterotaktischen Keimbildung". In: *physica status solidi (b)* 2.7, pp. 923–928. DOI: 10.1002/pssb.19620020710.

Klyuev, V. P. and B. Z. Pevzner (2003). "Thermal expansion and glass transition temperature of calcium borate and calcium aluminoborate glasses". In: *Glass Physics and Chemistry* 29.2, pp. 127–136. DOI: 10.1023/a:1023498823701.

Kocsis, L., P. Herman, and A. Eke (2006). "The modified Beer–Lambert law revisited". In: *Physics in Medicine and Biology* 51.5, N91–N98. DOI: 10.1088/0031-9155/51/5/n02.

Krueger, I. and H. K. Wedepohl (2003). "Composition and shapes of glass of the early medieval period (8^{th} to 10^{th} century AD) in Central Europe". In: *Échanges et commerce du verre dans le monde antique*, pp. 93–100.

Kunicki-Goldfinger, J. J., I. C. Freestone, I. McDonald, J. A. Hobot, H. Gilderdale-Scott, and T. Ayers (2014). "Technology, production and chronology of red window glass in the medieval period – rediscovery of a lost technology". In: *Journal of Archaeological Science* 41, pp. 89–105. DOI: 10.1016/j.jas.2013.07.029. (Visited on 09/13/2016).

Kurkjian, C. R. and W. R. Prindle (1998). "Perspectives on the history of glass composition". In: *Journal of the American Ceramic Society* 81.4, pp. 795–813. DOI: 10.1111/j.1151-2916.1998.tb02415.x.

Lahlil, S., I. Biron, M. Cotte, and J. Susini (Sept. 2010). "New insight on the in situ crystallization of calcium antimonate opacified glass during the Roman period". In: *Applied Physics A* 100.3, pp. 683–692. ISSN: 0947-8396, 1432-0630. DOI: 10.1007/s00339-010-5650-z.

Lahlil, S., I. Biron, M. Cotte, J. Susini, and N. Menguy (Jan. 2010). "Synthesis of calcium antimonate nano-crystals by the 18th dynasty Egyptian glassmakers". In: *Applied Physics A* 98.1, pp. 1–8. ISSN: 0947-8396, 1432-0630. DOI: 10.1007/s00339-009-5454-1.

Lahlil, S., M. Cotte, I. Biron, J. Szlachetko, N. Menguy, and J. Susini (2011). "Synthesizing lead antimonate in ancient and modern opaque glass". In: *Journal of Analytical Atomic Spectrometry* 26.5, p. 1040. DOI: 10.1039/c0ja00251h. URL: http://dx.doi.org/10.1039/c0ja00251h.

Landerer, X. (1859). "Ueber verschiedene in den alten Gräbern der Hellenen aufgefundene Gegenstände". In: *Das Ausland. Wochenschrift für Erd- und Völkerkunde* 32, pp. 684–686.

Lankton, J. W. (2003). *A bead timeline, vol. I: Prehistory to 1200 CE*. Washington, DC: The Bead Society of Greater Washington, pp. 14–19. ISBN: 978-0972506618.

Larkin, P. J. (2011). *Infrared and Raman spectroscopy. Principles and spectral interpretation*. Amsterdam: Elsevier.

Lauwers, D., A. G. Hutado, V. Tanevska, L. Moens, D. Bersani, and P. Vandenabeele (2014). "Characterisation of a portable Raman spectrometer for in situ analysis of art objects". In: *Spectrochimica Acta Part A: Molecular and Biomolecular Spectroscopy* 118, pp. 294–301. DOI: 10.1016/j.saa.2013.08.088.

Lazic, V., F. Colao, R. Fantoni, A. Palucci, V. Spizzichino, I. Borgia, B. G. Brunetti, and A. Sgamellotti (2003). "Characterisation of lustre and pigment composition in ancient pottery by laser induced fluorescence and breakdown spectroscopy". In: *Journal of Cultural Heritage* 4, pp. 303–308. DOI: 10.1016/s1296-2074(02)01212-8.

Lilyquist, C. and R. H. Brill (1993). *Studies in Early Egyptian glass*. Ed. by G. Felix and E. Powers. New York: Metropolitan Museum of Art.

Longuet-Higgins, H. C., U. Opik, M. H. L. Pryce, and R. A. Sack (1958). "Studies of the Jahn-Teller effect. II. The dynamical problem". In: *Proceedings of the Royal Society A: Mathematical, Physical and Engineering Sciences* 244.1236, pp. 1–16. DOI: 10.1098/rspa.1958.0022.

Lynch, M. E., D. C. Folz, and D. E. Clark (2007). "Use of FTIR reflectance spectroscopy to monitor corrosion mechanisms on glass surfaces". In: *Journal of Non-Crystalline Solids* 353.27, pp. 2667–2674. DOI: 10.1016/j.jnoncrysol.2007.05.012.

Maikala, R. V. (2010). "Modified Beer's law – historical perspectives and relevance in near-infrared monitoring of optical properties of human tissue". In: *International Journal of Industrial Ergonomics* 40.2, pp. 125–134. DOI: 10.1016/j.ergon.2009.02.011.

Maltoni, S. and A. Silvestri (2016). "Innovation and tradition in the fourth century mosaic of the Casa delle Bestie Ferite in Aquileia, Italy: archaeometric characterisation of the glass tesserae". In: *Archaeological and Anthropological Sciences*. DOI: https://doi.org/10.1007/s12520-016-0359-3.

Mäntele, W. and E. Deniz (2017). "UV–VIS absorption spectroscopy: Lambert-Beer reloaded". In: *Spectrochimica Acta Part A: Molecular and Biomolecular Spectroscopy* 173, pp. 965–968. DOI: 10.1016/j.saa.2016.09.037.

Mass, J. L., M. T. Wypyski, and R. E. Stone (2002). "Malkata and Lisht glassmaking technologies: Towards a specific link between second millennium BC". In: *Archaeometry* 44.1, pp. 67–82. DOI: 10.1111/1475-4754.00043.

Mass, J. L., M. T. Wypyski, and R. E. Stone (2001). "Evidence for the metallurgical origins of glass at two Ancient Egyptian glass factories". In: *MRS Bulletin* 26.1, pp. 38–43. DOI: 10.1557/mrs2001.17.

Mecking, O. (2012). "Medieval lead glass in Central Europe". In: *Archaeometry* 55.4, pp. 640–662. DOI: 10.1111/j.1475-4754.2012.00697.x.

Miliani, C., F. Rosi, A. Daveri, and B. G. Brunetti (2011). "Reflection infrared spectroscopy for the non-invasive in situ study of artists' pigments". In: *Applied Physics A* 106.2, pp. 295–307. DOI: 10.1007/s00339-011-6708-2.

Mirti, P., P. Davit, and M. Gulmini (2001). "Colourants and opacifiers in seventh and eighth century glass investigated by spectroscopic techniques". In: *Analytical and Bioanalytical Chemistry* 372.1, pp. 221–229. DOI: 10.1007/s00216-001-1183-9.

Mishchenko, M. I., L. D. Travis, and A. A. Lacis (2006). *Scattering, absorption, and emission of light by small particles*. Third, electronic edition. New York: NASA Goddard Institute for Space Studies.

Möncke, D., D. Palles, N. Zacharias, M. Kaparou, E. I. Kamitsos, and L. Wondraczek (2013). "Formation of an outer borosilicate glass layer on Late Bronze age Mycenaean blue vitrious relief fragments". In: *Physics and Chemistry of Glasses — European Journal of Glass Science and Technology Part B* 54.1, pp. 52–59.

Möncke, D., M. Papageorgiou, A. Winterstein-Beckmann, and N. Zacharias (June 2014). "Roman glasses coloured by dissolved transition metal ions: redox-reactions, optical

spectroscopy and ligand field theory". In: *Journal of Archaeological Science* 46, pp. 23–36. ISSN: 03054403. DOI: 10.1016/j.jas.2014.03.007.

Moran, W. L. (1992). *The Amarna letters*. Baltimore: Johns Hopkins University Press.

Müller, R., E. D. Zanotto, and V. M. Fokin (2000). "Surface crystallization of silicate glasses: nucleation sites and kinetics". In: *Journal of Non-Crystalline Solids* 274.1-3, pp. 208–231. DOI: 10.1016/s0022-3093(00)00214-3.

Nascimento, M. L. F. and E. D. Zanotto (2006). "Mechanisms and dynamics of crystal growth, viscous flow, and self-diffusion in silica glass". In: *Physical Review B* 73.2, pp. 024209-1–024209-7. DOI: 10.1103/physrevb.73.024209.

Nightingale, G. (2004). "Mykenisches Glas". In: *Althellenistische Technologie und Technik von der prähistorischen bis zur hellenistischen Zeit mit Schwerpunkt auf der prähistorischen Epoche*. Weilheim: Verein zur Förderung der Aufarbeitung der Hellenischen Geschichte e.V., 2004, pp. 171–189.

Opik, U. and M. H. L. Pryce (1957). "Studies of the Jahn-Teller effect. I. A survey of the static problem". In: *Proceedings of the Royal Society A: Mathematical, Physical and Engineering Sciences* 238.1215, pp. 425–447. DOI: 10.1098/rspa.1957.0010.

Oppenheim, A. L., R. H. Brill, D. Barag, and A. Von Saldern (1970). "The chemical interpretation of the texts". In: *Glass and glassmaking in ancient Mesopotamia*. Vol. 3. Corning Museum of Glass Monographs. New York: Corning Museum of Glass, pp. 105–128.

Outram, A. K. (2008). "Introduction to experimental archaeology". In: *World Archaeology* 40.1, pp. 1–6. DOI: 10.1080/00438240801889456.

Panagiotaki, M., L. Papazoglou-Manioudaki, C.-S. G., E. Andreopoulou-Mangou, Y. Maniatis, M. S. Tite, and A. Shortland (2003). "A glass workshop at the Mycenaean citadel of Tiryns in Greece". In: *Annales du 16^3 congrès de l'associacion internationale pour l'histoire du verre*. London, pp. 14–8.

Panagiotaki, M. (2008). "The technological development of Aegean vitreous materials in the Bronze Age". In: *Vitreous Materials in the Late Bronze Age Aegean* 9, pp. 34–63.

Peltenburg, E. (1971). "Some early developments of vitreous materials". In: *World Archaeology* 3.1, pp. 6–12. DOI: 10.1080/00438243.1971.9979489.

Picon, M. and M. Vichy (2003). "D'Orient en Occident: l'origine du verre à l'époque romaine et durant le haut Moyen Âge". In: *Échanges et commerce du verre dans le monde antique*, pp. 17–31.

Rehren, T. (2005). "Late Bronze Age Glass Production at Qantir-Piramesses, Egypt". In: *Science* 308.5729, pp. 1756–1758. DOI: 10.1126/science.1110466.

Reitzenstein, D. (2016). "*auri sanies*: Nero, Gold und *chrysocolla*". In: *Beiträge der Tübinger Summerschool vom 16. - 19. Juni 2014*. Ed. by K. B. Zimmer. Rahden / Westf., pp. 115–133.

Rempel, U. (2008). "Die frühneuzeitliche Weinglashütte bei Wieda/Südharz". In: *Glashüttenlandschaft Europa. Beiträge zum 3. Internationalen Glassymposium in Heigenbrücken / Spessart, 2006. Beiträge zum 3. Internationalen Glassymposium in Heigenbrücken / Spessart, 2006*. Ed. by P. Steppuhn, G. Himmelsbach, and H. Flachendecker. Regensburg: Schnell & Steiner, pp. 192–196. ISBN: 978-3-7954-2074-1.

Ricciardi, P., P. Colomban, A. Tournié, M. Macchiarola, and N. Ayed (2009). "A non-invasive study of Roman Age mosaic glass tesserae by means of Raman spectroscopy". In: *Journal of Archaeological Science* 36.11, pp. 2551–2559. DOI: 10.1016/j.jas.2009.07.008.

Schallin, A.-L. (2016). "Identities and 'precious' commodities at Midea and Dendra in the Mycenaean Argolid". In: *Papers and Monographs from the Norwegian Institute at Athens*. Vol. 40. Athens: The Norwegian Institute at Athens.

Schalm, O., K. Janssens, H. Wouters, and D. Caluwé (2007). "Composition of 12 –18th century window glass in Belgium: Non-figurative windows in secular buildings and stained-glass windows in religious buildings". In: *Spectrochimica Acta Part B: Atomic Spectroscopy* 62.6-7, pp. 663–668. DOI: 10.1016/j.sab.2007.03.006.

Schliemann, H. (1878). *Mykenae. Bericht über meine Forschungen und Entdeckungen in Mykenae*. Leipzig: Brockhaus. URL: http://digi.ub.uni-heidelberg.de/diglit/schliemann1878.

Schmelzer, J. W. P., V. M. Fokin, and A. S. Abyzov (2016). "Crystallization of glass: What we know, what we need to know". In: *International Journal of Applied Glass Science* 7.3, pp. 253–261. DOI: 10.1111/ijag.12212.

Schoer, B. and T. Rehren (2007). "The composition of glass and associated ceramics from Qantir". In: *Hochtemperatur-technologie in der Ramses-Stadt. Rubinglas für den Pharao*. Ed. by E. Pusch and M. Bietak. Vol. 6. Forschungen in der Ramses-Stadt. Hildesheim: Gebrüder Gerstenberg, pp. 171–199.

Shortland, A. J. (2002). "The use and origin of antimonate colorants in early Egyptian glass". In: *Archaeometry* 44.4, pp. 517–530. DOI: 10.1111/1475-4754.t01-1-00083.

Shortland, A. J. and M. S. Tite (2000). "Raw materials of glass from Amarna and implications for the origins of Egyptian glass". In: *Archaeometry* 42.1, pp. 141–151. DOI: 10.1111/j.1475-4754.2000.tb00872.x.

Shortland, A., N. Rogers, and K. Eremin (2007). "Trace element discriminants between Egyptian and Mesopotamian Late Bronze Age glasses". In: *Journal of Archaeological Science* 34.5, pp. 781–789. DOI: 10.1016/j.jas.2006.08.004.

Shortland, A., L. Schachner, I. Freestone, and M. Tite (2006). "Natron as a flux in the early vitreous materials industry: sources, beginnings and reasons for decline". In: *Journal of Archaeological Science* 33.4, pp. 521–530. DOI: 10.1016/j.jas.2005.09.011.

Shugar, A. N. (2000). "Byzantine opaque red glass *tesserae* from Beit Shean, Israel". In: *Archaeometry* 42.2, pp. 375–384. DOI: 10.1111/j.1475-4754.2000.tb00888.x.

Silvestri, A., G. Molin, and G. Salviulo (2005). "Roman and medieval glass from the Italian area: Bulk characterization and relationships with production technologies". In: *Archaeometry* 47.4, pp. 797–816. DOI: 10.1111/j.1475-4754.2005.00233.x.

Silvestri, A., G. Molin, G. Salviulo, and R. Schievenin (2006). "Sand for Roman glass production: an experimental and philological study on source of supply". In: *Archaeometry* 48.3, pp. 415–432. DOI: 10.1111/j.1475-4754.2006.00264.x.

Smart, R. M. and F. P. Glasser (1974). "Compound formation and phase equilibria in the system PbO-SiO_2". In: *Journal of the American Ceramic Society* 57.9, pp. 378–382. DOI: 10.1111/j.1151-2916.1974.tb11416.x.

Smirniou, M. and T. Rehren (2010). "Direct evidence of primary glass production in Late Bronze Age Amarna, Egypt". In: *Archaeometry* 53.1, pp. 58–80. DOI: 10.1111/j.1475-4754.2010.00521.x.

Smith, C. S. and J. G. Hawthorne (1974). "*Mappae clavicula*: A little key to the world of Medieval techniques". In: *Transactions of the American Philosophical Society* 64.4, p. 1. DOI: 10.2307/1006317.

Smith, G. D. and R. J. H. Clark (2004). "Raman microscopy in archaeological science". In: *Journal of Archaeological Science* 31.8, pp. 1137–1160. DOI: 10.1016/j.jas.2004.02.008.

Stapleton, C. P. and S. S. Swanson (2002). "Batch material processing and glassmaking technology of 9^{th} century B.C. artifacts excavated from the site of Hasanlu, Northwest Iran". In: *MRS Proceedings* 712. DOI: 10.1557/proc-712-ii7.4.

Steppuhn, P. (2006). *Waldglashütten im Taunus. Geschichte, Archäologie, Produkte.* German. Schriftenreihe des Hessischen Freilichtmuseums, Heft 13. Neu-Anspach: Freilichtmuseum Hessenpark.

– (in press). "270 kg Flachglas in der Grube – Ein Fundkomplex des späten 12. bis frühen 16. Jahrhunderts vom Areal der Domimmunität in Münster (Westfalen)". In: *Glas und Glashütten: Archäologische Belege zu Rohstoff, Verarbeitung, Handel und Nutzung. Arbeitskreis zur Erforschung des mittelalterlichen Handwerks, 15. Treffen Konstanz 22.-24.05.2014 sowie 6. Internationales Symposium zur Erforschung mittelalterlicher und frühneuzeitlicher Glashütten Europas, Tagung Baiersbronn 6.5.-8.5. 2016.* Forschungen und Berichte zur Archäologie in Baden-Württemberg. Esslingen: Landesamt für Denkmalpflege Baden-Württemberg. in press.

Stern, W. B. and Y. Gerber (2004). "Potassium-calcium glass: New data and experiments". In: *Archaeometry* 46.1, pp. 137–156. DOI: 10.1111/j.1475-4754.2004.00149.x.

Stookey, S. D. (1949). "Coloration of glass by gold, silver, and copper". In: *Journal of the American Ceramic Society* 32.8, pp. 246–249. DOI: 10.1111/j.1151-2916.1949.tb18957.x.

Stratis, J. A., G. A. Zachariadis, E. A. Dimitrakoudi, and V. Simeonov (1988). "Critical comparison of decomposition procedures for atomic absorption spectrometric analysis of prehistorical ceramics". In: *Fresenius' Zeitschrift für Analytische Chemie* 331.7, pp. 725–729. DOI: 10.1007/bf01105608.

Stroud, J. S. (1961). "Photoionization of Ce^{3+} in glass". In: *The Journal of Chemical Physics* 35.3, pp. 844–850. DOI: 10.1063/1.1701227.

Sturge, M. D. (1968). "The Jahn-Teller effect in solids". In: *Solid State Physics* 20, pp. 91–211. DOI: 10.1016/s0081-1947(08)60218-0.

Tammann, G. (1933). *Der Glaszustand.* Leipzig: Voss.

Tilley, R. J. D. (2011). *Colour and the optical properties of materials.* 2nd ed. Chichester: Wiley. ISBN: 9780470746967.

Tite, M., T. Pradell, and A. Shortland (2007). "Discovery, production and use of tin-based opacifiers in glasses, enamels and glazes from the Late Iron Age onwards: : A reassessment." In: *Archaeometry* 50.1, pp. 67–84. DOI: 10.1111/j.1475-4754.2007.00339.x.

Tite, M., A. Shortland, Y. Maniatis, D. Kavoussanaki, and S. Harris (Sept. 2006). "The composition of the soda-rich and mixed alkali plant ashes used in the production of glass". In: *Journal of Archaeological Science* 33.9, pp. 1284–1292. ISSN: 03054403. DOI: 10.1016/j.jas.2006.01.004.

Vandenabeele, P., H. G. M. Edwards, and J. Jehlička (2014). "The role of mobile instrumentation in novel applications of Raman spectroscopy: archaeometry, geosciences, and forensics". In: *Chemical Society Reviews* 43.8, p. 2628. DOI: 10.1039/c3cs60263j.

Vandenabeele, P. and M. K. Donais (2016). "Mobile spectroscopic instrumentation in archaeometry research". In: *Applied Spectroscopy* 70.1, pp. 27–41. DOI: 10.1177/0003702815611063.

Vilarigues, M. and R. C. da Silva (2006). "Characterization of potash-glass corrosion in aqueous solution by ion beam and IR spectroscopy". In: *Journal of Non-Crystalline Solids* 352.50-51, pp. 5368–5375. DOI: 10.1016/j.jnoncrysol.2006.08.032.

Vogel, W. (2011). *Glass chemistry*. Trans. by N. Kreidl and M. L. Barreto. 2nd ed. Berlin: Springer Science & Business Media.

Wedepohl, K. H. (1997). "Chemical composition of medieval glass from excavations in West Germany". In: *Glastech. Ber. Glass Sci. Technol.* 70.8, pp. 246–255.

Wedepohl, K. H. and A. Kronz (2009). "Die Glaszusammensetzung dreier spätmittelalterlicher Hütten auf dem Taunus-Kamm unweit Glashütten". In: *Berichte der Kommission für Archäologische Landesforschung in Hessen* 9, pp. 135–151.

Wedepohl, K. H. (Sept. 2003). *Glas in Antike und Mittelalter*. Stuttgart: Schweizerbart Science Publishers. ISBN: 9783510652075. URL: http://www.schweizerbart.de//publications/detail/isbn/9783510652075/Wedepohl%5C_Glas%5C_in%5C_Mittelalter%5C_und%5C_Antike.

Wedepohl, K. H. and K. Simon (2010). "The chemical composition of medieval wood ash glass from Central Europe". In: *Chemie der Erde - Geochemistry* 70.1, pp. 89–97. DOI: 10.1016/j.chemer.2009.12.006.

Wedler, G. and H.-J. Freund (2018). *Lehr- und Arbeitsbuch Physikalische Chemie*. 7th ed. Weinheim: Wiley VCH. ISBN: 3527346112.

Welter, N., U. Schüssler, and W. Kiefer (2006). "Characterisation of inorganic pigments in ancient glass beads by means of Raman microspectroscopy, microprobe analysis and X-ray diffractometry". In: *Journal of Raman Spectroscopy* 38.1, pp. 113–121. DOI: 10.1002/jrs.1637.

Weyl, W. A. (2016). *Coloured glasses*. 7th ed. Sheffield: Society of Glass Technology.

Wiesenberg, F. (2014). "Experimentelle Archäologie: Römische Glasöfen. Rekonstruktion und Betrieb einer Glashütte nach Römischem Vorbild in der Villa Borg". In: *Schriften des Archäologieparks Römische Villa Borg*. Vol. 6. Merzig: Kulturstiftung Merzig-Wadern.

– (2018). "Glasperlenherstellung am holzbefeuerten Lehmofen". In: *Experimentelle Archäologie in Europa, Jahrbuch 2018*. Ed. by U. Weller, T. Lessing-Weller, and E. Hanning. Vol. Heft 17. Unteruhldingern: Europäische Vereinigung zur Förderung der Experimentellen Archäologie e.V., pp. 87–100.

Anhang

Selbstständigkeitserklärung

Ich erkläre, dass ich die vorliegende Arbeit selbstständig und nur unter Verwendung der angegebenen Hilfsmittel, persönlichen Mitteilungen und Quellen angefertigt habe.

Jena, den _____

Unterschrift

Erklärung zu den Eigenanteilen des Promovenden / der Promovendin sowie der weiteren Doktoranden / Doktorandinnen als Koautoren an den Publikationen und Zweitpublikationsrechten bei einer kumulativen Dissertation

Für alle in dieser kumulativen Dissertation verwendeten Manuskripte liegen die notwendigen Genehmigungen der Verlage ("Reprint permissions") für die Zweitpublikation vor.

Die Co-Autoren der in dieser kumulativen Dissertation verwendeten Manuskripte sind sowohl über die Nutzung, als auch über die oben angegebenen Eigenanteile der weiteren Doktoranden / Doktorandinnen als Koautoren an den Publikationen und Zweitpublikationsrechten bei einer kumulativen Dissertation informiert und stimmen dem zu.

Die Anteile des Promovenden / der Promovendin sowie der weiteren Doktoranden / Doktorandinnen als Koautoren an den Publikationen und Zweitpublikationsrechten bei einer kumulativen Dissertation sind in der Anlage aufgeführt.

Ferdinand Drünert	_____	_____	_____
Name des Promovenden / der Promovendin	Datum	Ort	Unterschrift

Publikation: Copper-based opaque red glasses – Understanding the colouring mechanism of copper nanoparticles in archaeological glass samples

Name	Vorgeschlagene Publikationsäquivalente
Ferdinand Drünert	1
Magdalena Blanz	0.25
Kilian Pollok	
Zhiwen Pan	
Lothar Wondraczek	
Doris Möncke	

Publikation: Ancient Roman nano-technology: Insight into the manufacture of mosaic *tesserae* opacified by calcium antimonate

Name	Vorgeschlagene Publikationsäquivalente
Ferdinand Drünert	1
Eleni Palamara	
Nikolaos Zacharias	
Lothar Wondraczek	
Doris Möncke	

Publikation: Borosilicate glass layers on Mycenaean glass: surface alterations by glass – borax – gold interactions

Name	Vorgeschlagene Publikationsäquivalente
Ferdinand Drünert	1
Felix Lind	0.25
Peter Vontobel	
Efastratios I. Kamitsos	
Lothar Wondraczek	
Doris Möncke	